Collapse, Revival and Decoherence of Entanglement in Two Qubits Systems

Iskandar Bahari

PhD

University of York

Physics

January 2018

Abstract

We extend study of the Jaynes-Cummings model involving a pair of identical two-level atoms (or qubits) interacting with a single mode quantised field. We investigate the effects of replacing the radiation field mode with a 'big spin', comprising a collection of N qubits, or spin-1/2 particles. We demonstrate the similarities of this set-up to the qubits-field model in terms of the qubits state probability, occurrence of attractor states, generation of Schrödinger cat state, and in particular the collapse and revival of the entanglement between the two qubits in the qubit subsystem. We extend our analysis by taking into account a decoherence effect due to qubit imperfections. We study two cases of 'error' in the system for both the field mode and 'big spin' cases. In the first part, we consider the case of systems with non-resonance frequencies, and secondly we let the systems evolve with a difference in the dipole interaction strengths of the two qubits. We average over the errors in both of these parameters with distributions of varying width. We demonstrate the effects of such error modeling in both the field mode and the 'big spin' scenarios. We discover that increasing the width of the 'error' distribution increases suppression of the coherent dynamics of the coupled system, including the collapse and revival of the entanglement between the qubits. We also find out that the decoherence effects are more significant in the system with difference in the coupling strength as opposed to the non-resonance case that has higher robustness against errors. At the end of the study, we investigate the qubit-big spin system with a modest value of N to identify the smallest size of the big spin that exhibits the important events in such interacting model.

Contents

List of Figures

Acknowledgments

First of all, I would like to thank my supervisor, Professor Tim Spiller, for his support and guidance throughout my PhD journey. He was indeed very committed and patience in supervising me, besides always having time and answers to all my questions. I am also indebted to him, whose guidance has given my thesis its present shape.

I would also like to thank my sponsors, The Higher Educations of Malaysia and the International Islamic University Malaysia for their financial supports that made a PhD at York possible.

I have also been fortunate to have learned from many people over the last four years especially my PhD friends and colleagues in the Physics department, thank you for many interesting and fruitful discussions. To all my fellow Malaysian friends that provided me with uncountable helps and supports, may God bless all of you with the best in life.

I would also like to dedicate very special thanks to my families, especially my parents Mr Bahari Iberahim and Mrs Kamariah Napi for their undivided loves and supports from distant. Infinity thanks to my beloved wife Norlaila Md Nor, who has been very patient in accompanying me along my PhD journey. She has been very understanding, supportive and always stands by my side during my ups and downs. To my first son Irham Luqman, my daughter Laisara Iqlima who was born during the first year of my PhD, and my newly born son Indra Luthfy, all of you just made my PhD years a very beautiful experience and memory. Not to forget my very supportive siblings and in laws. Without them I would not have had the strength to pursue and complete this dissertation.

Finally, my gratitude to the Almighty for the good chance and life that have been gifted to me. This work has indeed bring me closer to Him.

Authors Declaration

The candidate confirms that the work in this dissertation was carried out in accordance with the requirements of the University's Regulations and Code of Practice for Research Degree Programmes and that it has not been submitted for any other academic award. The candidate confirms that any views expressed in the dissertation are those of the author and appropriate credit has been given within the thesis where reference has been made to the work of others.

Chapter 4, 6 and 7 are based on the publication:

I. Bahari, T.P.Spiller, S.Dooley, A.Hayes, and F.McCrossan,
Collapse and revival of entanglement in qubits with big spin system,
arXiv:1612.06444 (2016).

This publication has been submitted, accepted will be published in the International Journal of Quantum Information.

Timothy P. Spiller supervised the project. All other work is directly attibutable to Iskandar Bahari.

Chapter 1

Introduction

Quantum information technologies range all the way from communications with discrete resources, through metrology and simulation technologies to quantum computers that require large entangled quantum resources. Behind these technologies lie the fundamental features of quantum physics like entanglement, superposition, non-cloning properties, measurement, and many more. Based on these physical laws of quantum mechanics, quantum technology has a potential to revolutionise many areas of science and technology besides opening possibilities for new capabilities and applications.

Among many quantum information applications, quantum metrology is an emerging field that utilises the theory of entanglement to generate quantum resources via an interaction. It exploits quantum entanglement theory to enable highly sensitive measurements of physical parameters. 'Schrödinger cat' state is one example of potential resources for quantum metrology. It is a product of atom-field interaction system that can be used especially in the detection of weak forces [1, 2] and in enhancing the measurement precision [3, 2, 4, 5]. As opposed to the estimation precision by utilising separable states of N particles that is bounded by the Standard Quantum Limit of $\frac{1}{\sqrt{N}}$, by employing maximally entangled state like a 'Schrödinger cat' state, estimation precision can be improved to the Heisenberg Limit of $\frac{1}{N}$ [6, 7, 8].

Not only in quantum metrology, physical applications of an interaction between a two-level system (a qubit) with a field can be observed in many other different and interesting quantum systems, such as Rydberg atoms [9], Cooper Pair Boxes [10], Cavity Quantum Electrodynamics [11], trapped ions [12] and Circuit QED [13]. Amongst many, one of the most widely used atom-field interaction model is the Jaynes-Cummings model that was introduced by E. Jaynes and F. Cummings [14]. This model was studied to understand the predictions for the state evolution when a two-level atom is coupled to a quantised radiation field, in comparison with the semi-classical interaction model, the Rabi model [15]. Not only does this model exhibit many interesting phenomena, the Jaynes-Cummings model also provides a very important explanation about the event of spontaneous emission in quantum theory of radiation.

In the present day the Jaynes-Cummings model is widely used as a tool in many quantum fields. Not only because of the wide applicability of this model to a range of qubit-field systems, the significant potential for using qubits and fields together in quantum processing are also very promising. Therefore, we can easily find many applications of this model in quantum processing [16, 17, 18] and quantum computing systems [19, 20, 21].

Following the initial investigations, there have been numerous extended theoretical and computational studies of the Jaynes-Cummings model. These studies are conducted with a wide range of physical implementations in mind, to identify the similarities, differences, fundamental features and to extend potential applications of these systems. They first led to the discovery of qubit collapse and revival [22, 23] and more recently to the discoveries of many new interesting phenomena, such as sudden death of entanglement [24, 25, 26], collapse and revival of qubits entanglement [25, 27, 28], and cat-swapping [28].

In this thesis we study variants of some of these prior works, particularly those by C. Jarvis *et al* [27, 28] and S. Dooley *et al.* [29]. We propose a new model that incorporates some selected features of these earlier works into a different hybrid system with qubits that should also be a candidate for quantum information and processing applications. Our work demonstrates the appearance of a range of phenomena with potential application, including the collapse and revival of Rabi oscillations, the attractor and the spin Schrödinger cat states of the system, as well as the dynamics of the entanglement between the two initial qubits in the system.

This thesis is separated into 8 chapters. Later in this Chapter 1 some important terms, notations and operations that will be used throughout this thesis are introduced. It will then followed by a brief introduction of the standard quantum theory that is very important in influencing our models, and also many important concepts that are very useful when discussing the results in Chapter 2 and afterward.

In Chapter 2 we introduce the 'one-qubit Jaynes-Cummings model', a system that describes a single qubit interacting with a single mode of the field. We show the detailed calculations performed to understand the dynamics and and the properties of the model. By using the similar methods and understanding developed from this model, we show the calculations and the behaviours of an alternative model called the 'one-qubit big spin model' where a single qubit is allowed to interact with a collection of spin coherent states (called the 'big spin'). This chapter is the foundation to understand the quantum research in this thesis where in the subsequent chapters, all calculations will be based on and extended from the calculations made here.

We then proceed with Chapter 3 where we study both one-qubit Jaynes-Cummings model and one-qubit big spin model with non-zero detuning effects. We divided the studies into two parts, where in the first half of the chapter, we observe the effects of a finite frequencies detunings on both systems. On the other half, we introduce a concept of 'decoherence' on the systems, where we consider its effects with an ideal case of error in the detunings that is described by a distribution.

In Chapter 4, we extend both models by adding an extra qubit into the system and observe the behaviours of the interactions. This brings many new exciting dynamics to the system especially on the entanglement between the two qubits themselves. Phenomena such as 'attractor state', 'collapse and revival of qubits oscillations', 'qubits entropy' and 'collapse and revival of entanglement' are observed on both systems and these lead to the explorations of another dimensions in Chapter 5 and 6. In these chapters, we respectively study the decoherence effects on both interacting systems where in the first we let the systems evolve with errors in the detunings, and in the latter we consider the case of errors in the dipole-interaction strength between the qubits and the field (and big spin for the two-qubit big spin model).

We then proceed to extend the study on the two-qubit big spin model with modest numbers of spin-1/2 particles in the big spin, more relevant for current experimental possibilities. We observe the robustness of this model against the decreasing size of the 'big spin'. Chapter 8 concludes this thesis with some comparisons between the results produced in the preceding chapters.

1.1 Dirac Notation

In quantum mechanics, Dirac notation [30] is mainly used to represent state vectors. With such notation, we can represent pure states by kets $|\psi\rangle$ and their Hermitian conjugates by bras $\langle\psi|$. This notation has an equivalent matrix representation. As an example, a quantum bit state can written in Dirac notation as $|\psi\rangle = \alpha|e\rangle + \beta|g\rangle$ where α and β are the probability amplitudes written as complex numbers and $|e\rangle$ and $|g\rangle$ are the basis states that respectively indicate the excited and the ground state of the system. This ket state can be written in a matrix form as a column vector of

$$|\psi\rangle = \begin{pmatrix} \alpha \\ \beta \end{pmatrix}. \tag{1.1.1}$$

The bra $\langle\psi|$ that represents the conjugate transpose of the ket $|\psi\rangle$ has the form of $\langle\psi| = \alpha^*\langle e| + \beta^*\langle g|$ and can also be written as a row vector

$$\langle\psi| = \begin{pmatrix} \alpha^* & \beta^* \end{pmatrix}. \tag{1.1.2}$$

Intuitively, the bra-ket is then represented by $\langle\phi|\psi\rangle$ and the output value is called an inner product. This product is used to calculate the orthogonality of state. Two states are said to be orthogonal if the inner product is zero. For example,

$$\langle e|e\rangle = \langle g|g\rangle = 1 \tag{1.1.3}$$
$$\langle e|g\rangle = \langle g|e\rangle = 0 \tag{1.1.4}$$

therefore our qubit basis states $|e\rangle$ and $|g\rangle$ are orthogonal to each other.

With this inner product we may also check the normalisation of a vector by calculating if $\langle\psi|\psi\rangle = 1$. For a state $|\psi\rangle$ to be normalised, we need

$$\begin{aligned} \langle\psi|\psi\rangle &= (\alpha^*\langle e| + \beta^*\langle g|)(\alpha|\psi\rangle + \beta|\psi\rangle) && (1.1.5)\\ &= |\alpha|^2\langle e|e\rangle + \alpha\beta^*\langle g|e\rangle + \alpha^*\beta\langle e|g\rangle + |\beta|^2\langle g|g\rangle && (1.1.6)\\ &= |\alpha|^2 + |\beta|^2 = 1. && (1.1.7) \end{aligned}$$

Two states that are orthogonal and normalised are said to be orthonormal to each other.

1.1.1 Operators

With Dirac notation, we can form operators by considering the outer products

$$
\begin{aligned}
|\psi\rangle\langle\phi| &= (\alpha |e\rangle + \beta |g\rangle)(\delta^* \langle e| + \epsilon^* \langle g|) && (1.1.8)\\
&= \alpha\delta^* |e\rangle\langle e| + \beta\delta^* |g\rangle\langle e| + \alpha\epsilon^* |g\rangle\langle e| + \beta\epsilon^* |g\rangle\langle g| && (1.1.9)
\end{aligned}
$$

which can also be represented in a matrix form of

$$
\begin{aligned}
|\psi\rangle\langle\phi| &= \begin{pmatrix}\alpha\\ \beta\end{pmatrix}\begin{pmatrix}\delta^* & \epsilon^*\end{pmatrix} && (1.1.10)\\
&= \begin{pmatrix}\alpha\delta^* & \alpha\epsilon^*\\ \beta\delta^* & \beta\epsilon^*\end{pmatrix} && (1.1.11)
\end{aligned}
$$

Operators are usually distinguished from numbers by a hat above their symbols. For a system of a single qubit $|e\rangle\langle e|$, $|g\rangle\langle e|$, $|g\rangle\langle e|$ and $|g\rangle\langle g|$ are the possible operators. Pauli operators are example of these operators. They can be written in both matrix form as

$$
\hat{\sigma}^x = \begin{pmatrix}0 & 1\\ 1 & 0\end{pmatrix}, \quad \hat{\sigma}^y = \begin{pmatrix}0 & -i\\ i & 0\end{pmatrix}, \quad \hat{\sigma}^z = \begin{pmatrix}1 & 0\\ 0 & -1\end{pmatrix}. \tag{1.1.12}
$$

There are also raising and lowering operators given by

$$
\hat{\sigma}^+ = 2\begin{pmatrix}0 & 1\\ 0 & 0\end{pmatrix}, \quad \hat{\sigma}^- = 2\begin{pmatrix}0 & 0\\ 1 & 0\end{pmatrix}, \tag{1.1.13}
$$

where

$$
\sigma^{\pm} = \sigma^x \pm i\sigma^y \tag{1.1.14}
$$

and therefore the Pauli operators can be written in Dirac form as

$$
\begin{aligned}
\hat{\sigma}^x &= \frac{1}{2}(\hat{\sigma}^+ + \hat{\sigma}^-) = \frac{1}{2}(|e\rangle\langle g| + |g\rangle\langle e|), && (1.1.15)\\
\hat{\sigma}^y &= \frac{i}{2}(\hat{\sigma}^- - \hat{\sigma}^+) = \frac{i}{2}(|g\rangle\langle e| - |e\rangle\langle g|), && (1.1.16)\\
\hat{\sigma}^z &= \frac{1}{2}(\hat{\sigma}^+\hat{\sigma}^- - \hat{\sigma}^-\hat{\sigma}^+) = \frac{1}{2}(|e\rangle\langle e| - |g\rangle\langle g|). && (1.1.17)
\end{aligned}
$$

These operators obey the Pauli spin algebra (commutation relations)

$$[\hat{\sigma}^{+}, \hat{\sigma}^{-}] = \hat{\sigma}^{z} \tag{1.1.18}$$

$$[\hat{\sigma}^{z}, \hat{\sigma}^{\pm}] = \pm 2\hat{\sigma}^{\pm} \tag{1.1.19}$$

where the commutator of two operators $\hat{A}$ and $\hat{B}$ is defined as

$$[\hat{A}, \hat{B}] = \hat{A}\hat{B} - \hat{B}\hat{A}. \tag{1.1.20}$$

Another example of an operator is the Hamiltonian or energy operator of a system, which is a Hermitian operator. It is an operator that is its own adjoint. Therefore, it is also known as a self adjoint operator. A Hermitian operator is represented by a square matrix that satisfies $\hat{A} = \hat{A}^{\dagger}$. Given that all the diagonal elements are real, this Hermitian matrix can be diagnolised by a unitary matrix. It is a a square matrix that represents Unitary operators $\hat{U}$ and satisfies $\hat{U}\hat{U}^{\dagger} = \hat{U}^{\dagger}\hat{U} = \hat{I}_n$. $\hat{U}^{\dagger}$ is the conjugate transpose of $\hat{U}^{\dagger}$, and $\hat{I}_n$ is given the $n \times n$ identity matrix. All the eigenvalues of a Hermitian matrix are real and an eigenvector associated with a specific eigenvalue is orthogonal to another eigenvectors [31]. Given two Hermitian operators $\hat{A}$ and $\hat{B}$ and commutation relation $[\hat{A}, \hat{B}] = 0$, then the operators $\hat{A}$ and $\hat{B}$ are said to have a common set of eigenstates.

In this thesis, we will also be using the photon creation $\hat{a}^{\dagger}$ and annihilation $\hat{a}$ operators that satisfy

$$[\hat{a}^{\dagger}, \hat{a}] = 1. \tag{1.1.21}$$

These operators are usually associated with a field state where they act on photon number states $|n\rangle$. Unlike a qubit, a field has an infinite number of basis states, with n bounded from below, so $n = 0, 1, 2, ...$ The creation operator $\hat{a}^{\dagger}$ increases the number of quanta by one and on the other hand the annihilation $\hat{a}$ operator reduces it by one as follows:

$$\hat{a}^{\dagger} |n\rangle = \sqrt{n+1}\, |n+1\rangle \tag{1.1.22}$$

$$\hat{a} |n\rangle = \sqrt{n}\, |n-1\rangle \tag{1.1.23}$$

and since the state $|n\rangle$ are the eigenstates of the photon number operator $\hat{a}^{\dagger}\hat{a}$, therefore

$$\hat{a}^\dagger \hat{a} |n\rangle = n |n\rangle . \tag{1.1.24}$$

1.1.2 Hilbert Space

Hilbert space is a complex vector space of dimension appropriate for the physical system it is being used to describe. In a finite dimension, it is exactly the same as a complex inner product space. For instance, the Hilbert space $\mathcal{H}$ for a single qubit has a dimension 2. However, for a two qubit state the space is much bigger as it is now a combination of each qubit's Hilbert space, $\mathcal{H}_2 \otimes \mathcal{H}_2 = \mathcal{H}_4$ where $\otimes$ is a tensor product that expands vector spaces into a larger space. In a Dirac notation this symbol is usually hidden e.g. for two qubits, the qubits state is written as $|e\rangle \otimes |e\rangle = |e\rangle |e\rangle = |ee\rangle$ and in a matrix form this operation produce a larger vector as depicted in the example below.

$$\begin{bmatrix} a_{11} & a_{12} \\ a_{21} & a_{22} \end{bmatrix} \otimes \begin{bmatrix} b_{11} & b_{12} \\ b_{21} & b_{22} \end{bmatrix} = \begin{pmatrix} a_{11} \begin{bmatrix} b_{11} & b_{12} \\ b_{21} & b_{22} \end{bmatrix} & a_{12} \begin{bmatrix} b_{11} & b_{12} \\ b_{21} & b_{22} \end{bmatrix} \\ a_{21} \begin{bmatrix} b_{11} & b_{12} \\ b_{21} & b_{22} \end{bmatrix} & a_{22} \begin{bmatrix} b_{11} & b_{12} \\ b_{21} & b_{22} \end{bmatrix} \end{pmatrix} \tag{1.1.25}$$

$$= \begin{pmatrix} a_{11}b_{11} & a_{11}b_{12} & a_{12}b_{11} & a_{12}b_{12} \\ a_{11}b_{21} & a_{11}b_{22} & a_{12}b_{21} & a_{12}b_{22} \\ a_{21}b_{11} & a_{21}b_{12} & a_{22}b_{11} & a_{22}b_{12} \\ a_{21}b_{21} & a_{21}b_{22} & a_{22}b_{21} & a_{22}b_{2p} \end{pmatrix} \tag{1.1.26}$$

1.1.3 Expectation Value

If a system is described by any normalised state $|\psi\rangle$ in Hilbert space $\mathcal{H}$, the the observable quantity represented by an operator $\hat{O}_\phi = |\phi\rangle \langle\phi|$ is given by the expectation value

$$\left\langle \hat{O} \right\rangle = \frac{\int \psi^* \hat{O}_\phi \psi d\tau}{\int \psi^* \psi d\tau}. \tag{1.1.27}$$

This can also be written in terms of bra-ket notation as

$$P_\phi = \left\langle \hat{O} \right\rangle = \frac{\langle\psi| \hat{O}_\phi |\psi\rangle}{\langle\psi|\psi\rangle} \tag{1.1.28}$$

where P_ϕ is the probability of finding a particle in state $|\phi\rangle$ given an initial state $|\psi\rangle$.

1.2 Quantum Theory of Radiation

1.2.1 Coherent States

There are many photon distribution functions for a field and one of them that is our interest in this thesis are coherent states. Coherent states are a type of quantum harmonic oscillator with dynamics properties very close to the classical harmonic oscillation system or usually referred to as the most classical single-mode quantum state [32]. They are very close to the classical states, but are still quantum in nature. These states are the right eigenstates of the annihilation operator $\hat{a}$ and denoted as $|\alpha\rangle$. With a complex number α, the states satisfy

$$\hat{a}\,|\alpha\rangle = \alpha\,|\alpha\rangle \tag{1.2.1}$$

and a similar relation with the creation operator $\hat{a}^\dagger$ where

$$\langle\alpha|\,\hat{a}^\dagger = \alpha^*\,\langle\alpha|\,. \tag{1.2.2}$$

With a complete basis of number states $|n\rangle$, we expand $|\alpha\rangle$ and the states become

$$|\alpha\rangle = e^{|\alpha|^2/2}\sum_{n=0}^{\infty}\frac{\alpha^n}{\sqrt{n!}}\,|n\rangle \tag{1.2.3}$$

where

$$\alpha = |\alpha|e^{-i\theta}, \tag{1.2.4}$$

where the negative sign is just convention, which is adopted to be consistent with previous authors, $|n\rangle$ is the eigenstate of the photon number operator $\hat{n} = \hat{a}^\dagger\hat{a}$ with eigenvalue $n = 0, 1, 2..$, θ is the initial phase of the field and $|\alpha|$ is the size of the radiation field with

$$\bar{n} = \langle\alpha|\hat{n}|\alpha\rangle = |\alpha|^2. \tag{1.2.5}$$

The probability of detecting n photons in the field is given by a Poisson distribution with mean $\bar{n}$

$$P_n = | \langle n|\alpha \rangle |^2 = e^{-|\alpha|^2} \frac{|\alpha|^{2n}}{n!}. \tag{1.2.6}$$

For a large value of $\bar{n}$ we may rewrite the distribution as a Gaussian distribution of

$$e^{-\bar{n}} \frac{\bar{n}^n}{n!} = \frac{1}{\sqrt{2\pi\bar{n}}} e^{\frac{-(n-\bar{n})^2}{2\bar{n}}}. \tag{1.2.7}$$

The width of this probability distribution is $\sqrt{\bar{n}}$ and the following are the examples of the photon number probability distribution with two different values on $\bar{n} = |\alpha|^2$.

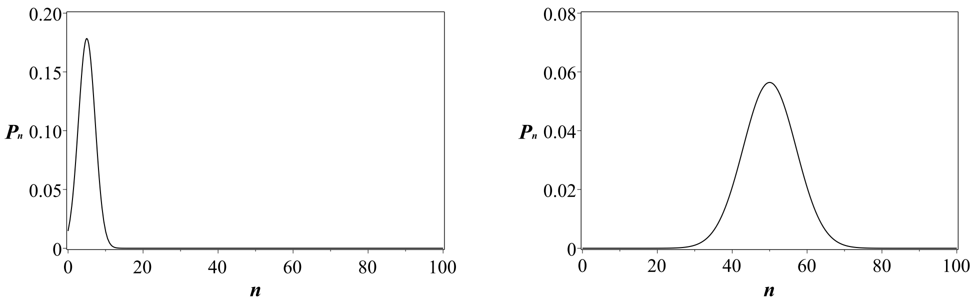

(a) $\bar{n} = 5$ (b) $\bar{n} = 50$

Figure 1.2.1: Plots of Coherent photon number distributions for two different values of $\bar{n}$

.

1.2.2 Spin Coherent States

In this section we will now introduce the analogues of optical coherent states for composite spin systems. In a two dimensional space where $\mathcal{H} = \mathcal{C}^2$ a quantum state can be written as a single spin-1/2 particle. It is one of the simplest examples of a state in such a state space and can be visualised in the Bloch sphere representation as a three dimensional vector $\boldsymbol{r}$, where $\boldsymbol{r} = (r_x, r_y, r_z)$ and $|\boldsymbol{r}| \leq 1$. A pure state has $|\mathbf{r}| = 1$ which means it is positioned on the surface of the sphere, and a mixed state is at inside the sphere with $|\boldsymbol{r}| < 1$ [33]. The definition of the pure and mixed states will be introduced and explained later in Section 1.3.

A spin-1/2 particle can be written in the form of $|\uparrow\rangle$ and $|\downarrow\rangle$ as

$$|\rightarrow\rangle = \frac{1}{\sqrt{2}}(|\uparrow\rangle + |\downarrow\rangle) \tag{1.2.8}$$

$$|\leftarrow\rangle = \frac{1}{\sqrt{2}}(|\uparrow\rangle - |\downarrow\rangle) \tag{1.2.9}$$

$$|\oplus\rangle = \frac{1}{\sqrt{2}}(|\uparrow\rangle + i\,|\downarrow\rangle) \tag{1.2.10}$$

$$|\odot\rangle = \frac{1}{\sqrt{2}}(|\uparrow\rangle - i\,|\downarrow\rangle) \tag{1.2.11}$$

where $|\uparrow\rangle = \begin{pmatrix}1\\0\end{pmatrix}$, $|\downarrow\rangle = \begin{pmatrix}0\\1\end{pmatrix}$, $\oplus$ is for the arrow pointing into the page and $\odot$ is for the arrow pointing out of the page. Associated with these states are the Pauli operators described in Section 1.1, that are given by Equation (1.1.12) to Equation (1.1.14) and obey the commutation relations given by Equation (1.1.15) to Equation (1.1.19). These operators act on the states as follows

$$\begin{array}{ccc} \hat{\sigma}^x\,|\rightarrow\rangle = |\rightarrow\rangle & \hat{\sigma}^y\,|\oplus\rangle = |\oplus\rangle & \hat{\sigma}^z\,|\uparrow\rangle = |\uparrow\rangle \\ \hat{\sigma}^x\,|\leftarrow\rangle = -\,|\leftarrow\rangle & \hat{\sigma}^y\,|\odot\rangle = -\,|\odot\rangle & \hat{\sigma}^z\,|\downarrow\rangle = -\,|\downarrow\rangle \end{array} \tag{1.2.12}$$

A system of two spin-1/2 particles lies in a four dimensional Hilbert space where $\mathcal{H} = \mathcal{C}^2 \otimes \mathcal{C}^2$. The states inside this state space can be written in the $|\uparrow\uparrow\rangle$, $|\uparrow\downarrow\rangle$, $|\downarrow\uparrow\rangle$ and $|\downarrow\downarrow\rangle$ basis. For example, a set of symmetric (under exchange of the two spins) triplet states are given as

$$|\uparrow\uparrow\rangle \quad ; \quad \tfrac{1}{\sqrt{2}}(|\uparrow\downarrow\rangle + |\downarrow\uparrow\rangle) \quad ; \quad |\downarrow\downarrow\rangle \tag{1.2.13}$$

and an additional antisymetric singlet state is given as

$$\frac{1}{\sqrt{2}}(|\uparrow\downarrow\rangle - |\downarrow\uparrow\rangle). \tag{1.2.14}$$

With N spin-1/2 particles, we have $\mathcal{H} = \mathcal{C}^2 \otimes \mathcal{C}^2 .. \otimes \mathcal{C}^2 = (\mathcal{C}^2)^{\otimes N}$ with collective spins operators

$$\hat{J}^x = \tfrac{1}{2}\textstyle\sum_{i=1}^{N} \hat{\sigma}^x_{(i)} \quad ; \quad \hat{J}^y = \tfrac{1}{2}\textstyle\sum_{i=1}^{N} \hat{\sigma}^y_{(i)} \quad ; \quad \hat{J}^z = \tfrac{1}{2}\textstyle\sum_{i=1}^{N} \hat{\sigma}^z_{(i)} \tag{1.2.15}$$

and the total spin operator is the given by

$$\hat{J}^2 = (\hat{J}^x)^2 + (\hat{J}^y)^2 + (\hat{J}^z)^2. \tag{1.2.16}$$

Associated with these operators are the Dicke states of the N spin system $|j,m\rangle_N$. These states are the simultaneous eigenstates of operator $\hat{J}^z$ and the total spin operator $\hat{J}^2$ such that

$$\hat{J}^z |j,m\rangle_N = m |j,m\rangle_N \tag{1.2.17}$$

$$\hat{J}^2 |j,m\rangle_N = j(j+1) |j,m\rangle_N \tag{1.2.18}$$

where the subscript N is to indicate that the state is a N spin system. There are also raising and lowering operators

$$\hat{J}^\pm = \hat{J}^x \pm i\hat{J}^y \tag{1.2.19}$$

that have the following commutation relations

$$[\hat{J}^+, \hat{J}^-] = -2\hat{J}^z \tag{1.2.20}$$

$$[\hat{J}^z, \hat{J}^\pm] = \pm\hat{J}^\pm \tag{1.2.21}$$

$$[\hat{J}^2, \hat{J}^\pm] = 0 \tag{1.2.22}$$

and act on the Dicke states as

$$\hat{J}^\pm |j,m\rangle_N = \sqrt{j(j+1) - m(m\pm 1)}\, |j, m\pm 1\rangle_N . \tag{1.2.23}$$

However, with the number of spin-1/2 larger than two, $N > 2$, the Dicke states $|j,m\rangle_N$ cannot form a complete basis for the system. The number of states is given by

$$\sum_{j=0}^{N/2} (2j+1) = (\frac{N}{2}+1)^2 \tag{1.2.24}$$

which is smaller than the total space 2^N spanned by the state $|j,m\rangle_N$. We may introduce an extra notation l to denote the missing spaces where in the j subspace the degeneracy is given by

$$\mu(j, N) = \begin{pmatrix} N \\ \frac{N}{2} - j \end{pmatrix} - \begin{pmatrix} N \\ \frac{N}{2} - j - 1 \end{pmatrix}. \tag{1.2.25}$$

This combinatorial factor gives us the total dimension

$$\sum_{j=0}^{N/2} \mu(j, N)(2j + 1) = 2^N \tag{1.2.26}$$

where $0 \leq j \leq \frac{N}{2}$. It represents the decomposition of the state space for a system with N spin-1/2 particles into the sum of subspaces with $\mathcal{C}^{2j+1}$ dimensions. Therefore, the Hilbert space becomes

$$\mathcal{H} = \bigoplus_{j=0}^{N/2} \mu(N, j)\mathcal{C}^{2j+1} \tag{1.2.27}$$

where the state space for each single spin-j particle is $2j+1$ dimensional subspace. For example, the state space for $j = \frac{N}{2}$ is $N+1$ dimensional, which is a subspace of the total 2^N dimensional state space. States in this eigenspace are symmetric with respect to exchange of two spins and in this thesis, we will consider the spin system of $j = \frac{N}{2}$ subspace.

In a Bloch sphere representation, a spin coherent state can be written in terms of Dicke state as

$$|j, (\theta, \phi)\rangle_N = \sum_{m=-j}^{j} \begin{pmatrix} 2j \\ m + j \end{pmatrix}^2 \left(\cos\frac{\theta}{2}\right)^{j-m} \left(e^{-i\phi} \sin\frac{\theta}{2}\right)^{j+m} |j, m\rangle_N \tag{1.2.28}$$

where θ is the polar angle and ϕ is the azimuthal angle. By letting $\theta = \pi$, we can make a stereographic projection of any point on the sphere from the north pole onto a complex plane through the equator. We can transform the the spherical coordinates (θ, ϕ) by a parameterisation that is given by

$$\zeta = e^{-i\phi} \tan\frac{\theta}{2}. \tag{1.2.29}$$

Therefore, the spin coherent state that is given by Equation (1.2.28) can now be rewritten as

$$|j,\zeta\rangle_N = \sum_{m=-j}^{j} \begin{pmatrix} 2j \\ j+m \end{pmatrix}^{1/2} \frac{1}{(1+|\zeta|^2)}^{j} \zeta^{j+m} |j,m\rangle_N \,. \tag{1.2.30}$$

In a $j = \frac{N}{2}$ eigenspace, a spin coherent state can be described as a state in which each of the N spins is in the same pure state [34, 35]. It is a separable state and with a given complex parameter ζ defined by Equation (1.2.29), the spin coherent state in such state space is written as

$$\left|\frac{N}{2},\zeta\right\rangle_N = \bigotimes_{i=1}^{N} \left(\frac{1}{\sqrt{1+|\zeta|^2}} \left|\downarrow^{(i)}\right\rangle + \frac{\zeta}{\sqrt{1+|\zeta|^2}} \left|\uparrow^{(i)}\right\rangle \right). \tag{1.2.31}$$

In terms of Dicke states, the equivalent representation of this spin coherent state is given as

$$|N,\zeta\rangle_N = \sum_{n=0}^{N} C_n \left|\frac{N}{2}, n-\frac{N}{2}\right\rangle_N \tag{1.2.32}$$

where

$$C_n = \frac{1}{(1+|\zeta|^2)^{N/2}} \sqrt{\frac{N!}{(N-n)!n!}}\zeta^n. \tag{1.2.33}$$

For this case, the Dicke state has a binomial distribution that is given by

$$\begin{pmatrix} 2j \\ m+j \end{pmatrix} P^{j+m}(1-P)^{j-m} \tag{1.2.34}$$

where $P = \sin^2\frac{\theta}{2}$, $j = \frac{N}{2}$and shown in Figure 1.2.2 for three values of P.

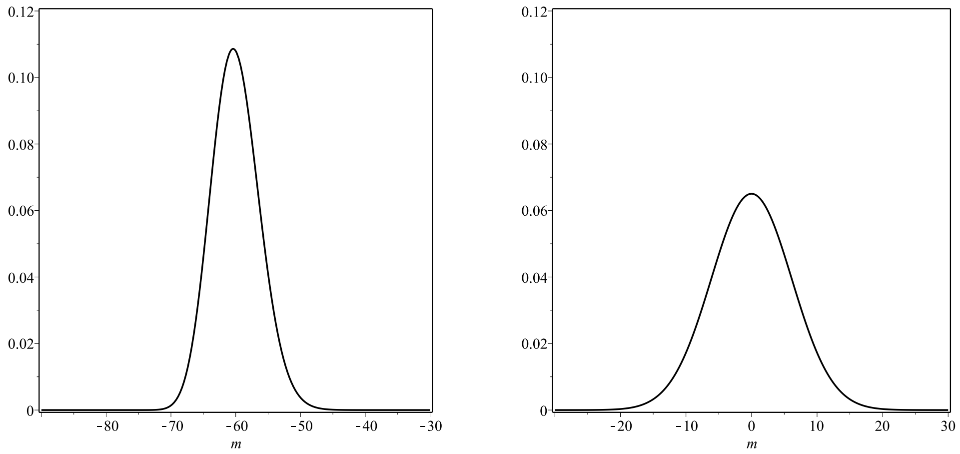

(a) $P = 0.1$ (b) $P = 0.5$

Figure 1.2.2: Distributions of Dicke states $\left|\frac{N}{2}, m\right\rangle_N$ for the spin coherent state $\left|\frac{N}{2}, (\theta, \phi)\right\rangle_N$ for two different values of P and with $N = 150$.

1.3 Mixed states and Density Matrix

Quantum systems with a well defined state are said to be in a pure state, where we know exactly about which state the system is in. However, there are quantum systems with states that can not be written as a single pure state vector, called the mixed state. Given a set of pure states $|\psi_i\rangle$ with probability P_i, we can write mixed states as a probabilistic sum P_i of several pure states $|\psi_i\rangle$ such that

$$\hat{\rho} = \sum_i P_i |\psi_i\rangle \langle\psi_i| . \tag{1.3.1}$$

This is called the density matrix or also known as a density operator and has the following properties

$$\hat{\rho} = \hat{\rho}^\dagger \tag{1.3.2}$$
$$\mathrm{Tr}(\hat{\rho}) = 1 \tag{1.3.3}$$
$$\left\langle \hat{O} \right\rangle = \mathrm{Tr}\left(\hat{\rho}\hat{O}\right). \tag{1.3.4}$$

Given a square m-by-m matrix with elements $a_{ij} \langle i|\hat{\rho}|j\rangle$ where $i = 1, 2..m$ and $j = 1, 2..m$, the trace of this matrix is defined as the sum of its eigenvalues, or the diagonal entries which is given by

$$\mathrm{Tr}(\hat{\rho}) = \sum_i \langle i|\hat{\rho}|i\rangle = \sum_{i=1}^{m} a_{ii}. \tag{1.3.5}$$

A pure state is a special case of a mixed state when $P_i = 1$ with only one state $|\psi_i\rangle$ in Equation (1.3.1). A pure state also always satisfies $\hat{\rho} = \hat{\rho}^2$ and always takes a trace value of $\mathrm{Tr}(\hat{\rho}^2) = 1$, whereas a mixed state takes $\mathrm{Tr}(\hat{\rho}^2) < 1$. While pure states are written as vectors, the mixed states are usually written as operators. The basis of eigenvectors is given by the smallest number of pure states that make up the mixed state and given by

$$\hat{\rho} = \sum_i^{D} \lambda_i |\epsilon_i\rangle \langle\epsilon_i| \tag{1.3.6}$$

where D is the Hilbert space, λ_i and $|\epsilon_i\rangle$ are respectively the are the eigenvalues and eigenvectors of the system.

There are many ways of writing a mixed state. For example, by simply changing the basis of the pure state $|\psi_i\rangle$ that forms the mixed state, we can have a state

$$\hat{M}_s = \frac{1}{2}(|e\rangle\langle e| + |g\rangle\langle g|) \tag{1.3.7}$$

written in the form of

$$\hat{M}_s = \frac{1}{2}(|+\rangle\langle +| + |-\rangle\langle -|) \tag{1.3.8}$$

where $|\pm\rangle = \frac{1}{\sqrt{2}}(|e\rangle\langle e| \pm |g\rangle\langle g|)$. In additional to these, a mixed state can also be represented in the basis of eigenvectors of pure states.

Density matrix and trace operations are very useful tools to deal with multi-particle systems. For example, a pure state for two systems A and B is given by $|\Psi_{AB}\rangle$ and the corresponding density matrix is then defined by

$$\hat{\rho}_{AB} = |\Psi_{AB}\rangle\langle\Psi_{AB}| \tag{1.3.9}$$

To analyse the information of system A only, we need to separate both systems by performing a trace operation over system B on this density matrix $\hat{\rho}_{AB}$. We will be left with a reduced density matrix of system A in the form of

$$\hat{\rho}_A = \mathrm{Tr}_B(\hat{\rho}_{AB}) \tag{1.3.10}$$

where Tr_B is the partial trace over system B.

1.4 Entanglement and measurements

The concept of entanglement was first introduced by Schrödinger [36, 37] and since it has become the essential foundation in quantum information processing [38, 39]. It is a very unique quantum property that explains the correlations of two or more quantum systems which has no classical counterpart.

A system is said to be entangled if it can not be decomposed and expressed as a product of states for each system component. For example let us consider a two-qubit state

$$\left|\Phi^+\right\rangle = (|ee\rangle + |gg\rangle)/\sqrt{2}. \tag{1.4.1}$$

For comparison, we also consider a system with two normalised qubits $|\psi\rangle = \alpha\,|e\rangle + \beta\,|g\rangle$ and $|\phi\rangle = \delta\,|e\rangle + \epsilon\,|g\rangle$. The state of this composite system of the two qubits can be written as

$$|\psi\rangle \otimes |\phi\rangle = (\alpha\,|e\rangle + \beta\,|g\rangle) \otimes (\delta\,|e\rangle + \epsilon\,|g\rangle \tag{1.4.2}$$

$$= \alpha\delta\,|ee\rangle + \alpha\epsilon\,|eg\rangle + \beta\delta\,|e\rangle + \beta\epsilon\,|e\rangle\,. \tag{1.4.3}$$

In order to to reduce this composite system into state $\left|\Phi^+\right\rangle$ we need $\alpha\epsilon = \beta\delta = 0$. However none of these α, β, δ or ϵ can take a value of zero to make state $\left|\Phi^+\right\rangle$. Therefore, we can conclude that this state is not separable and is said to be entangled. In fact, the two-qubit state $\left|\Phi^+\right\rangle$ is an example of a state with maximum entanglement. It is one of the following maximally entangled Bell states [40]

$$\left|\Phi^\pm\right\rangle = \frac{|ee\rangle \pm |gg\rangle}{\sqrt{2}}, \tag{1.4.4}$$

$$\left|\Psi^\pm\right\rangle = \frac{|eg\rangle \pm |ge\rangle}{\sqrt{2}}. \tag{1.4.5}$$

The density operator for state $|\Phi^+\rangle$ can be calculated by Equation (1.3.6) which gives us

$$\hat{\rho}_{AB} = \left(\frac{|ee\rangle + |gg\rangle}{\sqrt{2}}\right)\left(\frac{\langle ee| + \langle gg|}{\sqrt{2}}\right) \tag{1.4.6}$$

$$= \frac{|ee\rangle\langle ee| + |ee\rangle\langle gg| + |gg\rangle\langle ee| + |gg\rangle\langle gg|}{2} \tag{1.4.7}$$

$$= \frac{1}{2}\begin{pmatrix} 1 & 0 & 0 & 1 \\ 0 & 0 & 0 & 0 \\ 0 & 0 & 0 & 0 \\ 1 & 0 & 0 & 1 \end{pmatrix} \tag{1.4.8}$$

As given by Equation (1.3.10), to find the reduced matrix of qubit A, we trace out the qubit B such that

$$\hat{\rho}_A = \mathrm{Tr}_B\left(\hat{\rho}_{AB}\right) \tag{1.4.9}$$

$$= \mathrm{Tr}_B\left(\frac{|ee\rangle\langle ee| + |ee\rangle\langle gg| + |gg\rangle\langle ee| + |gg\rangle\langle gg|}{2}\right) \tag{1.4.10}$$

$$= \frac{|e\rangle\langle e| + |g\rangle\langle g|}{2} \tag{1.4.11}$$

$$= \frac{1}{2}\begin{pmatrix} 1 & 0 \\ 0 & 1 \end{pmatrix} \tag{1.4.12}$$

which gives us a mixed state as $\mathrm{Tr}\left(\hat{\rho}_A^2\right) = \frac{1}{2}$ and since $\hat{\rho}_{AB}$ is symmetric, it implies that $\hat{\rho}_A = \hat{\rho}_B$. Therefore, from this we can conclude that a partial trace of a maximally entangled state $\hat{\rho}_{AB}$ gives us a reduced density matrix $\hat{\rho}_A$ that is a maximally mixed state. It is also important to note that applying local unitary transformations like operators $\hat{U}$, $\hat{V}$ of $\hat{U} \otimes \hat{U}$ on a maximally entangled state would not change the amount of entanglement in the state [41].

A state that has no entanglement is called a separable state. It is the opposite of entangled state, where the two qubits can easily be separated and written as a product $|\psi\rangle \otimes |\phi\rangle$. There are also states that are neither maximally entangled nor separable, for example the state $\sqrt{\frac{19}{20}}\,|ee\rangle + \sqrt{\frac{1}{20}}\,|ee\rangle$ that will be used as an example later in Chapter 4, 5,6 and 7 of this thesis.

1.4.1 Entropy of Entanglement

For certain systems like a two entangled pure state, the amount of entanglement in a state can easily be quantified. However, quantifying entanglement is in mixed states is very hard as a single mixed state can be written in many different bases as shown the previous Section 1.3. While the amount of entanglement in the state is high in one basis, it could be the other way around if it is written in another basis. A mixed state is entangled if the following inequality holds, [42, 43]

$$\hat{\rho} \neq \sum_i P_i \left|\psi_i\right\rangle \left\langle\psi_i\right| \otimes \left|\phi_i\right\rangle \left\langle\phi_i\right| . \tag{1.4.13}$$

This means that if a mixed state can be written in a basis of product states then there is no entanglement present between the systems and the mixed state is called separable.

There are many different measures available to quantify mixed state entanglement between two qubits q_1 and q_2. Different methods would suggest different conclusions on the dimension of the entanglement. While one suggests that qubit q_1 is more entangled than qubit q_2, the other would suggest otherwise. However, all measures do agree on the degree of the entanglement, which to decide if both qubits $|\psi\rangle$ and $|\phi\rangle$ are separable or they are maximally entangled. In this section we will consider two measures of entanglement that are of significance to this thesis, which are entropy of entanglement and concurrence.

Entropy is a quantity used to measure purity of a quantum state and disturbance of a system. The are various types of entropy like von Neumann entropy [44, 45] and linear entropy [46]. Both measures range from zero which indicates the state being measured is pure, to one that tells us that the state is maximally mixed. However, linear entropy has an advantage over von Neumann entropy in terms of the amount of calculations involved. The linear entropy needs only the square of ρ, whereas the von Neumann requires diagonalisation of ρ to find its eigenvectors and eigenvalues at every point in time if a dynamical evolution is being considered. Therefore, throughout this thesis we will use linear entropy for it simplicity. It is denoted as S^L and given by the following formula

$$S^L = \frac{D}{D-1}\left(1 - \mathrm{Tr}(\hat{\rho}^2)\right) \tag{1.4.14}$$

where D is the dimension of Hilbert space.

It was shown earlier in this section that if we trace a single qubit out of a maximally entangled two-qubit system, the remaining reduced state is maximally mixed with $\mathrm{Tr}(\hat{\rho}_A^2) = 1/2$. In another study, Araki and Lieb have proven [47] that if an entangled system starts as a pure state, then the individual entropy of each component is the same throughout the interaction.

These facts are very important and very useful in many quantum systems as these allow us to use the entropy as a measure of entanglement. This method is known as the entropy of entanglement [48, 49]. As an example, we consider a quantum system in which two qubits q_1 and q_2 interact with a field mode f. We assume the whole system $\hat{\rho}_{q_1,q_2,f}$ is in a pure state and a partial trace on the field gives us

$$\hat{\rho}_{q_1,q_2} = \mathrm{Tr}_f(\hat{\rho}_{q_1,q_2,f}). \tag{1.4.15}$$

With this, we can calculate the entropy of the reduced density matrix $\hat{\rho}_{q_1,q_2}$ by using Equation (1.3.10). In a two-qubit Hilbert space, the linear entropy is calculated as

$$S^L = \frac{4}{3}(1 - \mathrm{Tr}(\hat{\rho}^2)). \tag{1.4.16}$$

We can then decide if the state being measured is pure or not. Based on the the calculated entropy too, we can observe if there is entanglement present between the two-qubit and the field subsystems. Zero value of this quantity means the state is pure and there is no entanglement between the two parts. On the other hand, a non-zero value tells us that the reduced density matrix is in a mixed state and there is entanglement present between the two subsystems. The value also indicates that there is maximum entanglement if the calculated entropy is unity. However, this method does not provide us the information about the entanglement between the two qubits, which requires another measurement called tangle (concurrence squared) that will be discussed shortly.

1.4.2 Concurrence and tangle

Previously, we have seen an example where linear entropy is used to calculate the purity of a quantum system, in which two qubits interact with a field mode. We can calculate the entropy of the whole interacting system or only the individual entropy of each subsystem. For a system that starts in a pure state, the individual entropy is much of interest, and it is used to measure the entanglement between the two-qubit and the field components. However, this quantity cannot be used to measure the degree of entanglement between the two qubits. A different quantity has to be used because the two-qubit state is sometimes a mixed state.

For this purpose, we will use a quantity called the mixed state tangle $\tau(\hat{\rho})$. This measurement is extracted from the entanglement of formation $E_F(\hat{\rho})$ that was introduced by Bennett *et al.* [50] as a measure of entanglement for two quantum systems of any size.

$$E_F(\hat{\rho}) = h\left[\frac{1+\sqrt{1-\tau(\hat{\rho})}}{2}\right] \tag{1.4.17}$$

where

$$h(x) = -x\log_2 x - (1-x)\log_2(1-x) \tag{1.4.18}$$

and $\tau(\hat{\rho})$ is the tangle of the state $\hat{\rho}$. It is hard to compute this entanglement of formation $E_F(\hat{\rho})$ for a general state, even by numerical computations. However, this quantity ranges from zero and monotonically increases in a similar magnitude as the value of tangle τ. The minimum and maximum of $\tau(\hat{\rho})$ respectively correspond to the minimum and maximum of $E_F(\hat{\rho})$ [49]. Therefore, it is sufficient for us to only use tangle (concurrence squared) as a measure of entanglement [51, 52]. For the purpose of this thesis where we consider the case of two-qubit systems, the quantity is defined as

$$\tau = \varsigma^2 = \left[\max\left(\sqrt{\chi_1} - \sqrt{\chi_2} - \sqrt{\chi_3} - \sqrt{\chi_4}, 0\right)\right]^2. \tag{1.4.19}$$

The χ's are the eigenvalues of matrix $\hat{\rho}_q(\sigma^y \otimes \sigma^y)\rho_q^*(\sigma^y \otimes \sigma^y)$ in decreasing order, where

$$\sigma^y \otimes \sigma^y = \begin{bmatrix} 0 & 0 & 0 & -1 \\ 0 & 0 & 1 & 0 \\ 0 & 1 & 0 & 0 \\ -1 & 0 & 0 & 0 \end{bmatrix}, \tag{1.4.20}$$

$\sigma^y = i(\sigma^- - \sigma^+)$ and $\hat{\rho}_q^*$ is the complex conjugate of the qubit density matrix $\hat{\rho}_q$ in the computational basis $|00\rangle$, $|01\rangle$, $|10\rangle$ and $|11\rangle$ [53, 51]. Similar to entropy, tangle takes a value from zero to unity to represent the strength of the entanglement where the first indicates no entanglement (separable) and the latter is for the maximum entanglement between two pure states. In this thesis, we will be using this quantity and its square root, concurrence $\varsigma(\hat{\rho}) = \sqrt{\tau(\hat{\rho})}$ to measure the entanglement between two qubits in Chapter 4, 5, 6 and 7.

1.4.3 Maximum Two-Qubit Entanglement and Entropy

A two-qubit pure state can have a tangle (and concurrence) value between zero and unity. A zero tangle value indicates a separable state with no entanglement, and unity is for the maximum entanglement between the two components. In between these minimum and maximum, there is a mixed state that has the maximum amount of tangle lower than unity in the two-qubit density matrix [54].

Studies by Munro *et al.* have discovered the amount of entanglement available to a state for a given value of the entropy [55, 49]. In their studies, they performed two measurements on the states of many randomly generated two-qubit density matrices. They calculated the linear entropy S^L and the tangle τ of the states and found the level of mixture in the two-qubit state with no trace operation performed. Therefore, the term entropy used here is not a similar quantity with the case where we find the entropy of entanglement with a part of the system is traced out and the density matrix represents a pure state, as discussed earlier in this section.

They also studied the relation between the two quantities, (the linear entropy and the tangle) by using a mixture of the maximally-entangled state and the maximally-mixed state, called a Werner state [56] that is given by

$$\hat{\rho}_w = \frac{1-\gamma}{4} I_2 \otimes I_2 + \gamma \left|\Phi_+\right\rangle \left\langle\Phi_+\right| \tag{1.4.21}$$

where I_2 is the 2-by-2 identity matrix and $|\Phi_+\rangle = \frac{1}{\sqrt{2}}(|00\rangle + |11\rangle)$ is a Bell state. This Werner state is an entangled state for $\gamma \geq 1/3$ and is a maximally entangled states when $\gamma = 1$ [57]. This relation is shown in Figure 1.4.1 for a range of γ value.

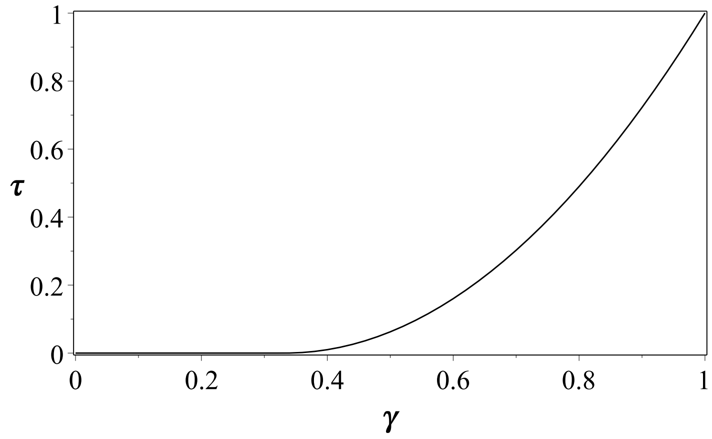

Figure 1.4.1: Plot of tangle for a different degree of entanglement parameterised by a positive integer γ in a Werner state $\hat{\rho}_w$.

For a specific value of S^L there is a state with the maximum value of entnaglement called the maximally entangled mixed state (MEMS) [58]. This state has the form of

$$\hat{\rho}_{MEMS} = \begin{pmatrix} g(\gamma)/2 & 0 & 0 & \gamma/2 \\ 0 & 1-2g(\gamma) & 0 & 0 \\ 0 & 1 & 0 & 0 \\ \gamma/2 & 0 & 0 & g(\gamma) \end{pmatrix}, \tag{1.4.22}$$

where

$$g(\gamma) = \begin{cases} \gamma/2, & \gamma \geq 2/3 \\ 1/3, & \gamma < 2/3. \end{cases} \tag{1.4.23}$$

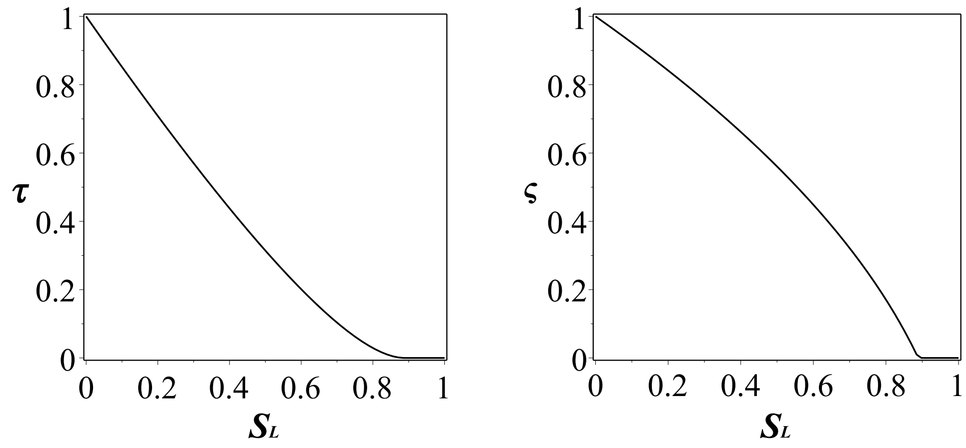

(a) Tangle vs linear entropy

(b) Concurrence vs linear entropy

Figure 1.4.2: Two measures of entanglement versus linear entropy for the Werner state $\hat{\rho}_w$.

The relation between the quantities can be seen in Figure 1.4.2 where the amount of entanglement for a given value of linear entropy is plotted. We plot in figure (a) the tangle versus the linear entropy and in figure (b) the concurrence versus the linear entropy for the Werner state (1.4.21).

1.5 Summary

We have now introduced all the tools required for the rest of the thesis. These tools are very important for calculations and understanding the physical behaviours of the systems. For example, the operators introduced in Section 1.1 are useful in formulating the Hamiltonian, the trace formula given by Equation (1.3.5) in Section 1.3 will be used to calculate the linear entropy, and the discussions on the entropy in Section 1.4 will guide us to understand the dynamics of entanglement between a qubit and a field state in a single qubit Jaynes-Cummings system that will be discussed further in the next Chapter 2.

Chapter 2

Single Qubit Interaction Models

2.1 Introduction

Interaction of a two-level system or a qubit with an external field is a very interesting topic in quantum physics. Depending on the properties of the field, either a quantised or a classical field is applied, and different picture of interactions can be observed. The differences are due to the ability of the quantum field to entangle with the qubit which therefore requires modelling the field as part of the whole quantum system, as opposed to the classical field that just interacts with the qubit as a source in the Hamiltonian [59].

One of the most well-known atom-classical field interaction models is the coupling of a two-level atom with a laser field that was first studied by I. Rabi in 1937 [15]. In this model, the field is classical and enters the qubit Hamiltonian as a source. It considers two-state atom coupled to an oscillatory driving electromagnetic field or in other words the atomic transition and the field's frequencies are similar or close enough to each other. This is a very good semi-classical interaction model involving only two atomic states that has many interesting phenomena like the continuous Rabi oscillations in atomic excitation probabilities [15, 23], which is very useful in modern optics.

This model was later further investigated by E. Jaynes and F. Cummings (thus named as Jaynes-Cumming model) in order to interpret its relationship to the quantum theory of radiation in describing the event of spontaneous emission [60]. Due to this unique phenomenon where the atomic population transitions in a quantised field can still occur even with the absence of photons, the model becomes a great reference in atomic physics, quantum optics and also theoretical and experimental quantum information. This model was later generalised by Tavis and Cumming for the case of multiple qubits [61].

Many interesting observations were discovered in a single qubit interacting model especially when a coherent state of the field is applied. In this chapter, we will discuss in detail this Jaynes-Cummings model and its various interesting characteristics. We will then extend our discussions to another interesting interacting model studied by S. Dooley on a system of a qubit coupled to a collection of N qubits or spin-1/2 particles called the "big spin" [29, 62, 63]. Detailed calculations and discussions on this single qubit and spin coherent state will be presented especially on its correspondence to the analogous Jaynes-Cummings model.

2.2 One-Qubit Jaynes-Cummings Model at Zero Detuning

The Jaynes-Cummings model considers a single two-level atom (also known as a qubit) interacting with a single-mode quantised electromagnetic field that made is up by a collection of energy or quanta (called photons), and represented by a harmonic oscillator. To study all the features in this interacting system, we will start off by finding its wavefunction, which will be calculated in detail in this section. Note that all these calculations are related to the works by C. Jarvis [64]. Here, we reproduce similar analytic calculations, and present the corresponding numerical results of the Jaynes-Cummings system. These calculations will provide the formalism and tools that we will use for the new calculations presented later in this thesis.

2.2.1 One-Qubit Jaynes-Cummings Hamiltonian

We consider a qubit with two energy levels or atomic states defined as $|e\rangle$ for excited state and $|g\rangle$ for its ground state. The atomic energy level is set to be zero halfway between these states, $E_e = -E_g = \frac{\hbar\Omega}{2}$ and the free atomic Hamiltonian may be calculated as

$$\hat{H}_A = \frac{1}{2}\left(E_e - E_g\right)\hat{\sigma}^z = \frac{1}{2}\hbar\Omega\hat{\sigma}^z. \tag{2.2.1}$$

where $\hat{\sigma}^z$ is a Pauli Z operator given by Equation (1.1.17). This qubit interacts with a quantised field that has the following form

$$\hat{\boldsymbol{E}} = \boldsymbol{\epsilon} \left(\frac{\hbar\omega}{\epsilon_0 V} \right)^{1/2} \left(\hat{a} + \hat{a}^\dagger \right) \sin(kz) \tag{2.2.2}$$

where $\boldsymbol{\epsilon}$ is a polarisation vector that is orthogonal to the z axis, ω is the coherent field's frequency, $\hat{a}^\dagger$ is the creation operator and $\hat{a}$ is the annihilation operator acting on the field given by Equation (1.1.22) and Equation (1.1.23) respectively [23].

The Hamiltonian that describes the atom-field interaction is given by

$$\begin{aligned} \hat{H}_I &= -\boldsymbol{d}.\boldsymbol{E} & (2.2.3) \\ &= \hat{d} g \left(\hat{a} + \hat{a}^\dagger \right) & (2.2.4) \end{aligned}$$

where

$$g = \left(\frac{\hbar\omega}{\epsilon_0 V} \right)^{1/2} \sin(kz) \tag{2.2.5}$$

and $\hat{d} = -\boldsymbol{d}.\boldsymbol{\epsilon}$, where $\boldsymbol{d}$ is an electric dipole moment that couples state $|e\rangle$ and $|g\rangle$ of a two-level atom. This can also be written in terms of atomic transition operators $\hat{\sigma}^+ = |e\rangle \langle g|$ and $\hat{\sigma}^- = |g\rangle \langle e|$ as

$$\boldsymbol{d} = \boldsymbol{d}_{ge}\hat{\sigma}^- + \boldsymbol{d}_{eg}\hat{\sigma}^+ + \boldsymbol{d}_{gg}\hat{\sigma}^-\hat{\sigma}^+ + \boldsymbol{d}_{ee}\hat{\sigma}^+\hat{\sigma}^-. \tag{2.2.6}$$

$\boldsymbol{d}_{ge} = \boldsymbol{d}_{ge}^*$ is the transition dipole moment which is also the non-zero off-diagonal elements $\langle g| \hat{d} |e\rangle = \langle e| \hat{d} |g\rangle = d$, while $\boldsymbol{d}_{gg}$ and $\boldsymbol{d}_{ee}$ are the permanent dipole moment which are in this case equal to zero, $\langle e| \hat{d} |e\rangle = \langle g| \hat{d} |g\rangle = 0$. Therefore, our dipole operator $\hat{d}$ is now

$$\begin{aligned} \hat{d} &= d\,|g\rangle \langle e| + d^* \,|e\rangle \langle g| & (2.2.7) \\ &= d\hat{\sigma}^- + d^*\hat{\sigma}^+ & (2.2.8) \\ &= d(\hat{\sigma}^+ + \hat{\sigma}^-) & (2.2.9) \end{aligned}$$

where d is real. Therefore our interaction Hamiltonian becomes

$$\hat{H}_I = \hbar\lambda \left(\hat{\sigma}^+ + \hat{\sigma}^- \right) \left(\hat{a} + \hat{a}^\dagger \right) \tag{2.2.10}$$

where $\lambda = dg/\hbar$ is the dipole-interaction strength between the two level system and the field.

The free-field Hamiltonian for the single mode of the cavity field with photon frequency ω is given by $\hat{H}_F = \hbar\omega \left(\hat{a}^\dagger\hat{a} + \frac{1}{2} \right)$ where the $\frac{1}{2}$ is coming from the

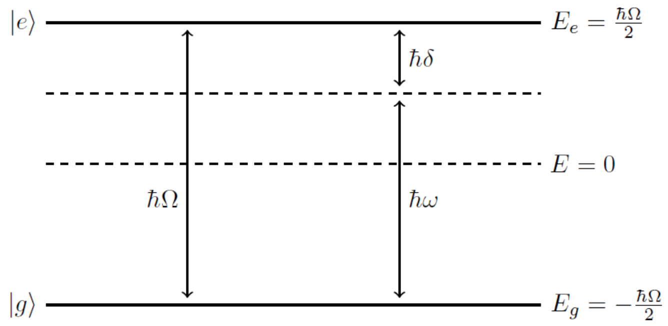

Figure 2.2.1: Energy levels for a qubit of frequency Ω, acting with a near resonant field of frequency ω. δ is the frequency difference between the cavity and the qubit and called qubit-cavity detuning.

zero-point (vacuum) energy and can be dropped from the total Hamiltonian. We can now write the total Hamiltonian of the system by a combination of these free-atomic, free-field and atom-field interaction Hamiltonian as

$$\begin{aligned} \hat{H}_{1,tot} &= \hat{H}_A + \hat{H}_F + \hat{H}_I && (2.2.11) \\ &= \frac{1}{2}\hbar\Omega\hat{\sigma}^z + \hbar\omega\hat{a}^\dagger\hat{a} + \hbar\lambda\left(\hat{\sigma}^+ + \hat{\sigma}^-\right)\left(\hat{a} + \hat{a}^\dagger\right) && (2.2.12) \\ &= \frac{1}{2}\hbar\Omega\hat{\sigma}^z + \hbar\omega\hat{a}^\dagger\hat{a} + \hbar\lambda\left(\hat{\sigma}^+\hat{a} + \hat{\sigma}^+\hat{a}^\dagger + \hat{\sigma}^-\hat{a} + \hat{\sigma}^-\hat{a}^\dagger\right) && (2.2.13) \end{aligned}$$

where the subscript “1,tot” is to highlight that this is the total Hamiltonian for a single qubit system and to differentiate this Hamiltonian with the two-qubit case that will be discussed in Chapter 4.

With the rotating wave approximation, all the rapid oscillating terms $\hat{\sigma}^+\hat{a}^\dagger$ and $\hat{\sigma}^-\hat{a}^\dagger$ are dropped [23, 65]. This is because in an interaction picture the bare frequency dependence is incorporated into the operators. It is in such an interaction picture that the terms can be thought of as rapidly oscillating. With these, we arrive to the approximation of the total Jaynes-Cummings Hamiltonian in the form of

$$\hat{H}_1 = \frac{1}{2}\hbar\Omega\hat{\sigma}^z + \hbar\omega\hat{a}^\dagger\hat{a} + \hbar\lambda\left(\hat{\sigma}^+\hat{a} + \hat{\sigma}^-\hat{a}^\dagger\right). \qquad (2.2.14)$$

The term $\hbar\lambda\left(\hat{\sigma}^+\hat{a} + \hat{\sigma}^-\hat{a}^\dagger\right)$ describes the interaction between the qubit and the field, where operators $\hat{\sigma}$ act only on the qubit state whereas the operators $\hat{a}$ and

$\hat{a}^\dagger$ act only on the field mode. If the qubit moves from an excited state $|e\rangle$ to the ground state $|g\rangle$, a photon is created and the number of photons in the field increases by one. Alternatively if the qubit moves from the ground state to the excited state, then a photon from the field is absorbed by the qubit (annihilated) and the number of photons in the cavity reduces by one.

The Hamiltonian H_1 given by Equation (2.2.14) commutes with an operator $\hat{M}_1$ that represents the total number of quanta and given as

$$\hat{M}_1 = \hat{a}^\dagger \hat{a} + \hat{\sigma}^+ \hat{\sigma}^-. \tag{2.2.15}$$

However, it does not commute with the full Hamiltonian $H_{1,tot}$ that is given by Equation (2.2.13) , although the expectation value of the excitation number is preserved by evolution under the full Hamiltonian. This is due to the dropped terms $\hat{\sigma}^+ \hat{a}^\dagger$ and $\hat{\sigma}^- \hat{a}^\dagger$ that do not commute with the operator $\hat{M}_1$. The commutation relation between this operator and Hamiltonian is

$$[\hat{H}_1, \hat{M}_1] = [\hat{H}_1, \hat{a}^\dagger \hat{a}] + [\hat{H}_1, \hat{\sigma}^+ \hat{\sigma}^-] \tag{2.2.16}$$

$$= \hbar\omega \Big[\hat{a}^\dagger \hat{a}, \hat{a}^\dagger \hat{a}\Big] + \frac{\hbar\Omega}{2}[\hat{\sigma}^z, \hat{a}^\dagger \hat{a}] + \hbar\lambda[\hat{a}\hat{\sigma}^+, \hat{a}^\dagger \hat{a}] + \hbar\lambda[\hat{a}^\dagger \hat{\sigma}^-, \hat{a}^\dagger \hat{a}]$$
$$+ \hbar\omega \Big[\hat{a}^\dagger \hat{a}, \hat{\sigma}^+ \hat{\sigma}^-\Big] + \frac{\hbar\Omega}{2}[\hat{\sigma}^z, \hat{\sigma}^+ \hat{\sigma}^-] + \hbar\lambda[\hat{a}\hat{\sigma}^+, \hat{\sigma}^+ \hat{\sigma}^-] + \hbar\lambda[\hat{a}^\dagger \hat{\sigma}^-, \hat{\sigma}^+ \hat{\sigma}^-]. \tag{2.2.17}$$

With the fact that an operator always commutes with itself, we can further simplify Equation (2.2.17) into

$$\Big[\hat{H}_1, \hat{M}_1\Big] = \hbar\lambda\Big(\hat{\sigma}^+ \Big[\hat{a}, \hat{a}^\dagger \hat{a}\Big] + \hat{\sigma}^- \Big[\hat{a}^\dagger, \hat{a}^\dagger \hat{a}\Big] + \hat{a}[\hat{\sigma}^+, \hat{\sigma}^+ \hat{\sigma}^-] + \hat{a}^\dagger[\hat{\sigma}^-, \hat{\sigma}^+ \hat{\sigma}^-]\Big) \tag{2.2.18}$$

and from commutation relation given by Equation (1.1.20), we expand Equation (2.2.18) into

$$\Big[\hat{H}_1, \hat{M}_1\Big] = \hbar\lambda\Big(\hat{\sigma}^+ \Big(\Big[\hat{a}, \hat{a}^\dagger\Big]\hat{a} + \hat{a}^\dagger[\hat{a}, \hat{a}]\Big) + \hat{\sigma}^- \Big(\Big[\hat{a}^\dagger, \hat{a}^\dagger\Big]\hat{a} + \hat{a}^\dagger[\hat{a}^\dagger, \hat{a}]\Big) - \hat{a}\hat{\sigma}^+ + \hat{a}^\dagger \hat{\sigma}^-\Big) \tag{2.2.19}$$

$$= \hbar\lambda\Big(\hat{a}\hat{\sigma}^+ - \hat{a}^\dagger \hat{\sigma}^- - \hat{a}\hat{\sigma}^+ + \hat{a}^\dagger \hat{\sigma}^-\Big). \tag{2.2.20}$$

Therefore, we have

$$\left[\hat{H}_1, \hat{a}^\dagger \hat{a} + \hat{\sigma}^+ \hat{\sigma}^-\right] = \left[\hat{H}, \hat{M}_1\right] = 0. \tag{2.2.21}$$

which means the quanta operator commutes with the Hamiltonian (2.2.14) and the number of excitations in the system is conserved under the rotating wave approximation.

2.2.2 Eigenvalues and Eigenvectors of Hamiltonian

To find the eigenvalues and eigenvectors of the Hamiltonian, we solve the eigenvalue equation

$$\hat{H}_1 \left|\psi\right\rangle = E \left|\psi\right\rangle . \tag{2.2.22}$$

where the general decomposition of an eigenstate solution to this equation is given by

$$\left|\Psi_1\right\rangle = \sum_{n=0}^{\infty} a_{e,n} \left|e, n\right\rangle + a_{g,n} \left|g, n\right\rangle . \tag{2.2.23}$$

At time $t = 0$, a wavefunction is assumed to be a general product state of the field and the qubit which is given by

$$\left|\Psi_1(0)\right\rangle = \left|\phi(0)\right\rangle \left|\psi_1(0)\right\rangle . \tag{2.2.24}$$

We will use this initial state at time $t = 0$ and from the eigenvalues we will decompose it into the eigenstates that will lead us to the general time dependence. With these, we can now solve Equation (2.2.22) by operating the Hamiltonian (2.2.14) on the general form for an eigenstate given by Equation (2.2.23). By changing the basis to be in terms of $\left|e, n\right\rangle$ and $\left|g, n+1\right\rangle$ and then rearranging the equation, we obtain

$$\begin{aligned}\hat{H}_1 \left|\Psi_1\right\rangle = \sum_{n=0}^{\infty} \Bigg[&\left(\hbar\omega n a_{e,n} + \frac{\hbar\Omega}{2} a_{e,n} + \hbar\lambda a_{g,n+1}\sqrt{n+1}\right) \left|e, n\right\rangle \\ &+ \left(\hbar\omega(n+1) a_{g,n+1} - \frac{\hbar\Omega}{2} a_{g,n+1} + \hbar\lambda a_{e,n}\sqrt{n+1}\right) \left|g, n+1\right\rangle \Bigg] \\ &- \hbar\frac{\Omega}{2} a_{g,0} \left|g, 0\right\rangle .\end{aligned} \tag{2.2.25}$$

With the conserved number of quanta, we can decompose the system into m_1 different decoupled sectors, where m_1 is the number of different values that the eigenvalue of $\hat{M}_1$ can take for this system. We can then write Equation (2.2.25) in a matrix form

$$\hat{H}_1 \left|\Psi_1\right\rangle = \sum_{n=0}^{\infty} \begin{pmatrix} \hbar\omega n + \frac{\hbar\Omega}{2} & \hbar\lambda\sqrt{n+1} \\ & \\ \hbar\lambda\sqrt{n+1} & \hbar\omega\left(n+1\right) - \frac{\hbar\Omega}{2} \end{pmatrix} \left|\Psi_1\right\rangle . \tag{2.2.26}$$

This matrix is for each of the m_1 sectors and these amplitudes will form doublets of states except for $\left|g, 0\right\rangle$ that is left on its own. It is then diagonalised to give us two eigenvalues

$$E_{\pm,n} = \hbar\omega n \pm \frac{\hbar}{2}\sqrt{\delta^2 + 4\lambda^2\left(n+1\right)} \tag{2.2.27}$$

and two corresponding eigenvectors

$$\left|\pm, n\right\rangle = \frac{\delta \pm \sqrt{\delta^2 + 4\lambda^2\left(n+1\right)}\left|e, n\right\rangle + 2\lambda\sqrt{n+1}\left|g, n+1\right\rangle}{\sqrt{2}\left(\delta^2 + 4\lambda^2\left(n+1\right) \pm \delta\sqrt{\delta^2 + 4\lambda^2\left(n+1\right)}\right)^{1/2}} \tag{2.2.28}$$

where $\delta = \Omega - \omega$ is the qubit-field detuning. These eigenvectors are often referred to as dressed states and can be written in a simpler form of $\sin\theta$ and $\cos\theta$ [23]

$$\left|+, n\right\rangle = \cos\theta_n\left|e, n\right\rangle + \sin\theta_n\left|g, n+1\right\rangle \tag{2.2.29}$$

$$\left|-, n\right\rangle = -\sin\theta_n\left|e, n\right\rangle + \cos\theta_n\left|g, n+1\right\rangle \tag{2.2.30}$$

where

$$\cos\theta_n = \frac{\delta \pm \sqrt{\delta^2 + 4\lambda^2\left(n+1\right)}}{\sqrt{2}\left(\delta^2 + 4\lambda^2\left(n+1\right) \pm \delta\sqrt{\delta^2 + 4\lambda^2\left(n+1\right)}\right)^{1/2}} \tag{2.2.31}$$

$$\sin\theta_n = \frac{2\lambda\sqrt{n+1}}{\sqrt{2}\left(\delta^2 + 4\lambda^2\left(n+1\right) \pm \delta\sqrt{\delta^2 + 4\lambda^2\left(n+1\right)}\right)^{1/2}} \tag{2.2.32}$$

2.2.3 Exact Solution

The Jaynes-Cummings model can be solved exactly by including the time dependence of the eigenstates and solving the time-dependent Schrödinger equation in the form of

$$|\Psi_1(t)\rangle = e^{-i\hat{H}_1 t/\hbar} |\Psi_1(0)\rangle \,. \tag{2.2.33}$$

To achieve that, we first transform the basis vectors $|e, n\rangle$ and $|g, n+1\rangle$ into the eigenvector terms in the form of $\sin\theta$ and $\cos\theta$

$$|e, n\rangle = \cos\theta_n |+, n\rangle - \sin\theta_n |-, n\rangle \tag{2.2.34}$$

$$|g, n+1\rangle = \sin\theta_n |+, n\rangle + \cos\theta_n |-, n\rangle \,. \tag{2.2.35}$$

Now the wavefunction at time $t = 0$ which is $|\Psi_1(0)\rangle$ and given by Equation (2.2.24) can be written in terms of the eigenvectors as

$$\begin{aligned}
|\Psi_1(0)\rangle &= |\phi(0)\rangle |\psi_1(0)\rangle && (2.2.36)\\
&= \sum_{n=0}^{\infty} C_n |n\rangle (C_e |e\rangle + C_g |g\rangle) && (2.2.37)\\
&= \sum_{n=0}^{\infty} [(C_e C_n \cos\theta_n + C_g C_{n+1} \sin\theta_n) |+, n\rangle \\
&\quad + (C_g C_{n+1} \cos\theta_n - C_e C_n \sin\theta_n) |-, n\rangle] + C_g C_0 |g, 0\rangle && (2.2.38)
\end{aligned}$$

where $\sum_{n=0}^{\infty} |C_n|^2 = 1$ and $|C_e|^2 + |C_g|^2 = 1$ for normalised initial states. This step relies on the decomposition of the initial state into a superposition of eigenstates across all the different m_1 sectors. Once this is done, the known time evolution of each eigenstate can be used to find the full state at a later time. This is a very useful approach because it doesn't need numerical integration of the time evolution, where errors can build up. Therefore, with this initial wavefunction we can calculate $|\Psi_1(t)\rangle$ by using the time-dependent Schrödinger Equation (2.2.33)

$$\begin{aligned}
|\Psi_1(t)\rangle &= e^{-i\hat{H}_1 t/\hbar} |\Psi_1(0)\rangle && (2.2.39)\\
&= C_g C_0 e^{i\delta t/2} |g, 0\rangle + \sum_{n=0}^{\infty} \Big[e^{-i\omega\left(n+\frac{1}{2}\right)t} \\
&\Big(e^{-it\sqrt{\delta^2+4\lambda^2(n+1)}/2} (C_e C_n \cos\theta_n + C_g C_{n+1} \sin\theta_n) |+, n\rangle && (2.2.40)\\
&+ e^{it\sqrt{\delta^2+4\lambda^2(n+1)}/2} (C_g C_{n+1} \cos\theta_n - C_e C_n \sin\theta_n) |-, n\rangle \Big) \Big].
\end{aligned}$$

We then rewrite the solution back into the basis $|e, n\rangle$ and $|g, n+1\rangle$ terms, replace the exponential into the *sine* and *cosine* terms where $e^{ix} = \cos x + i \sin x$, and obtain

$$
\begin{aligned}
|\Psi_1(t)\rangle = C_g C_0 e^{i\delta t/2} |g,0\rangle + \sum_{n=0}^{\infty} \Bigg[& e^{-i\omega\left(n+\frac{1}{2}\right)t} \\
& \Bigg(\left(C_e C_n \cos\left(t\sqrt{\delta^2 + 4\lambda^2 (n+1)}/2\right) + i \sin\left(t\sqrt{\delta^2 + 4\lambda^2 (n+1)}/2\right)\right. \\
& \left(C_e C_n \left(\sin^2\theta_n - \cos^2\theta_n\right) - 2 C_g C_{n+1} \cos\theta_n \sin\theta_n\right)) |e,n\rangle \\
& + (C_g C_{n+1} \cos\left(t\sqrt{\delta^2 + 4\lambda^2 (n+1)}/2\right) + i \sin\left(t\sqrt{\delta^2 + 4\lambda^2 (n+1)}/2\right) \\
& \left(C_g C_{n+1} \left(\cos^2\theta_n - \sin^2\theta_n\right) - 2 C_e C_n \cos\theta_n \sin\theta_n\right)) |g,n+1\rangle \Bigg) \Bigg].
\end{aligned} \tag{2.2.41}
$$

We consider the case of field and the qubit are on resonance, so that $\Omega = \omega$ and thus $\delta = 0$. These simplify the terms $\cos\theta_n = \sin\theta_n = \frac{1}{\sqrt{2}}$ as well as Equation (2.2.41) into

$$
\begin{aligned}
|\Psi_1(t)\rangle = \sum_{n=0}^{\infty} \Bigg[& e^{-i\omega\left(n+\frac{1}{2}\right)t} \Bigg(\left(C_e C_n \cos\left(\lambda t\sqrt{n+1}\right) + i \sin\left(\lambda t\sqrt{n+1}\right)\right) |e,n\rangle \\
& + \left(C_g C_{n+1} \cos\left(\lambda t\sqrt{n+1}\right) + i \sin\left(\lambda t\sqrt{n+1}\right)\right) |g,n+1\rangle \Bigg) \Bigg] \\
& + C_g C_0 |g,0\rangle .
\end{aligned} \tag{2.2.42}
$$

The solution given by Equation (2.2.42) is for the case of only operators are time dependent. In an interaction picture both operators and state vectors are time dependent. The time dependence of the operators is coming from the interaction part of the Hamiltonian, $\hat{H}_I = \hbar\lambda\left(\hat{\sigma}^+ + \hat{\sigma}^-\right)\left(\hat{a} + \hat{a}^\dagger\right)$, whereas the time dependence of the latter is given by $\hat{H}_0 = \hat{H}_F + \hat{H}_A = \hbar\omega\left(\frac{1}{2}\hat{\sigma}^z + \hat{a}^\dagger\hat{a}\right)$ and calculated as

$$
|\Psi_I(t)\rangle = e^{-i\hat{H}_0 t/\hbar} |\Psi(t)\rangle . \tag{2.2.43}
$$

Therefore, for state vectors $|e,n\rangle$ and $|g,n+1\rangle$, the time dependent terms are defined as

$$
e^{-i\hat{H}_0 t/\hbar} |e,n\rangle = e^{-i\omega\left(n+\frac{1}{2}\right)t} |e,n\rangle \tag{2.2.44}
$$
$$
e^{-i\hat{H}_0 t/\hbar} |g,n+1\rangle = e^{-i\omega\left(n+\frac{1}{2}\right)t} |g,n+1\rangle . \tag{2.2.45}
$$

With these, we can make the following transformations

$$e^{-i\frac{\omega}{2}t}\left|e\right\rangle \rightarrow \left|e\right\rangle \tag{2.2.46}$$

$$e^{i\frac{\omega}{2}t}\left|g\right\rangle \rightarrow \left|g\right\rangle \tag{2.2.47}$$

$$e^{-i\omega nt}\left|n\right\rangle \rightarrow \left|n\right\rangle \tag{2.2.48}$$

and Equation (2.2.42) becomes

$$\begin{aligned}\left|\Psi_1(t)\right\rangle = \sum_{n=0}^{\infty} \Big[&\left(C_e C_n \cos\left(\lambda t\sqrt{n+1}\right) + i \sin\left(\lambda t\sqrt{n+1}\right)\right)\left|e,n\right\rangle \\ &+ \left(C_g C_{n+1} \cos\left(\lambda t\sqrt{n+1}\right) + i \sin\left(\lambda t\sqrt{n+1}\right)\right)\left|g,n+1\right\rangle \Big] + C_g C_0 \left|g,0\right\rangle .\end{aligned} \tag{2.2.49}$$

2.2.4 Collapse and Revival at Zero Detuning

To further investigate the Jaynes Cumming model, we consider Equation (2.2.49) for the case of interaction between a qubit and coherent state $\left|\alpha\right\rangle$ given by Equation (1.2.3). Therefore the initial state of such system can be written as

$$\left|\Psi_1(0)\right\rangle = \left|\alpha\right\rangle \left(C_e\left|e\right\rangle + C_g\left|g\right\rangle\right) \tag{2.2.50}$$

$$= \sum_{n=0}^{\infty} C_n \left|n\right\rangle \left(C_e\left|e\right\rangle + C_g\left|g\right\rangle\right) \tag{2.2.51}$$

where

$$C_n = e^{-|\alpha|^2/2}\frac{\alpha^n}{\sqrt{n!}} \tag{2.2.52}$$

with $\bar{n} = |\alpha|^2$ is the average photon number in the coherent state and $\left|n\right\rangle$ are the number (energy) eigenstates of the field.

Many interesting observations can been made out of this interacting model. Figure 2.2.2 illustrates the time evolutions of the system for the case of field and the qubit are on resonance so that $\delta = 0$ and the qubit starts in a ground state $\left|g\right\rangle$. For numerical purposes, we use $n = 150$ for the sum over photon number and $|\alpha|^2 = 36$ for the average photon number in the field mode.

One of the most remarkable features of this model is the occurrence of a phenomenon called the 'collapse and revival' of Rabi oscillation in the qubit system

[23, 66, 67]. This is the event where the dynamics of qubit state probabilities appear to damp out before the oscillation totally disappear for a period of time. After some time this qubit oscillation revives at the same frequency, however not with a uniform amplitude. In contract to the system with a classical field, with an appropriate strength that is comparable to the coherent state $|\alpha\rangle$, we can observe that the Rabi oscillations appear with the same frequency as in this quantum Jaynes-Cummings model. However, these oscillations do not collapse and revive, but they just go on with a uniform amplitude permanently.

This event of 'collapse and revival' can be seen from the blue line in Figure 2.2.2, where there is collapse, total disappearance and succeeded by a revival in the qubit state probability. These collapse and revival occurrences are periodic and at longer times a sequence of collapse and revivals can be observed and these can be explained by the destructive and constructive interferences.

From Equations (2.2.50) and (2.2.51) the initial system is given by $|\Psi_1(0)\rangle = |\alpha\rangle\,|g\rangle$. The probability of the qubit remains in the state $|g\rangle$ or going to state $|e\rangle$ are given by

$$P_g(t) = \langle g|\hat{\rho}_q(t)|g\rangle = e^{-\bar{n}} \sum_{n=1}^{\infty} \frac{\bar{n}^n}{n!} \cos^2(\lambda t\sqrt{n}) \tag{2.2.53}$$

$$P_e(t) = \langle e|\hat{\rho}_q(t)|e\rangle = e^{-\bar{n}} \sum_{n=1}^{\infty} \frac{\bar{n}^n}{n!} \sin^2(\lambda t\sqrt{n}) \tag{2.2.54}$$

where $\hat{\rho}_q(t)$ is the reduced density matrix of the qubit system as defined by Equation (1.3.10) is the form of

$$\hat{\rho}_q(t) = \mathrm{Tr}_f(|\Psi_1(t)\rangle\,\langle\Psi_1(t)|). \tag{2.2.55}$$

By looking at the qubit probabilities Equations (2.2.53) and (2.2.54), it is clear that the probability of finding the qubit in a particular state at a certain time is the sum of oscillating terms, where each term oscillates with a specific frequency depending on the value of n. The collapse in the qubit state probabilities can easily be understood by considering the phase differences between these discrete frequency components. As two oscillating terms with different phases are added together, destructive interference occurs and if the terms are 180° out of phase, they cancel each other. As we allow the evolution to continue, at a later time the phase difference becomes smaller and this contributes to the rephasing of the oscillating terms. Constructive interference occurs and this results in a reverse event called the revival in the qubit probability dynamics. This event has a peak at the revival time t_r, where for a given positive integer j, the jth revival time can be calculated as

$$2\pi j = t_r(\omega_{n+1} - \omega_n) \tag{2.2.56}$$
$$= t_r(2\lambda\sqrt{\bar{n}+1} - 2\lambda\sqrt{\bar{n}}) \tag{2.2.57}$$
$$= t_r(2\lambda\sqrt{\bar{n}} + \frac{\lambda}{\sqrt{\bar{n}}} - 2\lambda\sqrt{\bar{n}}) \tag{2.2.58}$$
$$t_r = \frac{2\pi j\sqrt{\bar{n}}}{\lambda} \tag{2.2.59}$$

Since $\bar{n} = |\alpha|^2$, then for the case of $j = 1$ as shown in Figure 2.2.2, the revival time is then

$$t_r = \frac{2\pi\sqrt{\bar{n}}}{\lambda} = \frac{2\pi|\alpha|}{\lambda}. \tag{2.2.60}$$

2.2.5 One-Qubit Attractor States

Besides collapse and revival, another interesting feature that can be observed from the one-qubit Jaynes-Cummings model is a phenomenon called the 'attractor state' [22, 68]. C. Jarvis *et al.* [27] have demonstrated that for $\bar{n} \gg \lambda t$ the wavefunction $|\Psi_1(t)\rangle$ can be reduced into a simplified form of two distinct parts; the qubit state $\left|D_{\pm\frac{1}{2}}(t)\right\rangle$ and the field state $\left|\Phi_{\pm\frac{1}{2}}(t)\right\rangle$.

$$\left|\widetilde{\Psi}_1(t)\right\rangle = \beta_{+\frac{1}{2}}(t)\left|D_{+\frac{1}{2}}(t)\right\rangle\left|\Phi_{+\frac{1}{2}}(t)\right\rangle + \beta_{-\frac{1}{2}}(t)\left|D_{-\frac{1}{2}}(t)\right\rangle\left|\Phi_{-\frac{1}{2}}(t)\right\rangle \tag{2.2.61}$$

where

$$\beta_{\pm\frac{1}{2}}(t) = \frac{1}{\sqrt{2}}e^{\pm i\pi\frac{t}{t_r}(\bar{n}+1)}\left(e^{i\theta}C_e \mp C_g\right) \tag{2.2.62}$$
$$\left|D_{\pm\frac{1}{2}}(t)\right\rangle = \frac{1}{\sqrt{2}}\left(e^{-i\theta}|e\rangle \mp e^{\mp\pi\frac{t}{t_r}}|g\rangle\right) \tag{2.2.63}$$
$$\left|\Phi_{\pm\frac{1}{2}}(t)\right\rangle = e^{\pm\pi\frac{t}{t_r}}|\alpha\rangle\,. \tag{2.2.64}$$

In the original study on this model, Gea-Banacloche [22, 68] has shown that with $\bar{n} \gg 1$ approximation, at half way to the revival time, the qubit completely disentangles itself from the field and the initial qubit state evolves to a state known as an 'attractor state' [23] of the qubit. This is evident and can easily be seen by rewriting Equation (2.2.62) to Equation (2.2.64) in terms of $\frac{t_r}{2}$ that gives us the following:

$$\beta_{\pm\frac{1}{2}}(\frac{t_r}{2}) = \pm\frac{i}{\sqrt{2}}e^{\pm i\pi\bar{n}/2}\left(e^{i\theta}C_e \mp C_g\right) \tag{2.2.65}$$

$$\left|D_{\pm\frac{1}{2}}(\frac{t_r}{2})\right\rangle = \frac{1}{\sqrt{2}}\left(e^{-i\theta}\left|e\right\rangle + i\left|g\right\rangle\right) \tag{2.2.66}$$

$$\left|\Phi_{\pm\frac{1}{2}}(\frac{t_r}{2})\right\rangle = \left|\pm i\alpha\right\rangle . \tag{2.2.67}$$

Obviously at time $\frac{t_r}{2}$, the qubit states $\left|D_{+\frac{1}{2}}(\frac{t_r}{2})\right\rangle$ and $\left|D_{-\frac{1}{2}}(\frac{t_r}{2})\right\rangle$ are identical and this attractor state has the form of

$$\left|\psi^+_{1,att}\right\rangle = \frac{1}{\sqrt{2}}\left(e^{-i\theta}\left|e\right\rangle + i\left|g\right\rangle\right) . \tag{2.2.68}$$

The probability of the qubit being in this state $\left|\psi^+_{1,att}\right\rangle$ is calculated as

$$P^+_{1,att}(t) = \left\langle\psi^+_{1,att}|\hat{\rho}_q(t)|\psi^+_{1,att}\right\rangle \tag{2.2.69}$$

and the quantity is shown as an orange curve in Figure 2.2.2. It is clear that at time $\frac{t_r}{2}$ the probability goes very close to unity.

From Equation (2.2.66) it is noticeable that this attractor state is independent of the initial qubit state. There is no contribution of the initial coefficients C_e and C_g that have been used at the beginning of the interaction to this state. However, it depends on the phase of the initial coherent field state θ. Since at time $\frac{t_r}{2}$ the qubit state can be factorised out of the wavefunction, the qubit and the field are therefore a product state. Equation (2.2.61) then becomes

$$\left|\widetilde{\Psi}_1\left(\frac{t_r}{2}\right)\right\rangle = \frac{\left|\psi^+_{1,att}\right\rangle}{\sqrt{2}}\left(ie^{i\pi\bar{n}/2}(e^{i\theta}C_e - C_g)\left|i\alpha\right\rangle - ie^{-i\pi\bar{n}/2}(e^{i\theta}C_e + C_g)\left|-i\alpha\right\rangle\right) . \tag{2.2.70}$$

At this time too, all the information about the initial qubit state is swapped into the radiation field which happens to be in a Schrödinger cat state. It is a coherent superposition of two coherent states with opposite phase $|\alpha\rangle$ and $|-\alpha\rangle$ [69, 70] as seen in Equation (2.2.70) with coefficients that contain the information about the initial qubit state..

As the subsystems continue to interact, at the revival time t_r the field states $\left|\Phi_{\pm\frac{1}{2}}(t)\right\rangle$ evolve into an identical state where $\left|\Phi_{+\frac{1}{2}}(t_r)\right\rangle = \left|\Phi_{-\frac{1}{2}}(t_r)\right\rangle = |-\alpha\rangle$. The field is factorised out of the wavefunction and the system is once again a product state. Opposite to the system at $\frac{t_r}{2}$, all the information about the initial qubit state is transferred from the field back to the qubit.

Similar disentanglement is also observed at time $\frac{3t_r}{2}$, where the components are once again factorised. The qubit is again in a pure state in which it evolves to an attractor state, but this time it is orthogonal to the state $\left|\psi^{+}_{1,att}\right\rangle$ and can be written as $\left|\psi^{-}_{1,att}\right\rangle$. Therefore, at this time, as depicted in Figure 2.2.2 we can see the probability $P_{1,att}(t)$ approaches very close to zero. The interaction then continues with the field being in state $|\alpha\rangle$ at time $2t_r$ and the system repeatedly evolves from an entangled state to a product state and back again. Gea-Banacloche defined this phenomenon as a natural route to quantum state preparation [22] where at the attractor times all initial qubit states evolve to the same state with all initial qubit information been transferred and stored into the field.

2.2.6 Linear entropy

One way to quantify information about entanglement in a system is by using a quantity called 'entropy'. It is an evaluation of quantum state purity, disturbance or missing information due to incomplete measurement of the system [23] and accessible at any point of time of the system. A Jaynes-Cummings system always starts in a pure state and its evolution is always determined by the time-dependent Schrödinger dynamics. Therefore, provided that the initial state chosen is pure overall, this qubit-field interacting system will always be a pure state. With no decoherence, the entropy of the complete system stays constant at zero throughout the interactions. This means that no interesting dynamics of this quantity could be observed in this overall system.

However, we can observe many interesting events in the dynamics of the individual entropy, either the qubit or the field. Araki and Lieb [47] have discovered that for a system that starts with a pure state, the partial entropy of the subsystems are always equal. This means that, for our Jaynes-Cummings model, the partial entropy of the qubit is always equal to the partial entropy of the field throughout the evolution. This enables us to use only one of the quantities to observe the dynamics of the entropy, and therefore the entanglement in the system.

As discussed in Section 1.4.1, we know that we can use entropy to measure the

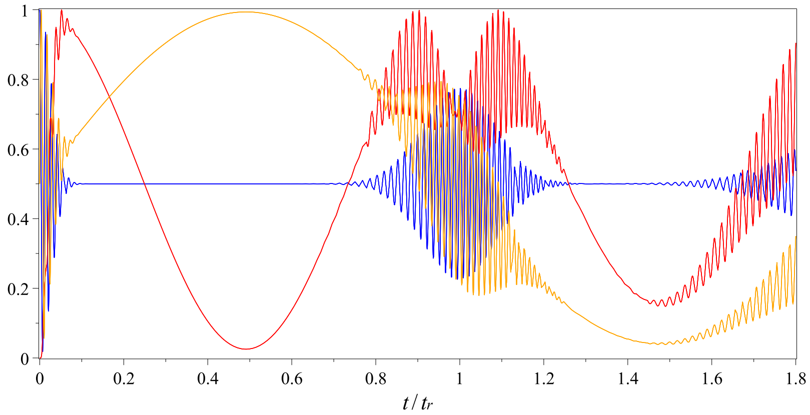

Figure 2.2.2: Time evolution for one-qubit Jaynes-Cummings model with the initial qubit state $|g\rangle$, $|\alpha|^2 = 36$ and the initial phase of the radiation field $\theta = 0$. The entropy of the qubit is shown as the red line, the probability of being in the state $|g\rangle$ is shown as the blue line and the probability of being in the attractor state $\left|\psi^{+}_{1,att}\right\rangle$ is shown as the orange line.

entanglement between two subsystems. Therefore, for the rest of the thesis only entropy of the qubit subsystem will be used, and we shall refer to the value of qubit's entropy only when entropy is mentioned. We will be using 'linear entropy' (impurity of a state) as a measure of entanglement between the qubit and the field for its simplicity over the Von Neuman entropy, where there is no diagonalisation needed on $\hat{\rho}$ in calculating the quantity. As given by Equation (1.4.16), the linear entropy is defined as

$$S^L_q(t) = 1 - \mathrm{Tr}(\hat{\rho}_q(t)^2). \tag{2.2.71}$$

where $\hat{\rho}_q(t)$ is the qubit's reduced density matrix given by Equation (2.2.71). This quantity ranges from zero to unity, where the former corresponds to a completely pure state and the latter corresponds to a completely (or maximally) mixed state. If the value of the entropy is non zero then the reduced density matrix is mixed, and it is a sign of some entanglement present between the qubit and the field.

The dynamics of qubit entropy in this system is illustrated as a red curve in Figure 2.2.2. From previous section, we know that at the attractor times $\frac{t_r}{2}$ and $\frac{3t_r}{2}$, the qubit is an attractor state, which is a pure state. The qubit disentangles itself from the field and there is no entanglement presents at these times. This explains the dips in the red line in the figure at these particular times, where we can see the entropy values $S^L_q(t)$ approach very close to zero.

At time t_r only a shallow dip in entropy can be seen. This suggests a mixed state or the presence of large entanglement between the qubit and the field. This is in contradiction to the analytic prediction made in the large $\bar{n}$ approximation where the qubit is expected to once again disentangle from the field, and be in a pure state which makes the entropy curve approaches very close to zero. The reason of such difference is the width of this dip is on a time that is much narrower than the entropy at $\frac{t_r}{2}$ [27, 64]. However, with a greater value of $\bar{n}$ in the numerical calculation, the value of the entropy at this time will get closer to zero.

2.3 One-Qubit Big Spin Interaction Model

From the previous section, we have seen many remarkable features revealed by a composite system of a single qubit interacting with a quantum field, named the Jaynes-Cummings model. Appearance of events like collapse and revival of the qubit oscillations, attractor states, Schrödinger cat states and the dynamics of entanglement between the qubit and the field have made this model a great reference in atomic physics, quantum optics and also theoretical and experimental quantum information.

Motivated by these findings, S. Dooley and collaborators have made further studies on the single qubit interacting system [29, 62, 63]. They investigated a system of a single qubit coupled to "big spin", which is a collection of N qubits or spin-1/2 particles. They demonstrated the correspondence of a spin coherent state with a coherent state for a field mode and further extended their analysis on a single qubit and big spin interacting system. From their research, they managed to demonstrate similarity of this model with the Jaynes-Cumming model, and also highlight the similar characteristics of the two models.

2.3.1 One-Qubit Big Spin Hamiltonian

In this model, we consider the interaction of a qubit with a big spin that is made of a collection of N qubits or spin-1/2 particles. In an $\frac{N}{2}$ eigenspace, which is the maximum angular momentum eigenspace of the N spins, a spin coherent state is a product of N spins that are all in the same pure state. The state is parametrised by a complex number $\zeta = \sqrt{\bar{n}}e^{-i\phi}$ and is written in the form of

$$|N, \zeta\rangle = \otimes_{i=1}^{N} \left(\frac{1}{\sqrt{1+|\zeta|^2}} \left|\downarrow^{(i)}\right\rangle + \frac{\zeta}{\sqrt{1+|\zeta|^2}} \left|\uparrow^{(i)}\right\rangle \right). \tag{2.3.1}$$

This state can also be represented in a Dicke state as

$$|N, \zeta\rangle \equiv |\zeta\rangle_N = \sum_{n=0}^{N} C_n \left| \frac{N}{2}, n - \frac{N}{2} \right\rangle \tag{2.3.2}$$

where

$$C_n = \frac{1}{(1+|\zeta|^2)^{N/2}} \sqrt{\frac{N!}{(N-n)!n!}} \zeta^n. \tag{2.3.3}$$

We can shift the label for Dicke state to avoid the redundant $\frac{N}{2}$ terms and a subscript N is placed to differentiate with the state of coherent field considered in previous sections.

$$\left| \frac{N}{2}, n - \frac{N}{2} \right\rangle \to |n\rangle_N . \tag{2.3.4}$$

The "n" used in this section is not to be confused with the one that has been used for the coherent state. In this model, it represents the number of excitations in the system, as opposed to the number of photons in the previous model. Similarly for the expectation value $\bar{n}$ where in this section it is for the spin coherent state such that $\bar{n} = |\zeta|^2$.

We consider a qubit and big spin interacting system with a scaled complex parameter ζ by a factor of $\frac{1}{\sqrt{N}}$, so that the initial spin coherent state is in the form of $\left| \frac{\zeta}{\sqrt{N}} \right\rangle_N$. This scaling is very important to maintain the correspondence of this system with the Jaynes-Cummings model when we consider $N \to \infty$ in which the spin coherent state is mapped to an oscillator coherent state of amplitude ζ [34, 35].

The spin coherent state may be written as

$$\left| \frac{\zeta}{\sqrt{N}} \right\rangle_N = \sum_{n=0}^{N} \frac{1}{\left(1 + \frac{|\zeta|^2}{N}\right)^{N/2}} \sqrt{\binom{N}{n}} \left(\frac{\zeta}{\sqrt{N}} \right)^n |n\rangle_N \tag{2.3.5}$$

$$= \sum_{n=0}^{N} \left[\binom{N}{n} (1-p)^{N-n} p^n \right]^{1/2} e^{-i\phi n} |n\rangle_N \tag{2.3.6}$$

where

$$p = \frac{|\zeta|^2/N}{1+|\zeta|^2/N}. \tag{2.3.7}$$

Then for $N \to \infty$ limit, we have $p \to 0$, $Np \to |\zeta|^2$ and

$$\lim_{N\to\infty} \left| \frac{\zeta}{\sqrt{N}} \right\rangle_N = \sum_{n=0}^{\infty} \left[e^{-|\zeta|^2} \frac{|\zeta|^{2n}}{n!} \right]^{1/2} e^{-i\phi n} |n\rangle \tag{2.3.8}$$

$$= e^{\frac{|\zeta|^2}{2}} \sum_{n=0}^{\infty} \frac{\zeta^n}{\sqrt{n!}} |n\rangle . \tag{2.3.9}$$

Clearly in this condition, our spin coherent state reduces to a coherent state of the field mode $|\zeta\rangle$.

In their study, S. Dooley *et al.* [29] have calculated and obtained the Hamiltonian for this interaction system. The modified Hamiltonian contains the bare Hamiltonians for the big spin $\hat{H}_B = \hbar\omega_N \left(\hat{J}^z + \frac{N}{2} \right)$ and the qubit $\hat{H}_A = \frac{\hbar\Omega}{2}\hat{\sigma}^z$, and then a coupling interaction $\hat{H}_I = \frac{\hbar\lambda}{\sqrt{N}} (\hat{J}^+\hat{\sigma}^- + \hat{J}^-\hat{\sigma}^+)$ with is the analogous term to the dipole coupling term in the Jaynes-Cummings system. Therefore, the Hamiltonian for this system is given by

$$\hat{H}_{1,N} = \hbar\omega_N \left(\hat{J}^z + \frac{N}{2} \right) + \frac{\hbar\Omega}{2}\hat{\sigma}^z + \frac{\hbar\lambda}{\sqrt{N}} (\hat{J}^+\hat{\sigma}^- + \hat{J}^-\hat{\sigma}^+) \tag{2.3.10}$$

where ω_N is the frequency of the big spin, $\hat{J}^z \equiv \sum_{i=1}^{N} \hat{\sigma}^z_{(i)}$ and $\hat{J}^\pm \equiv \sum_{i=1}^{N} \hat{\sigma}^\pm_{(i)}$ are operators that act on the big spin and $\hat{\sigma}^z_{(i)} = \left| e_{(i)} \right\rangle \left\langle e_{(i)} \right| - \left| g_{(i)} \right\rangle \left\langle g_{(i)} \right|$ acts on the individual spins that make up the big spin. The constant term $\frac{\omega_N N}{2}$ is introduced so that the ground state eigenvalue of the big spin Hamiltonian J^z is zero like the photon field with the vacuum energy neglected.

In a restriction of $\frac{N}{2}$ subspace, operators $\hat{J}^\pm$ can be written as

$$\frac{\hat{J}^+}{\sqrt{N}} = \sum_{n=0}^{N} \sqrt{(n+1)\left(1 - \frac{n}{N}\right)} \left| \frac{N}{2}, n+1-\frac{N}{2} \right\rangle \left\langle \frac{N}{2}, n-\frac{N}{2} \right| \tag{2.3.11}$$

$$\frac{\hat{J}^-}{\sqrt{N}} = \sum_{n=0}^{N} \sqrt{n\left(1 - \frac{n-1}{N}\right)} \left| \frac{N}{2}, n-1-\frac{N}{2} \right\rangle \left\langle \frac{N}{2}, n-\frac{N}{2} \right| \tag{2.3.12}$$

and operator $\hat{J}^z$ is

$$\hat{J}^z + \frac{N}{2} = \sum_{n=0}^{N} n \left| \frac{N}{2}, n-\frac{N}{2} \right\rangle \left\langle \frac{N}{2}, n-\frac{N}{2} \right| . \tag{2.3.13}$$

The similarities of the N-spin system with the field mode can be understood by considering a $N \to \infty$ limit. We can consider an embedding of this N-spin system in the Hilbert space of the coherent state by a linear mapping f where these operators can be transformed from a Dicke state $\left|\frac{N}{2}, n-\frac{N}{2}\right\rangle$ into the Fock state $|n\rangle$. In a $N \to \infty$ limit of $f\frac{\hat{J}^{+}}{\sqrt{N}}f^{\dagger}$ and $f\left(\hat{J}^{z}+\frac{N}{2}\right)f^{\dagger}$ operators (2.3.11-2.3.13) then become

$$\lim_{N\to\infty} f\frac{\hat{J}^{+}}{\sqrt{N}}f^{\dagger} = \sum_{n=0}^{\infty}\sqrt{(n+1)}\,|n+1\rangle\langle n| \tag{2.3.14}$$

$$\lim_{N\to\infty} f\frac{\hat{J}^{-}}{\sqrt{N}}f^{\dagger} = \sum_{n=0}^{\infty}\sqrt{(n-1)}\,|n+1\rangle\langle n| \tag{2.3.15}$$

$$\lim_{N\to\infty} f\left(\hat{J}^{z}+\frac{N}{2}\right)f^{\dagger} = \sum_{n=0}^{\infty} n\sqrt{n}\,|n+1\rangle\langle n|\,. \tag{2.3.16}$$

These are respectively the harmonic oscillator creation ($\hat{a}^{\dagger}$), annihilation ($\hat{a}$) and number ($\hat{a}^{\dagger}\hat{a}$) operators. It is clear that our qubit-big spin Hamiltonian (2.3.15) reduces to the Jaynes-Cummings Hamiltonian and our operators (2.3.11-2.3.13) transform into the harmonic oscillator operators.

In a bosonic limit, the corresponding big spin operators given by Equation (2.3.14) to Equation (2.3.16) obey the bosonic commutation relation $[\hat{a},\hat{a}^{\dagger}] = 1$ and $\left\langle[\hat{a},\hat{a}^{\dagger}]\right\rangle = 1$. However, when N is finite these conditions are not fulfilled by the operators because in this case we have

$$\left[\frac{\hat{J}_{-}}{\sqrt{N}},\frac{\hat{J}_{+}}{\sqrt{N}}\right] = 1-\frac{2}{N}\left(\hat{J}_{z}+\frac{N}{2}\right). \tag{2.3.17}$$

To satisfy the following conditions,

$$\left[\frac{\hat{J}^{-}}{\sqrt{N}},\frac{\hat{J}^{+}}{\sqrt{N}}\right] = 1 \tag{2.3.18}$$

and

$$\left\langle\left[\frac{\hat{J}^{-}}{\sqrt{N}},\frac{\hat{J}^{+}}{\sqrt{N}}\right]\right\rangle \approx 1; \tag{2.3.19}$$

we need to neglect the $\frac{2}{N}\left(\hat{J}_{z}+\frac{N}{2}\right)$ term. Since

$$\left\langle\zeta\left|\left(\hat{J}_{z}+\frac{N}{2}\right)\right|\zeta\right\rangle_{N} = \frac{|\zeta|^{2}/N}{1+|\zeta|^{2}/N} \tag{2.3.20}$$

a condition where $|\zeta|^2 \ll N$ is required so that the term is negligible and the correspondence between the qubit-big spin model and the Jaynes-Cummings model holds.

We introduce an operator $M_{1,N}$ that represents the total number of excitation in the system which is given as

$$M_{1,N} = \hat{J}^z + \hat{\sigma}^+\hat{\sigma}^-. \tag{2.3.21}$$

The subscript "1,N" is to differentiate the term with the one-qubit Jaynes Cumming model and later for the two qubits case that will be considered in Chapter 4 and the subsequent chapters. The commutation relation between this operator and Hamiltonian (2.3.15) is calculated as

$$\begin{aligned}
[\hat{H}_{1,N}, \hat{M}_{1,N}] &= [\hat{H}_{1,N}, \hat{J}^z] + [\hat{H}_{1,N}, \hat{\sigma}^+\hat{\sigma}^-] \qquad (2.3.22)\\
&= \hbar\omega\Big[\hat{J}^z + \frac{N}{2}, \hat{J}^z\Big] + \frac{\hbar\Omega}{2}[\hat{\sigma}^z, \hat{J}^z] + \frac{\hbar\lambda}{\sqrt{N}}[\hat{J}^-\hat{\sigma}^+, \hat{J}^z] + \frac{\hbar\lambda}{\sqrt{N}}[\hat{J}^+\hat{\sigma}^-, \hat{J}^z]\\
&\quad + \hbar\omega\Big[\hat{J}^z + \frac{N}{2}, \hat{\sigma}^+\hat{\sigma}^-\Big] + \frac{\hbar\Omega}{2}[\hat{\sigma}^z, \hat{\sigma}^+\hat{\sigma}^-] + \frac{\hbar\lambda}{\sqrt{N}}[\hat{J}^-\hat{\sigma}^+, \hat{\sigma}^+\hat{\sigma}^-]\\
&\qquad + \frac{\hbar\lambda}{\sqrt{N}}[\hat{J}^+\hat{\sigma}^-, \hat{\sigma}^+\hat{\sigma}^-]. \qquad (2.3.23)
\end{aligned}$$

Since an operator always commutes with itself, we can further simplify Equation (2.3.23) into

$$\Big[\hat{H}_{1,N}, \hat{M}_{1,N}\Big] = \frac{\hbar\lambda}{\sqrt{N}}\Big(\hat{\sigma}^+\Big[\hat{J}^-, \hat{J}^z\Big] + \hat{\sigma}^-\Big[\hat{J}^+, \hat{J}^z\Big] + \hat{J}^-[\hat{\sigma}^+, \hat{\sigma}^+\hat{\sigma}^-] + \hat{J}^+[\hat{\sigma}^-, \hat{\sigma}^+\hat{\sigma}^-]\Big) \tag{2.3.24}$$

and from commutation relation given by Equation (1.1.20), we expand Equation (2.3.24) then becomes

$$\begin{aligned}
\Big[\hat{H}_{1,N}, \hat{M}_{1,N}\Big] &= \frac{\hbar\lambda}{\sqrt{N}}\Big(\hat{\sigma}^+\Big(\Big[\hat{J}^-, \hat{J}^+\Big]\hat{J}^- + \hat{J}^+\Big[\hat{J}^-, \hat{J}^-\Big]\Big)\\
&\quad + \hat{\sigma}^-\Big(\Big[\hat{J}^+, \hat{J}^+\Big]\hat{J}^- + \hat{J}^+\Big[\hat{J}^+, \hat{J}^-\Big]\Big) - \hat{J}^-\hat{\sigma}^+ + \hat{J}^+\hat{\sigma}^-\Big) \qquad (2.3.25)\\
&= \frac{\hbar\lambda}{\sqrt{N}}\Big(\hat{J}^-\hat{\sigma}^+ - \hat{J}^+\hat{\sigma}^- - \hat{J}^-\hat{\sigma}^+ + \hat{J}^+\hat{\sigma}^-\Big). \qquad (2.3.26)
\end{aligned}$$

Therefore, we have

$$\left[\hat{H}_{1,N}, \hat{J}^z + \hat{\sigma}^+\hat{\sigma}^-\right] = \left[\hat{H}, \hat{M}_{1,N}\right] = 0. \tag{2.3.27}$$

which means the excitation number commutes with the Hamiltonian (2.2.14) and the number of excitations in the system is conserved.

2.3.2 Eigenvalues and Eigenvectors of Hamiltonian

Similar to the Jaynes-Cummings model discussed in the previous section, we can find the exact solutions to the dynamics of this one-qubit big spin model. We can achieve this by finding the eigenstates and eigenvalues of the Hamiltonian. We first solve the similar eigenvalue equation to that given by Equation (2.2.22)

$$\hat{H}_{1,N} |\psi\rangle_N = E |\psi\rangle_N \tag{2.3.28}$$

where the general decomposition of an eigenstate solution to this equation is given by

$$|\Psi_1\rangle_N = \sum_{n=0}^{N} a_{e,n} |e, n\rangle_N + a_{g,n} |g, n\rangle_N . \tag{2.3.29}$$

The initial state for the prepared wavefunction at time $t = 0$ has the form of

$$|\Psi_1(0)\rangle_N = |\phi(0)\rangle_N |\psi_1(0)\rangle . \tag{2.3.30}$$

It is assumed that this initial state is a general product state of the big spin and the qubit. We can then decompose it into the eigenstates that will lead us to the general time dependence (from the eigenvalues) for the initial state.

Now we can solve Equation (2.3.28) by operating the Hamitonian given by Equation (2.3.15) on the general form for an eigenstate Equation (2.3.29). We then obtain

$$\begin{aligned}\hat{H}_{1,N} |\Psi_1\rangle_N = \sum_{n=0}^{N} \Bigg[&\hbar\omega_N n\big(a_{e,n} |e, n\rangle_N + a_{g,n} |g, n\rangle_N \big) + \frac{\hbar\Omega}{2}\big(a_{e,n} |e, n\rangle_N \\ &- a_{g,n} |g, n\rangle_N \big) + \hbar\lambda\Big(a_{e,n}\sqrt{(n+1)\left(1 - \frac{n}{N}\right)} |g, n+1\rangle_N \\ &+ a_{g,n}\sqrt{n\left(1 - \frac{n-1}{N}\right)} |e, n-1\rangle_N \Big)\Bigg]\end{aligned} \tag{2.3.31}$$

Because of conservation of excitation number, we can decompose the system into $m_{1,N}$ different decoupled sectors, where $m_{1,N}$ is the number of different values that the eigenvalue of $M_{1,N}$ can take for this system. We change all the basis so that they are in the form of $|e,n\rangle_N$ and $|g,n+1\rangle_N$, and then we rearrange the equation so that

$$\begin{aligned}\hat{H}_{1,N}\,|\Psi_1\rangle_N = \sum_{n=0}^{N-1}\Bigg[&\left(\hbar\omega_N n a_{e,n} + \frac{\hbar\Omega}{2}a_{e,n} + \hbar\lambda a_{g,n+1}\sqrt{(n+1)\left(1-\frac{n}{N}\right)}\right)|e,n\rangle_N \\ &+\left(\hbar\omega_N(n+1)a_{g,n+1} - \frac{\hbar\Omega}{2}a_{g,n+1} + \hbar\lambda a_{e,n}\sqrt{(n+1)\left(1-\frac{n}{N}\right)}\right) \\ &|g,n+1\rangle_N\Bigg] + \hbar(\omega_N N + \frac{\Omega}{2})a_{e,N}\,|e,N\rangle_N\,\hbar\frac{\Omega}{2}a_{g,0}\,|g,0\rangle_N\end{aligned} \tag{2.3.32}$$

which may also be written in a matrix form of

$$\hat{H}_{1,N}\,|\Psi_1\rangle_N = \sum_{n=0}^{N}\begin{pmatrix}\hbar\omega_N n + \frac{\hbar\Omega}{2} & \hbar\lambda\sqrt{(n+1)\left(1-\frac{n}{N}\right)} \\ \hbar\lambda\sqrt{(n+1)\left(1-\frac{n}{N}\right)} & \hbar\omega_N(n+1) - \frac{\hbar\Omega}{2}\end{pmatrix}|\Psi_1\rangle_N\,. \tag{2.3.33}$$

This matrix is for each of the $m_{1,N}$ sectors and these amplitudes will form doublets of states except for the $|g,0\rangle$ and $|e,N\rangle$. The energies for these uncoupled states are respectively given by $E_{g,0} = -\hbar\frac{\Omega}{2}$ and $E_{e,N} = \hbar(\omega_N N + \frac{\Omega}{2})$. This matrix is then diagonalised and this gives us the following eigenvalues

$$E_{\pm,n} = \hbar\omega_N n \pm \frac{\hbar}{2}\mu_n(\delta) \tag{2.3.34}$$

where

$$\mu_n(\delta) = \sqrt{\delta^2 + 4\lambda^2\,(n+1)\left(1-\frac{n}{N}\right)} \tag{2.3.35}$$

and $\delta = \Omega - \omega_N$ is the detuning between the frequencies. The corresponding eigenvectors are then given by

$$|\pm,n\rangle_N = \frac{(\delta \pm \mu_n(\delta))\,|e,n\rangle_N + \mu_n(\delta)\,|g,n+1\rangle_N}{\sqrt{2}\big(\mu_n(\delta)^2 \pm \delta\mu_n(\delta)\big)^{1/2}} \tag{2.3.36}$$

and often referred to as dressed states. These eigenvectors can also be written in the form of

$$|+,n\rangle_N = \cos\phi_n\,|e,n\rangle_N + \sin\phi_n\,|g,n+1\rangle_N \tag{2.3.37}$$
$$|-,n\rangle_N = -\sin\phi_n\,|e,n\rangle_N + \cos\phi_n\,|g,n+1\rangle_N \tag{2.3.38}$$

where

$$\cos\phi_n = \frac{\mu_n(\delta)+\delta}{\sqrt{2}\sqrt{\mu_n(\delta)^2+\delta\mu_n(\delta)}} \tag{2.3.39}$$
$$= \frac{1}{\sqrt{2}}\left[\frac{\mu_n(\delta)+\delta}{\mu_n(\delta)}\right]^{1/2} \tag{2.3.40}$$

$$\sin\phi_n = \frac{\mu_n(\delta)-\delta}{\sqrt{2}\sqrt{\mu_n(\delta)^2-\delta\mu_n(\delta)}} \tag{2.3.41}$$
$$= \frac{1}{\sqrt{2}}\left[\frac{\mu_n(\delta)-\delta}{\mu_n(\delta)}\right]^{1/2} \tag{2.3.42}$$

2.3.3 Exact Solution

To observe the interacting system of one-qubit big spin, we need to solve the time-dependent Schrödinger equation similar to Equation (2.2.31).

$$|\Psi_1(t)\rangle = e^{-i\hat{H}_{1,N}t/\hbar}\,|\Psi_1(0)\rangle_N\,. \tag{2.3.43}$$

We first transform the basis vectors $|e,n\rangle_N$ and $|g,n+1\rangle_N$ into the trigonometric form of

$$|e,n\rangle_N = \cos\phi_n\,|+,n\rangle_N - \sin\phi_n\,|-,n\rangle_N \tag{2.3.44}$$
$$|g,n+1\rangle_N = \sin\phi_n\,|+,n\rangle_N + \cos\phi_n\,|-,n\rangle_N\,. \tag{2.3.45}$$

We may then rewrite the wavefunction at time $t=0$ as given by Equation (2.3.30) in terms of the eigenvectors as

$$
\begin{aligned}
|\Psi_1(0)\rangle_N &= |\phi(0)\rangle_N |\psi_1(0)\rangle_N = \sum_{n=0}^{N} C_n |n\rangle_N (C_e |e\rangle + C_g |g\rangle) && (2.3.46)\\
&= \sum_{n=0}^{N-1} \Big[C_e C_n \Big(\cos\phi_n |+, n\rangle_N - \sin\phi_n |-, n\rangle_N \Big) \\
&+ C_g C_{n+1} \big(\sin\phi_n |+, n\rangle_N + \cos\phi_n |-, n\rangle_N \big) \Big] && (2.3.47)\\
&+ C_e C_N |e, N\rangle_N + C_g C_0 |g, 0\rangle_N \\
&= \sum_{n=0}^{N-1} \Big[\Big(C_e C_n \cos\phi_n + C_g C_{n+1} \sin\phi_n \Big) |+, n\rangle_N \\
&+ \Big(C_g C_{n+1} \cos\phi_n - C_e C_n \sin\phi_n \Big) |-, n\rangle_N \Big] && (2.3.48)\\
&+ C_e C_N |e, N\rangle_N + C_g C_0 |g, 0\rangle_N
\end{aligned}
$$

with the normalised initial states, $\sum_{n=0}^{N-1} |C_n|^2 = 1$ and $|C_e|^2 + |C_g|^2 = 1$. This is based on the decomposition of the initial state into a superposition of eigenstates across all the different $m_{1,N}$ sectors. The known time evolution of each eigenstate can then be used to find the full state at a later time. By doing this, we do not need to apply numerical integration of the time evolution, which may cause errors. We can then calculate $|\Psi_1(t)\rangle_N$ as

$$
\begin{aligned}
|\Psi_1(t)\rangle_N &= e^{-i\hat{H}_{1,N} t/\hbar} |\Psi_1(0)\rangle_N && (2.3.49)\\
&= \sum_{n=0}^{N} \Big[e^{-i\omega_N \left(n+\frac{1}{2}\right)t} \Big(e^{-it\mu_n(\delta)/2} \left(C_e C_n \cos\phi_n + C_g C_{n+1} \sin\phi_n \right) |+, n\rangle_N \\
&+ e^{it\mu_n(\delta)/2} \left(C_g C_{n+1} \cos\phi_n - C_e C_n \sin\phi_n \right) \Big) |-, n\rangle_N \Big] \\
&+ C_e C_N e^{-it(\omega_N N + \frac{\Omega}{2})} |e, N\rangle_N + C_g C_0 e^{it\frac{\Omega}{2}} |g, 0\rangle_N \\
& && (2.3.50)
\end{aligned}
$$

We once again transform the basis so that they are in the bare basis terms of $|e, n\rangle_N$ and $|g, n+1\rangle_N$.

$$
\begin{aligned}
|\Psi_1(t)\rangle_N = \sum_{n=0}^{N-1} \Bigg[& e^{-i\omega_N\left(n+\frac{1}{2}\right)t} \Bigg(\Bigg(\cos\phi_n e^{-it\mu_n(\delta)/2} \left(C_e C_n \cos\phi_n + C_g C_{n+1}\sin\phi_n\right) \\
& - \sin\phi_n e^{it\mu_n(\delta)/2} \left(C_g C_{n+1}\cos\phi_n - C_e C_n \sin\phi_n\right) \Bigg) |e,n\rangle_N \\
& + \Bigg(\sin\phi_n e^{-it\mu_n(\delta)/2} \left(C_e C_n \cos\phi_n + C_g C_{n+1}\sin\phi_n\right) \\
& + \cos\phi_n e^{it\mu_n(\delta)/2} \left(C_g C_{n+1} C_e C_n \cos\phi_n \sin\phi_n\right) \Bigg) |g,n+1\rangle_N \Bigg) \Bigg] \\
& + C_e C_N e^{-it\left(\omega_N N + \frac{\Omega}{2}\right)} |e,N\rangle_N + C_g C_0 e^{it\frac{\Omega}{2}} |g,0\rangle_N
\end{aligned}
\tag{2.3.51}
$$

Finally, we further simplify this Equation (2.3.51) by rewriting the exponential terms as $e^{ix} = \cos x + i\sin x$ and obtain the following expression

$$
\begin{aligned}
|\Psi_1(t)\rangle = \sum_{n=0}^{N-1} \Bigg[& e^{-i\omega_N\left(n+\frac{1}{2}\right)t} \Bigg(\Bigg(C_e C_n \cos\left(\frac{t}{2}\mu_n(\delta)\right) + i\sin\left(\frac{t}{2}\mu_n(\delta)\right) \\
& \left(C_e C_n(\sin^2\phi_n - \cos^2\phi_n) - 2C_g C_{n+1}\cos\phi_n \sin\phi_n\right) \Bigg) |e,n\rangle_N \\
& + \Bigg(C_g C_{n+1} \cos\left(\frac{t}{2}\mu_n(\delta)\right) + i\sin\left(\frac{t}{2}\mu_n(\delta)\right) \\
& \left(C_g C_{n+1}(\cos^2\phi_n - \sin^2\phi_n) - 2C_e C_n \cos\phi_n \sin\phi_n \phi_n\right) \Bigg) |g,n+1\rangle_N \Bigg) \Bigg] \\
& + C_e C_N e^{-it\left(\omega_N N + \frac{\Omega}{2}\right)} |e,N\rangle_N + C_g C_0 e^{it\frac{\Omega}{2}} |g,0\rangle_N .
\end{aligned}
\tag{2.3.52}
$$

In this chapter, we will apply a similar condition as the case for the Jaynes-Cummings model in Section 2.2.4, where we let the qubit and the big spin to interact at the same frequency, so on resonance.. This means that there are no detunings in the system. The case where there is a non-zero detuning will be considered in the next chapter. As we let the frequency of the qubit Ω and frequency of the big spin ω_N to be at resonance, therefore $\delta = 0$ and we have

$$
\mu_n(0) = 2\lambda\sqrt{(n+1)\left(1 - \frac{n}{N}\right)}
\tag{2.3.53}
$$

and $\cos\phi_n = \sin\phi_n = \frac{1}{\sqrt{2}}$. The wavefunction $|\Psi_1(t)\rangle_N$ is then simplified into

$$
\begin{aligned}
&|\Psi_1(t)\rangle_N = \sum_{n=0}^{N-1} \Bigg[e^{-i\omega_N n t} \\
&\Bigg(\Bigg(C_e C_n \cos\left(\lambda t\sqrt{(n+1)(1-\frac{n}{N})}\right) - iC_g C_{n+1}\sin\left(\lambda t\sqrt{(n+1)(1-\frac{n}{N})}\right)\Bigg)|e,n\rangle_N \\
&+\Bigg(C_g C_{n+1}\cos\left(\lambda t\sqrt{(n+1)(1-\frac{n}{N})}\right) - iC_e C_n \sin\left(\lambda t\sqrt{(n+1)(1-\frac{n}{N})}\right)\Bigg)|g,n+1\rangle_N\Bigg)\Bigg] \\
&+ C_e C_N e^{-it(\omega_N N+\frac{\Omega}{2})}|e,N\rangle_N + C_g C_0 e^{-it(\omega_N-\frac{\Omega}{2})}|g,0\rangle_N
\end{aligned}
\tag{2.3.54}
$$

In the solution given by Equation (2.3.54) only operators that carry the time dependence terms which is coming from the interaction part of the Hamiltonian, $\hat{H}_I = \frac{\hbar\lambda}{\sqrt{N}}(\hat{J}^+\hat{\sigma}^- + \hat{J}^-\hat{\sigma}^+)$. We can include the time dependence of the states by defining the vectors in the interaction picture as

$$
|\Psi_I(t)\rangle_N = e^{-i\hat{H}_{0,N}t/\hbar}|\Psi(t)\rangle_N . \tag{2.3.55}
$$

$\hat{H}_{0,N}$ consists of the big spin and the qubit parts of the Hamiltonian, which is given by $\hat{H}_{0,N} = \hbar\omega_N\left(\hat{J}^z + \frac{N}{2}\right) + \frac{\hbar\Omega}{2}\hat{\sigma}^z$. Therefore, for state vectors $|e,n\rangle_N$ and $|g,n+1\rangle_N$, the time dependent terms are defined as

$$
e^{-i\hat{H}_{0,N}t/\hbar}|e,n\rangle_N = e^{-i\omega_N\left(n+\frac{1}{2}\right)t}|e,n\rangle_N \tag{2.3.56}
$$

$$
e^{-i\hat{H}_{0,N}t/\hbar}|g,n+1\rangle_N = e^{-i\omega_N\left(n+\frac{1}{2}\right)t}|g,n+1\rangle_N . \tag{2.3.57}
$$

With these, we can make the following transformations

$$
e^{-i\frac{\omega_N}{2}t}|e\rangle \to |e\rangle \tag{2.3.58}
$$

$$
e^{i\frac{\omega_N}{2}t}|g\rangle \to |g\rangle \tag{2.3.59}
$$

$$
e^{-i\omega_N n t}|n\rangle \to |n\rangle \tag{2.3.60}
$$

and obtain the solution of time-dependent Schrödinger equation with $\delta = 0$ that is now given by

$$
\begin{aligned}
|\Psi_1(t)\rangle_N = &\sum_{n=0}^{N-1} \\
&\Bigg[\Bigg(\left(C_eC_n\cos\left(\lambda t\sqrt{(n+1)(1-\frac{n}{N})}\right) - iC_gC_{n+1}\sin\left(\lambda t\sqrt{(n+1)(1-\frac{n}{N})}\right)\right)|e,n\rangle_N \\
&+\left(C_gC_{n+1}\cos\left(\lambda t\sqrt{(n+1)(1-\frac{n}{N})}\right) - iC_eC_n\sin\left(\lambda t\sqrt{(n+1)(1-\frac{n}{N})}\right)\right)|g,n+1\rangle_N\Bigg)\Bigg] \\
&+C_eC_N\,|e,N\rangle_N + C_gC_0\,|g,0\rangle_N\,.
\end{aligned}
\tag{2.3.61}
$$

2.3.4 Collapse and Revival at Zero Detuning

In Section 2.2.4, we have seen an event called the collapse and revival of qubit state probability in one-qubit Jaynes-Cummings model. It is an event in which the oscillations of the qubit state collapse for a period of time and then revive at the revival time t_r. In another study, S. Dooley *et al.* [29, 63] have also demonstrated similar occurrence in the one-qubit big spin system. With a scaled spin coherent state $\left|\frac{\zeta}{\sqrt{N}}\right\rangle_N$, they showed the correspondence of such events in both one-qubit big spin and the Jaynes-Cummings interacting systems.

Given that we start off with a single qubit interacting with a spin coherent state $\left|\frac{\zeta}{\sqrt{N}}\right\rangle_N$, the initial state for such an interacting system that was given by Equation(2.3.30) becomes

$$
|\Psi_1(0)\rangle_N = \sum_{n=0}^{N} C_n \left|\frac{\zeta}{\sqrt{N}}\right\rangle_N (C_e\,|e\rangle + C_g\,|g\rangle) \tag{2.3.62}
$$

where C_n is the coefficient for the big spin that has the form of

$$
C_n = \sum_{n=0}^{N} \frac{1}{\left(1+\frac{|\zeta|^2}{N}\right)^{N/2}} \sqrt{\frac{N!}{(N-n)!n!}} \left(\frac{\zeta}{\sqrt{N}}\right)^n, \tag{2.3.63}
$$

$\bar{n} = |\zeta|^2$ is the average excitation number in the spin coherent state and $|n\rangle$ are the energy eigenstates. We may then factor and write the solution as

$$
|\Psi_1(t)\rangle_N = |\psi_e(t)\rangle_N\,|e\rangle + |\psi_g(t)\rangle_N\,|g\rangle \tag{2.3.64}
$$

where $|\Psi_e(t)\rangle$ and $|\Psi_g(t)\rangle$ are the big spin components of $|\Psi_1(t)\rangle$ given by

$$|\psi_e(t)\rangle_N = \sum_{n=0}^{N} C_n \cos\left(\lambda t\sqrt{(n+1)(1-\frac{n}{N})}\right)|n\rangle \tag{2.3.65}$$

$$|\psi_g(t)\rangle_N = -i\sum_{n=0}^{N} C_n \sin\left(\lambda t\sqrt{(n+1)(1-\frac{n}{N})}\right)|n+1\rangle\,. \tag{2.3.66}$$

Therefore the probabilities of the qubit being in the excited or ground state are

$$P_e(t) = \langle e|\,\hat{\rho}_q(t)\,|e\rangle = \frac{N!}{(1+\frac{|\zeta|^2}{N})^N}\sum_{n=0}^{N}\frac{1}{(N-n)!n!}\left(\frac{\zeta^2}{N}\right)^n \sin^2\left(\lambda\sqrt{(n+1)(1-\frac{n}{N})}t\right) \tag{2.3.67}$$

$$P_g(t) = \langle g|\,\hat{\rho}_q(t)\,|g\rangle = \frac{N!}{(1+\frac{|\zeta|^2}{N})^N}\sum_{n=0}^{N}\frac{1}{(N-n)!n!}\left(\frac{\zeta^2}{N}\right)^n \cos^2\left(\lambda\sqrt{(n+1)(1-\frac{n}{N})}t\right). \tag{2.3.68}$$

The atomic inversion or the expectation value for the qubit $\langle\hat{\sigma}^z(t)\rangle$ can also be calculated as

$$W(t) = \langle\psi_e(t)|\psi_e(t)\rangle_N - \langle\psi_g(t)|\psi_g(t)\rangle_N \tag{2.3.69}$$

$$= \frac{N!}{(1+\frac{|\zeta|^2}{N})^N}\sum_{n=0}^{N}\frac{1}{(N-n)!n!}\left(\frac{\zeta^2}{N}\right)^n \cos\left(2\lambda t\sqrt{(n+1)(1-\frac{n}{N})}\right). \tag{2.3.70}$$

where $\hat{\rho}_q(t)$ is the reduced density matrix of the qubit system given by Equation (2.2.55).

To observe interesting properties of this interacting model, we plot Figure 2.3.1 which illustrates the time evolutions of the system for the case of big spin and the qubit are on resonance so that $\delta = 0$. For numerical purposes, we let the qubit start with a ground state $|g\rangle$ so that $C_e = 0$ and $C_g = 1$, $N = 120$ and $|\zeta|^2 = 16$. We plot the probability of the qubit being in the ground state $|g\rangle$ as a blue curve in Figure 2.3.1. From the plot, we can observe a similar event of collapse and revival in the qubit state oscillations. The dynamics of the state collapse and disappear completely for a period of time and then reappear at the revival time t_r. Similar as for the case of the standard Jaynes-Cummings model, such disappearance is due to the destructive interference of the individual qubit in the big spin which later revives as the phase of oscillating terms start to interfere constructively.

The time where the qubit expectation value revives can be estimated by using the maximum values of which the excitation number probability distribution are in phase. It is periodic with 2π intervals and occurs repeatedly. Given that k is a positive integer, the kth revival time for the one-qubit big spin model can the be calculated by

$$2\pi k = t_r\left(\omega_{\bar{n}+1} - \omega_{\bar{n}}\right) \tag{2.3.71}$$

$$= t_r\left(2\lambda\sqrt{(\bar{n}+1)\left(1-\frac{\bar{n}}{N}\right)} - 2\lambda\sqrt{\bar{n}\left(1-\frac{\bar{n}-1}{N}\right)}\right) \tag{2.3.72}$$

$$t_r = \frac{2\pi k}{\left(2\lambda\sqrt{(\bar{n}+1)\left(1-\frac{\bar{n}}{N}\right)} - 2\lambda\sqrt{\bar{n}\left(1-\frac{\bar{n}-1}{N}\right)}\right)}. \tag{2.3.73}$$

With binomial expansions and given that $\bar{n} = |\zeta|^2$, then for the case of $k = 1$, the revival time of the system is approximated as

$$t_r = \frac{2\pi\sqrt{\frac{N|\zeta|^2}{N+|\zeta|^2}}}{1 - \frac{3|\zeta|^2}{2(N+|\zeta|^2)} - \frac{N+|\zeta|^2}{N|\zeta|^2} + \frac{|\zeta|^2}{4N^2}\frac{N(|\zeta|^2-1)+|\zeta|^2(N-1)}{(N+|\zeta|^2)^2}}. \tag{2.3.74}$$

To simplify this equation but without neglecting the correspondence between this one-qubit big spin model and one-qubit Jaynes Cumming model, we have to observe the mean value condition of $|\zeta|^2 \ll N$. With this we may make an estimation and further simplify the revival time t_r. With the fact that $1 \ll \bar{n} \ll N$, which implies very small values of $\frac{\bar{n}}{N}$, we can therefore make appropriate approximations that give us the kth revival time as

$$2\pi k = t_r\left(2\lambda\sqrt{(\bar{n}+1)}\left(1-\frac{\bar{n}}{N}\right) - 2\lambda\sqrt{\bar{n}}\left(1-\frac{\bar{n}}{N}\right)\right) \tag{2.3.75}$$

$$= t_r\left(2\lambda\sqrt{\bar{n}} + \frac{\lambda}{\sqrt{\bar{n}}} - 2\lambda\sqrt{\bar{n}}\right)\left(1-\frac{\bar{n}}{N}\right) \tag{2.3.76}$$

$$\Rightarrow t_r = \frac{2\pi k\sqrt{\bar{n}}}{\lambda\left(1-\frac{\bar{n}}{N}\right)} \tag{2.3.77}$$

$$\tag{2.3.78}$$

where $k = 1, 2...$

Therefore, in a parameter regime that satisfies $1 \ll \bar{n} \ll N$, $k = 1$ and $\bar{n} = |\zeta|^2$ the equation for revival time t_r is simplified into

$$t_r = \frac{2\pi\sqrt{\bar{n}}}{\lambda\left(1-\frac{\bar{n}}{N}\right)} = \frac{2\pi|\zeta|}{\lambda\left(1-\frac{|\zeta|^2}{N}\right)}. \tag{2.3.79}$$

This simplified revival time t_r agrees with the results presented by S. Dooley [63]. Calculations also show that the numerical values for this equation are consistent with the revival time given by the first approximation (Equation (2.3.74)). Therefore, for the rest of this thesis, we will be referring to Equation (2.3.79) when mentioning the revival time t_r for the one-qubit big spin model.

2.3.5 One-Qubit Attractor States

In Section 2.2.5, we have shown that in a one-qubit Jaynes-Cummings model with $|\alpha|^2 \gg 1$, at a particular time $\frac{t_r}{2}$, the qubit disentangles itself from the system and evolves into an a special state called the 'attractor state' $\left|\psi_{1,att}^{+}\right\rangle$. In their study, S. Dooley *et al.* [29] have also shown that we can as well observe the similar event in a one-qubit big spin model. They have also proposed a method of creating spin cat states when the $1 \ll |\zeta|^2 \ll N$ condition is observed. In this parameter regime, we can rewrite the final solution to the one-qubit big spin system given by Equation (2.3.61) in the exponential form and then we collect the terms with the same frequency so that we have an equation with states $|e,n\rangle_N$ and $|g,n\rangle_N$ basis.

$$\begin{aligned}
|\Psi_1(t)\rangle_N = \sum_{n=0}^{N}\Bigg[\frac{C_n}{2}\Bigg(&\Bigg(e^{i\lambda\sqrt{(n+1)\left(1-\frac{n}{N}\right)}}\left(C_e - C_g\frac{C_{n+1}}{C_n}\right)|e,n\rangle_N \\
&+ e^{i\lambda\sqrt{n\left(1-\frac{n-1}{N}\right)}}\left(C_g - C_e\frac{C_{n-1}}{C_n}\right)|g,n\rangle_N\Bigg) \\
&+\Bigg(e^{-i\lambda\sqrt{(n+1)\left(1-\frac{n}{N}\right)}}\left(C_e + C_g\frac{C_{n+1}}{C_n}\right)|e,n\rangle_N \\
&+ e^{-i\lambda\sqrt{n\left(1-\frac{n-1}{N}\right)}}\left(C_g + C_e\frac{C_{n-1}}{C_n}\right)|g,n\rangle_N\Bigg)\Bigg)\Bigg]
\end{aligned} \tag{2.3.80}$$

Due to the form of C_n, for the terms n in the summation which give significant contribution we use the facts that $(n-\bar{n})$ is very small as compared to $\bar{n}$ and $\bar{n} \ll N$, to make the following approximations on the big spin's coefficients

$$
\begin{aligned}
\frac{C_{n+1}}{C_n} &= \left[\frac{\frac{\zeta}{\sqrt{N}}\sqrt{N-n}}{\sqrt{n+1}}\right] && (2.3.81)\\
&= \left[\frac{\frac{\zeta}{\sqrt{N}}\sqrt{N-\overline{n}}}{\sqrt{\overline{n}}}\right]\left(1-\frac{n-\overline{n}}{N-\overline{n}}\right)^{1/2}\left(1+\frac{n-\overline{n}+1}{\overline{n}}\right)^{-1/2} && (2.3.82)\\
&\approx \left[\frac{\frac{\zeta}{\sqrt{N}}\sqrt{N-\overline{n}}}{\sqrt{\overline{n}}}\right]\left(1-\frac{n-\overline{n}}{2(N-\overline{n})}+...\right)\left(1-\frac{n-\overline{n}+1}{2\overline{n}}+...\right) && (2.3.83)\\
&\approx \frac{\zeta}{|\zeta|}\left(1-\frac{|\zeta|}{2\sqrt{N}}+...\right)\left(1-\frac{1}{2N|\zeta|}-\frac{1}{2N|\zeta|^2}-\frac{1}{2N}+...\right) && (2.3.84)\\
&\approx \frac{\zeta}{|\zeta|} = e^{-i\phi} && (2.3.85)
\end{aligned}
$$

and similarly

$$
\frac{C_{n-1}}{C_n} \approx \frac{|\zeta|}{\zeta} = e^{i\phi}. \tag{2.3.86}
$$

Therefore we can write an approximation to the state $|\Psi_1(t)\rangle_N$ given by Equation (2.3.80) as $\left|\widetilde{\Psi}_1(t)\right\rangle_N$ which has the form of

$$
\begin{aligned}
\left|\widetilde{\Psi}_1(t)\right\rangle_N = \sum_{n=0}^{N}\Bigg[\frac{C_n}{2}\Bigg(&\Big(e^{i\lambda\sqrt{(n+1)\left(1-\frac{n}{N}\right)}}\left(C_e - e^{i\phi}C_g\right)|e,n\rangle_N\\
&+ e^{i\lambda\sqrt{n\left(1-\frac{n}{N}\right)}}\left(C_g - e^{-i\phi}C_e\right)|g,n\rangle_N\Big)\\
&+\Big(e^{-i\lambda\sqrt{(n+1)\left(1-\frac{n}{N}\right)}}\left(C_e - e^{i\phi}C_g\right)|e,n\rangle_N\\
&+ e^{-i\lambda\sqrt{n\left(1-\frac{n}{N}\right)}}\left(C_g - e^{-i\phi}C_e\right)|g,n\rangle_N\Big)\Bigg)\Bigg]
\end{aligned} \tag{2.3.87}
$$

To separate the qubit and the big spin parts we again use the binomial theorem to expand the square root, and we use the facts that, for significantly contributing terms in the summation, $(n-\bar{n})$ is very small as compared to $\bar{n}$ and $\bar{n} \ll N$ to make the following approximations

$$
\begin{aligned}
\sqrt{(n+l)\left(1-\frac{n}{N}\right)} &= (\bar{n}+(n-\bar{n})+l)^{\frac{1}{2}}\left(1-\frac{\bar{n}+(n-\bar{n})}{N}\right)^{\frac{1}{2}} && (2.3.88)\\
&\approx \left(\frac{\sqrt{\bar{n}}}{2}+\frac{n}{2\sqrt{\bar{n}}}+\frac{l}{2\sqrt{\bar{n}}}\right)\left(1-\frac{\bar{n}+(n-\bar{n})}{N}\right) && (2.3.89)\\
&\approx \left(\frac{\sqrt{\bar{n}}}{2}+\frac{n}{2\sqrt{\bar{n}}}+\frac{l}{2\sqrt{\bar{n}}}\right)\left(1-\frac{\bar{n}}{N}\right) && (2.3.90)
\end{aligned}
$$

where l is a parameter that takes on the value of 0 or 1.

We insert this approximation into Equation (2.3.87) and obtain

$$\begin{aligned}\left|\widetilde{\Psi}_1(t)\right\rangle_N = \sum_{n=0}^{N}\Bigg[\frac{C_n}{2}\Bigg(& e^{\frac{i\lambda\sqrt{\bar{n}}\left(1-\frac{\bar{n}}{N}\right)t}{2}} e^{\frac{i\lambda n\left(1-\frac{\bar{n}}{N}\right)t}{2\sqrt{\bar{n}}}}\Bigg(e^{\frac{i\lambda\left(1-\frac{\bar{n}}{N}\right)t}{2\sqrt{\bar{n}}}}\left(C_e - e^{i\phi}C_g\right)|e\rangle \\ &+\left(C_g - e^{-i\phi}C_e\right)|g\rangle\Bigg) \\ &+ e^{\frac{-i\lambda\sqrt{\bar{n}}\left(1-\frac{\bar{n}}{N}\right)t}{2}} e^{\frac{-i\lambda n\left(1-\frac{\bar{n}}{N}\right)t}{2\sqrt{\bar{n}}}}\Bigg(e^{\frac{-i\lambda\left(1-\frac{\bar{n}}{N}\right)t}{2\sqrt{\bar{n}}}}\left(C_e - e^{i\phi}C_g\right)|e\rangle \\ &+\left(C_g - e^{-i\phi}C_e\right)|g\rangle\Bigg)\Bigg)|n\rangle_N\Bigg].\end{aligned} \tag{2.3.91}$$

From this, we can now separate the qubit and the big spin terms as

$$\begin{aligned}\left|\widetilde{\Psi}_1(t)\right\rangle_N = &\frac{1}{2}\left(\sum_{n=0}^{N} e^{\frac{i\lambda\sqrt{\bar{n}}\left(1-\frac{\bar{n}}{N}\right)t}{2}} e^{\frac{i\lambda n\left(1-\frac{\bar{n}}{N}\right)t}{2\sqrt{\bar{n}}}}|n\rangle_N\right)\left(C_e - e^{i\phi}C_g\right)\left(e^{\frac{i\lambda\left(1-\frac{\bar{n}}{N}\right)t}{2\sqrt{\bar{n}}}}|e\rangle - e^{i\phi}|g\rangle\right) \\ &+\frac{1}{2}\left(\sum_{n=0}^{N} e^{\frac{-i\lambda\sqrt{\bar{n}}\left(1-\frac{\bar{n}}{N}\right)t}{2}} e^{\frac{-i\lambda n\left(1-\frac{\bar{n}}{N}\right)t}{2\sqrt{\bar{n}}}}|n\rangle_N\right)\left(C_e - e^{i\phi}C_g\right)\left(e^{\frac{-i\lambda\left(1-\frac{\bar{n}}{N}\right)t}{2\sqrt{\bar{n}}}}|e\rangle - e^{i\phi}|g\rangle\right)\end{aligned} \tag{2.3.92}$$

and with big spin $\left|\frac{\zeta}{\sqrt{N}}\right\rangle_N$ the wavefunction becomes

$$\begin{aligned}\left|\widetilde{\Psi}_1(t)\right\rangle_N = &\frac{1}{2}e^{\frac{i\lambda\sqrt{\bar{n}}\left(1-\frac{\bar{n}}{N}\right)t}{2}}\left|e^{\frac{i\lambda\left(1-\frac{\bar{n}}{N}\right)t}{2\sqrt{\bar{n}}}}\frac{\zeta}{\sqrt{N}}\right\rangle_N\left(C_e - e^{i\phi}C_g\right)\left(e^{\frac{i\lambda\left(1-\frac{\bar{n}}{N}\right)t}{2\sqrt{\bar{n}}}}|e\rangle - e^{i\phi}|g\rangle\right) \\ &+\frac{1}{2}e^{\frac{-i\lambda\sqrt{\bar{n}}\left(1-\frac{\bar{n}}{N}\right)t}{2}}\left|e^{\frac{-i\lambda\left(1-\frac{\bar{n}}{N}\right)t}{2\sqrt{\bar{n}}}}\frac{\zeta}{\sqrt{N}}\right\rangle_N\left(C_e - e^{i\phi}C_g\right)\left(e^{\frac{-i\lambda\left(1-\frac{\bar{n}}{N}\right)t}{2\sqrt{\bar{n}}}}|e\rangle - e^{i\phi}|g\rangle\right)\end{aligned} \tag{2.3.93}$$

which consists of two distinct parts; the big spin and the qubit parts. We can write the equation in a simplified form of

$$\left|\widetilde{\Psi}_1(t)\right\rangle_N = \eta_{+\frac{1}{2}}\left|Q_{+\frac{1}{2}}\right\rangle_N\left|\Phi_{+\frac{1}{2}}\right\rangle_N + \eta_{-\frac{1}{2}}\left|Q_{-\frac{1}{2}}\right\rangle\left|\Phi_{-\frac{1}{2}}\right\rangle_N \tag{2.3.94}$$

where $\eta_{\pm\frac{1}{2}}$ is a normalisation factor, $\left|Q_{\pm\frac{1}{2}}\right\rangle$ is a state of the qubit and $\left|\Phi_{\pm\frac{1}{2}}\right\rangle_N$ is a state of the big spin. Note that t_r is the revival time given by Equation (2.3.74).

$$\eta_{\pm\frac{1}{2}}(t) = \pm\frac{1}{\sqrt{2}}e^{\pm i\pi\frac{t}{t_r}(\bar{n}+1)}\left(e^{i\phi}C_e \mp C_g\right) \tag{2.3.95}$$

$$\left|Q_{\pm\frac{1}{2}}(t)\right\rangle = \frac{1}{\sqrt{2}}\left(e^{-i\phi}\left|e\right\rangle \mp e^{i\pi\frac{t}{t_r}}\left|g\right\rangle\right) \tag{2.3.96}$$

$$\left|\Phi_{\pm\frac{1}{2}}(t)\right\rangle_N = \left|e^{i\pi\frac{t}{t_r}}\frac{\zeta}{\sqrt{N}}\right\rangle_N. \tag{2.3.97}$$

This solution clearly shows that the wavefunction is separated by the big spin and the qubit parts. It can also be noticed that there are two different spin coherent states that are out of phase by $2\pi t/t_r = \lambda t(1-\frac{\bar{n}}{N})$. As it was also shown by S. Dooley [29] that in the $1 \ll |\zeta|^2 \ll N$ regime, at $\frac{t_r}{2}$ the qubit evolves to an attractor state. Equation (2.3.95) to Equation (2.3.97) therefore become

$$\eta_{\pm\frac{1}{2}}\left(\frac{t_r}{2}\right) = \pm\frac{i}{\sqrt{2}}e^{\pm i\pi\bar{n}/2}\left(e^{i\phi}C_e \mp C_g\right) \tag{2.3.98}$$

$$\left|Q_{\pm\frac{1}{2}}\left(\frac{t_r}{2}\right)\right\rangle = \frac{1}{\sqrt{2}}\left(e^{-i\phi}\left|e\right\rangle + i\left|g\right\rangle\right) \tag{2.3.99}$$

$$\left|\Phi_{\pm\frac{1}{2}}\left(\frac{t_r}{2}\right)\right\rangle_N = \left|\pm i\frac{\zeta}{\sqrt{N}}\right\rangle_N. \tag{2.3.100}$$

It can be seen that at half of the revival time $\frac{t_r}{2}$, the qubit and the big spin are disentangled. At this time too, we have qubit states $\left|Q_{+\frac{1}{2}}\left(\frac{t_r}{2}\right)\right\rangle = \left|Q_{-\frac{1}{2}}\left(\frac{t_r}{2}\right)\right\rangle$. The qubit approaches an attractor state that has a form of

$$\left|\psi_{1,att}^{+}\right\rangle_N = \frac{1}{\sqrt{2}}\left(e^{-i\phi}\left|e\right\rangle + i\left|g\right\rangle\right). \tag{2.3.101}$$

Similar to the attractor state in the Jaynes-Cummings model, this state is independent of the qubit's initial conditions, but depends on the initial phase of the spin coherent state ϕ. This can be seen from Equation (2.3.99), where there is no factor of coefficients C_e and C_g. To show the dynamics of the attractor state, we calculate the probability of the qubit for being in the state $\left|\psi_{1,att}^{+}\right\rangle_N$ by using Equation (2.2.69). We then plot a curve for this quantity as an orange line in Figure 2.3.1. From the figure, it is clear that at the attractor time $\frac{t_r}{2}$, the probability approaches very close to unity. At this particular time too, the qubit and the big spin are in a product state, therefore the wavefunction at $\frac{t_r}{2}$ is given as

$$\begin{aligned}\left|\widetilde{\Psi}_1\left(\frac{t_r}{2}\right)\right\rangle_N = \frac{\left|\psi_{1,att}^{+}\right\rangle_N}{\sqrt{2}}\Bigg(& ie^{i\pi\bar{n}/2}(e^{i\phi}C_e - C_g)\left|i\frac{\zeta}{\sqrt{N}}\right\rangle_N \\ & - ie^{-i\pi\bar{n}/2}(e^{i\phi}C_e + C_g)\left|-i\frac{\zeta}{\sqrt{N}}\right\rangle_N\Bigg).\end{aligned} \tag{2.3.102}$$

The big spin is now in a superposition of two adjacent states (opposite phase) $\left|\frac{\zeta}{\sqrt{N}}\right\rangle_N$ and $\left|-\frac{\zeta}{\sqrt{N}}\right\rangle_N$ called the spin cat state that contains all the information about the qubit's initial state.

As we let the system continue to evolve, we can later see the the evolution in the big spin's system. At time t_r, state $\left|\Phi_{\pm\frac{1}{2}}(t)\right\rangle_N$evolves into an identical state where $\left|\Phi_{+\frac{1}{2}}(t_r)\right\rangle_N = \left|\Phi_{-\frac{1}{2}}(t_r)\right\rangle = \left|-\frac{\zeta}{\sqrt{N}}\right\rangle_N$. The overall system is once again a product state and the big spin can be factorised out of the wavefunction. At this time, all the information about the initial qubit state is transferred from the big spin back to the qubit.

Similar disentanglement as at time $\frac{t_r}{2}$ is also observed at the second attractor time $\frac{3t_r}{2}$. The big spin and the qubit components are once again factorised, at which the qubit is again a pure state. It evolves to an orthogonal attractor state, $\left|\psi^-_{1,att}\right\rangle$. This makes the probability $P_{1,att}(t)$ curve depicted by orange line in Figure 2.2.2 approaches very close to zero.

The interaction then continues with the big spin evolving into state $\left|\frac{\zeta}{\sqrt{N}}\right\rangle_N$ at $2t_r$. The overall system then repeatedly evolves from an entangled state to a product state and then back again into an entangled state where the information in the qubit is transferred into the big spin and again back into the qubit. This is a similar phenomenon to the case of the Jaynes-Cummings model, that is defined by Gea-Banacloche as a natural route to quantum state preparation [22] and can be clearly seen by monitoring the entropy of the system.

2.3.6 Linear entropy

To understand the dynamics of the entanglement in the system, we observe the linear entropy of the qubit throughout its interaction with big spin. We use a similar linear entropy formula as Equation (2.2.71), but this time the big spin is traced over to give the reduced density matrix of the qubit $\hat{\rho}(t)$. The dynamics of this quantity are shown in the illustrated red curve in Figure 2.3.1.

From the analytical calculations made in Section 2.3.5, we know that at the attractor times $\frac{t_r}{2}$ and $\frac{3t_r}{2}$ the entropy $S^L_q(t)$ is zero to indicate that the qubit and the big spin form a product state. The qubit is an attractor state which is a pure state and disentangled form the big spin. This is supported by our numerical outputs where the red line in Figure 2.3.1 approaches very close to zero, thus there are dips in this quantity at these times. This confirms the system is indeed in a good approximation to a product state where there is very little entanglement between the qubit and big spin.

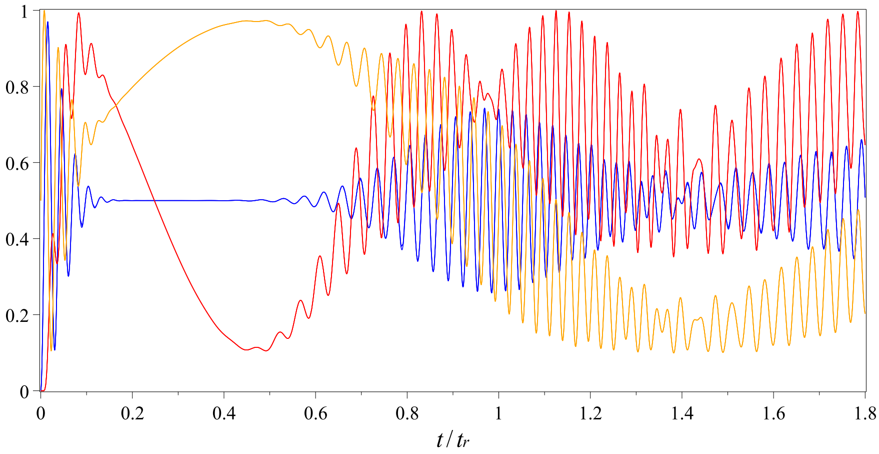

Figure 2.3.1: Time evolution for a system with one-qubit big spin model with the qubit starts in an initial state $|g\rangle$, $N = 120$ and $|\zeta|^2 = 16$. (a) red line is for the entropy of the qubit. (b) blue line is for the probability of being in the qubit's initial state $|g\rangle$. (c) orange line is for the probability of the qubit being in the attractor state $\left|\psi^{+}_{1,att}\right\rangle_N$.

Another dip in the entropy curve can also be seen at the revival time t_r. This is where the qubit and the big spin are expected to disentangle once again. However, a shallower dip is observed which seems to suggest the presence of large entanglement in the system while the analytical prediction states otherwise. Similar explanation with the case of Jaynes-Cummings model can be made where this happens as an effect of the narrow time scale on the width of this dip. With a greater value of $N \to \infty$ in the numerical calculation, the entropy at this time gets closer to zero and agrees with the analytical predictions. These observations on the properties of the linear entropy are similar to the analogous Jaynes-Cummings model.

2.4 Summary

We have investigated the dynamics and time evolutions of a single qubit interacting with a collection of N spins, called the big spin. We also have shown the correspondence of this interacting system with the one-qubit Jaynes-Cummings model. We started by reproducing the results of prior works by C. Jarvis *et al.* [64] to develop in depth understanding on a single qubit interacting model and later we used similar calculation methods to reproduce the results produced by a one-qubit big spin model studied by S. Dooley [63, 29].

We calculated and demonstrated many interesting phenomena resulting from such interactions. Quantities like the oscillations of qubits probabilities, the one-qubit attractor state with the attractor time, the linear entropy of the qubit subsystem, were plotted to visualise their interesting dynamics and properties.

A direct comparison can be made with similar quantities that are produced by the Jaynes-Cummings model. We see that all above-mentioned quantities behave in similar ways for both systems, and thus we can conclude the correspondence of our one-qubit big spin and Jaynes-Cummings models. Next, we will extend our research to understanding the dynamics of these systems including the effects of decoherence. Given the already observed correspondences, we can thus study both models side by side to further investigate their similarities and differences with errors in the frequencies, which will be considered in the next chapter. Subsequent chapters will then employ the formalism established here to consider two-qubit systems.

Chapter 3

Single Qubit Interaction Models With Non-Zero Frequencies Detuning

3.1 Introduction

In the previous chapter, we have considered the one-qubit Jaynes-Cummings model as well as the one-qubit big spin model with a resonant condition for the two frequencies in the Hamiltonian. In other words, we let the systems evolve with a zero detuning in the frequencies of the qubit Ω and the field ω (or big spin ω_N), and we analysed the time evolutions for both interacting systems. In this chapter, we will investigate and discuss the influences of a non-zero detuning between the frequencies on both systems.

In these set ups, we are dealing with a condition where there is difference in the energy levels, as depicted in Figure 2.2.1. This difference is due to a mismatch between the energy level separation in the qubit system and the energy of a photon in the field mode. As this difference in energy increases, fewer emitting and absorbing events take place. A study on the effects of non-zero detuning in the one-qubit Jaynes-Cumming model has been conducted by C.Jarvis in her thesis [64]. She demonstrated the changes in the time evolutions of this interacting system when there is an exact value of detuning as a result of $\delta = \Omega - \omega$. In this set up, the evolution was still Hamiltonian and reversible, but simply off-resonant. In the first part of this study, we will apply similar frequency detunings to the one-qubit big spin model where we are interested to investigate and observe the off-resonant attributes in the time evolution of the one-qubit big spin system.

We will then further extend our research by considering both one-qubit Jaynes-Cummings as well as one-qubit big spin interaction systems with error effects. In this case, we will consider the condition of which the desired system is an interaction with $\delta = 0$, but subject to a distribution of errors. In other words, we will deal with errors from the ideal case of zero detuning, and therefore the distribution is chosen to peak at zero. Such considerations are because in a real system, there are always the potential for decoherence, i.e. the transformation of a quantum-mechanical superposition state into a classical statistical mixture over time. It is a condition where there is an irreversible increase in the mixture of an ensemble of quantum systems with time. This could be due to a distribution of detunings, as we are considering here, or to interaction with some other form of environment or noise [23]. Therefore, to understand the realistic case of both forms of interacting system, it is important to study the behaviour of these models under the decoherence effects.

3.2 Jaynes-Cummings Model with Non-Zero Detuning

As shown in Section 2.2.3, by letting $\Omega \neq \omega$ we can find the solution for the one-qubit Jaynes-Cummings Hamiltonian which is in the form of Equation (2.2.41). In an interaction picture, we can apply the state transformations as given by Equations (2.2.46) to (2.2.48) and simplify the solution into

$$\begin{aligned}
|\Psi_1(t)\rangle = \sum_{n=0}^{\infty} \Bigg(& \Big(C_e C_n \cos\left(t\sqrt{\delta^2 + 4\lambda^2 (n+1)}/2\right) + i \sin\left(t\sqrt{\delta^2 + 4\lambda^2 (n+1)}/2\right) \\
& \left(C_e C_n \left(\sin^2\theta_n - \cos^2\theta_n\right) - 2C_g C_{n+1} \cos\theta_n \sin\theta_n\right) \Big) |e, n\rangle \\
& + \Big(C_g C_{n+1} \cos\left(t\sqrt{\delta^2 + 4\lambda^2 (n+1)}/2\right) + i \sin\left(t\sqrt{\delta^2 + 4\lambda^2 (n+1)}/2\right) \\
& \left(C_g C_{n+1} \left(\cos^2\theta_n - \sin^2\theta_n\right) - 2C_e C_n \cos\theta_n \sin\theta_n\right) \Big) |g, n+1\rangle \Bigg) \\
& + C_g C_0 e^{i\delta t/2} |g, 0\rangle
\end{aligned} \tag{3.2.1}$$

where $\delta = \Omega - \omega$, besides $\cos\theta_n$ and $\sin\theta_n$ are respectively given by Equations (2.2.31) and (2.2.32). In a system with a coherent state of the field, C_n is then given by Equation (2.2.52). We will use Equation (3.2.1) to calculate and show the dynamics of one-qubit Jaynes-Cummings model with an exact value of detuning in Section 3.2.1, and later we will consider the system with a distribution of detunings, leading to errors and decoherence, in Section 3.2.2 .

3.2.1 Finite Frequencies Detuning

As mentioned in the introduction, C. Jarvis has made a further analysis on the one-qubit Jaynes-Cummings model by studying the effects of non-zero detunings to the behaviour of such system with an exact value of δ [64]. She presented the changes in the system caused by non-zero detunings and the studies concluded that, as the value of δ increases the qubit state probabilities, together with a delay in the revival time.

To exhibit the results, we plot Figure 3.2.1 for several value of δ. Note that we define our time in the units of revival time t_r. Therefore, there is a corresponding conversion for the units of the angular frequency (and so δ) to units of ${t_r}^{-1}$. In this figure, we plot several curves of which each of them represents the probability of the qubit being in the ground state $P_g(t) = \langle g|\hat{\rho}_q(t)|g\rangle$ for different values of δ. From the graph, we can see it is evident that the qubit state probability increases to follow the increment in the δ value. As compared to the one-qubit Jaynes-Cummings system with $\delta = 0$ depicted as the red line in Figure 3.2.1, where the probability is always averaged at approximately $P_g(t) = 0.5$, it can be seen that the probability is shifted to a higher value for each different cases of $\delta > 0$.

Besides the changes in the qubit state probability $P_g(t)$, we can see that there is also adjustment in the revival time of this system with respect to the increasing detuning. From the plot, we can observe that the respected revival time for each value of detuning $t_{r,\delta}$, has become longer with the increment of δ. The revival time for each δ can be estimated by

$$
\begin{aligned}
2\pi &= t_{r,\delta}(\omega_{n+1} - \omega_n) && (3.2.2)\\
&= t_{r,\delta}\left(\sqrt{\delta^2 + 4\lambda^2(\bar{n}+1)} - \sqrt{\delta^2 + 4\lambda^2\bar{n}}\right) && (3.2.3)\\
t_{r,\delta} &= \frac{2\pi}{\sqrt{\delta^2 + 4\lambda^2(\bar{n}+1)} - \sqrt{\delta^2 + 4\lambda^2\bar{n}}} && (3.2.4)
\end{aligned}
$$

As an example, for the case of $\delta = 10$ the revival time is approximately at $t_{r,10} \approx 1.30$, but the revival time is longer for $\delta = 25$ which occurs approximately at $t_{r,25} \approx 2.29$.

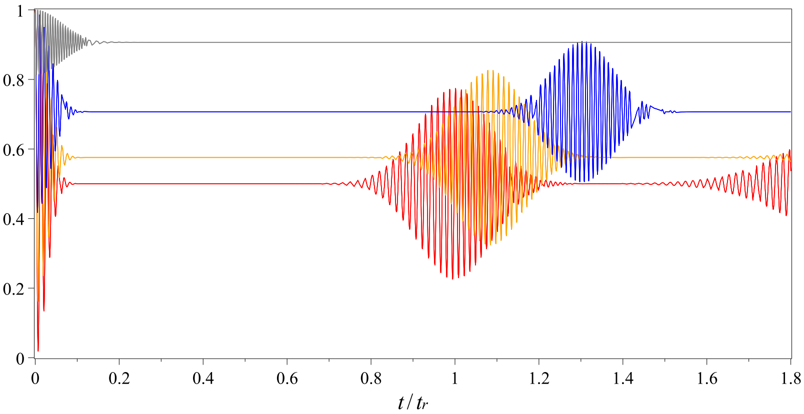

Figure 3.2.1: The probability of the qubit being in the state $|g\rangle$ for a one-qubit Jaynes-Cumming model with four different values of δ. The initial qubit state is $|g\rangle$ with $\bar{n} = 36$ and $\theta = 0$. The red curve is for $\delta = 0$, orange $\delta = 5$, blue $\delta = 10$ and grey $\delta = 25$.

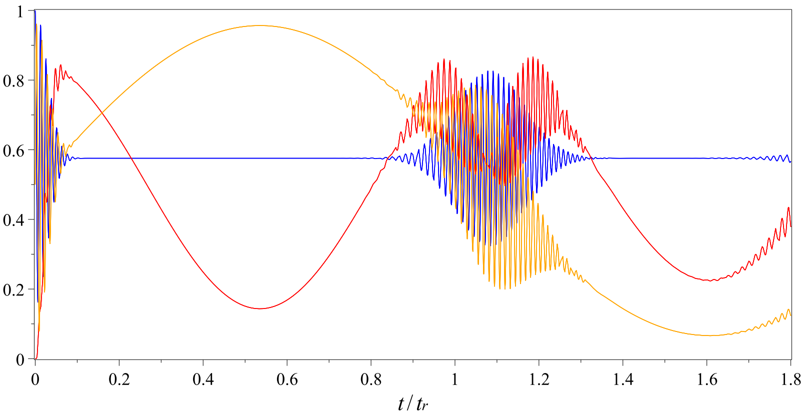

Figure 3.2.2: Time evolution of a one-qubit Jaynes-Cummings model when the qubit started in the initial state $|g\rangle$ with $\bar{n} = 36$, $\theta = 0$ and $\delta = 5$. The red curve is for the linear entropy $S_q^L(t)$ of the reduced density matrix, blue curve is for the probability of the qubit being in state $|g\rangle$ and orange is for the probability of the qubit being in attractor state $\left|\psi_{1,att}^{+}\right\rangle$.

Not only it changes the qubit probability and revival time, the increment in δ also influences the entanglement of the qubit and the field subsystems. To illustrate this fact, we plot the a curve in Figure 3.2.2 to show the linear entropy $S_q^L(t) = 1 - \mathrm{Tr}(\hat{\rho}_q(t)^2)$ of the qubit subsystem of one-qubit Jaynes-Cummings model with a specific value of error $\delta = 5$. We plot together the probability of the qubit being in the ground state $P_g(t)$, as well as the probability of the qubit being in the one-qubit attractor state $P^+_{1,att}(t) = \left\langle \psi^+_{1,att} | \hat{\rho}_q(t) | \psi^+_{1,att} \right\rangle$. A similar overall pattern of time evolutions can be seen in this figure as compared to the case of $\delta = 0$ shown in Figure 2.2.2. However, besides some delay in the revival time by approximately 0.1, changes can also be noticed in the linear entropy $S_q^L(t)$ as well as the attractor state probability $P^+_{1,att}(t)$ lines. We can see that at half of the revival time, $\frac{t_{r,5}}{2}$, the linear entropy curve does not approach very close to zero, while the probability of the qubit being in the one-qubit attractor state has slightly reduced, although still quite close to unity. These show that the detuning introduced has made the disentanglement between the qubit and the field subsystems harder, and therefore increases the mixture in the qubit state at that particular time.

These observations clearly demonstrate that a non-zero detuning has some significant effects on the time evolutions of one-qubit Jaynes-Cummings interacting model. Therefore, if the desired system evolution is the behaviours that seen in a system with zero detuning, having a finite non-zero detuning causes a deviation from these desired behaviours, as shown in the time-dependence of the various quantities described above.

3.2.2 Error Modelling: a Distribution of Errors

We have seen the effects of having a non-zero detuning in one-qubit Jaynes-Cummings system. It is clear that changes in δ have some influences in the probability of the qubit state, the revival time, and the entanglement of the qubit and the field (purity of the qubit state). In this section we discuss a Jaynes-Cummings system with different treatments on the detuning in the frequency of the qubit Ω and the coherent field ω. This time we analyse the system with realistic errors that usually occur in a practical system.

In an actual system, there will always errors that coming from unknown detunings, which will lead to disturbance in the system. In this thesis, we will focus on the case of a desired system with zero detuning, but with a potential errors that subject to a Gaussian distribution. We will use this distribution to average over the frequency differences δ with a distribution of error width Δ.

With a Gaussian distribution that is centered at an expectation value zero $\delta = 0$ and standard deviation Δ, the error can be written as

$$f(\delta|0,\Delta) = \frac{1}{\Delta\sqrt{2\pi}} e^{-\frac{\delta^2}{2\Delta^2}} \tag{3.2.5}$$

where δ is the error sampled over a range of its standard deviation. To analyse the system, in principle an integral should be done over all δ such that

$$\hat{\rho}_q(\Delta) = \int_{-\infty}^{\infty} d\delta f(\delta|0,\Delta)\, \hat{\rho}_q(t,\delta). \tag{3.2.6}$$

This is to evaluate the density matrix of the qubit for all of the δ values by averaging the density matrix over the errors. However, as this is not possible analytically, we use an approximation to this integral which involves a sufficiently large number of δ. This means, we consider a discrete approximation to this ensemble of system which can be calculated in the form of

$$\hat{\rho}_q(\Delta) \approx \sum_{\delta_i} \frac{f(\delta_i|0,\Delta)\, \hat{\rho}_q(t,\delta_i)}{\sum_{\delta_i} f(\delta_i|0,\Delta)} \tag{3.2.7}$$

where i indicates the number of the discrete events. The spacing in δ chosen is such that there is only a small error between our approximation and the analytic integral over all δ given by Equation (3.2.6) and as this number i increases, the function begins to resemble a distribution in the continuous regime as shown in Figure 3.2.3. It can be seen in subfigure (d) that as we set $i = 31$ the curve is very close to the original distribution shown in subfigure (a). This indicates that $i = 31$ is a sufficiently good approximation to our Gaussian distribution and will be used in our work. Note that we define the time of our system in the units of revival time t_r, so there is a corresponding conversion for the units of the angular frequency. Therefore, δ and Δ in this thesis are defined in units of ${t_r}^{-1}$.

We use Equation (3.2.7) and the error distribution properties to calculate the qubit's reduced density matrix over a distribution of δ values and then we evaluate the probability of the qubit being in ground state $P_g(t)$, the linear entropies $S_q^L(t)$ and the probabilities of the qubits being in the attractor state $P_{1,att}^{+}(t)$. We plot the time evolutions of this case of one-qubit Jaynes-Cummings model for a several values of error distribution width Δ and the results are presented as Figure 3.2.4.

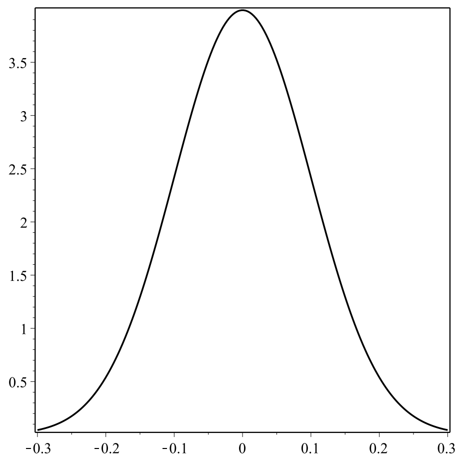

(a) continuous

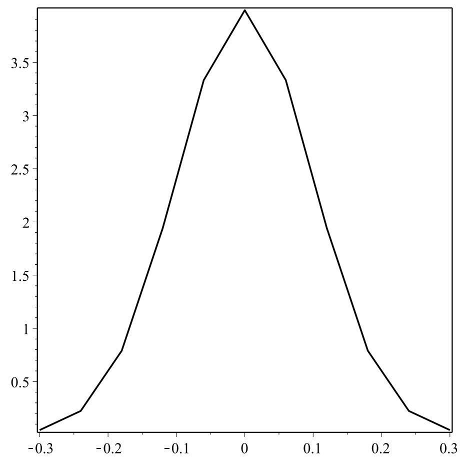

(b) discrete with i=11

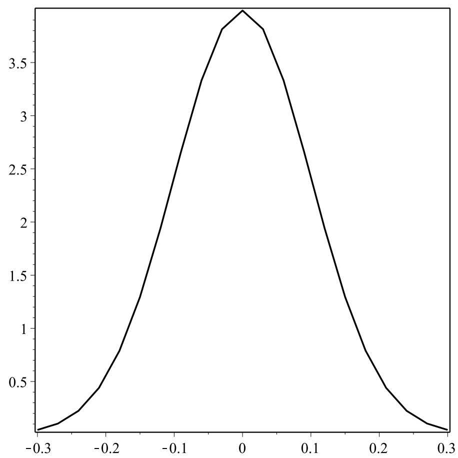

(c) discrete with i=21

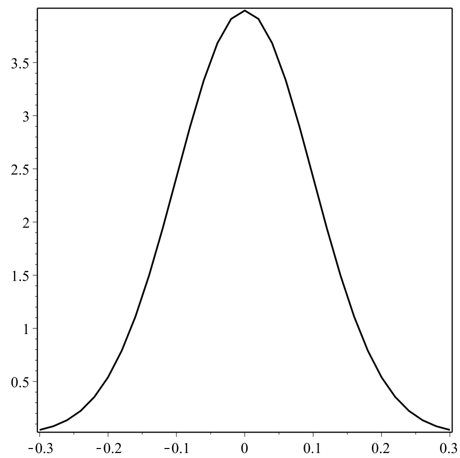

(d) discrete with i=31

Figure 3.2.3: Plots of Gaussian distribution with various values of discrete estimations, i. The distribution given by Equation (3.2.5) is centered at an expectation value zero $\delta = 0$ and standard deviation $\Delta = 0.3$

.

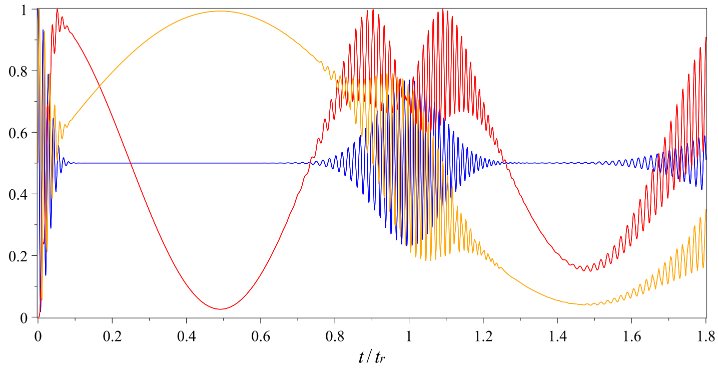

(a) $\Delta = 0.3$

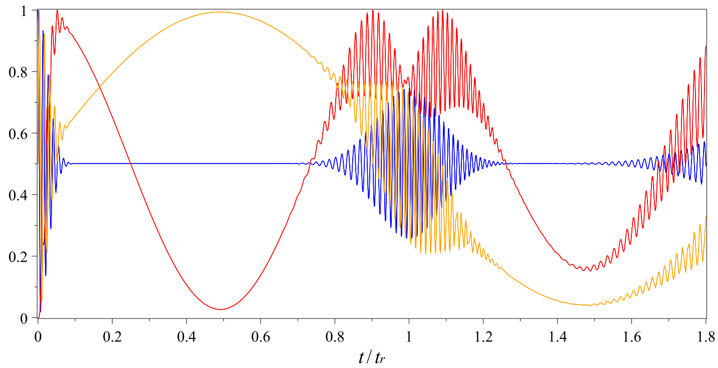

(b) $\Delta = 0.5$

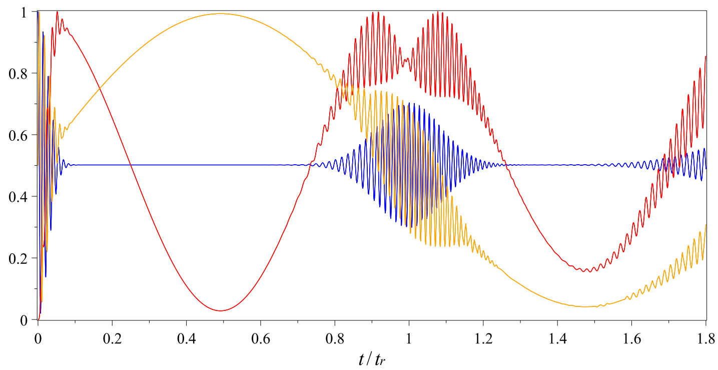

(c) $\Delta = 0.7$

Figure 3.2.4: Plots comparing qubit linear entropies (red), probability of the qubit being in state $|g\rangle$ (blue) and the probability of the qubit being in attractor state $\left|\psi^{+}_{1,att}\right\rangle$ (orange) for one-qubit Jaynes-Cummings model of initial qubit state $|g\rangle$, $\bar{n} = 36$ and the initial phase of the radiation field $\theta = 0$ with decoherence effects. Figure (a) shows the differences in the system with $\Delta = 0.3$, (b) shows the differences in the system with $\Delta = 0.5$ and (c) shows the differences in the system with $\Delta = 0.7$.

We choose $\Delta = 0.3$, $\Delta = 0.5$ and $\Delta = 0.7$ as comparisons to the case of one-qubit Jaynes-Cummings model with zero detuning value shown in Figure 2.2.2.

Unlike the results from Section 3.2.1 where the probabilities of the qubit being in state $|g\rangle$ are shifted to larger values with the increment in the frequency detunings, we can see the probabilities in this case remain averaged at around $P_g(t) = 0.5$ even with changes in the error values. At the attractor time $\frac{t_r}{2}$ no changes are observed in all quantities suggesting that no changes in the purity of the qubit subsystem and the one-qubit attractor state can still be observed at this particular time.

Perhaps the most obvious distinctions to the one-qubit Jaynes-Cummings model with zero detuning value can be noticed at the revival time t_r. Even though the changes are small, we may see that as we increase the error width Δ, the amplitude in the qubit state probabilities at this particular time have become smaller for both $P_g(t)$ and $P^+_{1,att}(t)$. Therefore, we can conclude that a single non-zero value of detuning shifts the revival (so changes the revival time) but with a distribution of detunings to model realistic errors in the system, the revival is suppressed. This is because of the different detunings in the ensemble distribution are causing revival at different times. Qubit information is also affected at this revival time t_r in which a shallower dip in the entropy line is observed for a larger value of error. This increment in the qubit entropy is due to additional entropy from the decoherence as a result of the distribution of detunings over the ensemble. This indicates that at this time the system is in a more mixed state, therefore there is addition to the entropy resulting from entanglement of the qubit with the field. This behaviour also suggests that the disentanglement between the qubit and the field subsystems become harder with the presence of larger decoherence effects.

To further investigate the effects of decoherence on the system, we extend our analysis with larger values of error. We aim to determine the maximum value of Δ that abolishes the revival of qubit's state probability. We plot Figure 3.2.5 with various values of $\Delta > 1$ and from the figure, we can see that as the Δ increases, the qubit state oscillations continue to revive with a lower amplitude, until with $\Delta = 3.0$, the revival diminishes completely. This shows that the errors have also interrupted the constructive interferences and affected the qubit state revival in the system. The death of oscillations can also be observed on the probability of the one-qubit attractor state, as well as the linear entropy evolutions where both quantities are flat, even at the revival time t_r as shown in Figure 3.2.5(c).

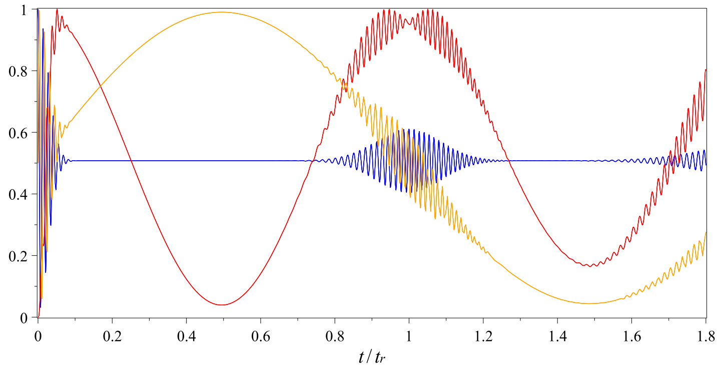

(a) $\Delta = 1.5$

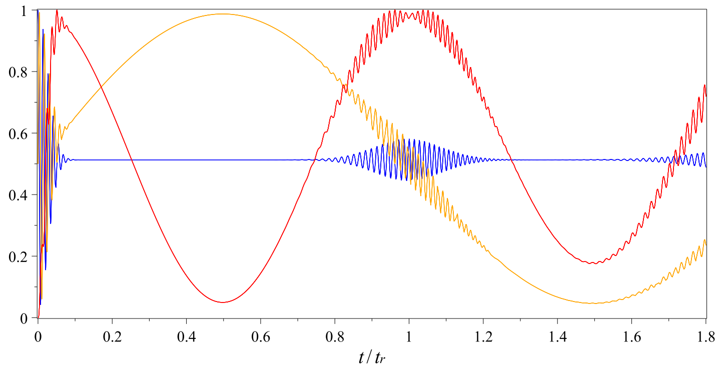

(b) $\Delta = 2.0$

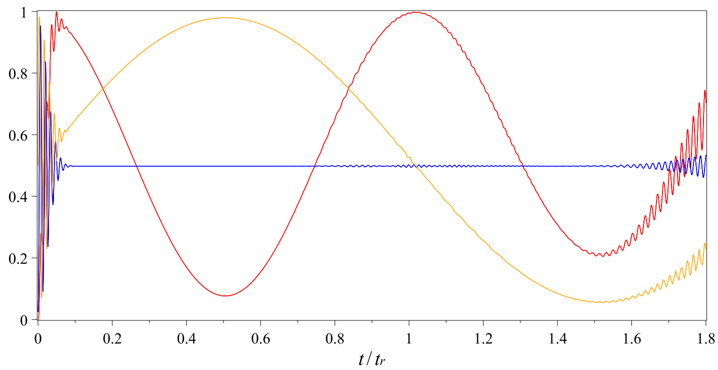

(c) $\Delta = 3.0$

Figure 3.2.5: Plots comparing qubit linear entropies (red), probability of the qubit being in state $|g\rangle$ (blue) and the probability of the qubit being in attractor state $\left|\psi_{1,att}^{+}\right\rangle$ (orange) for one-qubit Jaynes-Cummings model of initial qubit state $|g\rangle$, $\bar{n} = 36$ and the initial phase of the radiation field $\theta = 0$ with decoherence effects. Figure (a) shows the differences in the system with $\Delta = 1.5$, (b) shows the differences in the system with $\Delta = 2.0$ and (c) shows the differences in the system with $\Delta = 3.0$.

3.3 Single Qubit and Big Spin Model with Non-Zero Detuning

In the previous sections, we have seen the effects of having a finite non-zero frequency detuning, as well as the effects of a distribution of errors in one-qubit Jaynes-Cummings system. We will now extend our research to study the impacts of applying similar treatments on one-qubit big spin interacting model. In the first part of this section, we consider the case of a qubit of frequency Ω interacting with the big spin of frequency ω_N where we will observe the changes in the dynamics of this system when we have an exact value of non-zero detunings. We will then proceed with investigation on the case of which we have an ideal system but with a potential errors that subject to a Gaussian distribution as given by Equation (3.2.5).

In Section 2.3.2, we have calculated the eigenvalues and eigenvectors for one-qubit big spin system. We then obtained the solution for Hamiltonian (2.3.10) in the form of Equation (2.3.52). Within interaction picture assumption, we can apply the state transformations as given by Equations (2.3.58) to Equation (2.3.60), and 0we simplify the solution as

$$\begin{aligned}
|\Psi_1(t)\rangle = \sum_{n=0}^{N-1} \Bigg[& \left(C_e C_n \cos\left(\frac{t}{2}\mu_n(\Delta)\right) + i \sin\left(\frac{t}{2}\mu_n(\Delta)\right) \right. \\
& \left. (C_e C_n (\sin^2\phi_n - \cos^2\phi_n) - 2C_g C_{n+1} \cos\phi_n \sin\phi_n) \right) |e, n\rangle_N \\
& + \left(C_g C_{n+1} \cos\left(\frac{t}{2}\mu_n(\Delta)\right) + i \sin\left(\frac{t}{2}\mu_n(\Delta)\right) \right. \\
& \left. (C_g C_{n+1} (\cos^2\phi_n - \sin^2\phi_n) - 2C_e C_n \cos\phi_n \sin\phi_n \phi_n) \right) |g, n+1\rangle_N \Bigg] \\
& + C_e C_N e^{-it(\omega_N N + \frac{\Omega}{2})} |e, N\rangle_N + C_g C_0 e^{-it(\omega_N - \frac{\Omega}{2})} |g, 0\rangle_N .
\end{aligned} \tag{3.3.1}$$

where $\delta = \Omega - \omega_N$ and in the units of $\frac{1}{t_r}$, $\mu_n(\delta)$ is given by Equation (2.3.35), and $\cos\phi_n$ as well as $\sin\phi_n$ are respectively given by Equation (2.3.40) and Equation (2.3.42). We will use Equation (3.3.1) to investigate and demonstrate the changes that a detuning and an error can make in the time evolutions of this interacting system.

3.3.1 Finite Frequencies Detuning

From Equation (3.3.1), we plot Figure 3.3.1 to show the effects of four non-zero detuning values δ on the probability of the qubit being in the ground state $P_g(t)$ in one-qubit big spin model. We compare these results with the similar case of one-qubit Jaynes-Cummings model. A similar pattern of responds exhibited by both models towards the increased detuning value. It is clear that with a larger non-zero detuning, the qubit state probability increases from approximately $P_g(t) = 0.5$ for the case of the system with resonance frequencies as discussed in Section 2.3.4.

We can also observe that the system has a delayed revival time, as was observed in the corresponding one-qubit Jaynes-Cummings case. We can estimate the adjusted revival time as

$$2\pi = t_{r,\delta}(\omega_{n+1} - \omega_n) \tag{3.3.2}$$

$$= t_{r,\delta}\left(\sqrt{\delta^2 + 4\lambda^2(\bar{n}+1)\left(1 - \frac{\bar{n}}{N}\right)} - \sqrt{\delta^2 + 4\lambda^2\bar{n}\left(1 - \frac{\bar{n}-1}{N}\right)}\right) \tag{3.3.3}$$

$$t_{r,\delta} = \frac{2\pi}{\sqrt{\delta^2 + 4\lambda^2(\bar{n}+1)\left(1 - \frac{\bar{n}}{N}\right)} - \sqrt{\delta^2 + 4\lambda^2\bar{n}\left(1 - \frac{\bar{n}-1}{N}\right)}} \tag{3.3.4}$$

from which we may calculate the revival time values for each case of δ shown in Figure 3.3.1. For example, the new revival time for $\delta = 10$ is approximately $t_{r,10} \approx 1.78$ and for $\delta = 25$ the revival time is at $t_{r,25} \approx 3.61$.

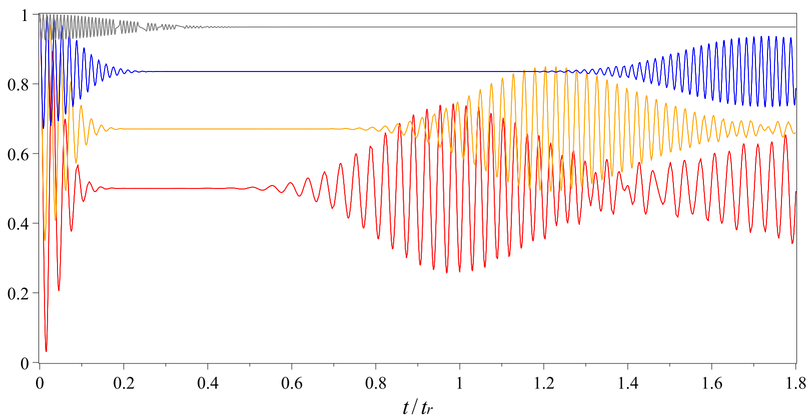

Figure 3.3.1: The probability of the qubit being in the state $|g\rangle$ for four different values of δ. The initial qubit state is $|g\rangle$ with $\bar{n} = 16$, $N = 120$ and $\phi = 0$. The red curve is for $\delta = 0$, orange $\delta = 5$, blue $\delta = 10$ and grey $\delta = 25$.

For a clearer picture on the overall effects of detuning to the one-qubit big spin system, we plot Figure 3.3.2 to show the changes in the system at detuning $\delta = 5$. From the figure we can see that not only does the non-zero detuning affect the average qubit state probability $P_g(t)$ and the revival time t_r, but it also changes the expected value of the attractor state $P^+_{1,att}(t)$ and linear entropy $S^L_q(t)$ of the qubit.

At the attractor time $\frac{t_{r,5}}{2}$, there is an increase in the entropy value. The quantity no longer approaches close to zero as it was observed in the system with zero detuning value. At the same time, in contrast the probability of being in the attractor state $P^+_{1,att}(t)$ reduces slightly from unity. Therefore, a conclusion on the entanglement or purity of the system can be made where we can say that the occurrence of detuning δ in this interacting model has prevented the qubit from easily disentangling with the big spin, and either subsystem remains as a more mixed state at this particular time. Again, these changes towards the increment in the δ value are similar to the effects shown in the one-qubit Jaynes-Cummings model with non-zero detunings.

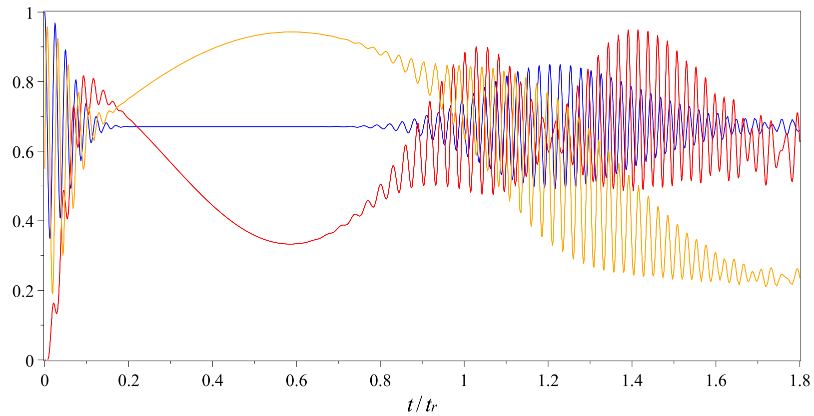

Figure 3.3.2: Time evolution of one-qubit big spin system when the qubits are started in the initial state $|g\rangle$ with $\bar{n} = 16$, $N = 120$, $\phi = 0$ and $\delta = 5$. The red curve is for entropy of the reduced density matrix, blue is for the probability of the qubit being in state $|g\rangle$ and orange is for the probability of the qubit being in attractor state $\left|\psi^+_{1,att}\right\rangle_N$.

3.3.2 Error Modelling: a Distribution of Detunings

In this section we consider one-qubit big spin interacting model with errors in the detunings. Similar to our discussion in Section 3.2.2, we apply an analogous method with the one-qubit Jaynes-Cumming model on this system, where we average over the detuning with a distribution of standard deviation Δ. To model the a practical scenario where the desired detuning is zero but allowing for errors, we consider a Gaussian distribution of detunings centred at expectation value zero as defined by Equation (3.2.5). A discrete approximation of density matrix with a sufficiently large number of δ values and averaged over the distributed error as given by Equation (3.2.7) is used to analyse the time evolutions of the erroneous system.

We calculate the probability of the qubit being in the ground states $P_g(t)$, the linear entropy $S_q^L(t)$ and the probability of the qubit being in the one-qubit attractor state $P^+_{1,att}(t)$. We plot Figure 3.2.4 to show the time evolutions of this interaction system for several values of error distribution widths Δ, and the results are presented as Figure 3.3.3. We choose $\Delta = 0.3$, $\Delta = 0.5$ and $\Delta = 0.7$ to compare with the desired system of zero detuning as depicted in Figure 2.3.1.

From the plot, we can observe some changes in the time evolutions which indicates the effects of decoherence on the system's dynamics especially at the revival time t_r. The probability of our qubit state remains averaged at approximately $P_g(t) = 0.5$. However, we can see that as we increase the value of error distribution width Δ, the amplitude of the revival at t_r decreases. This is due to the mixture over different revival times considered within the range of the error distribution. The same pattern of amplitude reductions with respect to the increasing error width is shown in the one-qubit attractor state probability $P^+_{1,att}(t)$ curve. At the revival time t_r, we can see that the amplitude of the orange line reduces significantly.

There are also changes in the linear entropy $S_q^L(t)$ of the system, where the dip in this quantity at time t_r has been filled in. This suggests that at the revival time, the error has its effects on the purity of the qubit subsystem. Although we can see an almost similar phenomena was also shown in Figure 3.3.1 for the case of $\Delta = 0$, where the dip in the entropy line does not goes near to zero at time t_r due to the very short time scale in this system with finite value of N, but the shallower dips in this quantity at the respective time as shown in Figure 3.3.3 are telling us that the subsystems now are more of a mixed state. This means that the disentanglement between the qubit and big spin components have becoming harder as Δ increases. This is due to the overall state of the system that is no longer a pure state as a result of decoherence.

We continue our study with larger values of error to investigate the maximum value of Δ that the revival of the qubit state oscillation can hold. We plot the qubit

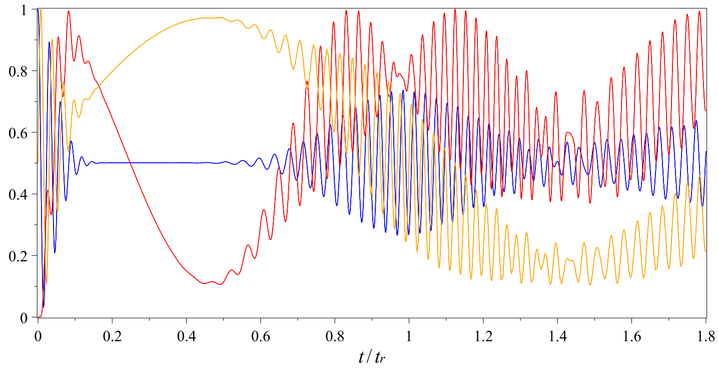

(a) $\Delta = 0.3$

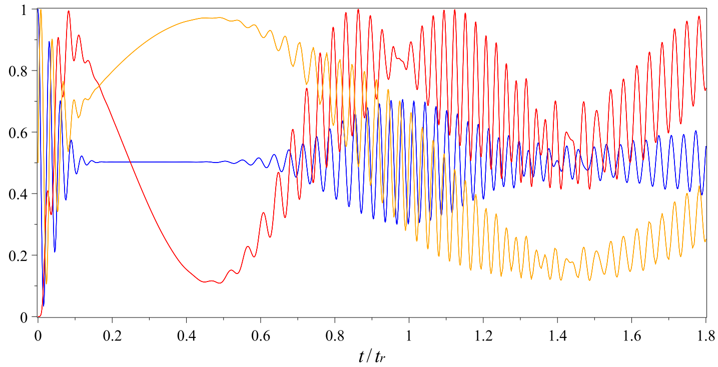

(b) $\Delta = 0.5$

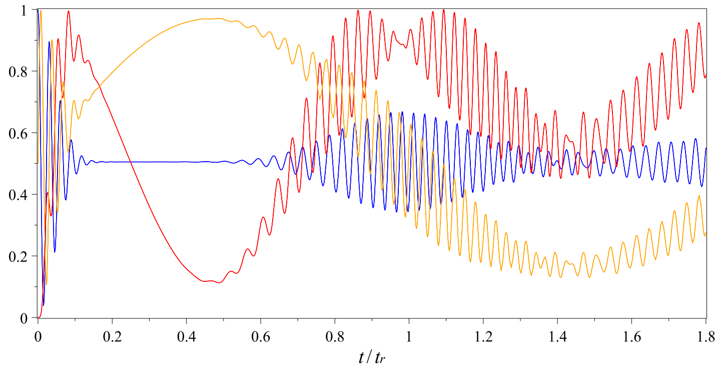

(c) $\Delta = 0.7$

Figure 3.3.3: Plots comparing qubit linear entropies (red), probability of the qubit being in state $|g\rangle$ (blue) and the probability of the qubit being in attractor state $\left|\psi^{+}_{1,att}\right\rangle_N$ (orange) for one-qubit big spin model of initial qubit state $|g\rangle$, $\bar{n} = 36$, $N = 120$ and the initial phase of the radiation field $\phi = 0$ with decoherence effects. Figure (a) shows the differences in the system with $\Delta = 0.3$, (b) shows the differences in the system with $\Delta = 0.5$ and (c) shows the differences in the system with $\Delta = 0.7$.

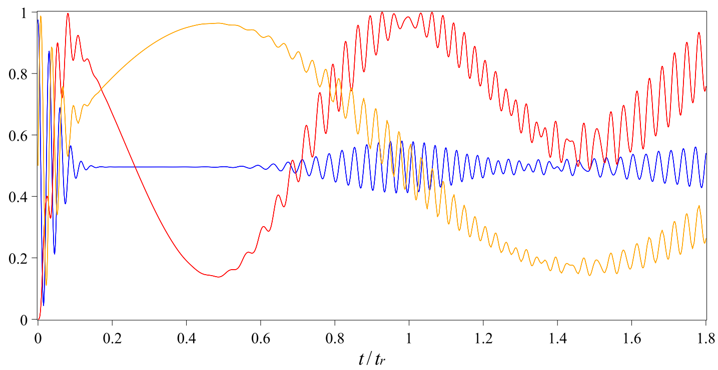

(a) $\Delta = 1.5$

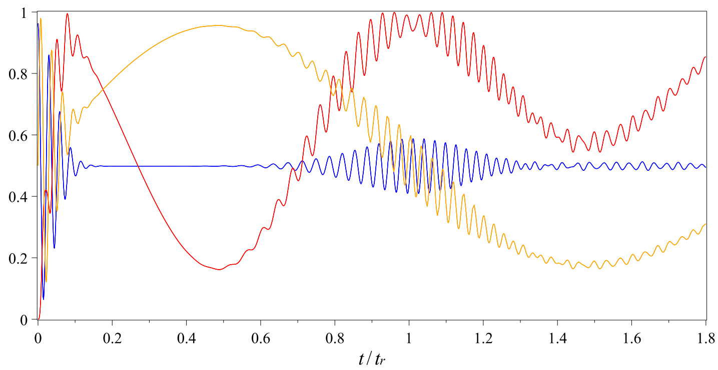

(b) $\Delta = 2.0$

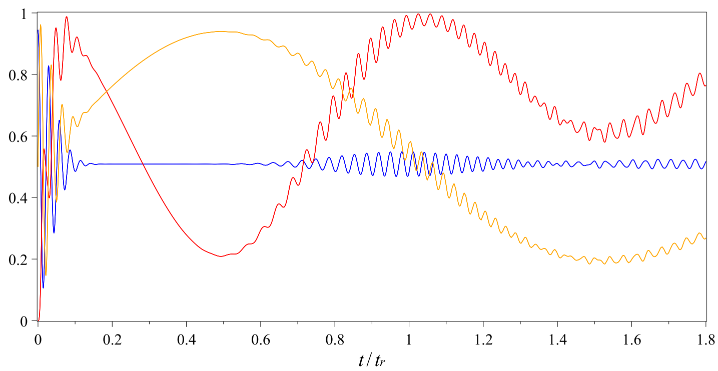

(c) $\Delta = 3.0$

Figure 3.3.4: Plots comparing qubit linear entropies (red), probability of the qubit being in state $|g\rangle$ (blue) and the probability of the qubit being in attractor state $\left|\psi^{+}_{1,att}\right\rangle_N$ (orange) for one-qubit big spin model of initial qubit state $|g\rangle$, $\bar{n} = 36$, $N = 120$ and the initial phase of the radiation field $\phi = 0$ with decoherence effects. Figure (a) shows the differences in the system with $\Delta = 1.5$, (b) shows the differences in the system with $\Delta = 2.0$ and (c) shows the differences in the system with $\Delta = 3.0$.

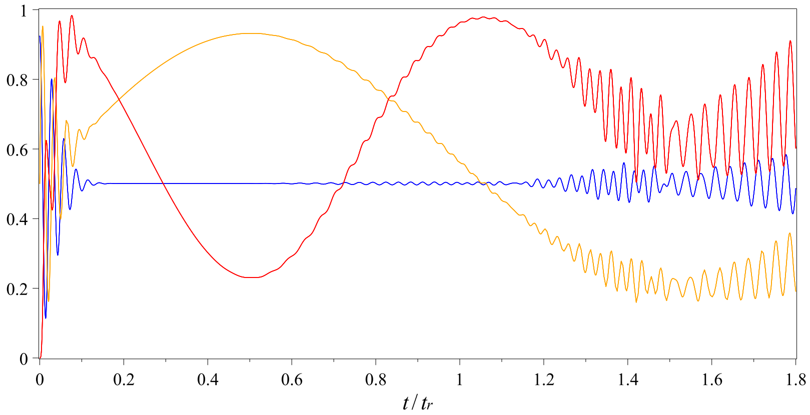

Figure 3.3.5: Time evolution of one-qubit big spin system when the qubit started in the initial state $|g\rangle$ with $\bar{n} = 16$, $N = 120$, $\phi = 0$ and $\Delta = 3.5$. The red curve is for entropy of the reduced density matrix, blue is for the probability of the qubit being in state $|g\rangle$ and orange is for the probability of the qubit being in attractor state $\left|\psi^{+}_{1,att}\right\rangle_{N}$.

state probability with various Δ values in Figure 3.3.4. For comparisons, we use similar error distribution width values to those for the case of one-qubit Jaynes-Cummings model plotted as Figure 3.2.5 in Section 3.2.2. From comparison, we can see similar attributes against the increment of Δ in our one-qubit big spin system, where a lower revival amplitude is observed in the system with a bigger value of Δ. However, as opposed to the one-qubit Jaynes-Cummings model where the revival completely diminished at $\Delta = 3.0$, a slower reaction to error is observed in our one-qubit big spin model. There is still revival in qubit state oscillation occurs at t_r. The oscillations only completely disappear at $\Delta = 3.5$ as shown in Figure 3.3.5, where the curves for both one-qubit attractor state and linear entropy also become a thin line.

3.4 Summary

We have shown the effects of detunings in both the one-qubit Jaynes-Cummings as well as the one-qubit big spin models. We first analysed the systems with a non-zero frequency detuning and observed the the differences Hamiltonian evolution of these systems when such detuning is applied.

We then considered the more realistic and practical case of detuning where we analysed both interacting systems with an error given by a Gaussian distribution of detunings. In this work, we limited our analysis to the error scenario where the desired evolution is for zero detuning, when the entangling and other effects are most pronounced. However, in an experiment which is deliberately set up to realise off-resonant dynamics, the detuning would be set to some chosen value. In this case we could model errors (and thus decoherence) by choosing a distribution that has a finite width but peaks at this value of detuning, instead of peaking at zero.

It is clear that such non-zero detunings have affected and changed the time evolutions of both one-qubit Jaynes-Cummings as well as one-qubit big spin interacting systems in similar manner. Nevertheless, the results also show that the big spin system is a little more resilient against increasing error width compared to the field mode case.

Chapter 4

Two-Qubit Interacting Systems

4.1 Introduction

There have been numerous extended studies of the Jaynes-Cummings model conducted to identify the similarities, differences, fundamental features and potential applications of these systems. For example Chumakov *et al.* have made a detailed study on the many-qubit Jaynes-Cummings model, where they analysed the interaction of multiple two-level atoms and a strong quantised electromagnetic field in a lossless cavity [71]. They presented the time evolution and demonstrated many interesting events coming out of such a system, like the factorisation of the wave function, trapping states, collapses and revivals of atomic inversion and the field distribution.

Other studies on similar multi-qubit models have also been conducted by considering a very large $\bar{n}$ approximation [27, 28, 72, 73, 74]. As a part of their works, a detailed study on a specific case of two qubits interacting with a coherent state have been carried out by C. Jarvis and collaborators [27, 64]. They have demonstrated the time evolution of the system and made many important discoveries especially on the occurrence of attractor state in the system, as well as qubit-qubit entanglement and their dependency on a set of qubits initial conditions.

In Section 2.3.1, we have seen the correspondence between a collection of N spin called 'the big spin' $\left|\frac{\zeta}{\sqrt{N}}\right\rangle$ with coherent state $|\alpha\rangle$. With this fact, a one-qubit big spin interaction model has been proposed [29] and discussed in the same section. In this chapter, by using a similar correspondence we propose a new model that incorporates some selected features of the earlier works into a different hybrid system with qubits, where in this model we investigate a system of two qubits interacting with the big spin.

We will start by introducing the two-qubit Jaynes-Cummings model and all its important features that have been discussed in [27, 64]. In the first half of this chapter, we will reproduce these results in order for us to understand the basics and all the features that come out of an interacting system with two qubits. We will then introduce the two-qubit big spin model and discuss its interesting time evolutions. We demonstrate the appearance of important phenomena including the collapse and revival of Rabi oscillations, the attractor and the cat states of the system, as well as the dynamics of the entanglement between the two specific qubits in the system.

4.2 Two Qubits Interacting With A Single Mode Of A Field At Zero Detuning

Adding an extra qubit into the one-qubit Jaynes-Cummings model indeed increases the complexity of the system. However, with an extra qubit in the system more interesting features can be studied from such interaction of the qubits and the field mode. For example, in this new set up, besides the entanglement between the qubits and the field, the entanglement between the qubits themselves can also be observed. To study all the features in the system, we have to find its wavefunction, which will be calculated in detail in this section. Note that all these calculation have been made by C.Jarvis [27, 64]. Here we reproduce these analytic calculations, and present equivalent numerical results, as we will then be using similar techniques and calculating comparable quantities in order to study our new system in the following Section 4.3.

4.2.1 Two-Qubit Jaynes-Cummings Hamiltonian

A multi-qubit Jaynes-Cummings Hamiltonian for the interaction of a bosonic field mode with q qubits can written in the form of

$$\hat{H}_q = \hbar\omega\hat{a}^\dagger\hat{a} + \frac{\hbar}{2}\sum_{i=1}^{q}\Omega_i\hat{\sigma}_i^z + \hbar\sum_{i=1}^{q}\lambda_i(\hat{a}^\dagger\hat{\sigma}_i^+ + \hat{a}\hat{\sigma}_i^-). \tag{4.2.1}$$

This is called Tavis-Cummings Hamiltonian [61] where $\hat{\sigma}_i^z = |e_i\rangle\langle e_i| - |g_i\rangle\langle g_i|$, $\hat{\sigma}_i^+ = |e_i\rangle\langle g_i|$ and $\hat{\sigma}_i^- = |g_i\rangle\langle e_i|$ are the qubit operators, $\hat{a}^\dagger$ and $\hat{a}$ are respectively the creation and annihilation operators for a photon with frequency ω, and λ_i is the cavity-i-th qubit coupling constant. Each qubit is labeled by a subscript i and has a ground state $|g_i\rangle$as well as an excited state $|e_i\rangle$. With an energy $\epsilon_{g,i}$ for the ground state and $\epsilon_{e,i}$ for the excited state, we may calculate each qubit frequency by $\hbar\Omega_i = \epsilon_{e,i} - \epsilon_{g,i}$.

In this section, we will consider the case of two identical qubits ($q = 2$) interacting with a coherent field $|\alpha\rangle$. The Hamiltonian (4.2.1) is then reduced to

$$\hat{H}_2 = \hbar\omega(\hat{a}^\dagger\hat{a}) + \frac{\hbar}{2}(\omega_1\hat{\sigma}_1^z + \omega_2\hat{\sigma}_2^z) + \hbar\lambda_1\left(\hat{a}\hat{\sigma}_1^+ + \hat{a}^\dagger\hat{\sigma}_2^-\right) + \hbar\lambda_2\left(\hat{a}\hat{\sigma}_2^+ + \hat{a}^\dagger\hat{\sigma}_2^-\right). \tag{4.2.2}$$

The total number of quanta in this two-qubit Jaynes-Cummings model case is represented as an operator

$$\hat{M}_2 = \hat{a}^\dagger\hat{a} + \hat{\sigma}_1^+\hat{\sigma}_1^- + \hat{\sigma}_2^+\hat{\sigma}_2^-. \tag{4.2.3}$$

This operator commutes with the Hamiltonian (4.2.2) as

$$\left[\hat{H}_2, \hat{M}_2\right] = 0. \tag{4.2.4}$$

So the number of excitations in this system is conserved.

For this two-qubit case, we assume that each qubit independently interacts with the field mode by a similar way to the one-qubit Jaynes-Cummings system and no direct interaction happens between the two qubits. With the possibility of each qubit absorbing at most one photon„ the field mode could now differ by up to two photons and the field could be in states $|n\rangle$, $|n+1\rangle$ and $|n+2\rangle$.

4.2.2 Eigenvalues, Eigenvectors and Exact Solution

In order to find the solution to the dynamics of two-qubit Jaynes-Cummings model, we first find the eigenvalues and the eigenvectors of the Hamiltonian by solving the eigenvalue equation

$$\hat{H}_2|\psi\rangle = E|\psi\rangle. \tag{4.2.5}$$

We will then take an initial state at time $t = 0$ and decompose it into these eigenstates that will lead us to the general time dependence (from the eigenvalues) for this initial state.

At time $t = 0$, the prepared wavefunction is assumed to be a general product state of the field and the qubits which is given by

$$|\Psi_2(0)\rangle = |\psi(0)\rangle|\psi_2(0)\rangle \tag{4.2.6}$$

and the general decomposition of an eigenstate solution to Equation (4.2.5) is in the form of

$$|\Psi_2\rangle = \sum_{n=0}^{\infty} \left(a_{ee,n}|ee,n\rangle + a_{eg,n}|eg,n\rangle + a_{ge,n}|ge,n\rangle + a_{gg,n}|gg,n\rangle\right) \tag{4.2.7}$$

where $|ee\rangle$ is shorthand for $|e_1\rangle|e_2\rangle$ and *etc.*

Now we can solve Equation (4.2.5) by operating the Hamitonian (4.2.2) on the general form for an eigenstate given by Equation (4.2.7). With the solutions and after we rearrange them in states with the same number of excitations $|ee,n\rangle$ $|eg,n+1\rangle$, $|ge,n+1\rangle$ and $|gg,n+2\rangle$, we get

$$\begin{aligned}
\hat{H}_2|\Psi_2\rangle = \sum_{n=0}^{\infty} \Bigg[\\
&+ \left[\hbar(\omega n + \frac{\Omega_1}{2} + \frac{\Omega_2}{2})a_{ee,n} + \hbar\sqrt{n+1}(\lambda_1 a_{ge,n+1} + \lambda_2 a_{eg,n+1})\right]|ee,n\rangle \\
&+ \left[\hbar\left(\omega(n+1) + \frac{\Omega_1}{2} - \frac{\Omega_2}{2}\right)a_{eg,n+1} + \hbar\lambda_1\sqrt{n+2}a_{gg,n+2} + \hbar\lambda_2\sqrt{n+1}a_{ee,n}\right]|eg,n+1\rangle \\
&+ \left[\hbar\left(\omega(n+1) - \frac{\Omega_1}{2} + \frac{\Omega_2}{2}\right)a_{ge,n+1} + \hbar\lambda_1\sqrt{n+1}a_{ee,n} + \hbar\lambda_2\sqrt{n+2}a_{gg,n+2}\right]|ge,n+1\rangle \\
&+ \left[\hbar\left(\omega(n+2) - \frac{\Omega_1}{2} - \frac{\Omega_2}{2}\right)a_{gg,n+2} + \hbar\sqrt{n+2}(\lambda_1 a_{eg,n+1} + \hbar\lambda_2 a_{ge,n+1})\right]|gg,n+2\rangle \Bigg] \\
&+ \left[(\hbar\omega - \frac{\hbar\Omega_1}{2} - \frac{\hbar\Omega_2}{2})a_{gg,1} + \hbar\lambda_1 a_{eg,0} + \hbar\lambda_2 a_{ge,0}\right]|gg,1\rangle \\
&+ \left[(-\frac{\hbar\Omega_1}{2} + \frac{\hbar\Omega_2}{2})a_{ge,0} + \lambda_2 a_{gg,1}\right]|ge,0\rangle + \left[(\frac{\hbar\Omega_1}{2} - \frac{\hbar\Omega_2}{2})a_{eg,0} + \lambda_1 a_{gg,1}\right]|eg,0\rangle \\
&- (\frac{\hbar\Omega_1}{2} + \frac{\hbar\Omega_2}{2})a_{gg,0}|gg,0\rangle .
\end{aligned} \tag{4.2.8}$$

Since the number of excitations is conserved, the system can be decomposed into m_2 decoupled sectors, where m_2 is a number of different sectors that is equal to the number of different values that the eigenvalue of $\hat{M}_2$ can take for this system. So we may put this equation into a matrix form given by

$$\hat{H}_2|\Psi_2\rangle = \sum_{n=0}^{\infty} \begin{pmatrix} \upsilon_{1,1} & \upsilon_{1,2} & \upsilon_{1,3} & \upsilon_{1,4} \\ \upsilon_{2,1} & \upsilon_{2,2} & \upsilon_{2,3} & \upsilon_{2,4} \\ \upsilon_{3,1} & \upsilon_{3,2} & \upsilon_{3,3} & \upsilon_{3,4} \\ \upsilon_{4,1} & \upsilon_{4,2} & \upsilon_{4,3} & \upsilon_{4,4} \end{pmatrix} |\Psi_2\rangle \tag{4.2.9}$$

where the entries are

$$
\begin{aligned}
&\upsilon_{1,1} = \hbar\omega n + \tfrac{\hbar\Omega_1}{2} + \tfrac{\hbar\Omega_2}{2} && \upsilon_{1,2} = \hbar\lambda_2\sqrt{n+1} \\
&\upsilon_{1,3} = \hbar\lambda_1\sqrt{n+1} && \upsilon_{1,4} = 0 \\
&\upsilon_{2,1} = \hbar\lambda_2\sqrt{n+1} && \upsilon_{2,2} = \hbar\omega(n+1) + \tfrac{\hbar\Omega_1}{2} - \tfrac{\hbar\Omega_2}{2} \\
&\upsilon_{2,3} = 0 && \upsilon_{2,4} = \hbar\lambda_1\sqrt{n+2} \\
&\upsilon_{3,1} = \hbar\lambda_1\sqrt{n+1} && \upsilon_{3,2} = 0 \\
&\upsilon_{3,3} = \hbar\omega(n+1) - \tfrac{\hbar\Omega_1}{2} + \tfrac{\hbar\Omega_2}{2} && \upsilon_{3,4} = \hbar\lambda_2\sqrt{n+2} \\
&\upsilon_{4,1} = 0 && \upsilon_{4,2} = \hbar\lambda_1\sqrt{n+2} \\
&\upsilon_{4,3} = \hbar\lambda_2\sqrt{n+2} && \upsilon_{4,4} = \hbar\omega(n+2) - \tfrac{\hbar\Omega_1}{2} - \tfrac{\hbar\Omega_2}{2}.
\end{aligned}
$$

This matrix is for each of the m_2 sectors and these amplitudes will form quartets of states except for $|gg,0\rangle$, $|ge,0\rangle$, $|eg,0\rangle$ and $|gg,1\rangle$ that are left out on their own.

In this chapter, we consider the atomic and the field inversion frequencies to be at resonance as well as the field and the qubits to be at a uniform dipole-interaction coupling. We will consider the cases of non-resonant frequency and different couplings in Chapter 5 and Chapter 6 respectively. So for all i in equations above, we have $\omega = \Omega_i$ and $\lambda = \lambda_i$ where $i = 1, 2$. We may find the eigenvalues and eigevectors for each of the m sectors by diagonalising Matrix (4.2.9) and this gives us four non-zero eigenvalues. For $n = 0$

$$E_{0,n} = E_{d,n} = \hbar\omega(n+1) \tag{4.2.10}$$

and for the case where $n \geq 1$

$$E_{\pm,n} = \hbar\omega(n+1) \pm \hbar\lambda\sqrt{2(2n+3)}. \tag{4.2.11}$$

For the lower energy levels from outside the summation, the eigenvalues are

$$E_{\pm,-1} = \pm\sqrt{2}\hbar\lambda \tag{4.2.12}$$

$$E_{d,-1} = 0 \tag{4.2.13}$$

$$E_{g,0} = -\hbar\omega. \tag{4.2.14}$$

From these eigenvalues, we find the corresponding eigenvectors. Three of them lie only in the symmetric (with respect to exchange of the two qubits) subspace and are given by

$$|\pm, n\rangle_2 = \sqrt{\frac{n+1}{2(2n+3)}}\,|ee, n\rangle \pm \frac{1}{2}(|eg, n+1\rangle + |ge, n+1\rangle) + \sqrt{\frac{n+2}{2(2n+3)}}\,|gg, n+2\rangle \tag{4.2.15}$$

$$|0, n\rangle_2 = -\sqrt{\frac{n+2}{2n+3}}\,|ee, n\rangle + \sqrt{\frac{n+1}{2n+3}}\,|gg, n+2\rangle \tag{4.2.16}$$

where the subscript "2" is used to differentiate these vectors from the vectors in the one qubit cases. Another eigenvector is in the antisymmetric subspace and is known as a dark state. It is a state where no photon emission occurs because as the first qubit emits a photon, the second photon will immediately absorb it and it is antisymmetric because the exchange of the qubits gives a minus sign. This state is written as

$$|d, n\rangle_2 = \frac{1}{\sqrt{2}}(|ge, n+1\rangle - |eg, n+1\rangle). \tag{4.2.17}$$

We can also find the rest of the unpaired eigenvectors and they are in the following forms:

$$|\pm, -1\rangle_2 = \pm\frac{1}{2}\,(|eg, 0\rangle + |ge, 0\rangle) + \frac{1}{\sqrt{2}}\,|gg, 1\rangle \tag{4.2.18}$$

$$|d, -1\rangle_2 = \frac{1}{\sqrt{2}}\,(|ge, 0\rangle - |eg, 0\rangle) \tag{4.2.19}$$

$$|gg, 0\rangle \tag{4.2.20}$$

We can transform the basis vectors $|ee, n\rangle$, $|eg, n+1\rangle$, $|ge, n+1\rangle$ and $|gg, n+2\rangle$ in terms of eigenvectors as

$$|ee,n\rangle = \sqrt{\frac{n+1}{2(2n+3)}}(|+,n\rangle + |-,n\rangle) - \sqrt{\frac{n+2}{2n+3}}\,|0,n\rangle \tag{4.2.21}$$

$$|eg,n+1\rangle = \frac{1}{2}(|+,n\rangle + |-,n\rangle) - \frac{1}{\sqrt{2}}\,|d,n\rangle \tag{4.2.22}$$

$$|ge,n+1\rangle = \frac{1}{2}(|+,n\rangle + |-,n\rangle) + \frac{1}{\sqrt{2}}\,|d,n\rangle \tag{4.2.23}$$

$$|gg,n+2\rangle = \sqrt{\frac{n+2}{2(2n+3)}}(|+,n\rangle + |-,n\rangle) - \sqrt{\frac{n+1}{2n+3}}\,|0,n\rangle \tag{4.2.24}$$

$$|eg,0\rangle = \frac{1}{2}(|+,-1\rangle + |-,-1\rangle) - \frac{1}{\sqrt{2}}\,|d,-1\rangle \tag{4.2.25}$$

$$|ge,0\rangle = \frac{1}{2}(|+,-1\rangle + |-,-1\rangle) + \frac{1}{\sqrt{2}}\,|d,-1\rangle \tag{4.2.26}$$

$$|gg,1\rangle = \frac{1}{\sqrt{2}}(|+,n\rangle + |-,n\rangle). \tag{4.2.27}$$

We can then decompose this general form into the eigenstates by using the state $|\Psi_2(0)\rangle$ as given by Equation (4.2.6). Therefore, we have

$$\begin{aligned}|\Psi_2(0)\rangle = \sum_{n=0}^{\infty} &(C_n C_{ee}\,|ee,n\rangle + C_{n+1}C_{eg}\,|eg,n+1\rangle + C_{n+1}C_{ge}\,|ge,n+1\rangle \\ &+ C_{n+2}C_{gg}\,|gg,n+2\rangle\,) + C_0C_{eg}\,|eg,0\rangle + C_0C_{ge}\,|ge,0\rangle + C_1C_{gg}\,|gg,1\rangle \\ &+ C_0C_{gg}\,|gg,0\rangle\end{aligned} \tag{4.2.28}$$

and by changing its basis, we have

$$\begin{aligned}|\Psi_2(0)\rangle = \sum_{n=0}^{\infty} \Bigg[\\ &\left(C_nC_{ee}\frac{\sqrt{n+1}}{\sqrt{2(2n+3)}} + \frac{C_{n+1}}{2}(C_{eg}+C_{ge}) + C_{n+2}C_{gg}\frac{\sqrt{n+2}}{\sqrt{2(2n+3)}}\right)|+,n\rangle \\ &+ \left(C_nC_{ee}\frac{\sqrt{n+1}}{\sqrt{2(2n+3)}} - \frac{C_{n+1}}{2}(C_{eg}+C_{ge}) + C_{n+2}C_{gg}\frac{\sqrt{n+2}}{\sqrt{2(2n+3)}}\right)|-,n\rangle \\ &+ \left(C_{n+2}C_{gg}\frac{\sqrt{n+1}}{\sqrt{n+1}} - C_nC_{ee}\frac{\sqrt{n+2}}{\sqrt{2n+3}}\right)|0,n\rangle + \frac{C_{n+1}}{\sqrt{2}}(C_{ge}-C_{eg})\,|d,n\rangle\Bigg] \\ &+ (\frac{C_0}{2}(C_{eg}+C_{ge}) + \frac{1}{\sqrt{2}}C_1C_{gg})\,|+,-1\rangle + \frac{C_0}{\sqrt{2}}(C_{ge}-C_{eg})\,|d,-1\rangle \\ &+ (-\frac{C_0}{2}(C_{eg}+C_{ge}) + \frac{1}{\sqrt{2}}C_1C_{gg})\,|-,-1\rangle + C_0C_{gg}\,|gg,0\rangle\end{aligned} \tag{4.2.29}$$

From this, we can now calculate

$$|\Psi_2(t)\rangle = e^{-i\hat{H}_2 t/\hbar}\,|\Psi_2(0)\rangle \tag{4.2.30}$$

by including the time dependence of the eigenstates and then rewrite the solution back in terms of $|ee, n\rangle$, $|eg, n+1\rangle$, $|ge, n+1\rangle$ and $|gg, n+2\rangle$. It is desirable to put the eigenstates back in terms of these basis states as these are the "logical" basis states that measurements would project to. With $e^{ix} = \cos x + i \sin x$, we get

$$\begin{aligned}
|\Psi_2(t)\rangle = \sum_{n=0}^{\infty} e^{-i\omega(n+1)} \Bigg(\Bigg[& \frac{C_n C_{ee}}{2n+3}\Big((n+1)\cos\Big(\lambda t\sqrt{2(2n+3)}\Big) + (n+2)\Big) \\
&+ C_{gg}C_{n+2}\frac{\sqrt{n+1}\sqrt{n+2}}{2n+3}\Big(\cos\Big(\lambda t\sqrt{2(2n+3)}\Big) - 1\Big) \\
&- iC_{n+1}\frac{\sqrt{n+1}}{\sqrt{2(2n+3)}}\sin\Big(\lambda t\sqrt{2(2n+3)}\Big)(C_{eg}+C_{ge})\Bigg]\,|ee, n\rangle \\
&+ \Bigg[-\frac{i\sin\Big(\lambda t\sqrt{2(2n+3)}\Big)}{\sqrt{2(2n+3)}}\Big(\sqrt{n+1}C_n C_{ee} + \sqrt{n+2}C_{n+2}C_{gg}\Big) \\
&+ \frac{C_{n+1}}{2}\cos\Big(\lambda t\sqrt{2(2n+3)}\Big)(C_{eg}+C_{ge}) + \frac{C_{n+1}}{2}(C_{eg}-C_{ge})\Bigg]\,|eg, n+1\rangle \\
&+ \Bigg[-\frac{i\sin\Big(\lambda t\sqrt{2(2n+3)}\Big)}{\sqrt{2(2n+3)}}\Big(\sqrt{n+1}C_n C_{ee} + \sqrt{n+2}C_{n+2}C_{gg}\Big) \\
&+ \frac{C_{n+1}}{2}\cos\Big(\lambda t\sqrt{2(2n+3)}\Big)(C_{eg}+C_{ge}) - \frac{C_{n+1}}{2}(C_{eg}-C_{ge})\Bigg]\,|ge, n+1\rangle \\
&+ \Bigg[C_{ee}C_n\frac{\sqrt{n+1}\sqrt{n+2}}{2n+3}\Big(\cos\Big(\lambda t\sqrt{2(2n+3)}\Big) - 1\Big) \\
&+ \frac{C_{gg}C_{n+2}}{2n+3}\Big((n+2)\cos\Big(\lambda t\sqrt{2(2n+3)}\Big) + (n+1)\Big) \\
&- iC_{n+1}\sqrt{\frac{n+2}{2(2n+3)}}\sin\Big(\lambda t\sqrt{2(2n+3)}\Big)(C_{eg}+C_{ge})\Bigg]\,|gg, n+2\rangle\Bigg) \\
&+ e^{-i\omega t}\Bigg[-\frac{iC_0}{\sqrt{2}}(C_{eg}+C_{ge})\sin\Big(\sqrt{2}\lambda t\Big) + \frac{1}{2}C_1 C_{gg}\cos\Big(\sqrt{2}\lambda t\Big)\Bigg]\,|gg, 1\rangle \\
&+ e^{-i\omega t}\Bigg[\frac{C_0}{2}(C_{eg}+C_{ge})\cos\Big(\sqrt{2}\lambda t\Big) - \frac{i}{\sqrt{2}}C_1 C_{gg}\sin\Big(\sqrt{2}\lambda t\Big)\Bigg](\,|eg, 0\rangle + |ge, 0\rangle\,) \\
&+ e^{-i\omega t}\frac{C_0}{2}(C_{eg}-C_{ge})(\,|ge, 0\rangle - |eg, 0\rangle\,) + e^{i\frac{\omega}{2}t}C_0 C_{gg}\,|gg, 0\rangle\,.
\end{aligned} \tag{4.2.31}$$

Similar to the single qubit case considered in Section 2.2.3, we can then transform into an interaction picture and remove basic time dependence of the states to become implicit for ease of calculations. This equation loses its dependency on ω by making the following state transformations

$$e^{-i\omega t}\left|ee\right\rangle \rightarrow \left|ee\right\rangle \tag{4.2.32}$$

$$\left|eg\right\rangle \rightarrow \left|eg\right\rangle \tag{4.2.33}$$

$$\left|ge\right\rangle \rightarrow \left|ge\right\rangle \tag{4.2.34}$$

$$e^{i\omega t}\left|gg\right\rangle \rightarrow \left|gg\right\rangle \tag{4.2.35}$$

$$e^{-i\omega n t}\left|n\right\rangle \rightarrow \left|n\right\rangle . \tag{4.2.36}$$

4.2.3 Two-Qubit Attractor States

In Section 2.2.5 we have seen that in a one-qubit Jaynes-Cummings model with large $\bar{n}$ approximation, every initial qubit state will approach a one-qubit attractor $\left|\psi^{\pm}_{1,att}\right\rangle$ at the attractor time $\frac{t_r}{2}$ regardless of the qubit initial state. C.Jarvis *et.al* then extended this analysis for the case of two qubits under the same $\bar{n}$ approximation [28, 27]. They discovered that different to the case of a single qubit, the attractor state in the case of two-qubit Jaynes-Cummings model behaves differently with respect to the initial state of the qubits as will be discussed in this section.

With the general solution given by Equation (4.2.31), we can now consider a two-qubit Jaynes-Cummings system with an initial state

$$\left|\Psi_2(0)\right\rangle = \left|\alpha\right\rangle \left|\psi_2\right\rangle , \tag{4.2.37}$$

where $\left|\alpha\right\rangle$ is a coherent state given by Equation (1.2.3)

$$\left|\alpha\right\rangle = e^{-\frac{|\alpha|^2}{2}} \sum_{n=0}^{\infty} \frac{\alpha^n}{\sqrt{n!}} \left|n\right\rangle \qquad , \qquad \alpha = |\alpha| e^{-i\theta} \tag{4.2.38}$$

and $\left|\psi_2\right\rangle$ is the two-qubit state in the form of

$$\left|\psi_2\right\rangle = C_{ee}\left|ee\right\rangle + C_{eg}\left|eg\right\rangle + C_{ge}\left|ge\right\rangle + C_{gg}\left|gg\right\rangle . \tag{4.2.39}$$

This state is normalised so that $|C_{ee}|^2 + |C_{eg}|^2 + |C_{ge}|^2 + |C_{gg}|^2 = 1$. With large $\bar{n}$, we may approximate

$$\sqrt{2(2n+3)} \approx 2\sqrt{n} \tag{4.2.40}$$
$$n+2 \approx n \tag{4.2.41}$$
$$n+1 \approx n \tag{4.2.42}$$

and we can also transform the *cosine* and *sine* terms into an exponential form of

$$\cos x = \frac{1}{2}\left(e^{ix} + e^{-ix}\right) \tag{4.2.43}$$
$$\sin x = \frac{1}{2i}\left(e^{ix} - e^{-ix}\right). \tag{4.2.44}$$

We may then rewrite Equation (4.2.31) as

$$\begin{aligned}
\left|\widetilde{\Psi}_2(t)\right\rangle = \sum_{n=0}^{\infty} \Bigg(& \frac{1}{2}\big[(C_{ee}C_n - C_{gg}C_{n+2})\left|ee,n\right\rangle \\
& + (C_{eg} - C_{ge})C_{n+1}(\left|eg,n+1\right\rangle - \left|ge,n+1\right\rangle) \\
& + (-C_{ee}C_n + C_{gg}C_{n+2})\left|gg,n+2\right\rangle\big] \\
& + \frac{e^{2i\lambda t\sqrt{n}}}{4}\big[(C_{ee}C_n + C_{gg}C_{n+2}) - (C_{eg} - C_{ge})C_{n+1}\left|ee,n\right\rangle \\
& + ((C_{eg} + C_{ge})C_{n+1} - C_{ee}C_n - C_{gg}C_{n+2})(\left|eg,n+1\right\rangle + \left|ge,n+1\right\rangle) \\
& (C_{ee}C_n + C_{gg}C_{n+2} - (C_{eg} - C_{ge})C_{n+1})\left|gg,n+2\right\rangle\big] \\
& + \frac{e^{-2i\lambda t\sqrt{n}}}{4}\big[(C_{ee}C_n + C_{gg}C_{n+2}) + (C_{eg} - C_{ge})C_{n+1}\left|ee,n\right\rangle \\
& + ((C_{eg} + C_{ge})C_{n+1} + C_{ee}C_n - C_{gg}C_{n+2})(\left|eg,n+1\right\rangle + \left|ge,n+1\right\rangle) \\
& (C_{ee}C_n + C_{gg}C_{n+2} - (C_{eg} + C_{ge})C_{n+1})\left|gg,n+2\right\rangle\big]\Bigg) + \left|C_R\right\rangle.
\end{aligned} \tag{4.2.45}$$

where $\left|C_R\right\rangle$ are all the quantum state terms outside the sum in Equation (4.2.31) that is given by

$$\begin{aligned}
\left|C_R\right\rangle = & \left(-\frac{iC_0}{\sqrt{2}}(C_{eg} + C_{ge})\sin\left(\sqrt{2}\lambda t\right) + \frac{1}{2}C_1C_{gg}\cos\left(\sqrt{2}\lambda t\right)\right)\left|gg,1\right\rangle \\
& + \left(\frac{C_0}{2}(C_{eg} + C_{ge})\cos\left(\sqrt{2}\lambda t\right) - \frac{i}{\sqrt{2}}C_1C_{gg}\sin\left(\sqrt{2}\lambda t\right)\right)(\left|eg,0\right\rangle + \left|ge,0\right\rangle) \\
& + \frac{C_0}{2}(C_{eg} - C_{ge})(\left|ge,0\right\rangle - \left|eg,0\right\rangle) + C_0C_{gg}\left|gg,0\right\rangle.
\end{aligned} \tag{4.2.46}$$

We can regroup the terms according to their basis $|ee,n\rangle$, $|eg,n\rangle$, $|ge,n\rangle$ and $|gg,n\rangle$ and the equation is now in the form of

$$
\begin{aligned}
\left|\widetilde{\Psi}_2(t)\right\rangle = \sum_{n=0}^{\infty} \frac{C_n}{2}\Bigg(\Bigg[&\left(C_{ee} - C_{gg}\frac{C_{n+2}}{C_n}\right)|ee,n\rangle \\
&+ (C_{eg} - C_{ge})(\,|eg,n\rangle - |ge,n\rangle\,) - \left(C_{ee}\frac{C_{n-2}}{C_n} - C_{gg}\right)|gg,n\rangle\Bigg] \\
&+ \frac{1}{2}\Bigg[e^{2i\lambda t\sqrt{n+2}}\left(C_{ee} + C_{gg}\frac{C_{n+2}}{C_n} - (C_{eg} + C_{ge})\frac{C_{n+1}}{C_n}\right)|ee,n\rangle \\
&+ e^{2i\lambda t\sqrt{n+1}}\left((C_{eg} + C_{ge}) - C_{ee}\frac{C_{n-1}}{C_n} - C_{gg}\frac{C_{n+1}}{C_n}\right)(\,|eg,n\rangle + |ge,n\rangle\,) \\
&+ e^{2i\lambda t\sqrt{n}}\left(C_{ee}\frac{C_{n-2}}{C_n} + C_{gg} - (C_{eg} + C_{ge})\frac{C_{n-1}}{C_n}\right)|gg,n\rangle\Bigg]\Bigg) \\
&+ \frac{1}{2}\Bigg[e^{-2i\lambda t\sqrt{n+2}}\left(C_{ee} + C_{gg}\frac{C_{n+2}}{C_n} + (C_{eg} + C_{ge})\frac{C_{n+1}}{C_n}\right)|ee,n\rangle \\
&+ e^{-2i\lambda t\sqrt{n+1}}\left((C_{eg} + C_{ge}) + C_{ee}\frac{C_{n-1}}{C_n} - C_{gg}\frac{C_{n+1}}{C_n}\right)(\,|eg,n\rangle + |ge,n\rangle\,) \\
&+ e^{-2i\lambda t\sqrt{n}}\left(C_{ee}\frac{C_{n-2}}{C_n} + C_{gg} + (C_{eg} + C_{ge})\frac{C_{n-1}}{C_n}\right)|gg,n\rangle\Bigg]\Bigg).
\end{aligned}
\tag{4.2.47}
$$

As $(n-\bar{n})$ is very small compared to $\bar{n}$, further approximations can be made on the coherent field's coefficients such that

$$
\frac{C_{n\pm1}}{C_n} = \frac{\alpha^{n\pm1}\sqrt{n!}}{\alpha^n\sqrt{(n+1)!}} = \frac{\sqrt{\bar{n}}e^{\mp i\theta}}{\sqrt{n+1}} \approx e^{\mp i\theta} \tag{4.2.48}
$$

and we may also expand $\sqrt{n+k}$ by applying a binomial expansion

$$
\sqrt{n+k} = \sqrt{\bar{n} + (n-\bar{n}) + k} \approx \frac{\sqrt{\bar{n}}}{2} + \frac{n}{2\sqrt{\bar{n}}} + \frac{k}{2\sqrt{\bar{n}}} \tag{4.2.49}
$$

where k is an arbitrary number -1, 0 or 1. With these, we can now separate Equation (4.2.47) into the field and the two qubits parts as

$$
\begin{aligned}
\left|\widetilde{\Psi}_2(t)\right\rangle = {} & \frac{1}{2}\left(\sum_{n=0}^{\infty} C_n \left|n\right\rangle\right)\Big[\left(e^{2i\theta}C_{ee} - C_{gg}\right)\left(e^{-2i\theta}\left|ee\right\rangle - \left|gg\right\rangle\right) \\
& + \left(C_{eg} - C_{ge}\right)\left(\left|eg\right\rangle - \left|ge\right\rangle\right)\Big] \\
& + \frac{e^{i\lambda\sqrt{\bar{n}}t}e^{2i\lambda t/\sqrt{\bar{n}}}}{4}\left(e^{2i\theta}C_{ee} - e^{i\theta}(C_{eg} + C_{ge}) + C_{gg}\right)\left(\sum_{n=0}^{\infty} C_n e^{in\lambda t/\sqrt{\bar{n}}}\left|n\right\rangle\right) \\
& \left(e^{-2i\theta}\left|ee\right\rangle - e^{-i\lambda t/\sqrt{\bar{n}}}e^{i\theta}(\left|eg\right\rangle + \left|ge\right\rangle) + e^{-2i\lambda t/\sqrt{\bar{n}}}\left|gg\right\rangle\right) \\
& + \frac{e^{-i\lambda\sqrt{\bar{n}}t}e^{2i\lambda t/\sqrt{\bar{n}}}}{4}\left(e^{2i\theta}C_{ee} - e^{i\theta}(C_{eg} + C_{ge}) + C_{gg}\right)\left(\sum_{n=0}^{\infty} C_n e^{-in\lambda t/\sqrt{\bar{n}}}\left|n\right\rangle\right) \\
& \left(e^{2i\theta}\left|ee\right\rangle - e^{i\lambda t/\sqrt{\bar{n}}}e^{i\theta}(\left|eg\right\rangle + \left|ge\right\rangle) + e^{2i\lambda t/\sqrt{\bar{n}}}\left|gg\right\rangle\right)
\end{aligned}
\tag{4.2.50}
$$

which can be simplified in the form of

$$
\left|\widetilde{\Psi}_2(t)\right\rangle = \sum_{k=-1}^{1} \beta_k(t)\left|D_k(t)\right\rangle \otimes \left|\Phi_k(t)\right\rangle \tag{4.2.51}
$$

where

$$
\beta_{\pm 1}(t) = \frac{e^{\pm 2i\pi t(\bar{n}+2)/t_r}}{2}\left(e^{2i\theta}C_{ee} \mp e^{i\theta}\left(C_{eg} + C_{ge}\right) + C_{gg}\right) \tag{4.2.52}
$$

$$
\beta_0 = \sqrt{\frac{|e^{2i\theta}C_{ee} - C_{gg}|^2 + |C_{eg} - C_{ge}|^2}{2}} \tag{4.2.53}
$$

$$
\left|D_{\pm 1}(t)\right\rangle = \frac{1}{2}\left(e^{-2i\theta}\left|ee\right\rangle \mp e^{\pm 2i\pi t/t_r}e^{-i\theta}\left(\left|eg\right\rangle + \left|ge\right\rangle\right) + e^{\mp 4i\pi t/t_r}\left|gg\right\rangle\right) \tag{4.2.54}
$$

$$
\left|D_0(t)\right\rangle = \frac{\left(e^{2i\theta}C_{ee} - C_{gg}(e^{-2i\theta}\left|ee\right\rangle - \left|gg\right\rangle) + (C_{eg} - C_{ge})(\left|eg\right\rangle - \left|ge\right\rangle)\right)}{\sqrt{2\left(|e^{2i\theta}C_{ee} - C_{gg}|^2 + |C_{eg} - C_{ge}|^2\right)}} \tag{4.2.55}
$$

$$
\left|\Phi_k(t)\right\rangle = \sum_{n=0}^{\infty} C_n e^{2ink\pi t/t_r}\left|n\right\rangle . \tag{4.2.56}
$$

Here, t_r is the one-qubit revival time as stated in Equation (2.2.59) and for coherent state, we have

$$
\left|\Phi_k(t)\right\rangle = \left|e^{2ik\pi t/t_r}\alpha\right\rangle . \tag{4.2.57}
$$

From Equation (4.2.54) it can be observed that the two-qubit states $\left|D_{\pm 1}(t)\right\rangle$ are actually the direct product state of one-qubit states $\left|D_{\pm\frac{1}{2}}(t)\right\rangle$ given by Equation (2.2.44) with time $t \to 2t$.

$$
\begin{aligned}
|D_{\pm 1}(t)\rangle &= \frac{1}{2}\left(e^{-2i\theta}|ee\rangle \mp e^{\pm 2i\pi t/t_r} e^{-i\theta}\left(|eg\rangle + |ge\rangle\right) + e^{\mp 4i\pi t/t_r}|gg\rangle\right) && (4.2.58)\\
&= \frac{1}{\sqrt{2}}\left(e^{-i\theta}|e\rangle \mp e^{\mp 2i\pi t/t_r}|g\rangle\right) \otimes \frac{1}{\sqrt{2}}\left(e^{-i\theta}|e\rangle \mp e^{\mp 2i\pi t/t_r}|g\rangle\right) && (4.2.59)\\
&= \left|D_{\pm\frac{1}{2}}(2t)\right\rangle \otimes \left|D_{\pm\frac{1}{2}}(2t)\right\rangle && (4.2.60)
\end{aligned}
$$

It was shown in Section 2.2.5 that at the attractor time $\frac{t_r}{2}$ the qubit state in a single qubit model evolves into an attractor state $\left|D_{\pm\frac{1}{2}}(t)\right\rangle = \left|\psi^{+}_{1,att}\right\rangle$. Given the correspondence between the one-qubit and the two-qubit systems, we therefore can predict a similar behaviour for the latter where the state evolves to a direct product of one qubit attractor states $\left|\psi^{+}_{1,att}\right\rangle$ at $t = \frac{t_r}{4}$.

$$
\begin{aligned}
\left|D_{\pm 1}\left(\frac{t_r}{4}\right)\right\rangle &= \left|D_{\pm\frac{1}{2}}\left(\frac{t_r}{2}\right)\right\rangle \otimes \left|D_{\pm\frac{1}{2}}\left(\frac{t_r}{2}\right)\right\rangle && (4.2.61)\\
&= \left|\psi^{+}_{1,att}\right\rangle \otimes \left|\psi^{+}_{1,att}\right\rangle && (4.2.62)\\
&= \left|\psi^{+}_{2,att}\right\rangle. && (4.2.63)
\end{aligned}
$$

Similar to the case of the one-qubit system, we can find the second attractor state of the two-qubit system $\left|\psi^{-}_{2,att}\right\rangle$ at half way between the first and the second revival, which is at time $\frac{3t_r}{4}$. So we can label and write our two-qubit attractor states as

$$
\left|\psi^{\pm}_{2,att}\right\rangle = \frac{1}{2}\left(e^{2i\theta}|ee\rangle \pm ie^{i\theta}\left(|eg\rangle + |ge\rangle\right) - |gg\rangle\right). \qquad (4.2.64)
$$

4.2.4 Basin Of Attraction

By using the two-qubit attractor state above, we may rewrite the wavefunction of the two-qubit Jaynes-Cummings system at the two-qubit attractor time as

$$
\begin{aligned}
\left|\widetilde{\Psi}_2\left(\frac{t_r}{4}\right)\right\rangle = -\frac{1}{2}\left|\psi^{+}_{2,att}\right\rangle \Big(&\left(e^{2i\theta}C_{ee} + C_{gg}\right)\left(e^{i\pi\bar{n}/2}|i\alpha\rangle + e^{-i\pi\bar{n}/2}|-i\alpha\rangle\right)\\
&- e^{i\theta}\left(C_{eg} + C_{ge}\right)\left(e^{i\pi\bar{n}/2}|i\alpha\rangle - e^{-i\pi\bar{n}/2}|-i\alpha\rangle\right)\Big) + \beta_0|D_0\rangle|\alpha\rangle
\end{aligned}
\qquad (4.2.65)
$$

From the above wavefunction, we can see that there are three components to the full time-evolving state of the system at $\frac{t_r}{4}$. If the last part of the equation vanishes, the first two components combine at half way to the two-qubit revival time into a product state of the field with the two-qubit states. Since at this time the two-qubit state is a two-qubit attractor state [75], there is neither entanglement between the two qubits and the field nor between the two qubits themselves. In another words, there's absolutely no entanglement in the system at this particular time.

We can thus say that the $\beta_0 |D_0\rangle |\alpha\rangle$ part of the time-evolving state has an important influence in quantifying the initial states of the two qubits that lead to the attractor states. C.Jarvis referred to this initial set of states as the 'basin of attraction' [27, 64]. One way we can eliminate this part and find the 'basin of attraction' of the system is by letting $\beta_0 = 0$. To satisfy this, the coefficients of the two-qubit states have to be $e^{i\theta} C_{ee} = e^{-i\theta} C_{gg} = a$ and $C_{eg} = C_{ge} = \sqrt{\frac{1}{2} - |a|^2}$. These give us an initial state of the form

$$|\psi_2\rangle = a \left(e^{-i\theta} |ee\rangle + e^{i\theta} |gg\rangle \right) + \sqrt{\frac{1}{2} - |a|^2} \left(|eg\rangle + |ge\rangle \right) \tag{4.2.66}$$

where θ is the initial phase of the radiation field and a is a complex variable parametrising the state and satisfies $0 \leq |a| \leq \frac{1}{\sqrt{2}}$.

Beside the attractor state, at time $\frac{t_r}{4}$ the wavefunction also contains two field states which are macroscopically distinct coherent states, $\left|\Phi_{\pm 1}\left(\frac{t_r}{4}\right)\right\rangle$. We can again rewrite the wavefunction in terms of these states as

$$\begin{aligned} \left| \widetilde{\Psi}_2 \left(\frac{t_r}{4} \right) \right\rangle &= -e^{i\theta} \left| \psi^+_{2,att} \right\rangle \\ &\quad \times \left(e^{i\pi\bar{n}/2} \left(a - \sqrt{\frac{1}{2} - |a|^2} \right) |i\alpha\rangle + e^{-i\pi\bar{n}/2} \left(a + \sqrt{\frac{1}{2} - |a|^2} \right) |-i\alpha\rangle \right). \end{aligned} \tag{4.2.67}$$

By writing the wavefunction in this form, the connection between the two-qubit initial states with the proportion of the field states $|\alpha\rangle$ and $|-\alpha\rangle$ is clearly visible. It also shows that the initial information in the state of the qubits is mapped into a cat state of the field while the two qubits evolve into an attractor state.

It was shown in Section 2.2.5 that for the one-qubit Jaynes-Cummings system, the qubit disentangled itself from the field at t_r and $2t_r$ so that the field states at these times are $\left|\Phi_{+\frac{1}{2}}(t_r)\right\rangle = \left|\Phi_{-\frac{1}{2}}(t_r)\right\rangle$ and $\left|\Phi_{+\frac{1}{2}}(2t_r)\right\rangle = \left|\Phi_{-\frac{1}{2}}(2t_r)\right\rangle$. Similar to the attractor state, relationship between the one-qubit system and two-qubit subsystem under $t \to 2t$ mapping can also be seen in the field states. It turns out that $|\Phi_{\pm 1}(t)\rangle = \left|\Phi_{\pm\frac{1}{2}}(2t)\right\rangle$. From this we can predict that $\left|\Phi_{+1}\left(\frac{t_r}{2}\right)\right\rangle = \left|\Phi_{-1}\left(\frac{t_r}{2}\right)\right\rangle$

and $|\Phi_{+1}(t_r)\rangle = |\Phi_{-1}(t_r)\rangle$. Clearly at time $\frac{t_r}{2}$ and t_r, the field part can be factorised out of the wavefunction and there is no entanglement present between the two qubits and the field at these times.

4.2.5 Numerical Results

The time evolutions of the two-qubit Jaynes-Cummings system are illustrated as Figure 4.2.1 and Figure 4.2.2 where the first shows the dynamics in the quantities of the system with an initial two-qubit state that lies inside the basin of attraction, while the latter is for the case of an initial state outside the basin of attraction. For the first case, we choose a two-qubit state of $\frac{1}{\sqrt{2}}(|ee\rangle + |gg\rangle)$ and we use state $\frac{1}{\sqrt{20}}|ee\rangle + \sqrt{\frac{19}{20}}|gg\rangle$ for the system with an initial state from outside the basin as a comparison to the previous works [27, 28]. We use $\bar{n} = 36$ and $\theta = 0$ for both cases.

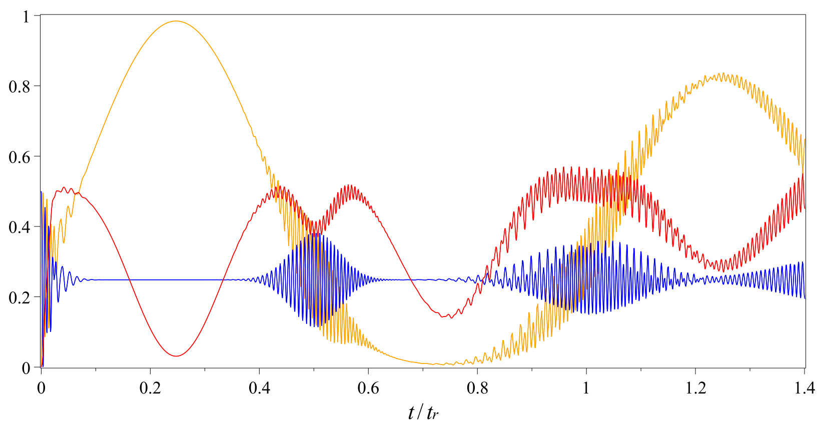

Figure 4.2.1: Time evolution for two-qubit Jaynes-Cummings system with the initial two-qubit state $\frac{1}{\sqrt{2}}(|ee\rangle+|gg\rangle)$, $\bar{n} = 36$ and the initial phase of the radiation field $\theta = 0$. The linear entropy of the qubits is shown as a red line, the probability of the two-qubit state being in state $|ee\rangle$ as a blue line and the probability of being in the two-qubit attractor state $\left|\psi^{+}_{2,att}\right\rangle$ as an orange line.

In the figures, we plot the linear entropy $S^L_q(t) = 1 - \mathrm{Tr}(\rho^2_q(t))$ as a red line. The entropy is associated with density matrix of the qubits at certain time when the field has been traced out, $\rho_q(t) = \mathrm{Tr}_f(|\Psi_2(t)\rangle\langle\Psi_2(t)|)$. This entropy of the two-qubit subsystem indicates entanglement between the two qubits and the field, as the overall system is in a pure state. This however, breaks down when we consider the decoherence cases in Chapter 5 and 6, where an average is

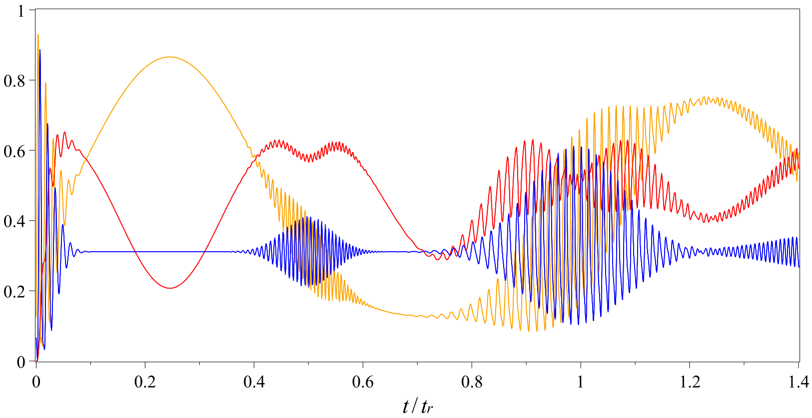

Figure 4.2.2: Time evolution for two-qubit Jaynes-Cummings system with the initial two-qubit state $\frac{1}{\sqrt{20}}\left|ee\right\rangle + \sqrt{\frac{19}{20}}\left|gg\right\rangle$, $\bar{n} = 36$ and the initial phase of the radiation field $\theta = 0$. The linear entropy of the qubits is shown as a red line, the probability of the two-qubit state being in state $\left|ee\right\rangle$ as a blue line and the probability of being in the two-qubit attractor state $\left|\psi^{+}_{2,att}\right\rangle$ as an orange line.

made over the qubit density matrix, as we can not know if the entropy is due to entanglement with the field or with the decoherence.

We also plot the probability of the two qubits being both in the excited state $\left|ee\right\rangle$ as a blue line by calculating $P_{ee}(t) = \sum_{n=0}^{\infty} \left|\left\langle ee, n | \Psi_2(t)\right\rangle\right|^2$ where $\left\langle ee, n\right|$ corresponds to the state that both qubits are in their excited state with n photons in the cavity. The probability of the two-qubit state being in the two-qubit attractor state of Equation (4.2.64) is also calculated by $P^{+}_{2,att}(t) = \left\langle \psi^{+}_{2,att} | \rho_q(t) | \psi^{+}_{2,att} \right\rangle$ and shown as the orange line.

From the figures, it is clear that the revival time of this two-qubit Jaynes-Cummings system is half of the revival time of the system with one qubit, which is t_r that is given by Equation (2.2.59). Regardless of the initial state of the two qubits, we can still see the event of collapse and revival of Rabi oscillations in this model. It can also be observed that the characteristics of the dips in entropy are different for each case of initial conditions. Even though for both cases the dips are observed at the similar times $\frac{t_r}{4}$ and $\frac{3t_r}{4}$, the entropy at the first is seen to be very small and nearer to zero with an initial two-qubit state from inside the basin of attraction.

At this time, the two qubits have disentangled themselves from the field again and are in a pure state known as the two-qubit attractor state $\left|\psi^{+}_{2,att}\right\rangle$. This fact is shown by the orange line in the graph, where the probability of the state being in the two-qubit attractor state is very close to unity. The system repeats this cycle at time $\frac{3t_r}{4}$ but this time the two qubits are in the orthogonal two-qubit attractor state $\left|\psi^-_{2,att}\right\rangle$. This is the reason for the probability of being in the two-qubit attractor state $\left|\psi^+_{2,att}\right\rangle$ approaching zero.

On the other hand, if the system starts with an initial state from outside the basin of attraction, it has a non-zero entropy value at times $\frac{t_r}{4}$ and $\frac{3t_r}{4}$. This is due to the relationship between entropy and entanglement, as the two-qubit state can not be factorised out of the wavefunction. The two qubits also will not be reduced into the two-qubit attractor state as $\beta_0 \neq 0$ in Equation (4.2.65). This can be seen from Figure 4.2.2 where the probability of being in the attractor state $\left|\psi^+_{2,att}\right\rangle$ at $\frac{t_r}{4}$ is small due to the reduction in the purity of the system.

From the analytical solutions in the previous section, the calculations show that with a very large $\bar{n}$ approximation, at times $\frac{t_r}{2}$ and t_r the system is once again factorised into the two-qubit and field parts if the two qubits start with a state from inside the basin of attraction. This is where we have $|\Phi_{-1}(t_r)\rangle = |\Phi_0(t_r)\rangle = |\Phi_1(t_r)\rangle = |\alpha\rangle$ and $|\Phi_{-1}(\frac{t_r}{2})\rangle = |\Phi_1(\frac{t_r}{2})\rangle = |-\alpha\rangle$. At these times, the two-qubit state is again pure and the the entropy is expected to approach zero. Similar behavior is also expected at time t_r for the case of initial two-qubit state from outside the basin of attraction. However, the plots in Figure 4.2.1 and Figure 4.2.2 show otherwise where there is no deep dip shown in the linear entropy line at these times indicating large entanglement between the qubits and the field. This is due to the very short time scale where the width of the gap between the peaks before and after this dip is much narrower as compared to the similar phenomena at time $\frac{t_r}{4}$ [27]. At this time a larger value of $\bar{n}$ would be needed in our numerical approximation to approach the analytical results.

4.2.6 Collapse, Revival, Death and Rebirth of Qubits Entanglement

Another interesting event that can be observed from the interaction of two qubits and a coherent field is the 'collapse and revival of entanglement' between the two qubits [27]. As opposed to the single qubit case where entanglement can only be measured between the qubit and the field, in two-qubit cases we can further measure the entanglement between the two qubits themselves.

To quantify the amount of entanglement between the two qubits, we may either use mixed state tangle $\tau(t)$ [51, 53] or concurrence, $\varsigma(t) = \sqrt{\tau(t)}$. Similar to entropy, these quantities take a value from zero to unity to represent the strength of the entanglement where the first indicates no entanglement and latter indicates maximum entanglement between the qubits. These quantities have been explained in Section 1.4.2 and the tangle is given by the formula

$$\tau(t) = [\max\{\chi_1 - \chi_2 - \chi_3 - \chi_4, 0\}]^2. \tag{4.2.68}$$

The dynamics by which these quantities disappear and reappear are very interesting. If they disappear with a finite slope, an event called 'sudden death of entanglement' (and then birth when they reappear) is observed. If they go smoothly to zero and then reappear also smoothly (with no discontinuous change in the gradient), then this event is called the 'collapse and revival of entanglement'.

C. Jarvis and collaborators have shown that it is possible to study the connection of the basin of attraction with the dynamics of the entanglement between the qubits [64, 27]. It was shown that similar to the entanglement of the two-qubit system with the field, the entanglement between the two qubits is very much dependent on their initial conditions too. States from inside and outside the basin of attraction present different time evolutions of the two-qubit entanglement [64, 27]. This is in agreement with the results of [76] which concludes that choosing proper initial conditions is very important in determining the behaviour of the entanglement in a two-qubit system.

Initial two-qubit state from inside the basin of attraction

In Section 4.2.4 we have calculated the basin of attraction for the initial states of a two-qubit Jaynes-Cummings model. C. Jarvis *et.al* have also demonstrated the level of entanglement with respect to the basin of attraction [64, 27]. They demonstrated that if the two qubits start with a state from inside the basin of attraction, there are only two possible states from the whole set where the initial entanglement measure $\tau(t) = 0$. These points are given by $a = \pm\frac{1}{2}$ indicating that there are only two product states in this basin of attraction. All other points represent entangled states and have entanglement values of either $\tau = 1$ and or in between zero and unity.

These entangled states evolve into the attractor state $\left|\psi^+_{2,att}\right\rangle$ at time $\frac{t_r}{4}$ and its orthogonal state $\left|\psi^-_{2,att}\right\rangle$ at time $\frac{3t_r}{4}$. From Equation (4.2.60), we know that these states are the products of two one-qubit attractor states which are pure and unentangled, such that $\left|\psi^+_{2,att}\right\rangle = \left|\psi^+_{1,att}\right\rangle \otimes \left|\psi^+_{1,att}\right\rangle$. Therefore, at these times we have a system with absolutely no entanglement, either between the two qubits and the field or between the qubits themselves. Similar to the one-qubit case, all the quantum information in the two-qubit initial state is transferred and encoded into the field state, producing a cat state of the field. The entanglement however returns into the system and recovers its initial value at the two-qubit revival time $\frac{t_r}{2}$ and later at time t_r. At these times, the value of the tangle or concurrence for the two-qubit state is expected to be exactly the same as its initial value at the beginning of the interaction. So we have $\tau(0) = \tau(\frac{t_r}{2}) = \tau(t_r)$. This interesting phenomenon is called 'collapse and revival of entanglement' [28, 64, 27, 25].

The dynamics of such entanglement is depicted in Figure 4.2.3 and Figure 4.2.4. In the first plot, we use tangle $\tau(t)$ as a measure of entanglement as a direct comparison with the previous works [28, 64, 27]. In the second figure we use concurrence $\varsigma(t)$ to display the entanglement and we will be using this quantity to describe the entanglement between the two qubits throughout this thesis. However, both quantities are shown as a black line in the respective figures.

Another interesting phenomenon can be seen in the dynamics of the qubit-qubit entanglement in which there are long periods of time for which this quantity remains near zero. This feature has been described as the 'death of entanglement' [24, 77, 26]. Therefore we can conclude that if we have a two-qubit Jaynes-Cummings system that starts with a two-qubit initial state from inside the basin of attraction, over time we will observe that the entanglement in the two qubits is exchanged for the qubits-field entanglement, and later for a superposition of field coherent states, or the cat states of the field. No entanglement is present at the two-qubit attractor time $\frac{t_r}{4}$, after which the entanglement exchange process starts to reverse. The entanglement between the two qubits and the field will start to reappear and again disappear at time $\frac{t_r}{2}$. At this point too, the concurrence returns to its initial value indicating the presence of entanglement in the two-qubit subsystem only.

In addition to the collapse, revival and death of entanglement features discussed above, from the figure we may also note another interesting phenomenon of this quantity by observing its disappearance and reappearance behaviour. We can see that at the two-qubit revival time $\frac{t_r}{2}$, the entanglement appears smoothly and then vanishes in a similar way. In the case of infinite finite size of the field strength n, the entanglement would go to it initial value and then zero again with a Gaussian envelope manner which can be explained by a detailed look at

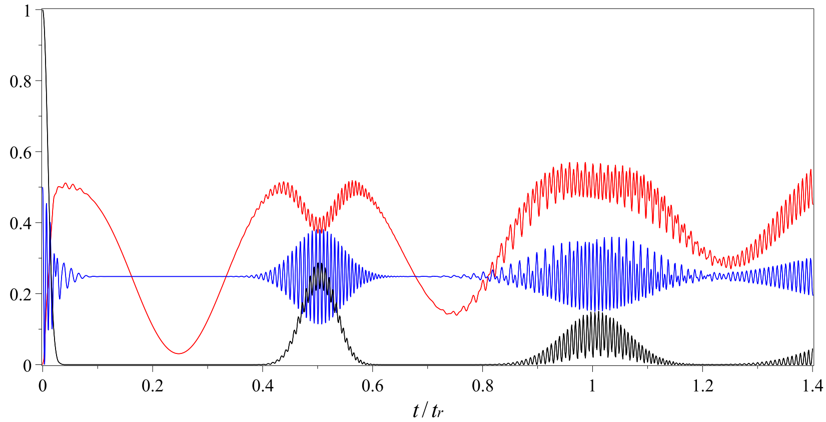

Figure 4.2.3: Time evolution for two qubits Jaynes-Cummings system with the initial qubits state $\frac{1}{\sqrt{2}}(|ee\rangle + |gg\rangle)$, $\bar{n} = 36$ and the initial phase of the radiation field $\theta = 0$. The linear entropy of the qubits is shown as a red line, the probability of the two-qubit state $|ee\rangle$ as a blue line and the tangle $\tau(t)$ as a black line.

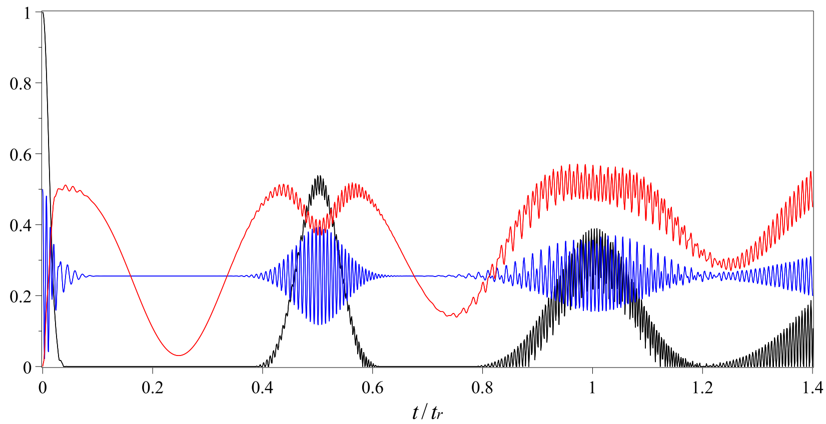

Figure 4.2.4: Time evolution for two qubits Jaynes-Cummings system with the initial qubits state $\frac{1}{\sqrt{2}}(|ee\rangle + |gg\rangle)$, $\bar{n} = 36$ and the initial phase of the radiation field $\theta = 0$. The linear entropy of the qubits is shown as a red line, the probability of the two-qubit state $|ee\rangle$ as a blue line and the concurrence $\varsigma(t)$ as a black line.

the eigenvalue expressions in Equation (4.2.69). However, in this case of finite system, there is not complete disentanglement of the field from the qubits, so the qubits cannot return to a maximally entangled pure state. Nevertheless, strong entanglement can still be seen in the considered finite system.

We have seen that our system wavefunction can be decomposed into the qubits and the field part a given by Equation (4.2.51). A state from inside the basin of attraction means that we have a wavefunction in the form of

$$\left|\widetilde{\Psi}_2(t)\right\rangle = \beta_{-1}(t)\left|D_{-1}(t)\right\rangle \otimes \left|\Phi_1(t)\right\rangle + \beta_1(t)\left|D_1(t)\right\rangle \otimes \left|\Phi_{-1}(t)\right\rangle . \tag{4.2.69}$$

This is a superposition of two product states and the reduced density matrix of this system $\rho_q(t)$ has only two non-zero eigenvalues. So, there is no need for *max* operation in Equation (4.2.68) as our eigenvalues χ_1 and χ_2 are never a negative value. This makes the collapse and the revival of the entanglement is smooth rather than evolving with a discontinuous change in gradient which is the case that we will discuss in the next section.

Initial two-qubit state from outside the basin of attraction

We have discussed interesting findings from a two-qubit Jaynes-Cummings model with an initial two-qubit state from inside the basin of attraction. It is the case where we satisfy the $\beta_0 = 0$ restriction in Equation (4.2.65). In this section, we will consider a similar two-qubit system, but with a different regime of initial two-qubit state where where we consider states from outside of the basin of attraction.

Considering such initial conditions means we are dealing with a system with a wavefunction given by Equation (4.2.65) restricted by $\beta_0 \neq 0$ inequality. The $\beta_0 \left|F_0\right\rangle \left|\alpha\right\rangle$ term prohibits the two-qubit subsystem to be factorised out of the wavefunction at $\frac{t_r}{4}$ and $\frac{3t_r}{4}$. This can be seen by the linear entropy plot depicted as a red line in Figure 4.2.5 where we plot the time evolutions of a two-qubit Jaynes-Cummings model with an initial two-qubit state from outside the basin of attraction. For a direct comparison with the results of previous studies [28, 64, 27, 26, 77, 78, 24, 25], we use an initial state $\frac{1}{\sqrt{20}}\left|ee\right\rangle + \sqrt{\frac{19}{20}}\left|gg\right\rangle$ and it is clear that the values of linear entropy are larger than zero at the two-qubit attractor times. This indicates that there is entanglement between the two qubits and the coherent field. This also means that the two-qubit subsystem is in a mixed state and will not approach the pure attractor state at these times.

We also plot the concurrence, $\varsigma(t)$ as a measure of qubit-qubit entanglement for the case of initial qubits state from outside the basin of attraction. Within this regime of initial condition, the quantity highlights many interesting events, especially the 'sudden death / birth of entanglement' [24, 25, 26] that occurs when the eigenvalues difference $\chi_1 - \chi_2 - \chi_4 - \chi_4$ in Equation (4.2.68) is negative. The *max* operation is then needed and this makes the value goes to zero with a finite gradient, as opposed to the Gaussian collapse and revival event as displayed in the case of initial states from inside the basin of attraction. This quantity is depicted by a black line in Figure 4.2.5.

In contrast to the case of a system with an initial two-qubit state from inside the basin of attraction with no entanglement measured between the two qubits at the attractor times, there are peaks with death / birth in this quantity for the system that starts with a state from outside the basin. This indicates that there is qubit-qubit entanglement occurring at the attractor times. These peaks are due to the fact that wavefunction (4.2.65) contains the $|D_0\rangle$ term. At time $\frac{t_r}{4}$, it was shown in Section 4.2.4 that at this time, the two-qubit state is an attractor state. We have $|D_{\pm 1}(\frac{t_r}{4})\rangle = \left|\psi^+_{2,att}\right\rangle$. This means there is no entanglement at all, even between the two qubits except if $\beta_0 \neq 0$. So, all the entanglements that occurs in the system at this time are coming from the $|D_0\rangle$ term.

The peaks in the concurrence can also be observed at times $\frac{t_r}{2}$ and t_r. This is similar to the case of an initial two-qubit state from inside the basin of attraction where the entanglement between the two qubits can be measured. We have seen from the analytical calculation for a large $\bar{n}$ approximation, at the second two-qubit revival time t_r, the field state can be factorised out of the wavefunction, where we have $|\Phi_0(t_r)\rangle = |\Phi_{-1}(t_r)\rangle = |\Phi_{+1}(t_r)\rangle = |-\alpha\rangle$. Therefore, the value of entanglement is also expected to be equal to its initial value at the beginning of the interaction. However, in Figure 4.2.5 we cannot see neither the complete qubits-field disentanglement nor the complete revival of qubit-qubit entanglement. These are because with $\bar{n} = 36$ the entropy will not approach zero, indicating there is entanglement between the qubits and the field which prevents the complete revival of the entanglement between the two qubits.

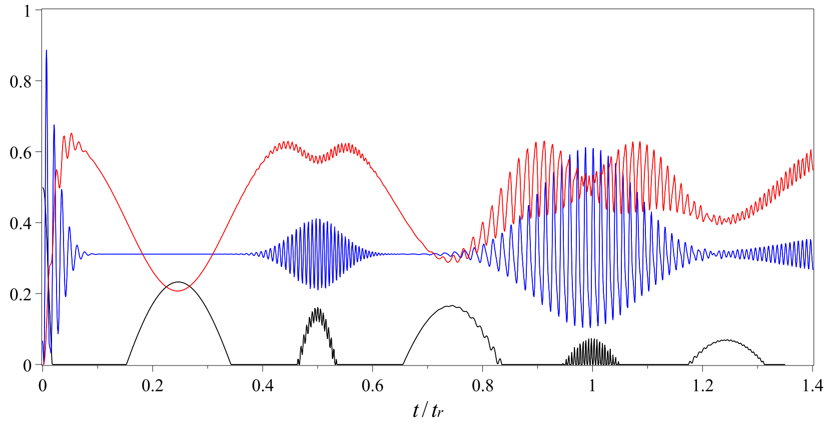

Figure 4.2.5: Time evolution for two qubits Jaynes-Cummings system with the initial qubits state $\frac{1}{\sqrt{20}}\left|ee\right\rangle+\sqrt{\frac{19}{20}}\left|gg\right\rangle$, $\bar{n}=36$ and the initial phase of the radiation field $\theta=0$. The linear entropy of the qubits is shown as a red line, the probability of the two-qubit state $\left|ee\right\rangle$ as a blue line and the concurrence $\varsigma(t)$ as a black line.

4.3 Two Qubits Big Spin Interaction Model

So far we have discussed the one-qubit Jaynes-Cummings model [[64, 27], the two-qubit Jaynes-Cummings model [75] as well as a one-qubit big spin model [29]. We studied these models and we reproduced the results that have been discovered and discussed by the previous researchers. We calculated the Hamiltonian, eigenvalues, eigenvectors and exact solutions for the respective systems. We evaluated the time evolutions for all these interacting systems and discussed a range of interesting properties resulting from these systems. All of these are important in helping us to understand the fundamentals of such qubit-field and qubit-big spin interacting systems.

In this section, we extend our analysis into a new area to explore the interaction between two qubits and a collection of N identical single spins in a pure state, or a big spin. We are interested in understanding the features of the dynamics produced by such an interacting system.

4.3.1 Two-Qubit Big Spin Hamiltonian

In Section 2.3.1 we have seen that the correspondence between one-qubit Jaynes-Cummings model and a one-qubit big spin model lies in the limit of $N\to\infty$. This is where a scaled spin coherent state $\left|\frac{\zeta}{\sqrt{N}}\right\rangle_N$ is equivalent to an oscillator coherent state of amplitude ζ.

With such correspondence and approximation, S.Dooley [29] has modelled the Hamiltonian of a one-qubit big spin model as given by Equation (2.3.10). We can expand the Hamiltonian to the multi-qubit case, so that the Hamiltonian for a system of multiple qubits interacting with a 'big spin' is given by:

$$\hat{H}_{q,N} = \hbar\omega_N(\hat{J}^z + \frac{N}{2}) + \frac{\hbar}{2}\sum_{i=1}^{q}\Omega_i\hat{\sigma}_i^z + \frac{\hbar}{\sqrt{N}}\sum_{i=1}^{q}\lambda_i(\hat{J}^+\hat{\sigma}_i^- + \hat{J}^-\hat{\sigma}_i^+) \tag{4.3.1}$$

where $\hat{J}^z \equiv \frac{1}{2}\sum\limits_{k=0}^{N}\hat{\sigma}_k^z$ and $\hat{J}^\pm \equiv \frac{1}{2}\sum\limits_{k=0}^{N}\hat{\sigma}_k^\pm$ are the operators for the big spin with requency ω_N and λ_i is the qubit$_i$-big spin coupling strength. $\hat{\sigma}_i^z = |e_i\rangle\langle e_i| - |g_i\rangle\langle g_i|$, $\hat{\sigma}_i^+ = |e_i\rangle\langle g_i|$ and $\hat{\sigma}_i^- = |g_i\rangle\langle e_i|$ are the individual qubit operators and the constant term $\frac{\omega N}{2}$ is introduced so that the ground state eigenvalue of the big spin Hamiltonian $\hat{J}^z$ is zero to prevent the ground state tending to negative infinite energy as N becomes very large. The subscript N is to differentiate this system from the two-qubit Jaynes-Cummings model.

In this chapter we limit our study to only a system of two qubits interacting with a big spin in a spin coherent state $\left|\frac{\zeta}{\sqrt{N}}\right\rangle_N$ as defined in Section 1.2.2. The $\frac{1}{\sqrt{N}}$ factors are inserted to anticipate the use of spin coherent states and the large N limit. The Hamiltonian is then reduced to

$$\begin{aligned}\hat{H}_{2,N} =& \hbar\omega_N\left(\hat{J}^z + \frac{N}{2}\right) + \frac{\hbar}{2}\left(\Omega_1\hat{\sigma}_1^z + \Omega_2\hat{\sigma}_2^z\right) + \frac{\hbar\lambda_1}{\sqrt{N}}\left(\hat{J}^+\hat{\sigma}_1^- + \hat{J}^-\hat{\sigma}_1^+\right)\\ &+ \frac{\hbar\lambda_2}{\sqrt{N}}\left(\hat{J}^+\hat{\sigma}_2^- + \hat{J}^-\hat{\sigma}_2^+\right).\end{aligned} \tag{4.3.2}$$

With an additional qubit in the system, the big spin could be in one of these $|n\rangle_N$, $|n+1\rangle_N$ and $|n+2\rangle_N$ states. The "n" used in this chapter is not to be confused with the one that has been used for the coherent state and similarly $\bar{n}$ in this section is for the spin coherent state such that $\bar{n} = |\zeta|^2$.

We assume independent interaction between each qubit and the big spin and so the interaction between the two qubits only happens via the big spin, which is the analogous case to compare with the field mode Jaynes-Cummings situation. We represent the total number of quanta in this two-qubit big spin model as an operator

$$\hat{M}_{2,N} = \hat{J}^z + \hat{\sigma}_1^+\hat{\sigma}_1^- + \hat{\sigma}_2^+\hat{\sigma}_2^-. \tag{4.3.3}$$

The number of excitations in this system is conserved since the above operator commutes with the Hamiltonian (4.3.1) as

$$\left[\hat{H}_{2,N}, \hat{M}_{2,N}\right] = 0. \tag{4.3.4}$$

4.3.2 Eigenvalues, Eigenvectors and Exact Solution

Now we are going to find the solutions to the dynamics of our two-qubit big spin model. We can do this by finding the eigenstates and eigenvalues of the Hamiltonian. We solve the eigenvalue equation

$$\hat{H} |\psi\rangle = E |\psi\rangle , \tag{4.3.5}$$

and then decompose the following initial state into the eigenstates and find the general time dependent solution. The wavefunction at time $t = 0$ is given by

$$|\Psi_2(0)\rangle_N = |\phi(0)\rangle_N |\psi_2(0)\rangle \tag{4.3.6}$$

By operating the Hamiltonian (4.3.2) on the following general decomposition of an eigenstate solution

$$|\Psi_2\rangle_N = \sum_{n=0}^{N} a_{ee,n} |ee, n\rangle_N + a_{eg,n} |eg, n\rangle_N + a_{ge,n} |ge, n\rangle_N + a_{gg,n} |gg, n\rangle_N \tag{4.3.7}$$

the eigenvalue equation (4.3.2) gives us the following solutions

$$\begin{aligned}
\hat{H}_{2,N} |\Psi_2\rangle_N = \sum_{n=0}^{N} \Bigg[& \\
& \hbar(\omega_N n + \frac{\Omega_1}{2} + \frac{\Omega_2}{2}) a_{ee,n} |ee, n\rangle_N + \hbar(\omega_N n + \frac{\Omega_1}{2} - \frac{\Omega_2}{2}) a_{eg,n} |eg, n\rangle_N \\
& + \hbar(\omega_N n - \frac{\Omega_1}{2} + \frac{\Omega_2}{2}) a_{ge,n} |ge, n\rangle_N + \hbar(\omega_N n - \frac{\Omega_1}{2} - \frac{\Omega_2}{2}) a_{gg,n} |gg, n\rangle_N \\
& + \hbar\sqrt{n\left(1 - \frac{n-1}{N}\right)} (\lambda_1 a_{ge,n} + \lambda_2 a_{eg,n}) |ee, n-1\rangle_N \\
& + \hbar\sqrt{n\left(1 - \frac{n-1}{N}\right)} a_{gg,n} (\lambda_1 |eg, n-1\rangle_N + \lambda_2 |ge, n-1\rangle_N) \\
& + \hbar\sqrt{(n+1)\left(1 - \frac{n}{N}\right)} a_{ee,n} (\lambda_1 |ge, n+1\rangle_N + \lambda_2 |eg, n+1\rangle_N) \\
& + \hbar\sqrt{(n+1)\left(1 - \frac{n}{N}\right)} (\lambda_1 a_{ge,n} + \lambda_2 a_{eg,n}) |gg, n+1\rangle_N \Bigg].
\end{aligned} \tag{4.3.8}$$

We then change the basis and rearrange the equation in terms of $|ee,n\rangle_N$, $|eg,n+1\rangle_N$, $|ge,n+1\rangle_N$ and $|gg,n+2\rangle_N$ states as

$$
\begin{aligned}
\hat{H}_{2,N}\,|\Psi_2\rangle_N = \sum_{n=0}^{N-2}\Bigg[&\Bigg((\hbar\omega_N n + \frac{\hbar\Omega_1}{2} + \frac{\hbar\Omega_2}{2})a_{ee,n} + \hbar\sqrt{(n+1)\Big(1-\frac{n}{N}\Big)} \\
&(\lambda_1 a_{ge,n+1} + \lambda_2 a_{eg,n+1})\Bigg)\,|ee,n\rangle_N \\
&+\Bigg((\hbar\omega_N(n+1) + \frac{\hbar\Omega_1}{2} - \frac{\hbar\Omega_2}{2})a_{eg,n+1} + \hbar\lambda_1\sqrt{(n+2)\Big(1-\frac{n+1}{N}\Big)}a_{gg,n+2} \\
&+\hbar\lambda_2\sqrt{(n+1)\Big(1-\frac{n}{N}\Big)}a_{ee,n}\Bigg)\,|eg,n+1\rangle_N \\
&+\Bigg((\hbar\omega_N(n+1) - \frac{\hbar\Omega_1}{2} + \frac{\hbar\Omega_2}{2})a_{ge,n+1} + \hbar\lambda_1\sqrt{(n+1)\Big(1-\frac{n}{N}\Big)}a_{ee,n} \\
&+\hbar\lambda_2\sqrt{(n+2)\Big(1-\frac{n+1}{N}\Big)}a_{gg,n+2}\Bigg)\,|ge,n+1\rangle_N \\
&+\Bigg((\hbar\omega_N(n+2) - \frac{\hbar\Omega_1}{2} - \frac{\hbar\Omega_2}{2})a_{gg,n+2} + \hbar\sqrt{(n+2)\Big(1-\frac{n+1}{N}\Big)} \\
&(\lambda_1 a_{eg,n+1} + \lambda_2 a_{ge,n+1})\Bigg)\,|gg,n+2\rangle_N\Bigg] + (-\frac{\hbar\Omega_1}{2} - \frac{\hbar\Omega_2}{2}) \\
&\times a_{gg,0}\,|gg,0\rangle_N + ((-\frac{\hbar\Omega_1}{2} + \frac{\hbar\Omega_2}{2})a_{ge,0} + \hbar\lambda_2 a_{gg,1})\,|ge,0\rangle_N \\
&+ ((\frac{\hbar\Omega_1}{2} - \frac{\hbar\Omega_2}{2})a_{eg,0} + \hbar\lambda_1 a_{gg,1})\,|eg,0\rangle_N + \Bigg((\hbar\omega_N - \frac{\hbar\Omega_1}{2} - \frac{\hbar\Omega_2}{2}) \\
&\times a_{gg,1} + \hbar\lambda_1 a_{eg,0} + \hbar\lambda_2 a_{ge,0}\Bigg)\,|gg,1\rangle_N + (\hbar\omega_N N + \frac{\hbar\Omega_1}{2} + \frac{\hbar\Omega_2}{2}) \\
&\times a_{ee,N}\,|ee,N\rangle_N + ((\hbar\omega_N N + \frac{\hbar\Omega_1}{2} - \frac{\hbar\Omega_2}{2})a_{eg,N} + \hbar\lambda_2 a_{ee,N-1})\,|eg,N\rangle_N \\
&+ ((\hbar\omega_N N - \frac{\hbar\Omega_1}{2} + \frac{\hbar\Omega_2}{2})a_{ge,N} + \hbar\lambda_1 a_{ee,N-1})\,|ge,N\rangle_N + ((\hbar\lambda_1 a_{ge,N} \\
&+ \hbar\lambda_2 a_{eg,N}) + (\hbar\omega_N N - \hbar\omega_N + \frac{\hbar\Omega_1}{2} + \frac{\hbar\Omega_2}{2})a_{ee,N-1} \\
&+ \hbar(\lambda_1 a_{ge,N} + \lambda_2 a_{eg,N}))\,|ee,N-1\rangle_N\,.
\end{aligned}
\tag{4.3.9}
$$

We have shown in Equation (4.3.4) that the number of excitations is conserved. So, we can decompose the system into $m_{2,N}$ different decoupled sectors that the eigenvalue of $\hat{M}_{2,N}$ can take for this system. We may then put this equation into a matrix form of

$$\hat{H}_{2,N}\left|\Psi_2\right\rangle_N = \sum_{n=0}^{N-2} \begin{pmatrix} \nu_{1,1} & \nu_{1,2} & \nu_{1,3} & \nu_{1,4} \\ \nu_{2,1} & \nu_{2,2} & \nu_{2,3} & \nu_{2,4} \\ \nu_{3,1} & \nu_{3,2} & \nu_{3,3} & \nu_{3,4} \\ \nu_{4,1} & \nu_{4,2} & \nu_{4,3} & \nu_{4,4} \end{pmatrix} \left|\Psi_2\right\rangle_N \tag{4.3.10}$$

where

$$\begin{aligned}
\nu_{1,1} &= \hbar\omega_N n + \tfrac{\hbar\Omega_1}{2} + \tfrac{\hbar\Omega_2}{2} & \nu_{1,2} &= \hbar\lambda_2\sqrt{(n+1)\left(1-\tfrac{n}{N}\right)} \\
\nu_{1,3} &= \hbar\lambda_1\sqrt{(n+1)\left(1-\tfrac{n}{N}\right)} & \nu_{1,4} &= 0 \\
\nu_{2,1} &= \hbar\lambda_2\sqrt{(n+1)\left(1-\tfrac{n}{N}\right)} & \nu_{2,2} &= \hbar\omega_N(n+1) + \tfrac{\hbar\Omega_1}{2} - \tfrac{\hbar\Omega_2}{2} \\
\nu_{2,3} &= 0 & \nu_{2,4} &= \hbar\lambda_1\sqrt{(n+2)\left(1-\tfrac{n+1}{N}\right)} \\
\nu_{3,1} &= \hbar\lambda_1\sqrt{(n+1)\left(1-\tfrac{n}{N}\right)} & \nu_{3,2} &= 0 \\
\nu_{3,3} &= \hbar\omega_N(n+1) - \tfrac{\hbar\Omega_1}{2} + \tfrac{\hbar\Omega_2}{2} & \nu_{3,4} &= \hbar\lambda_2\sqrt{(n+2)\left(1-\tfrac{n+1}{N}\right)} \\
\nu_{4,1} &= 0 & \nu_{4,2} &= \hbar\lambda_1\sqrt{(n+2)\left(1-\tfrac{n+1}{N}\right)} \\
\nu_{4,3} &= \hbar\lambda_2\sqrt{(n+2)\left(1-\tfrac{n+1}{N}\right)} & \nu_{4,4} &= \hbar\omega_N(n+2) - \tfrac{\hbar\Omega_1}{2} - \tfrac{\hbar\Omega_2}{2}
\end{aligned}$$

This matrix is for each of the $m_{2,N}$ sectors where the amplitudes will form quartets of states except for $|gg,0\rangle_N$, $|ge,0\rangle_N$, $|eg,0\rangle_N$, $|gg,1\rangle_N$, $|ee,N\rangle_N$, $|eg,N\rangle_N$, $|ge,N\rangle_N$ and $|ee,N-1\rangle_N$.

We consider an interacting system with two identical initial qubits, so that we have resonant inversion frequencies between the qubits and the big spin, $\omega_N = \Omega_1 = \Omega_2$. The dipole-interaction strengths between them are also assumed to be the same so that we have $\lambda = \lambda_1 = \lambda_2$. Note that we will study the case of errors in these parameters in Chapter 5 and 6 respectively. We obtain the following eigenvalues where for $n = 0$ we have

$$E_{0,n} = E_{d,n} = \hbar\omega_N(n+1). \tag{4.3.11}$$

and for $1 \leq n \leq N-2$ the eigenvalues are

$$E_{\pm,n} = \hbar\omega_N(n+1) \pm \hbar\lambda\sqrt{4n+6-\frac{4}{N}(n+1)^2}. \tag{4.3.12}$$

We also have the eigenvalues for the lower energy levels from outside the summation denoted as

$$E_{\pm,-1} = \pm\sqrt{2}\hbar\lambda \tag{4.3.13}$$

$$E_{d,-1} = 0 \tag{4.3.14}$$

$$E_{g,0} = -\hbar\omega_N \tag{4.3.15}$$

while for the upper energy levels their eigenvalues are given as

$$E_{\pm,N-1} = \hbar\omega_N N \pm \sqrt{2}\hbar\lambda \tag{4.3.16}$$

$$E_{d,N-1} = \hbar\omega_N N \tag{4.3.17}$$

$$E_{e,N} = \hbar\omega_N (N+1). \tag{4.3.18}$$

From these eigenvalues, we find the corresponding eigenvectors which are

$$\begin{aligned}|\pm, n\rangle_{2,N} = {} & \frac{\sqrt{(n+1)(1-\frac{n}{N})}}{\sqrt{4n+6-\frac{4}{N}(n+1)^2}}\,|ee,n\rangle_N \pm \frac{1}{2}(|eg,n+1\rangle + |ge,n+1\rangle_N) \\ & + \frac{\sqrt{(n+2)(1-\frac{n+1}{N})}}{\sqrt{4n+6-\frac{4}{N}(n+1)^2}}\,|gg,n+2\rangle_N\end{aligned} \tag{4.3.19}$$

$$\begin{aligned}|0, n\rangle_{2,N} = {} & -\frac{\sqrt{(n+2)(1-\frac{n+1}{N})}}{\sqrt{(n+1)(1-\frac{n}{N})+(n+2)(1-\frac{n+1}{N})}}\,|ee,n\rangle_N \\ & + \frac{\sqrt{(n+1)(1-\frac{n}{N})}}{\sqrt{(n+1)(1-\frac{n}{N})+(n+2)(1-\frac{n+1}{N})}}\,|gg,n+2\rangle_N\end{aligned} \tag{4.3.20}$$

The subscript "*2,N*" is used differentiate these vectors from the vectors in the one-qubit big spin as well as two-qubit Jaynes-Cummings models. Similar to case of the two-qubit Jaynes-Cummings model, we also have a dark state that lies in antisymmetric subspace as there is no excitation in the system. This state is written as

$$|d, n\rangle_{2,N} = \frac{1}{\sqrt{2}}(|ge,n+1\rangle_N - |eg,n+1\rangle_N) \tag{4.3.21}$$

The rest of the unpaired eigenvectors are given by

$$|\pm,-1\rangle_{2,N} = \frac{1}{\sqrt{2}}\,|gg,1\rangle_N \pm \frac{1}{2}(|eg,0\rangle_N + |ge,0\rangle_N) \tag{4.3.22}$$

$$|d,-1\rangle_{2,N} = \frac{1}{\sqrt{2}}(|ge,0\rangle_N - |eg,0\rangle_N) \tag{4.3.23}$$

$$|gg,0\rangle_N \tag{4.3.24}$$

$$|\pm,N-1\rangle_{2,N} = \frac{1}{\sqrt{2}}\,|ee,N-1\rangle_N \pm \frac{1}{2}(|eg,N\rangle_N + |ge,N\rangle_N) \tag{4.3.25}$$

$$|d,N-1\rangle_{2,N} = \frac{1}{\sqrt{2}}(|ge,N\rangle_N - |eg,N\rangle_N) \tag{4.3.26}$$

$$-\,|ee,N\rangle_N\,. \tag{4.3.27}$$

We can then transform and write all the basis vectors used in (4.3.7) to (4.3.9) in terms of the eigenvectors as

$$\begin{aligned}|ee,n\rangle_N = {} & \frac{\sqrt{(n+1)(1-\frac{n}{N})}}{\sqrt{4n+6-\frac{4}{N}(n+1)^2}}(|+,n\rangle_{2,N} + |-,n\rangle_{2,N}) \\ & - \frac{\sqrt{(n+2)(1-\frac{n+1}{N})}}{\sqrt{(n+1)(1-\frac{n}{N})+(n+2)(1-\frac{n+1}{N})}}\,|0,n\rangle_{2,N}\end{aligned} \tag{4.3.28}$$

$$|eg,n+1\rangle_N = \frac{1}{2}(|+,n\rangle_{2,N} - |-,n\rangle_{2,N}) - \frac{1}{\sqrt{2}}\,|d,n\rangle_{2,N} \tag{4.3.29}$$

$$|ge,n+1\rangle_N = \frac{1}{2}(|+,n\rangle_{2,N} - |-,n\rangle_{2,N}) + \frac{1}{\sqrt{2}}\,|d,n\rangle_{2,N} \tag{4.3.30}$$

$$\begin{aligned}|gg,n+2\rangle_N = {} & \frac{\sqrt{(n+2)(1-\frac{n+1}{N})}}{\sqrt{4n+6-\frac{4}{N}(n+1)^2}}(|+,n\rangle_{2,N} + |-,n\rangle_{2,N}) \\ & + \frac{\sqrt{(n+1)(1-\frac{n}{N})}}{\sqrt{(n+1)(1-\frac{n}{N})+(n+2)(1-\frac{n+1}{N})}}\,|0,n\rangle_{2,N}\end{aligned} \tag{4.3.31}$$

$$|eg,0\rangle_N = \frac{1}{2}(|+,-1\rangle_{2,N} - |-,-1\rangle_{2,N}) - \frac{1}{\sqrt{2}}|d,-1\rangle_{2,N} \tag{4.3.32}$$

$$|ge,0\rangle_N = \frac{1}{2}(|+,-1\rangle_{2,N} - |-,-1\rangle_{2,N}) + \frac{1}{\sqrt{2}}|d,-1\rangle_{2,N} \tag{4.3.33}$$

$$|gg,1\rangle_N = \frac{1}{\sqrt{2}}(|+,n\rangle_{2,N} + |-,n\rangle_{2,N}) \tag{4.3.34}$$

$$|eg,N\rangle_N = \frac{1}{2}(|+,N-1\rangle_{2,N} - |-,-1\rangle_{2,N}) - \frac{1}{\sqrt{2}}|d,N-1\rangle_{2,N} \tag{4.3.35}$$

$$|ge,N\rangle_N = \frac{1}{2}(|+,N-1\rangle_{2,N} - |-,-1\rangle_{2,N}) + \frac{1}{\sqrt{2}}|d,N-1\rangle_{2,N} \tag{4.3.36}$$

$$|ee,N-1\rangle_N = \frac{1}{\sqrt{2}}(|+,n\rangle_{2,N} + |-,n\rangle_{2,N}). \tag{4.3.37}$$

Then we use the initial state at $t = 0$, as given by Equation (4.3.7) to decompose the general state into eigenstates as

$$\begin{aligned}
|\Psi_2(0)\rangle_N = \sum_{n=0}^{N-2} \Big(& C_n C_{ee} |ee,n\rangle_N + C_{n+1} C_{eg} |eg,n+1\rangle_N + C_{n+1} C_{ge} |ge,n+1\rangle_N \\
& + C_{n+2} C_{gg} |gg,n+2\rangle_N \Big) + C_N C_{ee} |ee,N\rangle_N + C_{N-1} C_{ee} |ee,N-1\rangle_N \\
& + C_N C_{eg} |eg,N\rangle_N + C_N C_{ge} |ge,N\rangle_N + C_0 C_{eg} |eg,0\rangle_N + C_0 C_{ge} |ge,0\rangle_N \\
& + C_1 C_{gg} |gg,1\rangle_N + C_0 C_{gg} |gg,0\rangle_N
\end{aligned} \tag{4.3.38}$$

and by changing the basis of the states, we have

$$
\begin{aligned}
|\Psi_2(0)\rangle_N = \sum_{n=0}^{N-2} \Bigg[& |+,n\rangle_{2,N} \left(C_n C_{ee} \frac{\sqrt{(n+1)(1-\frac{n}{N})}}{\sqrt{4n+6-\frac{4}{N}(n+1)^2}} + \frac{C_{n+1}}{2}(C_{eg}+C_{ge}) \right. \\
& \left. + C_{n+2}C_{gg} \frac{\sqrt{(n+2)(1-\frac{n+1}{N})}}{\sqrt{4n+6-\frac{4}{N}(n+1)^2}} \right) + |-,n\rangle_{2,N} \left(C_n C_{ee} \frac{\sqrt{(n+1)(1-\frac{n}{N})}}{\sqrt{4n+6-\frac{4}{N}(n+1)^2}} \right. \\
& \left. - \frac{C_{n+1}}{2}(C_{eg}+C_{ge}) + C_{n+2}C_{gg} \frac{\sqrt{(n+2)(1-\frac{n+1}{N})}}{\sqrt{4n+6-\frac{4}{N}(n+1)^2}} \right) \\
& + |0,n\rangle_{2,N} \left(C_{n+2}C_{gg} \frac{\sqrt{(n+1)(1-\frac{n}{N})}}{\sqrt{(n+1)(1-\frac{n}{N})+(n+2)(1-\frac{n+1}{N})}} - C_n C_{ee} \right. \\
& \left. \frac{\sqrt{(n+2)(1-\frac{n}{N})}}{\sqrt{(n+1)(1-\frac{n}{N})+(n+2)(1-\frac{n+1}{N})}} \right) + |d,n\rangle_{2,N} \frac{C_{n+1}}{\sqrt{2}}(C_{ge}-C_{eg}) \Bigg] \\
& + |+,N-1\rangle_{2,N} \left(\frac{C_N}{2}(C_{eg}+C_{ge}) + \frac{1}{\sqrt{2}} C_{N-1}C_{ee} \right) \\
& + |-,N-1\rangle_{2,N} \left(-\frac{C_N}{2}(C_{eg}+C_{ge}) + \frac{1}{\sqrt{2}} C_{N-1}C_{ee} \right) \\
& + |d,N-1\rangle_{2,N} \left(\frac{C_N}{\sqrt{2}}(C_{ge}-C_{eg}) \right) - |ee,N\rangle_{2,N} C_N C_{ee} \\
& + |+,-1\rangle_{2,N} \left(\frac{C_0}{2}(C_{eg}+C_{ge}) + \frac{1}{\sqrt{2}} C_1 C_{gg} \right) \\
& + |-,-1\rangle_{2,N} \left(-\frac{C_0}{2}(C_{eg}+C_{ge}) + \frac{1}{\sqrt{2}} C_1 C_{gg} \right) \\
& + |d,-1\rangle_{2,N} \left(\frac{C_0}{\sqrt{2}}(C_{ge}-C_{eg}) \right) + |gg,0\rangle_{2,N} C_0 C_{gg}
\end{aligned}
\tag{4.3.39}
$$

where in this set up, C_n is the coefficient for the big spin coherent state as given by Equation (1.2.33).

$$
C_n = \sum_{n=0}^{N} \frac{1}{(1+|\zeta|^2)^{N/2}} \sqrt{\frac{N!}{(N-n)!n!}} \zeta^n. \tag{4.3.40}
$$

With the above Equations (4.3.39) and (4.3.27), we can include the time dependence of the eigenstates by

$$
|\Psi_2(t)\rangle_N = e^{-i\hat{H}_{2,N}t/\hbar} |\Psi_2(0)\rangle_N . \tag{4.3.41}
$$

We then expand the equation and put the solution back into the basis states that measurements would project to, in terms of $|ee, n\rangle_{2,N}$, $|eg, n+1\rangle_{2,N}$, $|ge, n+1\rangle_{2,N}$ and $|gg, n+2\rangle_{2,N}$ and we get

$$\begin{aligned}
|\Psi_2(t)\rangle_N = &\sum_{n=0}^{N-2} e^{-i\omega_N(n+1)t}\Bigg[e^{-i\lambda\sqrt{4n+6-\frac{4}{N}(n+1)^2}}\Bigg(C_n C_{ee}\frac{\sqrt{(n+1)(1-\frac{n}{N})}}{\sqrt{4n+6-\frac{4}{N}(n+1)^2}} \\
&+ \frac{C_{n+1}}{2}(C_{eg}+C_{ge}) + C_{n+2}C_{gg}\frac{\sqrt{(n+2)(1-\frac{n+1}{N})}}{\sqrt{4n+6-\frac{4}{N}(n+1)^2}}\Bigg)|+,n\rangle_{2,N} \\
&+ e^{-i\lambda\sqrt{4n+6-\frac{4}{N}(n+1)^2}}\Bigg(C_n C_{ee}\frac{\sqrt{(n+1)(1-\frac{n}{N})}}{\sqrt{4n+6-\frac{4}{N}(n+1)^2}} \\
&- \frac{C_{n+1}}{2}(C_{eg}+C_{ge}) + C_{n+2}C_{gg}\frac{\sqrt{(n+2)(1-\frac{n+1}{N})}}{\sqrt{4n+6-\frac{4}{N}(n+1)^2}}\Bigg)|-,n\rangle_{2,N} \\
&+ \Bigg(C_{n+2}C_{gg}\frac{\sqrt{(n+1)(1-\frac{n}{N})}}{\sqrt{(n+1)(1-\frac{n}{N})+(n+2)(1-\frac{n+1}{N})}} \\
&- C_n C_{ee}\frac{\sqrt{(n+2)(1-\frac{n}{N})}}{\sqrt{(n+1)(1-\frac{n}{N})+(n+2)(1-\frac{n+1}{N})}}\Bigg)|0,n\rangle_{2,N} \\
&+ \frac{C_{n+1}}{\sqrt{2}}(C_{ge}-C_{eg})\,|d,n\rangle_{2,N}\Bigg] \\
&+ e^{-i\omega_N N t}e^{-\sqrt{2}i\lambda t}\Big(\frac{C_N}{2}(C_{eg}+C_{ge}) + \frac{1}{\sqrt{2}}C_{N-1}C_{ee}\Big)|+,N-1\rangle_{2,N} \\
&+ e^{-i\omega_N N t}e^{\sqrt{2}i\lambda t}\Big(-\frac{C_N}{2}(C_{eg}+C_{ge}) + \frac{1}{\sqrt{2}}C_{N-1}C_{ee}\Big)|-,N-1\rangle_{2,N} \\
&+ e^{-i\omega_N N t}\Big(\frac{C_N}{\sqrt{2}}(C_{ge}-C_{eg})\Big)|d,N-1\rangle - e^{-i\omega_N(N+1)t}C_N C_{ee}\,|ee,N\rangle_{2,N} \\
&+ e^{-\sqrt{2}i\lambda t}\Big(\frac{C_0}{2}(C_{eg}+C_{ge}) + \frac{1}{\sqrt{2}}C_1 C_{gg}\Big)|+,-1\rangle_{2,N} \\
&+ e^{\sqrt{2}i\lambda t}\Big(-\frac{C_0}{2}(C_{eg}+C_{ge}) + \frac{1}{\sqrt{2}}C_1 C_{gg}\Big)|-,-1\rangle_{2,N} \\
&+ \Big(\frac{C_0}{\sqrt{2}}(C_{ge}-C_{eg})\Big)|d,-1\rangle_{2,N} + e^{i\omega_N t}C_0 C_{gg}\,|gg,0\rangle_{2,N}
\end{aligned} \tag{4.3.42}$$

Next, we transform the exponential terms into sin and cos form such that $e^{ix} = \cos x + i\sin x$ and simplify the equation to get the exact solution to the two-qubit big spin model in the form of

$$
\begin{aligned}
|\Psi_2(t)\rangle_N = \sum_{n=0}^{N-2} e^{-i\omega_N(n+1)t} \Bigg(\\
& \Bigg[C_n C_{ee} \Bigg(\frac{(n+1)(1-\frac{n}{N})}{2n+3-\frac{2}{N}(n+1)^2} \cos\Bigg(\lambda t \sqrt{4n+6-\frac{4}{N}(n+1)^2}\Bigg) \\
& + \frac{(n+2)(1-\frac{n+1}{N})}{(n+1)(1-\frac{n}{N})+(n+2)(1-\frac{n+1}{N})} \Bigg) \\
& + C_{gg} C_{n+2} \sqrt{(n+1)(1-\frac{n}{N})} \sqrt{(n+2)(1-\frac{n+1}{N})} \\
& \times \Bigg(\frac{\cos\Big(\lambda t \sqrt{4n+6-\frac{4}{N}(n+1)^2}\Big)}{2n+3-\frac{2}{N}(n+1)^2} - \frac{1}{(n+1)(1-\frac{n}{N})+(n+2)(1-\frac{n+1}{N})} \Bigg) \\
& - i C_{n+1} \frac{\sqrt{(n+1)(1-\frac{n}{N})}}{\sqrt{4n+6-\frac{4}{N}(n+1)^2}} \sin\Bigg(\lambda t \sqrt{4n+6-\frac{4}{N}(n+1)^2}\Bigg) (C_{eg}+C_{ge}) \Bigg] \\
& \times |ee,n\rangle_N + \Bigg[- \frac{i \sin\Big(\lambda t \sqrt{4n+6-\frac{4}{N}(n+1)^2}\Big)}{\sqrt{4n+6-\frac{4}{N}(n+1)^2}} \Bigg(\sqrt{(n+1)(1-\frac{n}{N})} C_n C_{ee} \\
& + \sqrt{(n+2)(1-\frac{n+1}{N})} C_{n+2} C_{gg} \Bigg) + \frac{C_{n+1}}{2} \cos\Bigg(\lambda t \sqrt{4n+6-\frac{4}{N}(n+1)^2}\Bigg) \\
& \times (C_{eg}+C_{ge}) + \frac{C_{n+1}}{2} (C_{eg}-C_{ge}) \Bigg] |eg,n+1\rangle_N \\
& + \Bigg[- \frac{i \sin\Big(\lambda t \sqrt{4n+6-\frac{4}{N}(n+1)^2}\Big)}{\sqrt{4n+6-\frac{4}{N}(n+1)^2}} \Bigg(\sqrt{(n+1)(1-\frac{n}{N})} C_n C_{ee} \\
& + \sqrt{(n+2)(1-\frac{n+1}{N})} C_{n+2} C_{gg} \Bigg) - \frac{C_{n+1}}{2} \cos\Bigg(\lambda t \sqrt{4n+6-\frac{4}{N}(n+1)^2}\Bigg) \\
& \times (C_{eg}+C_{ge}) - \frac{C_{n+1}}{2} (C_{eg}-C_{ge}) \Bigg] |ge,n+1\rangle_N \\
& + \Bigg[C_{ee} C_n \sqrt{(n+1)(1-\frac{n}{N})} \sqrt{(n+2)(1-\frac{n+1}{N})} \\
& \times \Bigg(\frac{\cos\Big(\lambda t \sqrt{4n+6-\frac{4}{N}(n+1)^2}\Big)}{2n+3-\frac{2}{N}(n+1)^2} - \frac{1}{(n+1)(1-\frac{n}{N})+(n+2)(1-\frac{n+1}{N})} \Bigg) \\
& + C_{gg} C_{n+2} \Bigg(\frac{(n+2)(1-\frac{n+1}{N})}{2n+3-\frac{2}{N}(n+1)^2} \cos\Bigg(\lambda t \sqrt{4n+6-\frac{4}{N}(n+1)^2}\Bigg) \\
& + \frac{(n+1)(1-\frac{n}{N})}{(n+1)(1-\frac{n}{N})+(n+2)(1-\frac{n+1}{N})} \Bigg) - i C_{n+1} \frac{\sqrt{(n+2)(1-\frac{n+1}{N})}}{\sqrt{4n+6-\frac{4}{N}(n+1)^2}} \\
& \times \sin\Bigg(\lambda t \sqrt{4n+6-\frac{4}{N}(n+1)^2}\Bigg) (C_{eg}+C_{ge}) \Bigg] |gg,n+2\rangle_N \Bigg)
\end{aligned}
$$

$$
\begin{aligned}
&+ e^{-i\omega_N(N+1)t} C_N \left| ee, N \right\rangle_N + e^{-i\omega_N N t}\left[\frac{-iC_N}{2}(C_{eg}+C_{ge})\sin\left(\sqrt{2}\lambda t\right)\right. \\
&\left.+ \frac{C_1 C_{gg}}{\sqrt{2}}\cos\left(\sqrt{2}\lambda t\right)\right] \left| ee, N-1 \right\rangle_N + e^{-i\omega_N N t}\left[\frac{C_N}{2}(C_{eg}+C_{ge})\cos\left(\sqrt{2}\lambda t\right)\right. \\
&\left.+ \frac{-iC_1 C_{gg}}{\sqrt{2}}\sin\left(\sqrt{2}\lambda t\right)\right]\left(\left| eg, N \right\rangle_N + \left| ge, N \right\rangle_N \right) \\
&+ \left[-\frac{iC_0}{2}(C_{eg}+C_{ge})\sin\left(\sqrt{2}\lambda t\right) + \frac{C_1 C_{gg}}{\sqrt{2}}\cos\left(\sqrt{2}\lambda t\right)\right] \left| gg, 1 \right\rangle_N \\
&+ \left[\frac{C_0}{2}(C_{eg}+C_{ge})\cos\left(\sqrt{2}\lambda t\right) - \frac{iC_1 C_{gg}}{\sqrt{2}}\sin\left(\sqrt{2}\lambda t\right)\right]\left(\left| eg, 0 \right\rangle_N + \left| ge, 0 \right\rangle_N \right) \\
&+ \frac{C_0}{2}(C_{eg}-C_{ge})\left(\left| ge, 0 \right\rangle_N - \left| eg, 0 \right\rangle_N \right) + C_0 C_{gg} \left| gg, 0 \right\rangle_N .
\end{aligned}
\tag{4.3.43}
$$

To simplify the calculations, similar to the single qubit case considered in Section 2.3.3 we may then remove the basic time dependence of the states by moving to an interaction picture with the following state transformations. With these, the equation loses its dependency on ω_N.

$$e^{-i\omega_N t} \left| ee \right\rangle \rightarrow \left| ee \right\rangle , \tag{4.3.44}$$

$$\left| eg \right\rangle \rightarrow \left| eg \right\rangle , \tag{4.3.45}$$

$$\left| ge \right\rangle \rightarrow \left| ge \right\rangle , \tag{4.3.46}$$

$$e^{i\omega_N t} \left| gg \right\rangle \rightarrow \left| gg \right\rangle , \tag{4.3.47}$$

$$e^{-i\omega_N n t} \left| n \right\rangle_N \rightarrow \left| n \right\rangle_N , \tag{4.3.48}$$

4.3.3 Two-Qubit Attractor States

Similar to the previous models, we can find the attractor state for our two qubits and big spin model. In Section 2.3.5 we have demonstrated that in a parameter regime $1 \ll |\zeta|^2 \ll N$ where $\bar{n} = |\zeta|^2$, a qubit state in a one-qubit big spin model will approach an attractor state regardless of its initial state. We then showed that for the case of two-qubit Jaynes Cumming model, whether or not the two-qubit attractor state is approached is dependent on the initial state of the qubits.

To find the attractor state for our model, we start by rewriting the *cosine* and *sine* terms in the exponential forms as

$$\cos x = \frac{1}{2}\left(e^{ix} + e^{-ix}\right) \tag{4.3.49}$$

$$\sin x = \frac{1}{2i}\left(e^{ix} - e^{-ix}\right). \tag{4.3.50}$$

and then we collect the terms with the same frequency. Equation (4.3.43) above now becomes

$$
\begin{aligned}
|\Psi_2(t)\rangle_N = \sum_{n=0}^{N-2} \Bigg(& \\
& \Bigg[\Bigg(\frac{(n+2)(1-\frac{n+1}{N})}{2n+3-\frac{2}{N}(n+1)^2} C_{ee}C_n - \frac{\sqrt{(n+1)(1-\frac{n}{N})}\sqrt{(n+2)(1-\frac{n+1}{N})}}{(n+1)(1-\frac{n}{N})+(n+2)(1-\frac{n+1}{N})} \\
& \times C_{gg}C_{n+2}\Bigg)|ee,n\rangle_N + \frac{C_{eg}-C_{ge}}{2} C_{n+1}(\,|eg,n+1\rangle_N - |ge,n+1\rangle_N\,) \\
& \times \Bigg(- \frac{\sqrt{(n+1)(1-\frac{n}{N})}\sqrt{(n+2)(1-\frac{n+1}{N})}}{(n+1)(1-\frac{n}{N})+(n+2)(1-\frac{n+1}{N})} C_{ee}C_n + \frac{(n+1)(1-\frac{n}{N})}{2n+3-\frac{2}{N}(n+1)^2} \\
& \times C_{gg}C_{n+2}\Bigg)|gg,n+2\rangle_N\Bigg] \\
& + \frac{e^{i\lambda t\sqrt{4n+6-\frac{4}{N}(n+1)^2)}}}{2}\Bigg[\Bigg(\frac{(n+1)(1-\frac{n}{N})}{2n+3-\frac{2}{N}(n+1)^2} C_{ee}C_n \\
& + \frac{\sqrt{(n+1)(1-\frac{n}{N})}\sqrt{(n+2)(1-\frac{n+1}{N})}}{2n+3-\frac{2}{N}(n+1)^2} C_{gg}C_{n+2} - \frac{\sqrt{(n+1)(1-\frac{n}{N})}}{\sqrt{4n+6-\frac{4}{N}(n+1)^2}} \\
& \times (C_{eg}+C_{ge})C_{n+1}\Bigg)|ee,n\rangle_N + \Bigg(\frac{C_{eg}+C_{ge}}{2} C_{n+1} - \frac{\sqrt{(n+1)(1-\frac{n}{N})}}{\sqrt{4n+6-\frac{4}{N}(n+1)^2}} C_{ee}C_n \\
& - \frac{\sqrt{(n+2)(1-\frac{n+1}{N})}}{\sqrt{4n+6-\frac{4}{N}(n+1)^2}} C_{gg}C_{n+2}\Bigg)(\,|eg,n+1\rangle_N + |ge,n+1\rangle_N\,) \\
& + \Bigg(\frac{\sqrt{(n+1)(1-\frac{n}{N})}\sqrt{(n+2)(1-\frac{n+1}{N})}}{2n+3-\frac{2}{N}(n+1)^2} C_{ee}C_n + \frac{(n+2)(1-\frac{n+1}{N})}{2n+3-\frac{2}{N}(n+1)^2} \\
& - \frac{\sqrt{(n+2)(1-\frac{n+1}{N})}}{\sqrt{4n+6-\frac{4}{N}(n+1)^2}}(C_{eg}+C_{ge})C_{n+1}\Bigg)|gg,n+2\rangle_N\Bigg] + ..
\end{aligned}
$$

$$
\begin{aligned}
&+\frac{e^{-i\lambda t\sqrt{4n+6-\frac{4}{N}(n+1)^2)}}}{2}\Bigg[\Bigg(\frac{(n+1)(1-\frac{n}{N})}{2n+3-\frac{2}{N}(n+1)^2}C_{ee}C_n \\
&+\frac{\sqrt{(n+1)(1-\frac{n}{N})}\sqrt{(n+2)(1-\frac{n+1}{N})}}{2n+3-\frac{2}{N}(n+1)^2}C_{gg}C_{n+2}+\frac{\sqrt{(n+1)(1-\frac{n}{N})}}{\sqrt{4n+6-\frac{4}{N}(n+1)^2}} \\
&\times(C_{eg}+C_{ge})C_{n+1}\Bigg)|ee,n\rangle_N+\Bigg(\frac{C_{eg}+C_{ge}}{2}C_{n+1}+\frac{\sqrt{(n+1)(1-\frac{n}{N})}}{\sqrt{4n+6-\frac{4}{N}(n+1)^2}}C_{ee}C_n \\
&-\frac{\sqrt{(n+2)(1-\frac{n+1}{N})}}{\sqrt{4n+6-\frac{4}{N}(n+1)^2}}C_{gg}C_{n+2}\Bigg)(|eg,n+1\rangle_N+|ge,n+1\rangle_N) \\
&+\Bigg(\frac{\sqrt{(n+1)(1-\frac{n}{N})}\sqrt{(n+2)(1-\frac{n+1}{N})}}{2n+3-\frac{2}{N}(n+1)^2}C_{ee}C_n+\frac{(n+2)(1-\frac{n+1}{N})}{2n+3-\frac{2}{N}(n+1)^2} \\
&+\frac{\sqrt{(n+2)(1-\frac{n+1}{N})}}{\sqrt{4n+6-\frac{4}{N}(n+1)^2}}(C_{eg}+C_{ge})C_{n+1}\Bigg)|gg,n+2\rangle_N\Bigg]\Bigg)+|C_R\rangle_N
\end{aligned}
\tag{4.3.51}
$$

where $|C_R\rangle_N$ are all quantum state terms from outside the sum in Equation (4.3.43) that is given by

$$
\begin{aligned}
|C_R\rangle_N =&C_N|ee,N\rangle_N+\Bigg[\frac{-iC_N}{2}(C_{eg}+C_{ge})\sin\Big(\sqrt{2}\lambda t\Big) \\
&+\frac{C_1C_{gg}}{\sqrt{2}}\cos\Big(\sqrt{2}\lambda t\Big)\Bigg]|ee,N-1\rangle_N+\Bigg[\frac{C_N}{2}(C_{eg}+C_{ge})\cos\Big(\sqrt{2}\lambda t\Big) \\
&+\frac{-iC_1C_{gg}}{\sqrt{2}}\sin\Big(\sqrt{2}\lambda t\Big)\Bigg](|eg,N\rangle_N+|ge,N\rangle_N) \\
&+\Bigg[-\frac{iC_0}{2}(C_{eg}+C_{ge})\sin\Big(\sqrt{2}\lambda t\Big)+\frac{C_1C_{gg}}{\sqrt{2}}\cos\Big(\sqrt{2}\lambda t\Big)\Bigg]|gg,1\rangle_N \\
&+\Bigg[\frac{C_0}{2}(C_{eg}+C_{ge})\cos\Big(\sqrt{2}\lambda t\Big)-\frac{iC_1C_{gg}}{\sqrt{2}}\sin\Big(\sqrt{2}\lambda t\Big)\Bigg](|eg,0\rangle_N+|ge,0\rangle_N) \\
&+\frac{C_0}{2}(C_{eg}-C_{ge})(|ge,0\rangle_N-|eg,0\rangle_N)+C_0C_{gg}|gg,0\rangle_N\,.
\end{aligned}
\tag{4.3.52}
$$

Within a regime of $1 \ll |\zeta|^2 \ll N$ where $\bar{n}=|\zeta|^2$, we can make the following approximations

$$(n+1)(1-\frac{n}{N}) \approx n(1-\frac{n}{N}) \tag{4.3.53}$$

$$(n+2)(1-\frac{n+1}{N}) \approx n(1-\frac{n}{N}) \tag{4.3.54}$$

$$\sqrt{4n+6-\frac{4}{N}(n+1)^2} \approx 2\sqrt{n(1-\frac{n}{N})} \tag{4.3.55}$$

we further simplify Equation (4.3.52) as

$$\begin{aligned}
\left|\widetilde{\Psi}_2(t)\right\rangle_N = \sum_{n=0}^{N-2} \Bigg(& \frac{1}{2}\big[(C_{ee}C_n - C_{gg}C_{n+2})\left|ee,n\right\rangle_N \\
&+ (C_{eg}-C_{ge})C_{n+1}\big(\left|eg,n+1\right\rangle_N - \left|ge,n+1\right\rangle_N\big) \\
&+ \big(-C_{ee}C_n + C_{gg}C_{n+2}\big)\left|gg,n+2\right\rangle_N\big] \\
&+ \frac{e^{2i\lambda t\sqrt{n\left(1-\frac{n}{N}\right)}}}{4}\big[(C_{ee}C_n + C_{gg}C_{n+2}) - (C_{eg}-C_{ge})C_{n+1}\left|ee,n\right\rangle_N \\
&+ \big((C_{eg}+C_{ge})C_{n+1} - C_{ee}C_n - C_{gg}C_{n+2}\big)\big(\left|eg,n+1\right\rangle_N + \left|ge,n+1\right\rangle_N\big) \\
&\big(C_{ee}C_n + C_{gg}C_{n+2} - (C_{eg}-C_{ge})C_{n+1}\big)\left|gg,n+2\right\rangle_N\big] \\
&+ \frac{e^{-2i\lambda t\sqrt{n\left(1-\frac{n}{N}\right)}}}{4}\big[(C_{ee}C_n + C_{gg}C_{n+2}) + (C_{eg}-C_{ge})C_{n+1}\left|ee,n\right\rangle_N \\
&+ \big((C_{eg}+C_{ge})C_{n+1} + C_{ee}C_n - C_{gg}C_{n+2}\big)\big(\left|eg,n+1\right\rangle_N + \left|ge,n+1\right\rangle_N\big) \\
&\big(C_{ee}C_n + C_{gg}C_{n+2} - (C_{eg}+C_{ge})C_{n+1}\big)\left|gg,n+2\right\rangle_N\big]\Bigg) + \left|C_R\right\rangle_N .
\end{aligned} \tag{4.3.56}$$

We regroup the terms based on their state basis $\left|ee,n\right\rangle_N$, $\left|eg,n+1\right\rangle_N$, $\left|ge,n+1\right\rangle_N$ and $\left|gg,n+2\right\rangle_N$ and obtain

$$
\begin{aligned}
\left|\widetilde{\Psi}_2(t)\right\rangle_N &= \sum_{n=0}^{N-2} \frac{C_n}{2}\Bigg(\Bigg[\Bigg(C_{ee} - C_{gg}\frac{C_{n+2}}{C_n}\Bigg)\left|ee,n\right\rangle_N \\
&+ (C_{eg} - C_{ge})\big(\left|eg,n\right\rangle_N - \left|ge,n\right\rangle_N\big) - \Bigg(C_{ee}\frac{C_{n-2}}{C_n} - C_{gg}\Bigg)\left|gg,n\right\rangle_N\Bigg] \\
&+ \frac{1}{2}\Bigg[e^{2i\lambda t\sqrt{(n+2)\left(1-\frac{n+2}{N}\right)}}\Bigg(C_{ee} + C_{gg}\frac{C_{n+2}}{C_n} - (C_{eg} + C_{ge})\frac{C_{n+1}}{C_n}\Bigg)\left|ee,n\right\rangle_N \\
&+ e^{2i\lambda t\sqrt{(n+1)\left(1-\frac{n+1}{N}\right)}}\Bigg((C_{eg} + C_{ge}) - C_{ee}\frac{C_{n-1}}{C_n} - C_{gg}\frac{C_{n+1}}{C_n}\Bigg)\big(\left|eg,n\right\rangle_N - \left|ge,n\right\rangle_N\big) \\
&+ e^{2i\lambda t\sqrt{n\left(1-\frac{n}{N}\right)}}\Bigg(C_{ee}\frac{C_{n-2}}{C_n} + C_{gg} - (C_{eg} + C_{ge})\frac{C_{n-1}}{C_n}\Bigg)\left|gg,n\right\rangle_N\Bigg]\Bigg) \\
&+ \frac{1}{2}\Bigg[e^{-2i\lambda t\sqrt{(n+2)\left(1-\frac{n+2}{N}\right)}}\Bigg(C_{ee} + C_{gg}\frac{C_{n+2}}{C_n} + (C_{eg} + C_{ge})\frac{C_{n+1}}{C_n}\Bigg)\left|ee,n\right\rangle_N \\
&+ e^{-2i\lambda t\sqrt{(n+1)\left(1-\frac{n+1}{N}\right)}}\Bigg((C_{eg} + C_{ge}) + C_{ee}\frac{C_{n-1}}{C_n} - C_{gg}\frac{C_{n+1}}{C_n}\Bigg)\big(\left|eg,n\right\rangle_N - \left|ge,n\right\rangle_N\big) \\
&+ e^{-2i\lambda t\sqrt{n\left(1-\frac{n}{N}\right)}}\Bigg(C_{ee}\frac{C_{n-2}}{C_n} + C_{gg} + (C_{eg} + C_{ge})\frac{C_{n-1}}{C_n}\Bigg)\left|gg,n\right\rangle_N\Bigg]\Bigg)
\end{aligned}
\tag{4.3.57}
$$

A further approximation can be made if the relevant values of n are such that $(n - \bar{n}) \ll \bar{n}$, which simplifies the big spin's coefficient as

$$
\begin{aligned}
\frac{C_{n+1}}{C_n} &= \left[\frac{\frac{\zeta}{\sqrt{N}}\sqrt{N-n}}{\sqrt{n+1}}\right] &(4.3.58)\\
&= \left[\frac{\frac{\zeta}{\sqrt{N}}\sqrt{N-\overline{n}}}{\sqrt{\overline{n}}}\right]\left(1 - \frac{n-\overline{n}}{N-\overline{n}}\right)^{1/2}\left(1 + \frac{n-\overline{n}+1}{\overline{n}}\right)^{-1/2} &(4.3.59)\\
&\approx \left[\frac{\frac{\zeta}{\sqrt{N}}\sqrt{N-\overline{n}}}{\sqrt{\overline{n}}}\right]\left(1 - \frac{n-\overline{n}}{2(N-\overline{n})} + ...\right)\left(1 - \frac{n-\overline{n}+1}{2\overline{n}} + ...\right) &(4.3.60)\\
&\approx \frac{\zeta}{|\zeta|}\left(1 - \frac{|\zeta|}{2\sqrt{N}} + ...\right)\left(1 - \frac{1}{2N|\zeta|} - \frac{1}{2N|\zeta|^2} - \frac{1}{2N} + ...\right) &(4.3.61)\\
&\approx \frac{\zeta}{|\zeta|} = e^{-i\phi} &(4.3.62)
\end{aligned}
$$

and similarly, we have

$$
\frac{C_{n-1}}{C_n} \approx \frac{|\zeta|}{\zeta} = e^{i\phi}. \tag{4.3.63}
$$

With the facts that $(n-\bar{n})$ is small compared to $\bar{n}$ and $\bar{n} \ll N$, we can separate the two-qubit and the big spin parts by using binomial theorem to expand the following square roots and then simplify the terms inside.

$$\sqrt{(n+l)\left(1-\frac{n}{N}\right)} = (\bar{n}+(n-\bar{n})+l)^{\frac{1}{2}}\left(1-\frac{\bar{n}+(n-\bar{n})}{N}\right)^{\frac{1}{2}} \tag{4.3.64}$$

$$\approx \left(\sqrt{\bar{n}}+\frac{(n-\bar{n})}{2\sqrt{\bar{n}}}+\frac{l}{2\sqrt{\bar{n}}}\right)\left(1-\frac{\bar{n}}{N}\right) \tag{4.3.65}$$

$$\approx \left(\frac{\sqrt{\bar{n}}}{2}+\frac{n}{2\sqrt{\bar{n}}}+\frac{l}{2\sqrt{\bar{n}}}\right)\left(1-\frac{\bar{n}}{N}\right) \tag{4.3.66}$$

where l in this case is a parameter that takes on the value of -1, 0 or 1.

$$\begin{aligned}\left|\widetilde{\Psi}_2(t)\right\rangle_N =& \frac{1}{2}\left(\sum_{n=0}^{N} C_n \left|n\right\rangle_N\right)\Big[\left(e^{2i\phi}C_{ee}-C_{gg}\right)\left(e^{-2i\phi}\left|ee\right\rangle-\left|gg\right\rangle\right)\\ &+\left(C_{eg}-C_{ge}\right)\left(\left|eg\right\rangle-\left|ge\right\rangle\right)\Big]+\left(e^{2i\phi}C_{ee}-e^{i\phi}(C_{eg}+C_{ge})+C_{gg}\right)\\ &\times\Bigg[\frac{e^{i\lambda\sqrt{\bar{n}}\left(1-\frac{\bar{n}}{N}\right)t}e^{2i\lambda\left(1-\frac{\bar{n}}{N}\right)t/\sqrt{\bar{n}}}}{4}\left(\sum_{n=0}^{N}C_n e^{in\left(1-\frac{\bar{n}}{N}\right)\lambda t/\sqrt{\bar{n}}}\left|n\right\rangle_N\right)\\ &\left(e^{-2i\phi}\left|ee\right\rangle-e^{-i\lambda\left(1-\frac{\bar{n}}{N}\right)t/\sqrt{\bar{n}}}e^{i\phi}(\left|eg\right\rangle+\left|ge\right\rangle)+e^{-2i\lambda t/\sqrt{\bar{n}}}\left|gg\right\rangle\right)\\ &+\frac{e^{-i\lambda\sqrt{\bar{n}}\left(1-\frac{\bar{n}}{N}\right)t}e^{2i\lambda\left(1-\frac{\bar{n}}{N}\right)t/\sqrt{\bar{n}}}}{4}\left(\sum_{n=0}^{N}C_n e^{-in\left(1-\frac{\bar{n}}{N}\right)\lambda t/\sqrt{\bar{n}}}\left|n\right\rangle_N\right)\\ &\left(e^{2i\phi}\left|ee\right\rangle-e^{i\lambda\left(1-\frac{\bar{n}}{N}\right)t/\sqrt{\bar{n}}}e^{i\phi}(\left|eg\right\rangle+\left|ge\right\rangle)+e^{2i\lambda t/\sqrt{\bar{n}}}\left|gg\right\rangle\right)\Bigg].\end{aligned} \tag{4.3.67}$$

It is clear that there are two distinct parts in this equation which can be simplified in the form of

$$\left|\widetilde{\Psi}_2(t)\right\rangle_N = \sum_{k=-1}^{1}\eta_k(t)\left|Q_k(t)\right\rangle\otimes\left|\Phi_k(t)\right\rangle_N \tag{4.3.68}$$

where $\eta_k(t)$ is normalisation factor, $|Q_k(t)\rangle$ is the two-qubit state, $|\Phi_k(t)\rangle_N$ is a state of the big spin state and k takes a value of $-1, 0$ or 1. With t_r as the one-qubit big spin revival time and given by Equation (2.3.78), these terms are then written as

$$\eta_{\pm 1}(t) = \frac{e^{\pm 2i\pi t(\bar{n}+2)/t_r}}{2}\left(e^{2i\phi}C_{ee} \mp e^{i\phi}\left(C_{eg}+C_{ge}\right)+C_{gg}\right) \tag{4.3.69}$$

$$\eta_0 = \sqrt{\frac{|e^{2i\phi}C_{ee}-C_{gg}|^2+|C_{eg}-C_{ge}|^2}{2}} \tag{4.3.70}$$

$$|Q_{\pm 1}(t)\rangle = \frac{1}{2}\left(e^{-2i\phi}|ee\rangle \mp e^{\pm 2i\pi t/t_r}e^{-i\phi}\left(|eg\rangle+|ge\rangle\right)+e^{\mp 4i\pi t/t_r}|gg\rangle\right) \tag{4.3.71}$$

$$|Q_0(t)\rangle = \frac{(e^{2i\phi}C_{ee}-C_{gg}(e^{-2i\phi}|ee\rangle-|gg\rangle)+(C_{eg}-C_{ge})(|eg\rangle-|ge\rangle))}{\sqrt{2\left(|e^{2i\phi}C_{ee}-C_{gg}|^2+|C_{eg}-C_{ge}|^2\right)}} \tag{4.3.72}$$

$$|\Phi_k(t)\rangle_N = \sum_{n=0}^{N} C_n e^{2ink\pi t/t_r}|n\rangle_N . \tag{4.3.73}$$

The term $|Q_0(t)\rangle$ is time-independent and with this the qubit is a maximally entangled qubit state at all times if $C_{eg} = C_{ge}$. With a spin coherent state, we have

$$|\Phi_k(t)\rangle_N = \left|e^{2ik\pi t/t_r}\frac{\zeta}{\sqrt{N}}\right\rangle_N . \tag{4.3.74}$$

We can see that the two-qubit states $|Q_{\pm 1}(t)\rangle$ given by Equation (4.3.69) are actually direct products of the single qubit states $\left|Q_{\pm\frac{1}{2}}(t)\right\rangle$ with a mapping of time $t \to 2t$.

$$|Q_{\pm 1}(t)\rangle = \frac{1}{2}\left(e^{-2i\phi}|ee\rangle \mp e^{\pm 2i\pi t/t_r}e^{-i\phi}\left(|eg\rangle+|ge\rangle\right)+e^{\mp 4i\pi t/t_r}|gg\rangle\right) \tag{4.3.75}$$

$$= \frac{1}{\sqrt{2}}\left(e^{-i\phi}|e\rangle \mp e^{\mp 2i\pi t/t_r}|g\rangle\right) \otimes \frac{1}{\sqrt{2}}\left(e^{-i\phi}|e\rangle \mp e^{\mp 2i\pi t/t_r}|g\rangle\right) \tag{4.3.76}$$

$$= \left|Q_{\pm\frac{1}{2}}(2t)\right\rangle \otimes \left|Q_{\pm\frac{1}{2}}(2t)\right\rangle . \tag{4.3.77}$$

From Section 2.3.5 we know that the qubit state in the one-qubit big spin model evolves into an attractor state at the attractor time $\frac{t_r}{2}$, such that $\left|Q_{\pm\frac{1}{2}}(\frac{t_r}{2})\right\rangle = \left|\psi^{+}_{1,att}\right\rangle$. We have also seen the correspondence of attractor states for the one-qubit and two-qubit Jaynes-Cummings models in Section 4.2.3 where the two-qubit state $|Q_{\pm 1}(t)\rangle$ becomes a direct product of $\left|Q_{\pm\frac{1}{2}}(t)\right\rangle$ at time $\frac{t_r}{4}$. Therefore we can conclude that the attractor state for our two-qubit big spin model will behave in the same way where

$$\left|Q_{\pm1}\left(\frac{t_r}{4}\right)\right\rangle = \left|Q_{\pm\frac{1}{2}}\left(\frac{t_r}{2}\right)\right\rangle \otimes \left|Q_{\pm\frac{1}{2}}\left(\frac{t_r}{2}\right)\right\rangle \tag{4.3.78}$$

$$= \left|\psi^{+}_{1,att}\right\rangle_N \otimes \left|\psi^{+}_{1,att}\right\rangle_N \tag{4.3.79}$$

$$= \left|\psi^{+}_{2,att}\right\rangle_N . \tag{4.3.80}$$

We can also find the second two-qubit attractor state of the two-qubit big spin system $\left|\psi^{-}_{2,att}\right\rangle_N$ which is orthogonal to $\left|\psi^{+}_{2,att}\right\rangle_N$ at time $\frac{3t_r}{4}$ which we label and write both two-qubit attractor states as

$$\left|\psi^{\pm}_{2,att}\right\rangle_N = \frac{1}{2}\left(e^{2i\phi}\left|ee\right\rangle \pm ie^{i\phi}\left(\left|eg\right\rangle + \left|ge\right\rangle\right) - \left|gg\right\rangle\right). \tag{4.3.81}$$

We may note that these states are exactly in the same form as the two-qubit attractor states of the two-qubit Jaynes-Cummings model given by Equation (4.2.64). This shows the correspondence of the two models in the $N \to \infty$ approximation.

4.3.4 Basin of attraction

We have seen that the initial two-qubit state for the case of the two-qubit Jaynes-Cummings model is bounded by a regime called the basin of attraction given by Equation (4.2.66). The correspondence of our two-qubit big spin model with the two-qubit Jaynes-Cummings model enables us to find a similar basin of attraction *i.e.* all two-qubit initial conditions that lead to the two-qubit attractor states $\left|\psi^{\pm}_{2,att}\right\rangle_N$. The wavefunction for the whole system at time $\frac{t_r}{4}$ can be written in terms of the two-qubit attractor state and spin coherent state as

$$\begin{aligned}\left|\widetilde{\Psi}_2\left(\frac{t_r}{4}\right)\right\rangle_N = &-\frac{1}{2}\left|\psi^{+}_{2,att}\right\rangle_N\Bigg[\left(e^{2i\phi}C_{ee}+C_{gg}\right)\left(e^{i\pi\bar{n}/2}\left|i\frac{\zeta}{\sqrt{N}}\right\rangle_N\right.\\ &\left.+\,e^{-i\pi\bar{n}/2}\left|-i\frac{\zeta}{\sqrt{N}}\right\rangle_N\right) - e^{i\phi}\left(C_{eg}+C_{ge}\right)\left(e^{i\pi\bar{n}/2}\left|i\frac{\zeta}{\sqrt{N}}\right\rangle_N\right.\\ &\left.-\,e^{-i\pi\bar{n}/2}\left|-i\frac{\zeta}{\sqrt{N}}\right\rangle_N\right)\Bigg] + \eta_0\left|Q_0\right\rangle\left|\frac{\zeta}{\sqrt{N}}\right\rangle_N\end{aligned} \tag{4.3.82}$$

By writing the equation in this form, it is clear that the two qubits and the big spin parts in this equation will be in a product state when the $\eta_0\left|Q_0\right\rangle\left|\frac{\zeta}{\sqrt{N}}\right\rangle$ part vanishes. This is when the linear entropy goes to zero, indicating that there is no entanglement between the two qubits and the big spin. At this two-qubit attractor time too, there is no presence of entanglement between the two qubits.

To find the 'basin of attraction' of the system we start by letting $\eta_0 = 0$. This is only possible if the coefficients of the two-qubit states in Equation (4.3.72) are $e^{i\phi}C_{ee} = e^{-i\phi}C_{gg} = b$ and $C_{eg} = C_{ge} = \sqrt{\frac{1}{2} - |b|^2}$. With these we have an initial state of the form of

$$|\psi_2\rangle = b\left(e^{-i\phi}|ee\rangle + e^{i\theta}|gg\rangle\right) + \sqrt{\frac{1}{2} - |b|^2}\,(|eg\rangle + |ge\rangle) \tag{4.3.83}$$

where ϕ is the initial phase of the spin coherent state and b is a complex variable parameterising the state and satisfies $0 \le |b| \le \frac{1}{\sqrt{2}}$. Obviously this basin of attraction is identical to the two-qubit Jaynes Cumming case a given by Equation (4.2.66). We have similar set of initial two-qubit states that lie in the symmetric subspace and will lead to two-qubit attractor states.

At this two-qubit attractor time too, all the information inside the qubits system has been transferred into the big spin, which is now a spin cat state [29, 63, 62] . From the wavefunction, we can see that Equation (4.3.82) contains two distinct spin coherent states $|\Phi_{\pm 1}(\frac{t_r}{4})\rangle$. We can rewrite the equation to see a clear connection between the two-qubit initial states with the proportion of the spin coherent states $\left|\frac{\zeta}{\sqrt{N}}\right\rangle$ and $\left|-\frac{\zeta}{\sqrt{N}}\right\rangle$ as

$$\begin{aligned}\left|\widetilde{\Psi}_2\left(\frac{t_r}{4}\right)\right\rangle_N &= -e^{i\phi}\left|\psi^+_{2,att}\right\rangle_N \\ &\times\left(e^{i\pi\bar{n}/2}\left(b - \sqrt{\frac{1}{2} - |b|^2}\right)\left|i\frac{\zeta}{\sqrt{N}}\right\rangle + e^{-i\pi\bar{n}/2}\left(b + \sqrt{\frac{1}{2} - |b|^2}\right)\left|-i\frac{\zeta}{\sqrt{N}}\right\rangle\right).\end{aligned} \tag{4.3.84}$$

This also explains how the information from the two-qubit initial state is encoded into the big spin while the two qubits evolve into an attractor state at time $\frac{t_r}{4}$.

The connection between the big spin state in the two-qubit model with the one-qubit case can also be seen under the $t \to 2t$ time mapping. Similar to the two-qubit Jaynes-Cummings model, we have $|\Phi_{\pm 1}(t)\rangle_N = \left|\Phi_{\pm\frac{1}{2}}(2t)\right\rangle_N$. We also know from the one-qubit case that at time t_r and $2t_r$ the big spin and the qubit become unentangled, so $\left|\Phi_{+\frac{1}{2}}(t_r)\right\rangle = \left|\Phi_{-\frac{1}{2}}(t_r)\right\rangle_N$ and $\left|\Phi_{+\frac{1}{2}}(2t_r)\right\rangle_N = \left|\Phi_{-\frac{1}{2}}(2t_r)\right\rangle_N$. With these results, we can write $|\Phi_{+1}(\frac{t_r}{2})\rangle_N = |\Phi_{-1}(\frac{t_r}{2})\rangle_N$ and $|\Phi_{+1}(t_r)\rangle_N = |\Phi_{-1}(t_r)\rangle_N$. This shows that at times $\frac{t_r}{2}$ and t_r, the big spin part can be factorised out of the wavefunction and there is no entanglement present between the two qubits and the big spin at these particular times.

4.3.5 Numerical Results

We plot the time evolutions of the two-qubit big spin system as Figure 4.3.1 and Figure 4.3.2. The first figure shows the dynamics in the interacting system with an initial two-qubit state that lies inside the basin of attraction, while the second figure is for the case of the initial state outside the basin of attraction. As comparisons to the two-qubit Jaynes-Cummings model considered in the previous section, we use a similar $\frac{1}{\sqrt{2}}(|ee\rangle + |gg\rangle)$ as the initial state from inside the basin of attraction, and state $\frac{1}{\sqrt{20}}|ee\rangle + \sqrt{\frac{19}{20}}|gg\rangle$ for the case of an initial state from outside the basin. For both cases, we let $\bar{n} = 25$, $N = 150$ and $\phi = 0$.

The linear entropy associated with the density matrix of the two qubits at all times when the big spin has been traced out $S_q^L(t)$ is plotted as a red line to show the purity of the two-qubit system. We also plot the probability of both qubits being in the excited state $P_{ee}(t)$ as the a blue line and the probability of the two-qubit state being in the two-qubit attractor state $P_{2,att}^{+}(t)$ is shown as an orange line. Both figures show the presence of collapse and revival in the two-qubit state probability regardless of the initial state where the blue lines show probability peaks at certain times. From the figures, we can see that the first revival for this two-qubit big spin system happens at $\frac{t_r}{2}$, which is half the revival time of the system with one qubit t_r given by Equation (2.3.78).

At the two-qubit attractor time $\frac{t_r}{4}$, with an initial two-qubit state from inside the basin of attraction, the qubits and the big spin are essentially unentangled. This result can be seen by the linear entropy line (red) approaching zero at this particular time, indicating little entanglement present between the two subsystems. In addition to that, the qubits are now in an approximate pure state known as two-qubit attractor state $\left|\psi_{2,att}^{+}\right\rangle_N$. This is demonstrated through the fidelity against this state, shown as an orange line in Figure 4.3.1. This means that there is no entanglement present in the system with the quantum information of the initial two-qubit state now encoded into the big spin which is now a spin cat state [29, 63, 62]. This is however not the case if the qubits start with a state from outside the basin of attraction. It is because the two-qubit state in this interacting system can not be factorised out of the wavefunction given by Equation (4.3.82). The non-zero η_0 value prohibits the factorisation of the wavefunction into the two-qubit and the big spin parts thus; the entropy will be non-zero. This is clearly shown in Figure 4.3.2 where the red line has a significant value at time $\frac{t_r}{4}$ indicating some entanglement between the big spin and the two-qubit subsystem. Furthermore, the two-qubit system does not approach the two-qubit attractor state as shown by the orange line, where the probability of being in the two-qubit attractor state $P^{+}_{2,att}(t)$ does not approach unity at time $\frac{t_r}{4}$. Similar behaviour emerges at the second two-qubit attractor time $\frac{3t_r}{4}$ except for the attractor state probability where the orthogonal two-qubit state $\left|\psi^{-}_{2,att}\right\rangle_N$ is the relevant attractor.

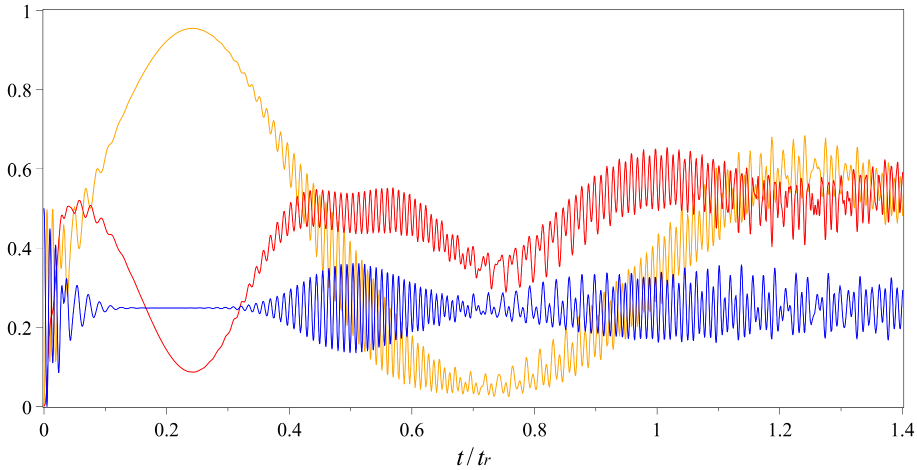

Figure 4.3.1: Time evolution for two-qubit big spin system with the initial two-qubit state $\frac{1}{\sqrt{2}}(|ee\rangle + |gg\rangle)$, $\bar{n} = 36$, $N = 150$ and the initial phase of the radiation field $\phi = 0$. The linear entropy of the qubits is plotted as a red line, the probability of the two-qubit state $|ee\rangle$ as a blue line and the probability of being in the two qubit 'attractor' state $\left|\psi^{+}_{2,att}\right\rangle_N$ as an orange line.

From the previously considered analytical solutions with large $\bar{n}$ where $1 \ll \bar{n} \ll N$, we know that regardless of the initial conditions, the system will once again be factorised into the two-qubit and the big spin parts at time t_r. Similar behaviour is also predicted at time $\frac{t_r}{2}$ if the two qubits start with a state that lies inside the basin of attraction. At these times, the two qubits are again in a pure state and their entropy are therefore expected to be zero. The dips in the linear entropy line is expected to be very near to zero to indicate the absence of entanglement between the subsystems. However, we can see this is not the case in the graphs. Unlike the behaviour at $\frac{t_r}{4}$ in the figures that can be approximately understood from the analytics, we cannot make a similar conclusion with the behaviour of the system at later times. There are no deep dips shown by the red line at $\frac{t_r}{2}$ and t_r in Figure 4.3.1 as well as at time t_r in Figure 4.3.2. This

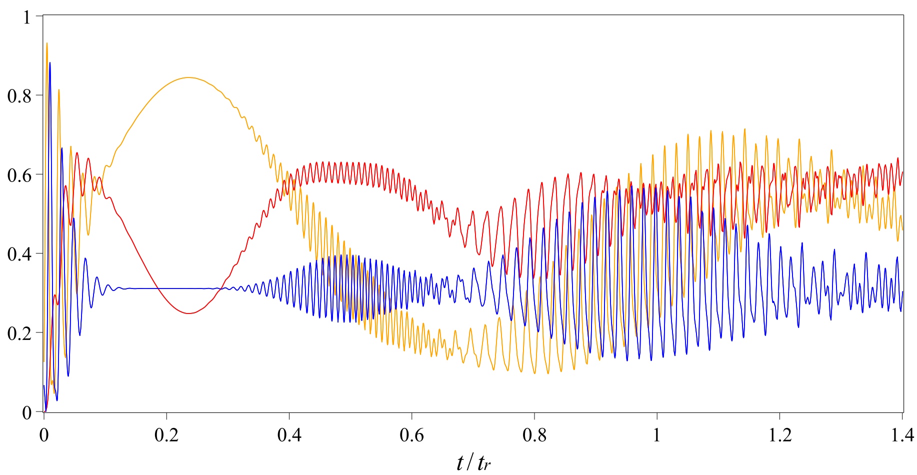

Figure 4.3.2: Time evolution for two-qubit big spin system with the initial two-qubit state $\frac{1}{\sqrt{20}}|ee\rangle + \sqrt{\frac{19}{20}}|gg\rangle$, $\bar{n} = 25$, $N = 150$ and the initial phase of the radiation field $\phi = 0$. The linear entropy of the qubits is plotted as a red line, the probability of the two-qubit state $|ee\rangle$ as a blue line and the probability of being in the two qubit 'attractor' state $\left|\psi^{+}_{2,att}\right\rangle_N$ as an orange line.

means that the parameters used in the numerical calculations are insufficient to approach the $N \to \infty$ conditions required for the analytic results to apply.

4.3.6 Collapse, Revival, Death and Rebirth of Qubits Entanglement

As shown in Section 4.2.6, in a two-qubit system we can measure not only the entanglement between the qubits and the field, but also between the two qubits themselves. While we use linear entropy to measure the first entanglement, we use a quantity called concurrence $\varsigma(t) = \sqrt{\tau(t)}$ as a measurement of the latter, where $\tau(t)$ is the mixed state tangle that is calculated by using Equation (4.2.68). We have discussed the linear entropy behaviour in our two-qubit big spin model in the previous section. So here we will further investigate the qubit-qubit entanglement in the system. This will reveal interesting phenomena resulting from the interaction of the two qubits and the big spin. These phenomena are known as the 'collapse and revival' as well as 'the sudden death / birth' of entanglement between the two qubits and they are analogous to the two-qubit Jaynes-Cummings model behaviour[64, 27].

It was also shown that in the two-qubit Jaynes-Cummings model, the the events depend on the two-qubit initial state, which is bounded by the basin of attraction described by Equation (4.2.66). Given the similarities of the two models, it is possible for us to study the connection of the phenomena 'collapse and revival' as well as the 'death and birth' of entanglement with the basin of attraction in our two-qubit big spin model.

Initial two-qubit state from inside the basin of attraction

The basin of attraction for the initial states of a two-qubit big spin model is given by Equation (4.3.83). It is parameterised by a single complex variable b and similar to the basin of attraction for the case of two-qubit Jaynes-Cummings model as given by Equation (4.2.66). As was demonstrated by C.Jarvis *et.al* [64, 27], we can calculate the level of entanglement associated with the states inside the basin of attraction. We plot Figure 4.3.3 to demonstrate the connection of concurrence $\varsigma(t)$ and parameter b. This figure shows that all possible levels of entanglement are represented in the basin of attraction. It shows that there are only two points where we have $\varsigma(t) = 0$, indicating that there are only two product states in this basin of attraction which are at $b = \pm\frac{1}{2}$. All other points represent entangled states with the entanglement varying between zero and the maximum value of unity. All the points representing states with maximum (unit) entanglement are given by the circle $b = \frac{e^{i\varphi}}{\sqrt{2}}$ and the line $Re(b) = 0$, where φ is an arbitrary phase.

At time $\frac{t_r}{4}$, all initial states inside the basin evolve into a two-qubit attractor state $\left|\psi^+_{2,att}\right\rangle_N$ given by Equation (4.3.78), and at time $\frac{3t_r}{4}$ they evolve into the orthogonal two-qubit attractor state $\left|\psi^-_{2,att}\right\rangle_N$. These states are pure and unentangled with the big spin, so there is no entanglement between the two qubits and the big spin at these times. We also know from Section 4.2.3 that the two-qubit attractor states is simply a direct product of two one-qubit attractor state $\left|\psi^+_{1,att}\right\rangle_N$ which are also pure and unentangled. Therefore, if the system starts with any state from inside the basin of attraction, there will be no qubit-qubit entanglement present and we will have a system with absolutely no entanglement either between the subsystems or between the two qubits at these times. Since the state of our composite system is pure at all times, the big spin must also be in a pure state at these times $\frac{t_r}{4}$ and $\frac{3t_r}{4}$. Similar to the single qubit case, all quantum information in the two-qubit initial state has been transferred into the big spin, even though in this case the two-qubit state contains entanglement.

From the analytical solutions, we know that with a large number of spin where $N \to \infty$ where $1 \ll \bar{n} \ll N$, at the two-qubit revival time $\frac{t_r}{2}$ the two-qubit

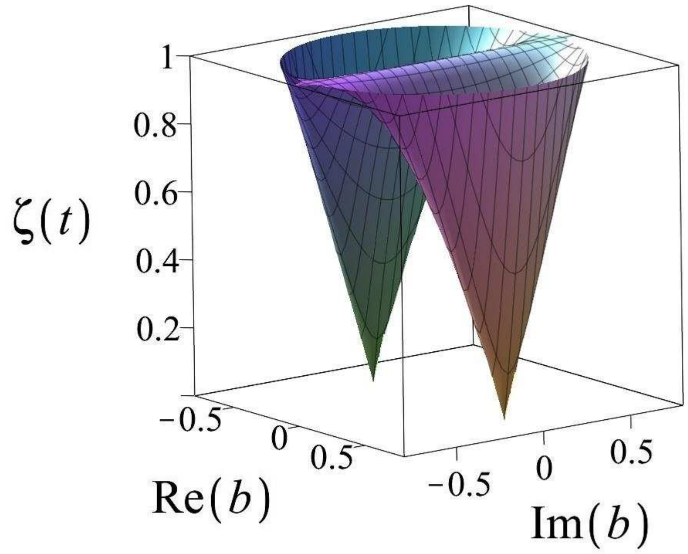

Figure 4.3.3: The value of the concurrence for the states in the basin of attraction for different values of b.

entanglement returns into the system and concurrence will regain its initial value. This also happens at the second two-qubit revival time t_r. The phenomenon is called 'collapse and revival of entanglement' [28, 64, 27, 25] and is observed at the times where $\varsigma(0) = \varsigma(\frac{t_r}{2}) = \varsigma(t_r)$. In between these times another interesting phenomenon called the 'death of entanglement' [24, 77, 26] can be seen. We plot Figure 4.3.4 to demonstrate these interesting phenomena. With $b = \frac{1}{\sqrt{2}}$ or equivalently an initial two-qubit state of $|\psi_2\rangle = \frac{1}{\sqrt{2}}(|ee\rangle + |gg\rangle)$, the figure clearly exhibits the events of 'collapse, revival and death' of entanglement in a two-qubit big spin interacting model with a two-qubit initial state selected from inside the basin of attraction. In this figure, we plot a black line to represent $\varsigma(t)$, the value of entanglement measured between the two qubits. Although the quantity does not actually return to unity, a strong qubit-qubit entanglement revival can be seen. The discrepancy and difference between the analytical and numerical results are due to the finite size of the big spin and its spin coherent state. Clearly with $N = 150$ the entropy does not go to zero, so for this finite system there is not complete disentanglement of the big spin from the qubits, so the qubits cannot return to a maximally entangled pure state.

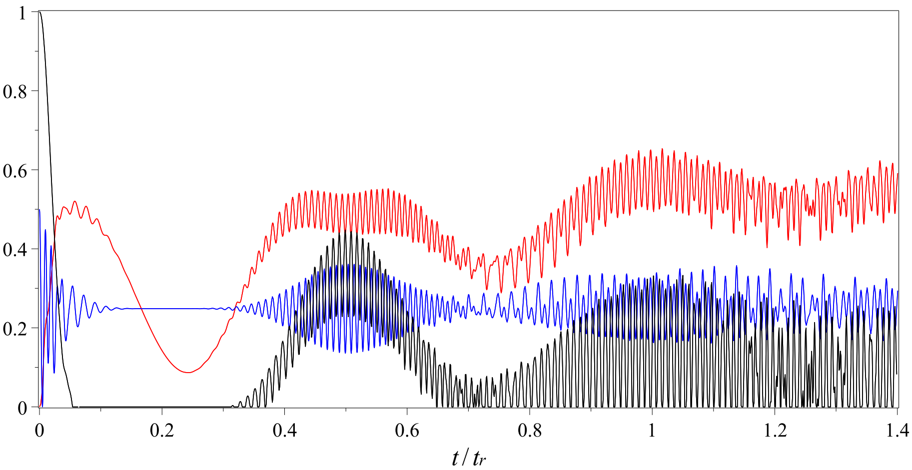

Figure 4.3.4: Time evolution for two-qubit big spin system with the initial two-qubit state $\frac{1}{\sqrt{2}}(|ee\rangle + |gg\rangle)$, $\bar{n} = 25$, $N = 150$ and the initial phase of the radiation field $\phi = 0$. The linear entropy of the qubits is shown as a red line, the probability of the two-qubit state $|ee\rangle$ as a blue line and the concurrence $\varsigma(t)$ as a black line.

As we let two entangled qubits interact with a collection of N spins, over time there will be evolution in the initial entanglement of the qubits. There will be exchange in the value of the qubit-qubit entanglement for the value of the two-qubit big spin entanglement and then for a superposition state of the big spin. This can be seen in Figure 4.3.4 where the value of $\varsigma(t)$ approaches zero at time $\frac{t_r}{4}$. This is why we find no entanglement present in the system at the first two-qubit attractor time, before the process reverses. The entanglement between the two qubits and the big spin returns into the system and expected to reach its maximum while the entanglement between the two qubits starts to reappear. Then both entanglements are also expected regain their initial values at time $\frac{t_r}{2}$, where the entanglement between the qubits and the big spin is again disappears and the value of entanglement between the two qubits goes to its maximum. However, with $N = 150$ in our numerical analysis, these entanglement disappearance and revival processes could not be completed as shown by the red and black curves in the Figure 4.3.4.

It is interesting to note that during the disappearance of the entanglement between the two qubits, the value goes smoothly to zero in a manner that has been described as a Gaussian envelope [64, 27] which is a similar case to the two-qubit Jaynes-Cummings system. The value of the entanglement collapses but the eigenvalues of Equation (4.2.66) never go negative so no *max* operation on the eigenvalues is needed to calculate $\varsigma(t)$ as described in Section 4.2.6. This makes the collapse goes smoothly rather than disappear and reappear with a finite gradient, which is the case of a system with an initial two-qubit state from outside the basin of attraction that will be discussed in the next section.

Initial two-qubit state from outside the basin of attraction

We have seen many interesting attributes of a two-qubit big spin interacting system in the previous sections. We have also seen the event of collapse, death and revival of entanglement between the two qubits that resulted from an interaction of a two-qubit initial state from inside the basin of attraction and the big spin. In this section we will extend our research by studying the system with an initial state selected from outside the basin.

Here we are considering a case where we let $\eta_0 \neq 0$ in Equation (4.3.79). With such a restriction, the equation maintains its last term $\eta_0 \left|Q_0\right\rangle \left|\frac{\zeta}{\sqrt{N}}\right\rangle_N$. This makes the wavefunction inseparable into a product state of the two-qubit and big spin subsystems at the two-qubit attractor times $\frac{t_r}{4}$ and $\frac{3t_r}{4}$. As the qubits cannot be factorised out of the wavefunction, there will be non-zero entropy in the system. The qubits will not approach the two-qubit attractor state. To illustrate the time evolutions for an interacting system involving a big spin and two qubits with an initial state from outside the basin of attraction, we plot Figure 4.3.5. We choose a two-qubit initial state from outside the basin of attraction which in the form of $\frac{1}{\sqrt{20}}\left|ee\right\rangle + \sqrt{\frac{19}{20}}\left|gg\right\rangle$.

We can see that the time evolutions produced are different to the case when the initial state is from inside the basin and in this section, we will focus only on the entanglement between the two qubits which is plotted in the figure as a black line. In this system we can observe an occurrence of a different phenomenon called 'sudden death / birth of entanglement' [24, 25, 26]. With a negative value of the eigenvalue difference, the *max* operation in Equation (4.2.68) influences the behaviour of the entanglement, where the value $\varsigma(t)$ goes to zero with a finite gradient instead of collapsing smoothly.

In the case of an initial two-qubit state from inside the basin of attraction where $\eta_0 = 0$ in Equation (4.3.82), there is no entanglement presents at times $\frac{t_r}{4}$ and $\frac{3t_r}{4}$. From our analysis in Section 4.3.3, we have shown that for this case at these times we have a two-qubit attractor state $\left|Q_{\pm 1}(\frac{t_r}{4})\right\rangle = \left|\psi^{\pm}_{2,att}\right\rangle$ that is pure

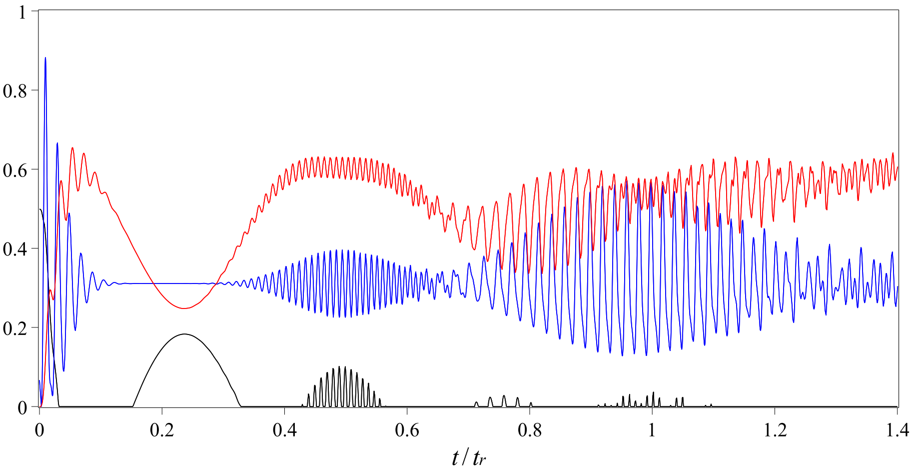

Figure 4.3.5: Time evolution a for two-qubit big spin system with the initial two-qubit state $\frac{1}{\sqrt{20}}\,|ee\rangle+\sqrt{\frac{19}{20}}\,|gg\rangle$, $\bar{n}=25$, $N=150$ and the initial phase of the radiation field $\theta=0$. The linear entropy of the qubits is shown as a red line, the probability of the two-qubit state $|ee\rangle$ as a blue line and the concurrence $\varsigma(t)$ as a black line.

and unentangled. However, we can see a different picture here, where there are peaks in the $\varsigma(t)$ at these times for the case of an initial state from outside the basin. We know that for this case, $\eta_0 \neq 0$. Therefore, if there is any measurement of entanglement at these times, then it has to be the contribution of $|Q_0\rangle$ term in the wavefunction (4.3.79). This event is shown in the concurrence plot in Figure 4.3.5 where we can see peaks at these times.

Anyway, this is not always the case. We may have a two-qubit big spin system that starts with an initial two-qubit state from outside the basin of attraction but not showing any peaks at times $\frac{t_r}{4}$ and $\frac{3t_r}{4}$. It is when the $|Q_0\rangle$ is a product state, then no entanglement presents in the qubits system. On the other hand, if it is an entangled state, then there is a chance that entanglement exists between the two qubits, and there is also possibility of no entanglement because a mixture of an entangled and a product state is not necessarily entangled. To illustrate this, we plot Figure 4.3.6 to show the different dynamics of concurrence $\varsigma(t)$ that is measured between the two qubits with three different initial states.

For comparison, Figure 4.3.6(a) is for a system that starts with a state from inside the basin of attraction while the last two with states from outside. It shows the event of Gaussian collapse and revival with smooth decay in the entanglement as compared to the other two which exhibit the event of sudden death / birth in the

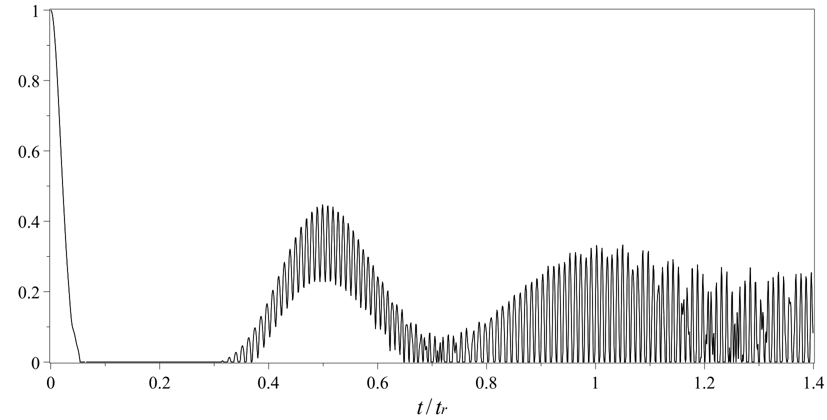

(a) $|\psi_2\rangle = \frac{1}{\sqrt{2}}(|ee\rangle + |gg\rangle)$

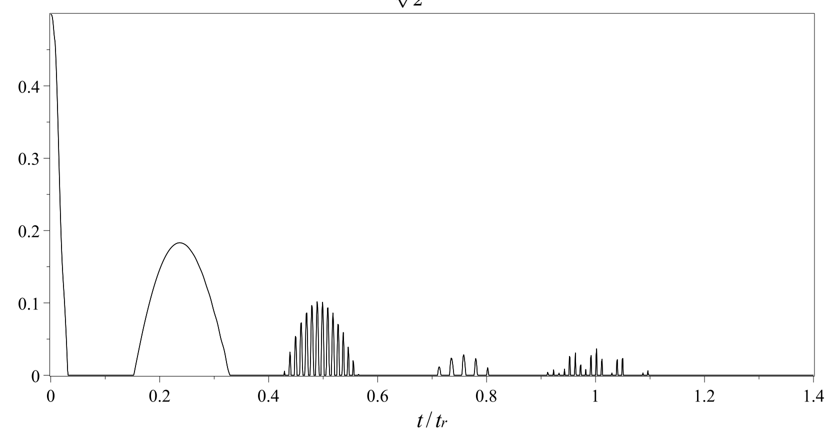

(b) $|\psi_2\rangle = \frac{1}{\sqrt{14}}\,|ee\rangle + \sqrt{\frac{14}{15}}\,|gg\rangle$

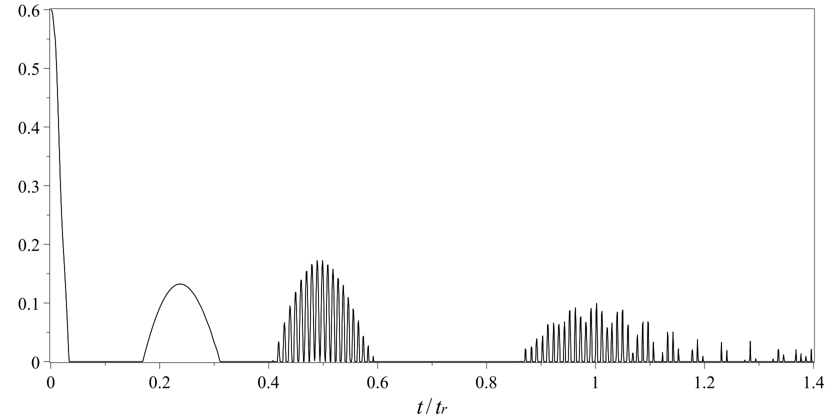

(c) $|\psi_2\rangle = \frac{1}{\sqrt{10}}\,|ee\rangle + \sqrt{\frac{9}{10}}\,|gg\rangle$

Figure 4.3.6: Plots comparing value of concurrence $\varsigma(t)$ as a measurement of two qubits entanglement with different initial two-qubit states, $\bar{n} = 36$, $N = 150$ and the initial phase of the spin coherent state $\phi = 0$.

entanglement between the two qubits. From Figure 4.3.6(b) and Figure 4.3.6(c) we can see the difference in the entanglement measurement at time $\frac{3t_r}{4}$. Unlike in Figure (b) there is no peak in concurrence in Figure (c) eventhough both systems start with an initial two-qubit state from outside the basin of attraction.

From our theoretical analysis for large $\bar{n}$ and $1 \ll \bar{n} \ll N$ in Section 4.3.4, we have seen that at time t_r the system has zero entropy and can be decomposed into the qubits and the big spin subsystems. At this time the big spin system $\Phi_{-1}(t_r) = \Phi_0(t_r) = \Phi_1(t_r) = \left|\frac{\zeta}{\sqrt{N}}\right\rangle$ and the amount of qubit-qubit entanglement returns to its value at the beginning of the interaction $\varsigma(0) = \varsigma(t_r)$. Some indication of this is shown in Figure 4.3.6 where there are peaks in the entanglement measurement for both cases of initial state, from inside and outside of the basin of attraction. However, with $\bar{n} = 25$ and a limited value of $N = 150$, the revival will not be complete and the concurrence will not show the full recovery of its initial value. There cannot be perfect two-qubit entanglement again if the entropy of the two-qubit subsystem is not allowed to return to zero because of the entanglement with the big spin not vanishing in this finite version of the system.

4.4 Summary

We have investigated the dynamics and time evolutions of a system with two qubits interacting with a collection of N spins. We also have shown the correspondence of this interacting system with the two-qubit Jaynes-Cummings model. We started by reproducing the results of prior works by C. Jarvis *et.al* [27, 64, 28] to develop in depth understanding on a two-qubit interacting model and later for a comparison with our two-qubit big spin model.

We calculated and demonstrated many interesting phenomena resulting from such interactions. Quantities like the Rabi oscillations of qubits probabilities, the linear entropy of the qubits system, the two-qubit attractor state, basin of attraction and lastly the entanglement between the two qubits with respect to their initial state were plotted to visualise their dynamics.

A direct comparison can be made with similar quantities that are produced by the two-qubit Jaynes-Cummings model. We see that all above-mentioned quantities behave in similar ways for both systems, and thus we can conclude the correspondence of our two-qubit big spin and two-qubit Jaynes-Cummings models. Next, we will extend our research to understanding the dynamics of these systems including the effects of decoherence. Given the already observed correspondences, we can thus study both models side by side to further investigate their similarities and differences with errors in the frequencies and dipole interaction strength.

Chapter 5

Two-Qubit Interacting Systems with Non-Zero Frequency Detuning

5.1 Introduction

In Chapter 3 we have seen the effects of frequency detunings on the one-qubit Jaynes-Cummings model and the one-qubit big spin model. We have also considered the two-qubit Jaynes-Cummings model and extended our analysis on the two-qubit big spin model with a resonant condition for the system frequencies in Chapter 4. In this chapter, we will study the effects of non-zero frequency detunings on both two-qubit interacting systems. We investigate the changes in the time evolutions of both systems with respect to the changes in the detunings.

Unlike the cases of single qubit systems, the study on the frequency detunings for the two-qubit cases will be more complicated as an extra qubit is involved. For example, instead of only $\delta = \omega - \Omega$ as for the case of one-qubit Jaynes-Cummings system, more variables need to be considered where in this new set up, there will be two values of δ. However, more interesting features like the decoherence in the entanglement between the qubits can be studied.

In Chapter 3, we undertook our frequency detuning analysis on single qubit interacting systems in two stages. First we considered a single non-zero detuning by taking a mismatch between the frequencies of the qubit and the field (and big spin for the case of one-qubit big spin model). Here the evolution was still Hamiltonian, but differed from the zero detuning resonant case. Following this, we analysed the systems by considering a distribution of detunings to model the realistic errors that usually occur in actual systems. In this chapter however, we will only focus on the latter, as we are interested on the effects of decoherence in both interacting systems, particularly on the dynamics of the entanglement between the qubits.

5.2 Collapse, Revival and Decoherence of Entanglement in Two-Qubit Jaynes-Cummings Model

To analyse and observe the effects of non-resonant frequencies in a two-qubit Jaynes-Cummings system we consider a case where the field mode's frequency, ω is positioned in between the two qubits frequencies, Ω_1 and Ω_2 as shown in Figure 5.2.1. We label the mismatches in the frequencies as $\hbar\delta_1 = \hbar(\Omega_1 - \omega)$ and $\hbar\delta_2 = -\hbar(\Omega_2 - \omega)$.

We solve the dynamics of this system by first solving the eigenvalue equation given by Equation (4.2.5). Rearranging the states with the same number of excitations, (4.2.8) now takes the form

$$
\begin{aligned}
\hat{H}_2 \left|\Psi_2\right\rangle = \sum_{n=0}^{\infty} \Bigg[& \\
& \left[\hbar\big(\omega\,(n+1) + \frac{\hbar}{2}\,(\delta_1 - \delta_2)\,\big)a_{ee,n} + \hbar\sqrt{n+1}\big(\lambda_1 a_{ge,n+1} + \lambda_2 a_{eg,n+1}\big)\right] \left|ee, n\right\rangle \\
& \left[\hbar\left(\omega\,(n+1) + \frac{\hbar}{2}\,(\delta_1 + \delta_2)\right) a_{eg,n+1} + \hbar\lambda_1\sqrt{n+2}a_{gg,n+2} + \hbar\lambda_2\sqrt{n+1}a_{ee,n}\right] \left|eg, n+1\right\rangle \\
& \left[\hbar\left(\omega\,(n+1) - \frac{\hbar}{2}\,(\delta_1 + \delta_2)\right) a_{ge,n+1} + \hbar\lambda_1\sqrt{n+1}a_{ee,n} + \hbar\lambda_2\sqrt{n+2}a_{gg,n+2}\right] \left|ge, n+1\right\rangle \\
& \left[\hbar\left(\omega\,(n+1) - \frac{\hbar}{2}\,(\delta_1 - \delta_2)\right) a_{gg,n+2} + \hbar\lambda_1\sqrt{n+2}\big(a_{eg,n+1} + \hbar\lambda_2 a_{ge,n+1}\big)\right] \left|gg, n+2\right\rangle \Bigg] \\
& + \left[- (\frac{\hbar\delta_1}{2} + \frac{\hbar\delta_2}{2})a_{gg,1} + \hbar\lambda_1 a_{eg,0} + \hbar\lambda_2 a_{ge,0}\right] \left|gg, 1\right\rangle \\
& + \left[- (\frac{\hbar\delta_1}{2} - \frac{\hbar\delta_2}{2})a_{ge,0} + \lambda_2 a_{gg,1}\right] \left|ge, 0\right\rangle + \left[- (\frac{\hbar\delta_1}{2} - \frac{\hbar\delta_2}{2})a_{eg,0} + \lambda_1 a_{gg,1}\right] \left|eg, 0\right\rangle \\
& - (\hbar\omega + \frac{\hbar\delta_1}{2} + \frac{\hbar\delta_2}{2})a_{gg,0} \left|gg, 0\right\rangle .
\end{aligned}
\tag{5.2.1}
$$

As was discussed in Section 4.2.2, we may then put this equation into a matrix form given by

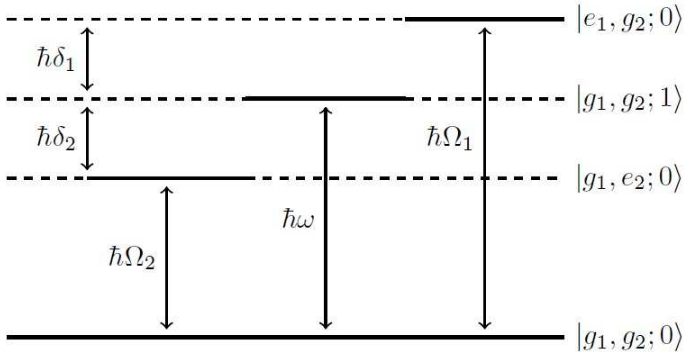

Figure 5.2.1: Two-level energy of field mode and qubits frequencies.

$$\hat{H}_2 |\Psi_2\rangle = \sum_{n=0}^{\infty} \begin{pmatrix} \upsilon_{1,1} & \upsilon_{1,2} & \upsilon_{1,3} & \upsilon_{1,4} \\ \upsilon_{2,1} & \upsilon_{2,2} & \upsilon_{2,3} & \upsilon_{2,4} \\ \upsilon_{3,1} & \upsilon_{3,2} & \upsilon_{3,3} & \upsilon_{3,4} \\ \upsilon_{4,1} & \upsilon_{4,2} & \upsilon_{4,3} & \upsilon_{4,4} \end{pmatrix} |\Psi_2\rangle \tag{5.2.2}$$

where

$$\begin{aligned}
&\upsilon_{1,1} = \hbar\omega\,(n+1) + \tfrac{\hbar}{2}\,(\delta_1 - \delta_2) && \upsilon_{1,2} = \hbar\lambda_2\sqrt{n+1} \\
&\upsilon_{1,3} = \hbar\lambda_1\sqrt{n+1} && \upsilon_{1,4} = 0 \\
&\upsilon_{2,1} = \hbar\lambda_2\sqrt{n+1} && \upsilon_{2,2} = \hbar\omega\,(n+1) + \tfrac{\hbar}{2}\,(\delta_1 + \delta_2) \\
&\upsilon_{2,3} = 0 && \upsilon_{2,4} = \hbar\lambda_1\sqrt{n+2} \\
&\upsilon_{3,1} = \hbar\lambda_1\sqrt{n+1} && \upsilon_{3,2} = 0 \\
&\upsilon_{3,3} = \hbar\omega\,(n+1) - \tfrac{\hbar}{2}\,(\delta_1 + \delta_2) && \upsilon_{3,4} = \hbar\lambda_2\sqrt{n+2} \\
&\upsilon_{4,1} = 0 && \upsilon_{4,2} = \hbar\lambda_1\sqrt{n+2} \\
&\upsilon_{4,3} = \hbar\lambda_2\sqrt{n+2} && \upsilon_{4,4} = \hbar\omega\,(n+1) - \tfrac{\hbar}{2}\,(\delta_1 - \delta_2)
\end{aligned}$$

There are many possible ways to analyse this interacting system off resonance, and in general this requires two independent detuning parameters. Given the calculational complexity required to explore this space, in this thesis we will consider a condition where the frequency of the field ω is equidistantly positioned in between the qubit frequencies Ω_1 and Ω_2. With this we eliminate the $\delta_1 - \delta_2$ terms and we can assign $\delta = \delta_1 + \delta_2$. This enables us to explore the off resonant case as a function of a single detuning parameter δ. We also assume the case of equal dipole interaction strength between the field and both qubits so that we have $\lambda_1 = \lambda_2 = \lambda$ (A mismatch in dipole coupling is explored separately in Chapter 6). This condition further simplifies the the equations and we can then find the eigenvalues of the Matrix (5.2.2). For the case of $n = 0$, we obtain

$$E_{0,n} = E_{d,n} = \hbar\omega(n+1) \tag{5.2.3}$$

and for $n \geq 1$, the eigenvalues are

$$E_{\pm,n} = \hbar\omega(n+1) \pm \frac{\hbar}{2}\sqrt{\delta^2 + 8\lambda^2(2n+3)}. \tag{5.2.4}$$

We also have the eigenvalues for the lower energy levels given as

$$E_{\pm,-1} = \pm\frac{\hbar}{2}\sqrt{\delta^2 + 8\lambda^2} \tag{5.2.5}$$

$$E_{d,-1} = 0 \tag{5.2.6}$$

$$E_{g,0} = -\hbar\omega. \tag{5.2.7}$$

From these eigenvalues, we find the corresponding eigenvectors that are given as

$$|\pm, n\rangle_2 = P\,|ee, n\rangle \pm Q\,|eg, n+1\rangle \pm R\,|ge, n+1\rangle + S\,|gg, n+2\rangle \tag{5.2.8}$$

$$|0, n\rangle_2 = -\frac{P_0}{\sqrt{P_0^2 + S_0^2}}\,|ee, n\rangle + \frac{S_0}{\sqrt{P_0^2 + S_0^2}}\,|gg, n+2\rangle \tag{5.2.9}$$

$$|d, n\rangle_2 = \frac{Q_0}{\sqrt{Q_0^2 + R_0^2}}\,|ge, n+1\rangle - \frac{R_0}{\sqrt{Q_0^2 + C_0^2}}\,|eg, n+1\rangle \tag{5.2.10}$$

where

$$P = \frac{\sqrt{8\lambda^2\left(n+1\right)}\sqrt{\left(\delta^2+4\lambda^2\left(2n+3\right)+\delta\sqrt{\delta^2+8\lambda^2\left(2n+3\right)}\right)}}{\left(\delta+\sqrt{\delta^2+8\lambda^2\left(2n+3\right)}\right)\sqrt{\delta^2+8\lambda^2\left(2n+3\right)+\delta\sqrt{\delta^2+8\lambda^2\left(2n+3\right)}}} \tag{5.2.11}$$

$$Q = \sqrt{2}\frac{\sqrt{\left(\delta^2+4\lambda^2(2n+3)+\delta\sqrt{\delta^2+8\lambda^2(2n+3)}\right)}}{2\sqrt{\delta^2+8\lambda^2(2n+3)+\delta\sqrt{\delta^2+8\lambda^2(2n+3)}}} \tag{5.2.12}$$

$$R = \sqrt{2}\frac{\sqrt{\left(\delta^2+4\lambda^2(2n+3)+\delta\sqrt{\delta^2+8\lambda^2(2n+3)}\right)}}{2\sqrt{\delta^2+8\lambda^2(2n+3)+\delta\sqrt{\delta^2+8\lambda^2(2n+3)}}} \tag{5.2.13}$$

$$S = \frac{\sqrt{8\lambda^2\left(n+2\right)}\sqrt{\left(\delta^2+4\lambda^2\left(2n+3\right)+\delta\sqrt{\delta^2+8\lambda^2\left(2n+3\right)}\right)}}{\left(\delta+\sqrt{\delta^2+8\lambda^2\left(2n+3\right)}\right)\sqrt{\delta^2+8\lambda^2\left(2n+3\right)+\delta\sqrt{\delta^2+8\lambda^2\left(2n+3\right)}}} \tag{5.2.14}$$

$$P_0 = \sqrt{8\lambda^2\left(n+1\right)}\sqrt{\left(\delta^2+4\lambda^2\left(2n+3\right)+\delta\sqrt{\delta^2+8\lambda^2\left(2n+3\right)}\right)} \tag{5.2.15}$$

$$Q_0 = \frac{1}{\sqrt{2}}\sqrt{\left(\delta^2+4\lambda^2(2n+3)+\delta\sqrt{\delta^2+8\lambda^2(2n+3)}\right)} \tag{5.2.16}$$

$$R_0 = -\frac{1}{\sqrt{2}}\sqrt{\left(\delta^2+4\lambda^2(2n+3)+\delta\sqrt{\delta^2+8\lambda^2(2n+3)}\right)} \tag{5.2.17}$$

$$S_0 = \sqrt{8\lambda^2\left(n+2\right)}\sqrt{\left(\delta^2+4\lambda^2\left(2n+3\right)+\delta\sqrt{\delta^2+8\lambda^2\left(2n+3\right)}\right)} \tag{5.2.18}$$

Note that we can make a check on all these eigenvalue and eigenvector expressions by letting $\Omega_1 = \Omega_2 = \omega$, and recover the results for resonance case discussed in Chapter 4. We follow the similar steps as in Section 4.2.2 to find the exact solution to this system's Hamiltonian. By transforming into the interaction picture and using the analogues of the state transformations (4.2.32) to (4.2.36), the solution reduces the into the following equation :

$$
\begin{aligned}
|\Psi_2(t)\rangle = \sum_{n=0}^{\infty}\Bigg(\Bigg[&C_nC_{ee}\bigg(2P^2\cos\bigg(\frac{t}{2}\sqrt{\delta^2+8\lambda^2(2n+3)}\bigg)+\frac{S_0^2}{P_0^2+S_0^2}\bigg)\\
&+C_{gg}C_{n+2}\bigg(2PS\cos\bigg(\frac{t}{2}\sqrt{\delta^2+8\lambda^2(2n+3)}\bigg)-\frac{P_0S_0}{P_0^2+S_0^2}\bigg)\\
&-iC_{n+1}P\sin\bigg(\frac{t}{2}\sqrt{\delta^2+8\lambda^2(2n+3)}\bigg)(C_{eg}+C_{ge})\Bigg]|ee,n\rangle\\
&+\Bigg[-i\sin\bigg(\frac{t}{2}\sqrt{\delta^2+8\lambda^2(2n+3)}\bigg)\bigg(C_nC_{ee}P+C_{n+2}C_{gg}S\bigg)\\
&+C_{n+1}Q\cos\bigg(\frac{t}{2}\sqrt{\delta^2+8\lambda^2(2n+3)}\bigg)(C_{eg}+C_{ge})+C_{n+1}R(C_{eg}-C_{ge})\Bigg]|eg,n+1\rangle\\
&+\Bigg[-i\sin\bigg(\frac{t}{2}\sqrt{\delta^2+8\lambda^2(2n+3)}\bigg)\bigg(C_nC_{ee}P+C_{n+2}C_{gg}S\bigg)\\
&+C_{n+1}Q\cos\bigg(\frac{t}{2}\sqrt{\delta^2+8\lambda^2(2n+3)}\bigg)(C_{eg}+C_{ge})-C_{n+1}R(C_{eg}-C_{ge})\Bigg]|ge,n+1\rangle\\
&+\Bigg[C_{ee}C_n\bigg(2PS\cos\bigg(\frac{t}{2}\sqrt{\delta^2+8\lambda^2(2n+3)}\bigg)-\frac{P_0S_0}{P_0^2+S_0^2}\bigg)\\
&+C_{gg}C_{n+2}\bigg(2S^2\cos\bigg(\frac{t}{2}\sqrt{\delta^2+8\lambda^2(2n+3)}\bigg)+\frac{P_0^2}{P_0^2+S_0^2}\bigg)\\
&-iC_{n+1}S\sin\bigg(\frac{t}{2}\sqrt{\delta^2+8\lambda^2(2n+3)}\bigg)(C_{eg}+C_{ge})\Bigg]|gg,n+2\rangle\Bigg)+|C_R\rangle
\end{aligned}
\tag{5.2.19}
$$

where $|C_R\rangle$ are all other state terms outside the sum given as

$$
\begin{aligned}
|C_R\rangle =&\big(-\hbar\delta a_{gg,1}+\hbar\lambda_1 a_{eg,0}+\hbar\lambda_2 a_{ge,0}\big)|gg,1\rangle+\hbar\lambda_2 a_{gg,1}|ge,0\rangle\\
&+\hbar\lambda_1 a_{gg,1}|eg,0\rangle-\hbar(\omega+\delta)a_{gg,0}|gg,0\rangle\,.
\end{aligned}
\tag{5.2.20}
$$

With this solution, we will analyse the system with respect to the errors as modelled in Section 3.2.2. With the single parametrisation of the detuning as a function of δ, we consider a practical system where the desired case is both qubits on resonance with the field mode, but where there are detuning errors across an ensemble of systems in this two-qubit Jaynes-Cummings model, in which the errors are distributed by Gaussian statistics given by Equation (3.2.5).

$$
f(\delta|0,\Delta)=\frac{1}{\Delta\sqrt{2\pi}}e^{-\frac{\delta^2}{2\Delta^2}}
\tag{5.2.21}
$$

where δ is the error sampled over its width, Δ. This represents errors distributed over δ but centred on zero, to model the ideal detuning case with decoherence (due to errors) effects.

We average over this frequency difference with distributions of varying width by averaging the density matrix over the error distribution. As explained in section 3.2.2, we achieve this with a discrete approximation given by Equation (3.2.7) that has the form of

$$\hat{\rho}_q(t) \approx \sum_{\delta_i} \frac{f\left(\delta_i|0,\Delta\right)\hat{\rho}_q(t,\delta_i)}{\sum_{\delta_i} f\left(\delta_i|0,\Delta\right)} \tag{5.2.22}$$

where i indicates the number of the discrete events.

Similar to the case of two-qubit and field mode with resonant frequencies, we can study the time evolutions of this system with different initial qubit state regimes. We observe the decoherence effects of systems with initial qubit states from both inside and outside of the basin of attraction given by Equation (4.2.66)

$$|\psi_2\rangle = a\left(e^{-i\theta}|ee\rangle + e^{i\theta}|gg\rangle\right) + \sqrt{\frac{1}{2} - |a|^2}\left(|eg\rangle + |ge\rangle\right) \tag{5.2.23}$$

where θ is the initial phase of the radiation field and a is a complex variable parameterising the state and satisfies $0 \leq |a| \leq \frac{1}{\sqrt{2}}$.

5.2.1 Initial two-qubit state from inside the basin of attraction

Equation (5.2.19) gives us the solution for a two-qubit Jaynes-Cummings model with a difference in the qubits' and the field's frequencies. With this equation and properties given by Equation (4.2.32), Equation (4.2.33) and Equation (4.2.34), we calculate the probability of the two qubits being in excited states $P_{ee}(t)$, the linear entropy of the two-qubit subsystem $S_q^L(t)$, the probability of the two qubits being in the attractor state $P^+_{2,att}(t)$ and the concurrence $\varsigma(t)$ of the two qubits entanglement. We then plot Figure 5.2.2 to show the time evolutions of this two qubits-field mode model for three different values of error, for the case of the initial two-qubit state of the qubits lying inside the basin of attraction.

Many interesting observations can be made from this Figure 5.2.2 especially when we compare these time evolutions with the case of two qubits-field system on resonance frequency, as shown in Figure 4.2.1 and Figure 4.2.4. By comparing the figures, we first observe that at this two-qubit attractor time $\frac{t_r}{4}$, the changes that emerge with increasing error distribution width are rather small. The linear entropy stays very close to zero and the two-qubit attractor state probability stays close to unity, meanwhile the two-qubit probability and tangle lines remain flat, as

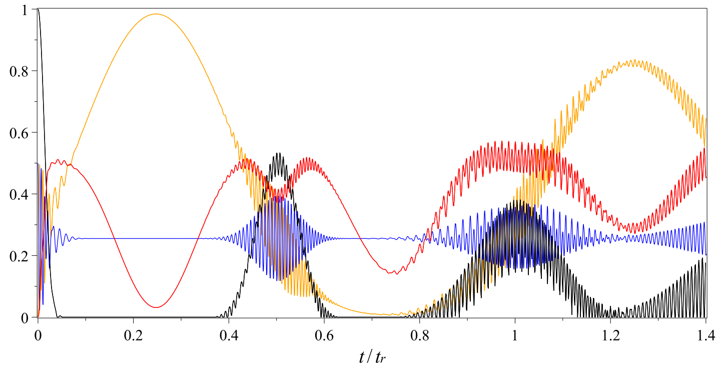

(a) $\Delta = 0.4$

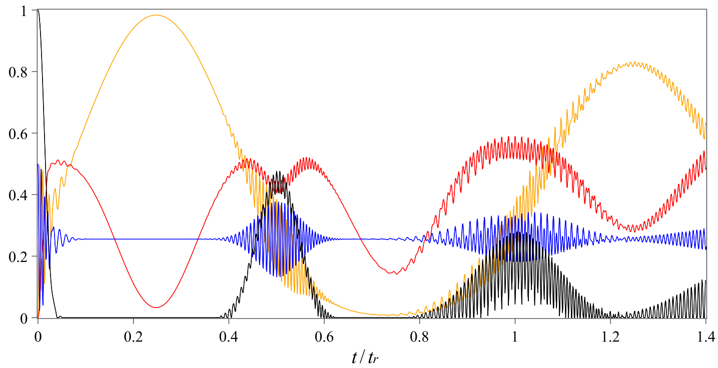

(b) $\Delta = 1.0$

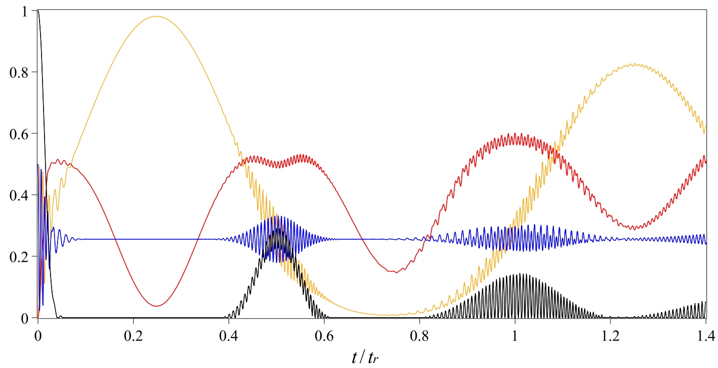

(c) $\Delta = 2.0$

Figure 5.2.2: Plots comparing qubits linear entropies (red), probability of the two-qubit state $|ee\rangle$ (blue), the probability of being in the two-qubit attractor state $\left|\psi^{+}_{2,att}\right\rangle$ (orange), and concurrence $\varsigma(t)$ (black) for two qubits-field mode models of initial two-qubit qubit state $\frac{1}{\sqrt{2}}(|ee\rangle + |gg\rangle)$, $\bar{n} = 36$ and the initial phase of the radiation field $\theta = 0$, with decoherence effects in frequency. Figure (a) shows the differences in the system with $\Delta = 0.4$, (b) shows the differences in the system with $\Delta = 1.0$ and (c) shows the differences in the system with $\Delta = 2.0$.

they were in the zero detuning system. This indicates that there are rather small changes in the purity of the two-qubit subsystem. Similar observations can be made at the second two-qubit attractor time $\frac{3t_r}{4}$ where again minimal changes to the entanglement indicators can be seen. This shows us that the detuning errors introduced have no or very small effect on the system at these particular times.

However, interesting behavioural changes are visible at the two-qubit revival time, $\frac{t_r}{2}$. This is where in a system with a very large $\bar{n}$, the two-qubit subsystem is expected to once again disentangle from the field and the linear entropy approach zero. With errors in the system, we can see that there is some disturbance to the linear entropy of the qubits. As the error distribution width increases the dip in the entropy curve becomes shallower indicating that the purity of the qubits system is lowered and the level of mixture increased. The value has now moving away from near zero to a larger value. This increase in the two-qubit entropy at the revival time is due to additional entropy from the decoherence due to the distribution of detunings over the ensemble, adding to entropy resulting from entanglement of the qubit with the field.

Beside the linear entropy, changes in the qubit probabilities can also be seen at this time. Although the effect is negligible on the probability of the qubit being in the two-qubit attractor state $P^{+}_{2,att}(t)$, as a function of increasing error width we observe a reduction in the amplitude of oscillation of the probability of the two qubits to be in the ground state $P_{ee}(t)$. The revival amplitude of the qubit at this time thus becomes smaller with increasing error width.

At time $\frac{t_r}{2}$ too, with a perfect revival the concurrence would be expected to return to the same value as it was for the initial state of the qubits at the beginning of the interaction $\varsigma(0) = \varsigma(\frac{t_r}{2})$. However, as shown in the numerical analysis in Section 4.2.5, with $\bar{n} = 36$, no perfect revival would be observed. Besides that, the results shown in Figure 5.2.2 also suggest that this quantity is also affected by the detuning errors in the system. As the error distribution width increases, the two-qubit entanglement becomes smaller as shown in the figure where the concurrence revival peak reduces in size. This shows that there are some effects on the entanglement value between the two qubits where it becomes smaller with the appearance of error.

5.2.2 Initial two-qubit state from outside the basin of attraction

We have considered the two-qubit Jaynes-Cummings model with initial qubit states from inside the basin of attraction. Considering such an initial condition of qubit states means that we are dealing with a two-qubit Jaynes-Cummings model with a restriction of $\eta_0 = 0$ on Equation (4.2.65). For the case of resonance, we have seen the effects of neglecting such a restriction on the system in Section 4.2.6. Here, we will study the model with $\eta_0 \neq 0$ and non-zero detuning. This means that we will explore the system outside the basin of attraction under the effect of increasing errors in the detuning.

With Equation (5.2.19) and properties given by Equations (5.2.21), (5.2.22) and (5.2.23), we calculate the probability of the two qubits being in ground states $P_{ee}(t)$, the linear entropy of the qubits system $S_q^L(t)$ and the probability of the two qubits being in the two-qubit attractor state $P_{2,att}^{+}(t)$. We also calculate the concurrence $\varsigma(t)$ to show the sudden death / birth of two-qubit entanglement in the system. We plot Figure 5.2.3 to show the time evolution of the two-qubit Jaynes-Cummings model with an initial qubit state from outside the basin of attraction and an increasing detuning error distribution width. We compare the results to the ideal model plotted as Figure 4.2.2 and Figure 4.2.5 in Chapter 4.

Similar to the case of resonance (zero detuning), without the $\eta_0 = 0$ restriction, the two-qubit state cannot be factorised out of the wavefunction at $\frac{t_r}{4}$ and $\frac{3t_r}{4}$. With this fact, the two qubits will not go towards the attractor state. The entropy will also be non-zero at these times. All this can be seen by the $P_{2,att}^{+}(t)$ shown as an orange line, which has its maximum significantly less than unity at the first two-qubit attractor time. The red linear entropy line has only shallow dips towards zero at the two attractor times, but does not approach close to zero. The amount of entanglement is shown as the black line and unlike for the case of initial states from inside the basin, clearly there are peaks at $\frac{t_r}{4}$ and $\frac{3t_r}{4}$. However, no significant changes can be observed on all of the dynamics at these times, even with error value $\Delta = 2.0$. This shows that the detuning introduced have rather limited effects on the system at the two-qubit attractor times.

At the two-qubit revival time $\frac{t_r}{2}$ as well as the one-qubit revival time t_r, we observe changes to the system as a function of increasing error distribution width. First, on the probability of the qubits being in the two-qubit attractor state $\left|\psi_{2,att}^{+}\right\rangle$ and being both in the excited state $|ee\rangle$. There is suppression of the revival oscillations in both probabilities with increasing errors. This can be seen by blue and orange lines where they become flatter at both times.

At the one-qubit revival time t_r too, the entropy is predicted to be near zero as the the qubit states can again be factorized out of the wavefunction. However, we can see that the entropy dips are filled in with increasing errors. Similarly, the

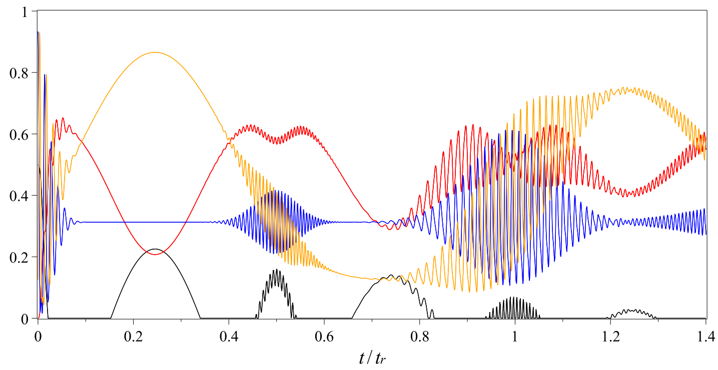

(a) $\Delta = 0.4$

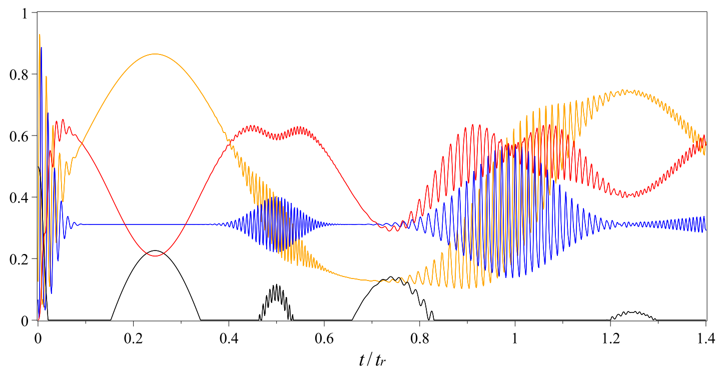

(b) $\Delta = 1.0$

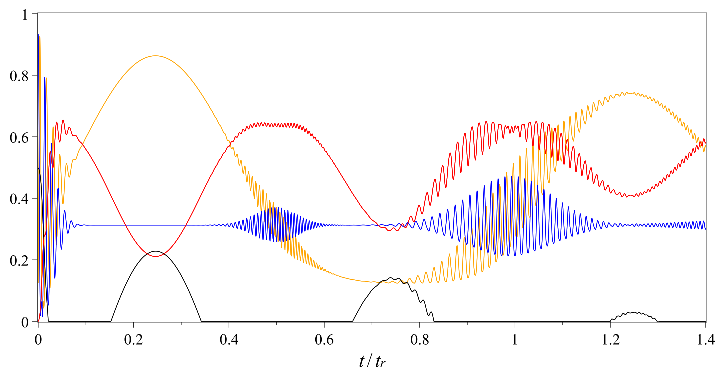

(c) $\Delta = 2.0$

Figure 5.2.3: Plots comparing qubits linear entropies (red), probability of the two qubits state $|ee\rangle$ (blue) and concurrence $\varsigma(t)$ (black) for two qubits-field mode models of initial qubit state $\frac{1}{\sqrt{20}}\,|ee\rangle + \sqrt{\frac{19}{20}}\,|ee\rangle$, $\bar{n} = 36$ and the initial phase of the radiation field $\theta = 0$, with decoherence effects in frequency. Figure (a) shows the differences in the system with $\Delta = 0.4$, (b) shows the differences in the system with $\Delta = 1.0$ and (c) shows the differences in the system with $\Delta = 2.0$.

concurrence also suffers with increasing decoherence due to detuning errors. In an ideal revival, the entanglement should be the same as at the start and at the revival time of interaction $\varsigma(0) = \varsigma(t_r)$. However, with $\bar{n} = 36$, it is not enough to see this happening in the system. Furthermore, with errors in the detunings, the occurrence of this quantity is now affected where the entanglement revivals decrease with increasing errors. The black line shows that the entanglement peaks at both times completely disappear with error distribution width $\Delta = 2.0$. This indicates that the expected revival of entanglement between the qubits is very sensitive to increasing detuning errors.

5.3 Collapse, Revival and Decoherence of Entanglement in Two-Qubit Big Spin Model

We have seen the effects of errors in the detuning on the two-qubit Jaynes-Cummings model. In this section, we will extend similar analysis on the two-qubit big spin model. We will investigate the system by considering a detuning error distribution modelled by Equation (5.2.21) and we will average the density matrix of the system over this error distribution. We will use a similar discrete approximation to the systems given by Equation (5.2.22).

We start with solving the dynamics of this system by finding the eigenvalues equation given by Equation (4.3.5). Rearranging the states with the same number of excitations, Equation (4.3.9) becomes

$$
\begin{aligned}
\hat{H}\left|\Psi_2(t)\right\rangle = \sum_{n=0}^{N-2} \Bigg[& \Bigg((\hbar\omega_N n + \frac{\hbar}{2}\left(\delta_1 - \delta_2\right)) a_{ee,n}(t) + \hbar\sqrt{(n+1)\Big(1 - \frac{n}{N}\Big)} \\
& \times \left(\lambda_1 a_{ge,n+1}(t) + \lambda_2 a_{eg,n+1}(t)\right)\Bigg) \left|ee, n\right\rangle_N \\
& + \Bigg((\hbar\omega_N (n+1) + \frac{\hbar}{2}\left(\delta_1 + \delta_2\right)) a_{eg,n+1}(t) + \hbar\lambda_1\sqrt{(n+2)\Big(1 - \frac{n+1}{N}\Big)} \\
& a_{gg,n+2}(t) + \hbar\lambda_2\sqrt{(n+1)\Big(1 - \frac{n}{N}\Big)} a_{ee,n}(t)\Bigg) \left|eg, n+1\right\rangle_N \\
& + \Bigg((\hbar\omega_N (n+1) - \frac{\hbar}{2}\left(\delta_1 + \delta_2\right)) a_{ge,n+1}(t) + \hbar\lambda_1\sqrt{(n+1)\Big(1 - \frac{n}{N}\Big)} \\
& a_{ee,n}(t) + \hbar\lambda_2\sqrt{(n+2)\Big(1 - \frac{n+1}{N}\Big)} a_{gg,n+2}(t)\Bigg) \left|ge, n+1\right\rangle_N \\
& + \Bigg((\hbar\omega_N (n+2) + \frac{\hbar}{2}\left(\delta_1 - \delta_2\right)) a_{gg,n+2}(t) + \hbar\sqrt{(n+2)\Big(1 - \frac{n+1}{N}\Big)} \\
& \times \left(\lambda_1 a_{eg,n+1}(t) + \lambda_2 a_{ge,n+1}(t)\right)\Bigg) \left|gg, n+2\right\rangle_N \Bigg] \\
& + (- \frac{\hbar\delta_1}{2} - \frac{\hbar\delta_2}{2}) a_{gg,0} \left|gg, 0\right\rangle_N + [(- \frac{\hbar\delta_1}{2} + \frac{\hbar\delta_2}{2}) a_{ge,0} + \hbar\lambda_2 a_{gg,1}] \left|ge, 0\right\rangle_N \\
& + [(\frac{\hbar\delta_1}{2} + \frac{\hbar\delta_2}{2}) a_{ge,0} + \hbar\lambda_1 a_{gg,1}] \left|eg, 0\right\rangle_N \\
& + [\Big((\hbar\omega_N + \frac{\hbar\delta_1}{2} - \frac{\hbar\delta_2}{2}) a_{gg,1}(t) + \hbar\lambda_1 a_{eg,0}(t) + \hbar\lambda_2 a_{ge,0}(t)\Big)] \left|gg, 1\right\rangle_N \\
& + (\hbar\omega_N N + \frac{\hbar\delta_1}{2} + \frac{\hbar\delta_2}{2}) a_{ee,N}(t) \left|ee, N\right\rangle_N \\
& + (\hbar\omega_N N + \frac{\hbar\delta_1}{2} - \frac{\hbar\delta_2}{2}) a_{eg,N}(t) \left|eg, N\right\rangle_N \\
& + (\hbar\omega_N N - \frac{\hbar\delta_1}{2} + \frac{\hbar\delta_2}{2}) a_{ge,N}(t) \left|ge, N\right\rangle_N + ((\hbar\lambda_1 a_{ge,N}(t) + \hbar\lambda_2 a_{eg,N}(t)) \\
& + (\hbar\omega_N N - \hbar\omega_N + \frac{\hbar\delta_1}{2} + \frac{\hbar\delta_2}{2}) a_{ee,N-1}(t)) \left|ee, N-1\right\rangle_N
\end{aligned}
\tag{5.3.1}
$$

We then put this equation into a matrix form of

$$
\hat{H}\left|\Psi_2(t)\right\rangle = \sum_{n=0}^{N-2} \begin{pmatrix} \nu_{1,1} & \nu_{1,2} & \nu_{1,3} & \nu_{1,4} \\ \nu_{2,1} & \nu_{2,2} & \nu_{2,3} & \nu_{2,4} \\ \nu_{3,1} & \nu_{3,2} & \nu_{3,3} & \nu_{3,4} \\ \nu_{4,1} & \nu_{4,2} & \nu_{4,3} & \nu_{4,4} \end{pmatrix} \left|\Psi(t)\right\rangle \tag{5.3.2}
$$

where

$$
\begin{aligned}
\nu_{1,1} &= \hbar\omega_N(n+1) + \tfrac{\hbar}{2}\left(\delta_1 - \delta_2\right) & \nu_{1,2} &= \hbar\lambda_2\sqrt{(n+1)\left(1-\tfrac{n}{N}\right)} \\
\nu_{1,3} &= \hbar\lambda_1\sqrt{(n+1)\left(1-\tfrac{n}{N}\right)} & \nu_{1,4} &= 0 \\
\nu_{2,1} &= \hbar\lambda_2\sqrt{(n+1)\left(1-\tfrac{n}{N}\right)} & \nu_{2,2} &= \hbar\omega_N(n+1) + \tfrac{\hbar}{2}\left(\delta_1 + \delta_2\right) \\
\nu_{2,3} &= 0 & \nu_{2,4} &= \hbar\lambda_1\sqrt{(n+2)\left(1-\tfrac{n+1}{N}\right)} \\
\nu_{3,1} &= \hbar\lambda_1\sqrt{(n+1)\left(1-\tfrac{n}{N}\right)} & \nu_{3,2} &= 0 \\
\nu_{3,3} &= \hbar\omega_N(n+1) - \tfrac{\hbar}{2}\left(\delta_1 + \delta_2\right) & \nu_{3,4} &= \hbar\lambda_2\sqrt{(n+2)\left(1-\tfrac{n+1}{N}\right)} \\
\nu_{4,1} &= 0 & \nu_{4,2} &= \hbar\lambda_1\sqrt{(n+2)\left(1-\tfrac{n+1}{N}\right)} \\
\nu_{4,3} &= \hbar\lambda_2\sqrt{(n+2)\left(1-\tfrac{n+1}{N}\right)} & \nu_{4,4} &= \hbar\omega_N(n+1) + \tfrac{\hbar}{2}\left(\delta_1 - \delta_2\right)
\end{aligned}
$$

Similar to the case of the two-qubit and coherent field model, we consider a condition where the frequency of the big spin ω_N is equidistantly positioned in between the qubits frequencies Ω_1 and Ω_2 as depicted in Figure 5.2.1. In this case we replace the coherent field frequency ω with the big spin's frequency ω_N.

Again, in order to simplify the exploration of the detuning parameter space to a single parameter, we can eliminate the $\delta_1 - \delta_2$ terms and assign $\delta = \delta_1 + \delta_2$. We also assume the case of equal dipole interaction strength between the field and both qubits so that we have $\lambda_1 = \lambda_2 = \lambda$ which further simplify the equations. We will consider the case of mismatch in coupling where $\lambda_1 \neq \lambda_2$ in the next chapter.

We can then find the eigenvalues by diagonalising Matrix (5.3.2). For $n = 0$ and $1 \leq n \leq N-2$, we respectively have

$$E_{0,n} = E_{d,n} = \hbar\omega_N(n+1) \tag{5.3.3}$$

$$
\begin{aligned}
E_{\pm,n} &= \hbar\omega_N(n+1) \pm \frac{\hbar}{2}\sqrt{\delta^2 + 4\lambda^2\left((4n+6) - \frac{4}{N}(n+1)^2\right)} && (5.3.4)\\
&= \hbar\omega_N(n+1) \pm \frac{\hbar}{2}\sqrt{\delta^2 + 4\lambda^2\xi}. && (5.3.5)
\end{aligned}
$$

For the lower energy levels, the eigenvalues are

$$E_{\pm,-1} = \frac{\hbar}{2}\sqrt{\delta^2 + 8\lambda^2} \tag{5.3.6}$$

$$E_{d,-1} = 0 \tag{5.3.7}$$

$$E_{g,0} = -\hbar\omega_N \tag{5.3.8}$$

and for the upper energy levels we have

$$E_{\pm,N-1} = \hbar\omega_N N \pm \frac{\hbar}{2}\sqrt{\delta^2 + 8\lambda^2} \tag{5.3.9}$$

$$E_{d,N-1} = \hbar\omega_N N \tag{5.3.10}$$

$$E_{e,N} = \hbar\omega_N (N+1). \tag{5.3.11}$$

From these eigenvalues, we find the corresponding eigenvectors that are given as

$$|\pm, n\rangle_{2,N} = P\,|ee, n\rangle \pm Q\,|eg, n+1\rangle + R\,|ge, n+1\rangle + S\,|gg, n+2\rangle \tag{5.3.12}$$

$$|0, n\rangle_{2,N} = -\frac{P_0}{\sqrt{P_0^2 + S_0^2}}\,|ee, n\rangle + \frac{S_0}{\sqrt{P_0^2 + S_0^2}}\,|gg, n+2\rangle \tag{5.3.13}$$

$$|d, n\rangle_{2,N} = \frac{Q_0}{\sqrt{Q_0^2 + R_0^2}}\,|ge, n+1\rangle - \frac{R_0}{\sqrt{Q_0^2 + R_0^2}}\,|eg, n+1\rangle \tag{5.3.14}$$

where

$$P = \frac{8N\lambda\sqrt{(n+1)(1-\frac{n}{N})}\sqrt{N\left(\delta^2 + 2\lambda^2\xi + \delta\sqrt{\delta^2 + 4\lambda^2\xi}\right)}}{\sqrt{N\left(\delta^2 + 4\lambda^2\xi + \delta\sqrt{\delta^2 + 4\lambda^2\xi}\right)}\left(\delta N + N\sqrt{\delta^2 + 4\lambda^2\xi}\right)} \tag{5.3.15}$$

$$Q = \sqrt{2}\frac{\sqrt{N\left(\delta^2 + 2\lambda^2\xi + \delta N\sqrt{\delta^2 + 4\lambda^2\xi}\right)}}{2\sqrt{N\left(\delta^2 + 4\lambda^2\xi + \delta\sqrt{\delta^2 + 4\lambda^2\xi}\right)}} \tag{5.3.16}$$

$$R = \sqrt{2}\frac{\sqrt{N\left(\delta^2 + 2\lambda^2\xi + \delta N\sqrt{\delta^2 + 4\lambda^2\xi}\right)}}{2\sqrt{N\left(\delta^2 + 4\lambda^2\xi + \delta\sqrt{\delta^2 + 4\lambda^2\xi}\right)}} \tag{5.3.17}$$

$$S = \frac{8N\lambda\sqrt{(n+2)(1-\frac{n+1}{N})}\sqrt{N\left(\delta^2+2\lambda^2\xi+\delta\sqrt{\delta^2+4\lambda^2\xi}\right)}}{\sqrt{N\left(\delta^2+4\lambda^2\xi+\delta\sqrt{\delta^2+4\lambda^2\xi}\right)\left(\delta N+N\sqrt{\delta^2+4\lambda^2\xi}\right)}} \tag{5.3.18}$$

$$P_0 = 8N\lambda\sqrt{(n+1)(1-\frac{n}{N})}\sqrt{N\left(\delta^2+2\lambda^2\xi+\delta\sqrt{\delta^2+4\lambda^2\xi}\right)} \tag{5.3.19}$$

$$Q_0 = \frac{1}{\sqrt{2}}\sqrt{N\left(\delta^2+2\lambda^2\xi+\delta N\sqrt{\delta^2+4\lambda^2\xi}\right)} \tag{5.3.20}$$

$$R_0 = -\frac{1}{\sqrt{2}}\sqrt{N\left(\delta^2+2\lambda^2\xi+\delta N\sqrt{\delta^2+4\lambda^2\xi}\right)} \tag{5.3.21}$$

$$S_0 = 8N\lambda\sqrt{(n+2)(1-\frac{n+1}{N})}\sqrt{N\left(\delta^2+2\lambda^2\xi+\delta\sqrt{\delta^2+4\lambda^2\xi}\right)} \tag{5.3.22}$$

Note that by letting $\Omega_1 = \Omega_2 = \omega_N$ we recover the eigenvalue and eigenvector expressions for resonance case discussed in Chapter 4. We solve the equation and find the exact solution to this system's Hamiltonian, and by transforming into the interaction picture and using the analogues of the state transformations given by Equations (4.3.44) to (4.3.48), the solution reduces the into the following equation :

$$
\begin{aligned}
|\Psi_2(t)\rangle = \sum_{n=0}^{N-2} \Bigg(\Bigg[& C_n C_{ee} \Big(2P^2 \cos\Big(\frac{t}{2}\sqrt{\delta^2 + 8\lambda^2(2n+3)}\Big) + \frac{S_0^2}{P_0^2 + S_0^2} \Big) \\
& + C_{gg} C_{n+2} \Big(2PS \cos\Big(\frac{t}{2}\sqrt{\delta^2 + 8\lambda^2(2n+3)}\Big) - \frac{P_0 S_0}{P_0^2 + S_0^2} \Big) \\
& - i C_{n+1} P \sin\Big(\frac{t}{2}\sqrt{\delta^2 + 8\lambda^2(2n+3)}\Big) (C_{eg} + C_{ge}) \Bigg] |ee, n\rangle \\
& + \Bigg[- i \sin\Big(\frac{t}{2}\sqrt{\delta^2 + 8\lambda^2(2n+3)}\Big) \Big(C_n C_{ee} P + C_{n+2} C_{gg} S \Big) \\
& + C_{n+1} Q \cos\Big(\frac{t}{2}\sqrt{\delta^2 + 8\lambda^2(2n+3)}\Big) (C_{eg} + C_{ge}) + C_{n+1} R (C_{eg} - C_{ge}) \Bigg] |eg, n+1\rangle \\
& + \Bigg[- i \sin\Big(\frac{t}{2}\sqrt{\delta^2 + 8\lambda^2(2n+3)}\Big) \Big(C_n C_{ee} P + C_{n+2} C_{gg} S \Big) \\
& + C_{n+1} Q \cos\Big(\frac{t}{2}\sqrt{\delta^2 + 8\lambda^2(2n+3)}\Big) (C_{eg} + C_{ge}) - C_{n+1} R (C_{eg} - C_{ge}) \Bigg] |ge, n+1\rangle \\
& + \Bigg[C_{ee} C_n \Big(2PS \cos\Big(\frac{t}{2}\sqrt{\delta^2 + 8\lambda^2(2n+3)}\Big) - \frac{P_0 S_0}{P_0^2 + S_0^2} \Big) \\
& + C_{gg} C_{n+2} \Big(2S^2 \cos\Big(\frac{t}{2}\sqrt{\delta^2 + 8\lambda^2(2n+3)}\Big) + \frac{P_0^2}{P_0^2 + S_0^2} \Big) \\
& - i C_{n+1} S \sin\Big(\frac{t}{2}\sqrt{\delta^2 + 8\lambda^2(2n+3)}\Big) (C_{eg} + C_{ge}) \Bigg] |gg, n+2\rangle \Bigg) + |C_R\rangle_N
\end{aligned}
\tag{5.3.23}
$$

where $|C_R\rangle_N$ are all other state terms outside the sum given as

$$
\begin{aligned}
|C_R\rangle_N = & (-\frac{\hbar\delta_1}{2} - \frac{\hbar\delta_2}{2}) a_{gg,0} |gg, 0\rangle_N + [(-\frac{\hbar\delta_1}{2} + \frac{\hbar\delta_2}{2}) a_{ge,0} + \hbar\lambda_2 a_{gg,1}] |ge, 0\rangle_N \\
& + [(\frac{\hbar\delta_1}{2} + \frac{\hbar\delta_2}{2}) a_{ge,0} + \hbar\lambda_1 a_{gg,1}] |eg, 0\rangle_N \\
& + [\Big((\hbar\omega_N + \frac{\hbar\delta_1}{2} - \frac{\hbar\delta_2}{2}) a_{gg,1}(t) + \hbar\lambda_1 a_{eg,0}(t) + \hbar\lambda_2 a_{ge,0}(t) \Big)] |gg, 1\rangle_N \\
& + (\hbar\omega_N N + \frac{\hbar\delta_1}{2} + \frac{\hbar\delta_2}{2}) a_{ee,N}(t) |ee, N\rangle_N \\
& + (\hbar\omega_N N + \frac{\hbar\delta_1}{2} - \frac{\hbar\delta_2}{2}) a_{eg,N}(t) |eg, N\rangle_N \\
& + (\hbar\omega_N N - \frac{\hbar\delta_1}{2} + \frac{\hbar\delta_2}{2}) a_{ge,N}(t) |ge, N\rangle_N + ((\hbar\lambda_1 a_{ge,N}(t) + \hbar\lambda_2 a_{eg,N}(t)) \\
& + (\hbar\omega_N N - \hbar\omega_N + \frac{\hbar\delta_1}{2} + \frac{\hbar\delta_2}{2}) a_{ee,N-1}(t)) |ee, N-1\rangle_N .
\end{aligned}
\tag{5.3.24}
$$

5.3.1 Initial two-qubit state from inside the basin of attraction

We use the solutions given by Equation (5.3) and error modelling properties given by Equations (5.2.21) and (5.2.22) to calculate the probability of the two qubits being in the excited states $P_{ee}(t)$, the linear entropy of the two-qubit subsystem $S_q^L(t)$, the probability of the qubits being in the two-qubit attractor state $P_{2,att}^{+}(t)$ and the measure of entanglement, concurrence $\varsigma(t)$ of the two-qubit subsystem. We consider the case of an initial two-qubit state that lies inside the basin of attraction, and we then plot Figure 5.3.1 to show the time evolutions of the two-qubit big spin system for three error values in the frequency detuning. With the figure, we compare the results with the case of a system with resonance frequency considered in Chapter 4 and depicted as Figure 4.3.1 and Figure 4.3.4.

From the plot, we can see that at the two-qubit attractor times $\frac{t_r}{4}$ and $\frac{3t_r}{4}$, the effects of error on the system's time evolutions are very minimal with increasing error distribution width. The linear entropy curve stays very close to zero and the two-qubit attractor state probability stays close to unity (and zero at the second attractor time $\frac{3t_r}{4}$). Furthermore, the qubits probability and concurrence plots maintain flat at zero, as they were observed in the system with zero detuning. This indicates that there are only very small changes in the purity of the two-qubit subsystem at these times, meaning that the two-qubit state remains pure and unentangled. So, it is very interesting to see that even with errors as high as $\Delta = 2.0$, we may still observe the two-qubit attractor state of the qubits, as well as the spin cat state of the big spin at these times.

Interesting changes can be seen at the two-qubit revival time $\frac{tr}{2}$, as well as at time t_r. At these times, in a perfect system with a very large vslue of N, the two-qubit subsystem is expected to once again disentangle from the big spin and the linear entropy curve approaches zero. However, we have seen in Section 4.2.5 that with $\bar{n} = 25$, this disentanglement process will not complete. In addition to that, for a system with decoherence in the detuning, we can see from Figure 5.3.1 that the dip in the red line has become shallower as the error distribution width increases. This suggests that there is some disturbance in the linear entropy of the qubits, where the purity is lowered and the level of mixture increased as the effects of the errors in the detuning. We can also note the effects of decoherence in the amplitude of the probability for the two qubits being in the state $|gg\rangle$ at these times. The revival peak of the two-qubit probability $P_{ee}(t)$ decreases with the increment of error distribution width. Similar behavioral change can also be seen in the probability of the two-qubit attractor state $P_{2,att}^{+}(t)$, where the amplitude

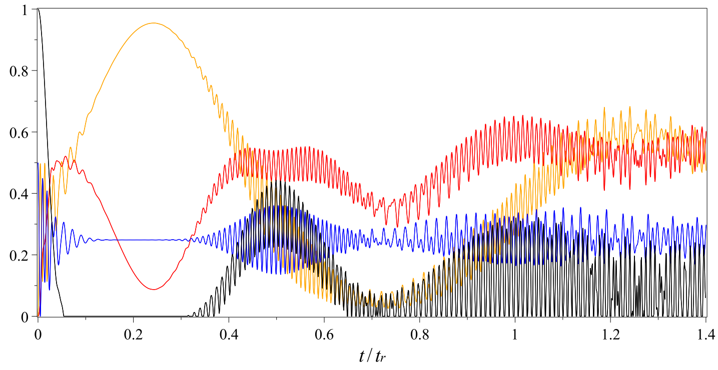

(a) $\Delta = 0.4$

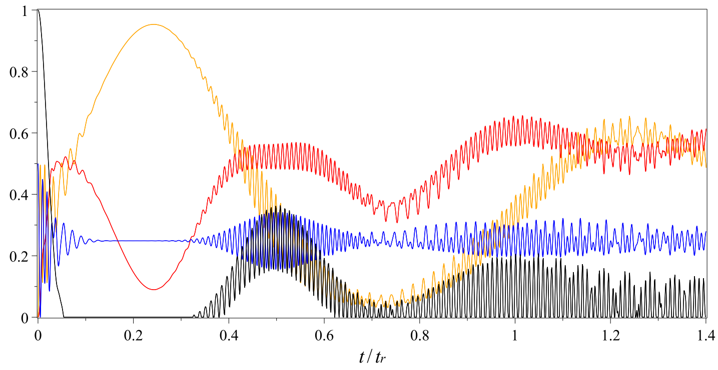

(b) $\Delta = 1.0$

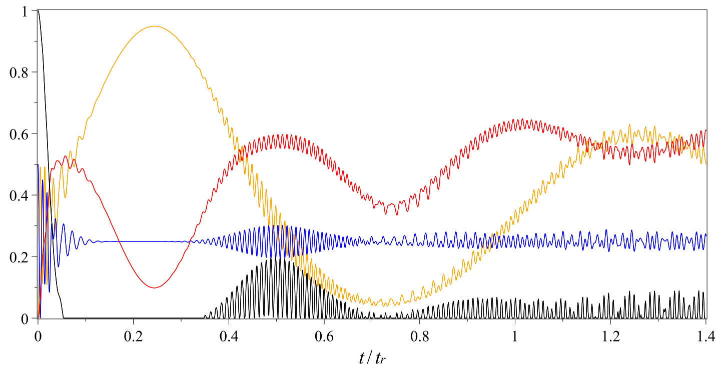

(c) $\Delta = 2.0$

Figure 5.3.1: Plots comparing qubits linear entropies (red), probability of the two qubits state $|ee\rangle$ (blue), probability of the two qubits being a two-qubit attractor state $\left|\psi^{+}_{2,att}\right\rangle_N$ (orange), and concurrence $\varsigma(t)$ (black) for two qubits-big spin models of initial qubit state $\frac{1}{\sqrt{2}}(|ee\rangle + |gg\rangle)$, $|\zeta|^2 = 25$, $N = 150$ and the big spin's initial phase $\phi = 0$, with decoherence effects in the frequency. Figure (a) shows the differences in the system with $\Delta = 0.4$, (b) shows the differences in the system with $\Delta = 1.0$ and (c) shows the differences in the system with $\Delta = 2.0$.

reduces significantly with the increasing error.

The plotted figure also suggests that at times $\frac{tr}{2}$ and t_r the qubit-qubit entanglement is also affected by the decoherence in the frequency of the system. The peaks in the value of concurrence can be seen to reduce with the increasing error distribution width as compared to the non-zero detuning case as depicted in Figure 4.3.4. This suggests that the entanglement between the two qubits are getting weaker with a larger value of decoherence.

5.3.2 Initial two-qubit state from outside basin of attraction

To analyse a two-qubit big spin model with non-zero detuning and with initial qubit states from outside of the basin of attraction, we plot Figure 5.3.2. The figure shows the time evolutions of the system where we plot similar quantities we used in the previous section when we considered the case of initial qubit states from inside the basin of attraction.

From the case of resonance system considered in Section 4.3.6 and depicted as Figure 4.3.2 and Figure 4.3.5, we know that for a system with initial qubit states form outside the basin of attraction, the two-qubit states cannot be factorised out of the wavefunction at the two-qubit attractor times. This means that at times $\frac{t_r}{4}$ and $\frac{3t_r}{4}$, the two-qubit states are not pure and will not be a two-qubit attractor state. The probability of the two qubits being in an attractor state $P^{+}_{2,att}(t)$ (shown as an orange curve) is far from unity, and the linear entropy $S^L_q(t)$ (shown as a red curve) does not approach zero. The peak in the concurrence can also be observed indicating non-zero entanglement between the two qubits. From Figure 5.3.2, we can see that similar to the case of initial two-qubit states from inside the basin of attraction, no significant changes can be observed on these quantities even with an error distribution width $\Delta = 2.0$ at times $\frac{t_r}{4}$ and $\frac{3t_r}{4}$.

The effects of the decoherence in a two-qubit big spin system with non-zero detunings can be seen at the two-qubit revival time $\frac{t_r}{2}$ as well as at the one-qubit revival time t_r. From Figure 5.3.2 we can see that the revival amplitude of both the probability of the two-qubit attractor state $P^{+}_{2,att}(t)$ as well as the probability of the two qubits being in the state $|ee\rangle$ are reduced as the error distribution width increases. The value of linear entropy has also increased at these times and the dip in the red curve is filled and become shallower with the increment of error value. This indicates that there is increase in the mixture of the two-qubit subsystem at these times.

The decoherece effects at times $\frac{t_r}{2}$ and t_r can also be observed on the black

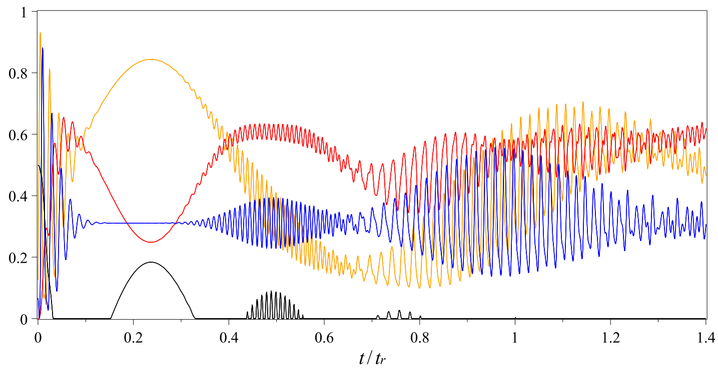

(a) $\Delta = 0.4$

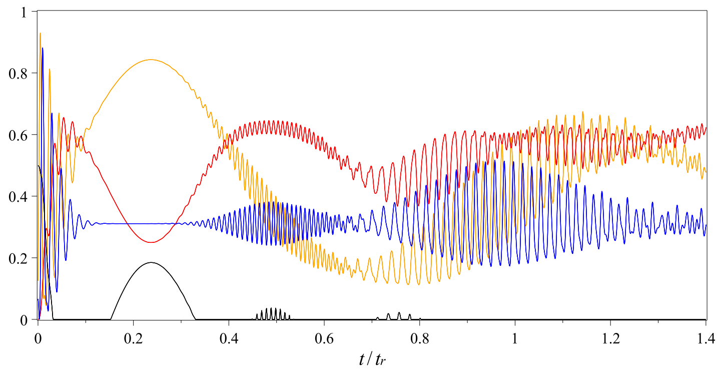

(b) $\Delta = 1.0$

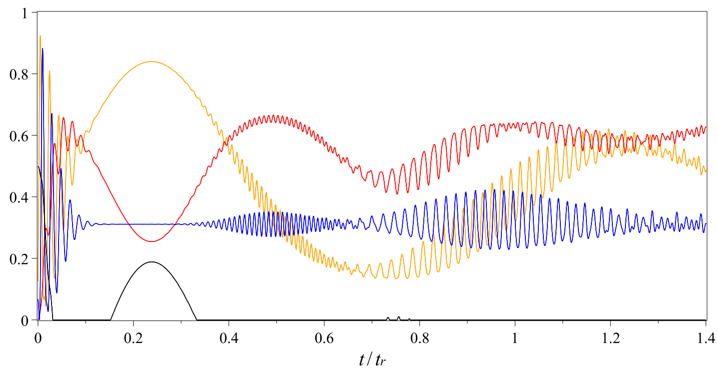

(c) $\Delta = 2.0$

Figure 5.3.2: Plots comparing qubits linear entropies (red), probability of the two qubits state $|ee\rangle$ (blue), probability of the two qubits being a two-qubit attractor state $\left|\psi^{+}_{2,att}\right\rangle_N$ (orange), and concurrence $\varsigma(t)$ (black) for two qubits-big spin model of initial qubit state $\frac{1}{\sqrt{20}}|ee\rangle + \sqrt{\frac{19}{20}}|gg\rangle$, $|\zeta|^2 = 25$, $N = 150$ and the big spin's initial phase $\phi = 0$, with decoherence effects in the frequency. Figure (a) shows the differences in the system with $\Delta = 0.4$, (b) shows the differences in the system with $\Delta = 1.0$ and (c) shows the differences in the system with $\Delta = 2.0$.

concurrence curve. The plots in Figure 5.3.2 shows that this quantity is very sensitive to the increment of decoherence in the system with an initial two-qubit state from outside the basin of attraction. The peak that resulted from the birth of entanglement between the two qubits reduces in size as the error distribution width increases, and it become totally flat at these particular times with $\Delta_0 = 2.0$.

5.4 Summary

We have considered both the two-qubit Jaynes-Cummings model as well as the two-qubit big spin model, both with the effect of non-zero detuning between the qubits and the field mode or big spin. In principle the detuning space has two independent parameters, so in order to simplify and make the investigations calculationally practical, we reduced this to a single parameter by detuning the qubits either side of the fieldmode and the big spin frequency. We then analysed the systems by taking a desired scenario of zero detuning, and for each example considering an ensemble of systems with a distribution of detunings, subject to a Gaussian distribution peaked at zero, with different chosen widths. We have demonstrated how the decoherence introduced by these detuning errors affects both the field mode and big spin systems, for states both inside and outside the basins of attraction.

From these studies, we have demonstrated that both the two-qubit Jaynes-Cummings model as well as the two-qubit big spin model react in a similar manner to the errors introduced, for both forms of system in their equivalent initial state regimes. All quantities like the probability of the two qubits being in the two-qubit attractor state, the Rabi oscillations, the linear entropy and the concurrence considered in both interacting systems show similar effects with increasing width of error distribution.

In additional to the presented results, we can also observe the characteristic of changes in the time evolutions for both two-qubit models with respect to decoherence. In this thesis, we use concurrence ς as an example where we show the decrement in this quantity with respect to the increasing error distribution width, Δ. For that purpose, we plot Figure 5.4.1 that exhibits and compares the changes in the amount of two-qubit entanglement between the two-qubit Jaynes Cummings and two-qubit big spin models. By considering both cases of initial two-qubit state from inside (Figure 5.4.1(a)) and outside (Figure 5.4.1(b)) the basin of attraction, we plot the values of concurrence at time $\frac{t_r}{2}$ against their specific Δ. Although there are significant gaps in the value of concurrence between the two models, we can see that for each initial two-qubit state, both models exhibit almost similar decrement trends in the changes as the results of increasing decoherence.

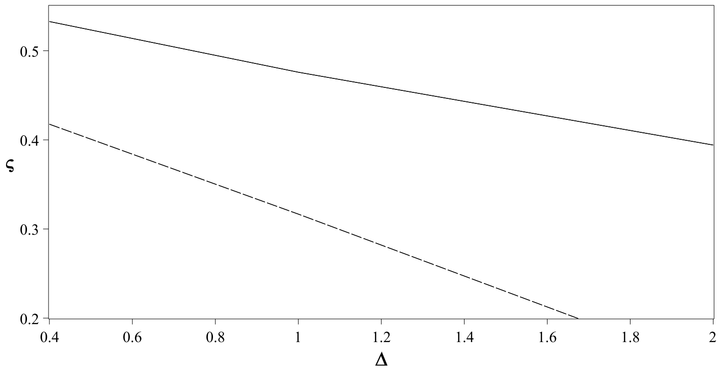

(a) Two-qubit state from inside the basin of attraction at time $\frac{t_r}{2}$

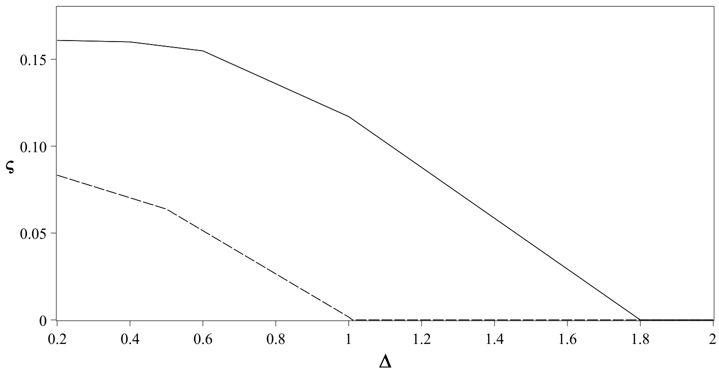

(b) Two-qubit state from outside the basin of attraction at time $\frac{t_r}{2}$

Figure 5.4.1: Measure of entanglement (concurrence) versus error distribution width (decoherence) for two-qubit Jaynes Cummings model (solid line) and two-qubit big spin (dashed line) model.

Chapter 6

Two-Qubit Interacting Systems with Non-Zero Dipole Interaction Detuning

6.1 Introduction

With an extra qubit in the system, the study on the the two-qubit interacting models are more complicated. More variables are involved and have to be considered. So far in all our analysis on the two-qubit interacting models, we have made an assumption that the interaction strength λ between the two qubits with the field (or with the big spin) are uniform such that we have $\lambda_1 = \lambda_2 = \lambda$. With this assumption, we have studied the resonant cases of two-qubit Jaynes-Cummings model and two-qubit big spin model in Chapter 4, as well as both models with a non-resonant condition for the system frequencies in Chapter 5. This led to a study of decoherence due to errors in the resonant condition.

In this chapter, we will study the effects of non-zero mismatch in dipole interaction strength (or errors) on the two-qubit Jaynes-Cummings model and then will extend our analysis on the two-qubit big spin model. We will investigate the changes in the time evolutions of both systems with respect to the changes in the dipole strength differences, particularly the entanglement between the two qubits. Similar to the case of non-zero frequency detunings, we will analyse the systems by considering a distribution of dipole strength differences to model the realistic errors that usually occur in actual systems.

6.2 Collapse, Revival and Decoherence of Entanglement in Two-Qubit Jaynes-Cummings Model

To analyse and observe the effects of non-zero difference in the dipole interaction strength of a two-qubit Jaynes-Cummings system, we consider a case where the dipole interaction strength of the first qubit λ_1 and the second qubit λ_2 are different. In order to isolate the effects just due to to the coupling mismatch, this time we we let the frequency of both qubits and the field mode to be resonant such that $\omega = \Omega_1 = \Omega_2$. We solve the dynamics of this system by first solving the eigenvalue equation given by Equation (4.2.5). By rearranging the states with the same number of excitations, Equation (4.2.7) now takes the form

$$\begin{aligned}
\hat{H}_2 \left|\Psi_2\right\rangle = \sum_{n=0}^{\infty} \Bigg[\\
& \left[\hbar\omega\left(n+1\right)a_{ee,n} + \hbar\sqrt{n+1}\left(\lambda_1 a_{ge,n+1} + \lambda_2 a_{eg,n+1}\right)\right]\left|ee,n\right\rangle \\
& \left[\hbar\omega\left(n+1\right)a_{eg,n+1} + \hbar\lambda_1\sqrt{n+2}a_{gg,n+2} + \hbar\lambda_2\sqrt{n+1}a_{ee,n}\right]\left|eg,n+1\right\rangle \\
& \left[\hbar\omega\left(n+1\right)a_{ge,n+1} + \hbar\lambda_1\sqrt{n+1}a_{ee,n} + \hbar\lambda_2\sqrt{n+2}a_{gg,n+2}\right]\left|ge,n+1\right\rangle \\
& \left[\hbar\omega\left(n+1\right)a_{gg,n+2} + \hbar\lambda_1\sqrt{n+2}\left(a_{eg,n+1} + \hbar\lambda_2 a_{ge,n+1}\right)\right]\left|gg,n+2\right\rangle \Bigg] \\
& + \left[\hbar\lambda_1 a_{eg,0} + \hbar\lambda_2 a_{ge,0}\right]\left|gg,1\right\rangle + \lambda_2 a_{gg,1}\left|ge,0\right\rangle + \lambda_1 a_{gg,1}\left|eg,0\right\rangle \\
& - \hbar\omega a_{gg,0}\left|gg,0\right\rangle .
\end{aligned} \tag{6.2.1}$$

As was discussed in Section 4.2.2, we may then put this equation into a matrix form given by

$$\hat{H}_2 \left|\Psi_2\right\rangle = \sum_{n=0}^{\infty} \begin{pmatrix} \upsilon_{1,1} & \upsilon_{1,2} & \upsilon_{1,3} & \upsilon_{1,4} \\ \upsilon_{2,1} & \upsilon_{2,2} & \upsilon_{2,3} & \upsilon_{2,4} \\ \upsilon_{3,1} & \upsilon_{3,2} & \upsilon_{3,3} & \upsilon_{3,4} \\ \upsilon_{4,1} & \upsilon_{4,2} & \upsilon_{4,3} & \upsilon_{4,4} \end{pmatrix} \left|\Psi_2\right\rangle \tag{6.2.2}$$

where

$$\upsilon_{1,1} = \hbar\omega\,(n+1) \quad \upsilon_{1,2} = \hbar\lambda_2\sqrt{n+1}$$

$$\upsilon_{1,3} = \hbar\lambda_1\sqrt{n+1} \quad \upsilon_{1,4} = 0$$

$$\upsilon_{2,1} = \hbar\lambda_2\sqrt{n+1} \quad \upsilon_{2,2} = \hbar\omega\,(n+1)$$

$$\upsilon_{2,3} = 0 \quad \upsilon_{2,4} = \hbar\lambda_1\sqrt{n+2}$$

$$\upsilon_{3,1} = \hbar\lambda_1\sqrt{n+1} \quad \upsilon_{3,2} = 0$$

$$\upsilon_{3,3} = \hbar\omega\,(n+1) \quad \upsilon_{3,4} = \hbar\lambda_2\sqrt{n+2}$$

$$\upsilon_{4,1} = 0 \quad \upsilon_{4,2} = \hbar\lambda_1\sqrt{n+2}$$

$$\upsilon_{4,3} = \hbar\lambda_2\sqrt{n+2} \quad \upsilon_{4,4} = \hbar\omega\,(n+1)$$

By diagonalising the Matrix (6.2.2), we then find the eigenvalues of the Hamiltonian. For $n = 0$, it is given by

$$E_{0,n} = E_{d,n} = \hbar\omega(n+1). \tag{6.2.3}$$

and for the case of $n \geq 1$ the eigenvalues are

$$\begin{aligned} E_{\pm,n} &= \hbar\omega(n+1) \\ &\pm \frac{\hbar}{2}\left[(4n+6)(\lambda_1^2+\lambda_2^2) + 2\sqrt{(4n+6)^2\lambda_1^2\lambda_2^2 + (\lambda_1-\lambda_2)^2(\lambda_1+\lambda_2)^2}\right]^{1/2}. \end{aligned} \tag{6.2.4}$$

We can also calculate the eigenvalues for the case of lower energy levels which are given as

$$E_{\pm,-1} = \pm\hbar\sqrt{\lambda_1^2+\lambda_2^2} \tag{6.2.5}$$

$$E_{d,-1} = 0 \tag{6.2.6}$$

$$E_{g,0} = -\hbar\omega. \tag{6.2.7}$$

From these eigenvalues, we find the corresponding eigenvectors that are given as

$$|\pm, n\rangle_2 = P\,|ee, n\rangle \pm Q\,|eg, n+1\rangle + R\,|ge, n+1\rangle + S\,|gg, n+2\rangle \tag{6.2.8}$$

$$|0, n\rangle_2 = -\frac{P_0}{\sqrt{P_0^2 + S_0^2}}\,|ee, n\rangle + \frac{S_0}{\sqrt{P_0^2 + S_0^2}}\,|gg, n+2\rangle \tag{6.2.9}$$

$$|d, n\rangle_2 = \frac{Q_0}{\sqrt{Q_0^2 + R_0^2}}\,|ge, n+1\rangle - \frac{R_0}{\sqrt{Q_0^2 + R_0^2}}\,|eg, n+1\rangle \tag{6.2.10}$$

where

$$P = \frac{(\lambda_1 + \lambda_2)\sqrt{n+1}}{\left((4n+6)(\lambda_1^2 + \lambda_2^2 + \lambda_1\lambda_2) + \sqrt{(4n+6)^2\lambda_1^2\lambda_2^2 + (\lambda_1 - \lambda_2)^2(\lambda_1 + \lambda_2)^2}\right)^{1/2}} \tag{6.2.11}$$

$$Q = \frac{\left((4n+6)(\lambda_1^2 + \lambda_2^2) + 2\sqrt{(4n+6)^2\lambda_1^2\lambda_2^2 + (\lambda_1 - \lambda_2)^2(\lambda_1 + \lambda_2)^2}\right)^{1/2}}{2\left((4n+6)(\lambda_1^2 + \lambda_2^2 + \lambda_1\lambda_2) + \sqrt{(4n+6)^2\lambda_1^2\lambda_2^2 + (\lambda_1 - \lambda_2)^2(\lambda_1 + \lambda_2)^2}\right)^{1/2}} \tag{6.2.12}$$

$$R = \frac{\left((4n+6)(\lambda_1^2 + \lambda_2^2) + 2\sqrt{(4n+6)^2\lambda_1^2\lambda_2^2 + (\lambda_1 - \lambda_2)^2(\lambda_1 + \lambda_2)^2}\right)^{1/2}}{2\left((4n+6)(\lambda_1^2 + \lambda_2^2 + \lambda_1\lambda_2) + \sqrt{(4n+6)^2\lambda_1^2\lambda_2^2 + (\lambda_1 - \lambda_2)^2(\lambda_1 + \lambda_2)^2}\right)^{1/2}} \tag{6.2.13}$$

$$S = \frac{(\lambda_1 + \lambda_2)\sqrt{n+2}}{\left((4n+6)(\lambda_1^2 + \lambda_2^2 + \lambda_1\lambda_2) + \sqrt{(4n+6)^2\lambda_1^2\lambda_2^2 + (\lambda_1 - \lambda_2)^2(\lambda_1 + \lambda_2)^2}\right)^{1/2}} \tag{6.2.14}$$

$$P_0 = (\lambda_1 + \lambda_2)\sqrt{n+1} \tag{6.2.15}$$

$$Q_0 = \frac{1}{2}\Big((4n+6)(\lambda_1^2+\lambda_2^2) + 2\sqrt{(4n+6)^2\lambda_1^2\lambda_2^2 + (\lambda_1-\lambda_2)^2(\lambda_1+\lambda_2)^2}\Big)^{1/2} \tag{6.2.16}$$

$$R_0 = -\frac{1}{2}\Big((4n+6)(\lambda_1^2+\lambda_2^2) + 2\sqrt{(4n+6)^2\lambda_1^2\lambda_2^2 + (\lambda_1-\lambda_2)^2(\lambda_1+\lambda_2)^2}\Big)^{1/2} \tag{6.2.17}$$

$$S_0 = (\lambda_1 + \lambda_2)\sqrt{n+2} \tag{6.2.18}$$

Note that we can make a check on all these eigenvalue and eigenvector expressions by letting the two couplings tend to the same λ, and recover the results shown in Chapter 4.

We follow the similar steps as in Section 4.2.2 to find the exact solution to this system's Hamiltonian. By transforming into the interaction picture and using the same state transformations (4.2.32) to (4.2.36), the solution reduces the into the following equation:

$$\begin{aligned}
|\Psi_2(t)\rangle = |C_R\rangle + \sum_{n=0}^{\infty}\Bigg(&\Bigg[C_nC_{ee}\Big(2P^2\cos\Big(\frac{t}{2}\sqrt{Z}\Big) + \frac{S_0^2}{P_0^2+S_0^2}\Big) + C_{gg}C_{n+2} \\
&\times\Big(2PS\cos\Big(\frac{t}{2}\sqrt{Z}\Big) - \frac{P_0S_0}{P_0^2+S_0^2}\Big) - iC_{n+1}P\sin\Big(\frac{t}{2}\sqrt{Z}\Big)(C_{eg}+C_{ge})\Bigg]|ee,n\rangle \\
&+\Bigg[-i\sin\Big(\frac{t}{2}\sqrt{Z}\Big)\Big(C_nC_{ee}P + C_{n+2}C_{gg}S\Big) \\
&+C_{n+1}Q\cos\Big(\frac{t}{2}\sqrt{Z}\Big)(C_{eg}+C_{ge}) + C_{n+1}C(C_{eg}-C_{ge})\Bigg]|eg,n+1\rangle \\
&+\Bigg[-i\sin\Big(\frac{t}{2}\sqrt{Z}\Big)\Big(C_nC_{ee}P + C_{n+2}C_{gg}S\Big) \\
&+C_{n+1}Q\cos\Big(\frac{t}{2}\sqrt{Z}\Big)(C_{eg}+C_{ge}) - C_{n+1}C(C_{eg}-C_{ge})\Bigg]|ge,n+1\rangle \\
&+\Bigg[C_{ee}C_n\Big(2PS\cos\Big(\frac{t}{2}\sqrt{Z}\Big) - \frac{P_0S_0}{P_0^2+S_0^2}\Big) + C_{gg}C_{n+2} \\
&\times\Big(2S^2\cos\Big(\frac{t}{2}\sqrt{Z}\Big) + \frac{P_0^2}{P_0^2+S_0^2}\Big) - iC_{n+1}S\sin\Big(\frac{t}{2}\sqrt{Z}\Big)(C_{eg}+C_{ge})\Bigg]|gg,n+2\rangle\Bigg)
\end{aligned} \tag{6.2.19}$$

where $Z = (4n+6)(\lambda_1^2+\lambda_2^2) + 2\sqrt{(4n+6)^2\lambda_1^2\lambda_2^2 + (\lambda_1-\lambda_2)^2(\lambda_1+\lambda_2)^2}$ and $|C_R\rangle$ are all other states outside the sum given by

$$\begin{aligned}|C_R\rangle &= \left(\hbar\lambda_1 a_{eg,0} + \hbar\lambda_2 a_{ge,0}\right)|gg,1\rangle + \lambda_2 a_{gg,1}|ge,0\rangle + \lambda_1 a_{gg,1}|eg,0\rangle \\ &\quad - \hbar\omega a_{gg,0}|gg,0\rangle\,.\end{aligned} \tag{6.2.20}$$

With this equation, we will analyse the two-qubit Jaynes-Cummings system with respect to the errors as modelled in Section 3.2.2. We let the difference in the dipole interaction strength of both qubits (or error) is given by δ such that $\lambda_2 = \lambda_1 + \delta$. With the single parametrisation of the mismatch as a function of δ, we consider a desired case of a realistic system with both qubits having equal dipole interaction strengths with the field mode. However we then consider unavoidable errors across an ensemble of this two-qubit subsystem, in which the errors are distributed by Gaussian statistics given by

$$f\left(\delta|0,\Delta\right) = \frac{1}{\Delta\sqrt{2\pi}}e^{-\frac{\delta^2}{2\Delta^2}} \tag{6.2.21}$$

where δ is the error sampled over its width, Δ. This represents errors distributed over δ but centered on zero, to model the ideal case of equal dipole interaction strength of both qubits with decoherence (due to errors) effects.

We average over this frequency difference with distributions of varying width by averaging the density matrix over the error distribution. We achieve this with a discrete approximation as explained in Section 3.2.2 that has the form of

$$\hat{\rho}_q(\Delta) \approx \sum_{\delta_i} \frac{f\left(\delta_i|0,\Delta\right)\hat{\rho}_q(t,\delta_i)}{\sum_{\delta_i} f\left(\delta_i|0,\Delta\right)} \tag{6.2.22}$$

where i indicates the number of the discrete events.

We can observe the time evolutions of this system in a similar way to the cases of two-qubit and field mode with resonance and non-resonance frequencies where the observation can be made on this system with different initial qubit state regimes. We will study and observe the decoherence effects of the systems with initial qubit states from both inside and outside of the basin of attraction that given by Equation (4.2.66)

$$|\psi_2\rangle = a\left(e^{-i\theta}|ee\rangle + e^{i\theta}|gg\rangle\right) + \sqrt{\frac{1}{2} - |a|^2}\left(|eg\rangle + |ge\rangle\right) \tag{6.2.23}$$

where θ is the initial phase of the radiation field and a is a complex variable parametrising the state and satisfies $0 \leq |a| \leq \frac{1}{\sqrt{2}}$.

6.2.1 Initial two-qubit state from inside the basin of attraction

Equation (6.2) gives us the solution to the Hamiltonian of a two-qubit Jaynes-Cummings model with a mismatch in the qubits' dipole interaction coupling to the field. With this equation, we calculate the probability of the two qubits both being in the excited state $P_{ee}(t)$, the linear entropy of the two-qubit subsystem $S_q^L(t)$, the probability of the two qubits being in the attractor state $P_{2,att}^{+}(t)$ and the concurrence $\varsigma(t)$ of the two qubits entanglement. To illustrate these quantities with respect to an initial two-qubit state from inside the basin of attraction, we plot Figure 6.2.1 for three different error distribution widths, Δ. We can make many interesting comparisons in the time evolutions of an interacting system with an error in the dipole interaction strength as depicted in the Figure 6.2.1 with the standard two-qubit Jaynes-Cummings system as depicted in Figure 4.2.1 and Figure 4.2.4.

In a standard Jaynes-Cummings system where the overall state of the system is pure, at the two-qubit attractor time $\frac{t_r}{4}$ the system is expected to have no entanglement, either between the two qubits and the field or between the two qubits themselves. The two-qubit subsystem is a two-qubit attractor state which is pure and disentangled from the field. These facts can be seen by observing Figure 4.2.1 where the linear entropy of the two-qubit subsystem represented by the red line approaching close to zero, and the probability of the two qubits being in the two-qubit attractor state $\left|\psi_{2,att}^{+}\right\rangle$ represented by the orange line approaching close to unity. It is interesting to note that with of $\bar{n} = 36$, although it is very close to zero, there is still a non-zero value of entropy can be observed in the red curve. This is due to some residual entanglement of the two qubits with the field. However, with increasing decoherence in the system, both quantities show some changes. The red entropy curves in Figure 6.2.1 show a weaker approach to zero and the orange probability curves show a weaker approach to unity, with increasing error distribution width Δ. This indicates that the purity of the two-qubit subsystem has been affected by the decoherence introduced into the system. There is an increase in the two-qubit mixture, with a little bit still attributable to entanglement with the field, but the increase is due to the decoherence. This is reflected in the plots by the entropy and probabilities deviating further from the pure state cases at this particular time as the error distribution width is increased. Similar observations can be made at the second attractor time $\frac{3t_r}{4}$ but with affected purity of the orthogonal two-qubit attractor state $\left|\psi_{2,att}^{-}\right\rangle$.

In a large $\bar{n}$ approximation, at the two-qubit revival time $\frac{t_r}{2}$ the two-qubit

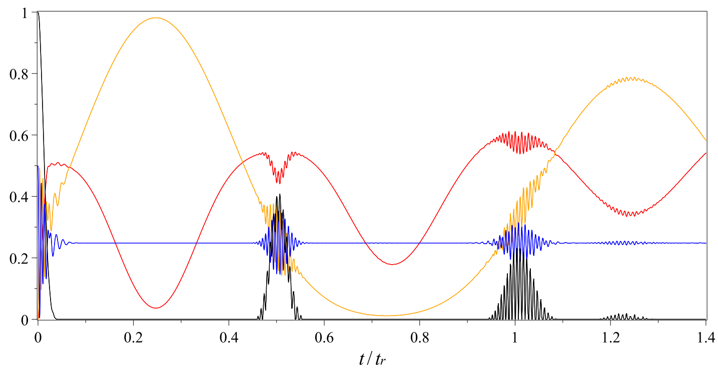

(a) $\Delta = 0.1$

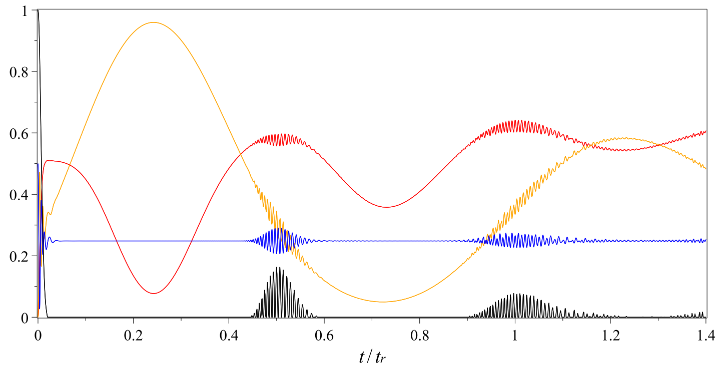

(b) $\Delta = 0.3$

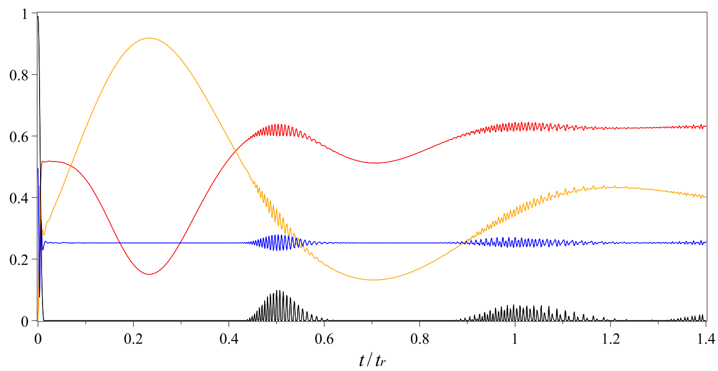

(c) $\Delta = 0.5$

Figure 6.2.1: Plots comparing qubits linear entropies (red), probability of the two-qubit state $|ee\rangle$ (blue), the probability of being in the two-qubit attractor state $\left|\psi^{+}_{2,att}\right\rangle$ (orange), and concurrence $\varsigma(t)$ (black) for two qubits-field mode models of initial qubit state $\frac{1}{\sqrt{2}}(|ee\rangle + |gg\rangle)$, $\bar{n} = 36$ and the initial phase of the radiation field $\theta = 0$, with decoherence effects in dipole interaction strength. Figure (a) shows the differences in the system with $\Delta = 0.1$, (b) shows the differences in the system with $\Delta = 0.3$ and (c) shows the differences in the system with $\Delta = 0.5$.

subsystem is expected to once again disentangle from the field, and thus the linear entropy is again very close to zero. However, with decoherence in the system, interesting changes are visible where there is some disturbance to the linear entropy of the two qubits. We can see that as the error distribution width increases the entropy value has become larger than zero, and the dip in the red line becomes shallower which indicates the decrement in the purity of the two-qubit subsystem. The decoherence has increase the mixture of the system and therefore we can see the dip in the linear entropy curve is filled in.

Beside the linear entropy, changes in the qubit probabilities can also be seen at time $\frac{t_r}{2}$. Although very small effects of decoherence can be seen on the probability of the qubits being in the two-qubit attractor state $P^{+}_{2,att}(t)$, a significant reduction in the amplitude of oscillation of the probability of the two qubits to be in the excited state $P_{ee}(t)$ is observed. The revival amplitude of the two qubits state at this time becomes smaller as a function of increasing error width where we can see from Figure 6.2.1, even with $\Delta = 0.1$, the revival envelope has shrunk significantly and the blue line has become almost a flat line at both $\frac{t_r}{2}$ and t_r with $\Delta = 0.5$.

The decoherence effects can also be seen in the value of entanglement between the two qubits. At time $\frac{t_r}{2}$ in a perfect system, the tangle value is expected to return to the same value as it has at the beginning of the interaction, so that $\varsigma(0) = \varsigma(\frac{t_r}{2})$. The numerical results for a system with $\bar{n} = 36$ is shown in Figure 4.2.4. However, as shown in the Figure 6.2.1 the concurrence decreases with the peak of its revival reduces to a lower value as the error distribution width Δ increases. This shows that there is a significant effect of decoherence on the entanglement value between the two qubits. Anyway, it is very interesting to see the fact that there is still some entanglement revival showing even with error distribution width at the scale of $\Delta = 0.5$, means that there is a good robustness of the entanglement against errors in the dipole interaction strength.

In Section 4.2.6 we have discussed that at the two-qubit revival time $\frac{t_r}{2}$ the process where the entanglement in the two qubits is exchanged for the qubits-field entanglement, and later for a superposition of field coherent states. However, in this case we cannot make a similar conclusion about the trade-off between the qubit-qubit and the qubits-field entanglements even though from the Figure 6.2.1 we can see there is an additional entropy being added by the increasing error width. This is because with the decoherence in the system, we can no longer have a promise that the total state of the system is still pure. Therefore, we can only conclude that it is certainly the case that the entanglement between the two qubits weakens with increasing error distribution widths Δ, but this does not necessarily imply the increment in the entanglement between the two qubits and the field.

6.2.2 Initial two-qubit state from outside the basin of attraction

Similar to the case of non-resonant frequencies, we can also study our model with errors in the dipole interaction strength with an initial two-qubit state that comes from outside the basin of attraction as given by Equation (6.2.23). With Equation (6.2) and an approximation given by Equation (6.2.22), we calculate the probability of the two qubits being in the excited states $P_{ee}(t)$, the linear entropy of the two-qubit subsystem $S_q^L(t)$, the probability of the two qubits being in the two-qubit attractor state $P_{2,att}^{+}(t)$ and also the concurrence $\varsigma(t)$ as a measurement of the entanglement between the two qubits. These quantities are plotted in Figure 6.2.2 that shows the time evolution of the two-qubit Jaynes-Cummings model that begins with an initial two-qubit state from outside the basin of attraction and considers an increasing error distribution width in the dipole interaction strength between the two qubits and the field.

We compare the results to the standard case of the Jaynes-Cummings model plotted in Figure 4.2.1 and Figure 4.2.4. Similar to the case with $\lambda_1 = \lambda_2$, without the $\eta_0 = 0$ condition in Equation (4.2.65), we cannot factorise the two-qubit state out of the wavefunction at times $\frac{t_r}{4}$ and $\frac{3t_r}{4}$. This prohibits the two-qubit subsystem from approaching the two-qubit attractor state and thus the entropy will be non-zero at these times. These are shown by the $P_{2,att}^{+}(t)$ plotted as an orange line, which has its maximum significantly less than unity at the first two-qubit attractor time. The red linear entropy line has only shallow dips towards zero at the two attractor times, but does not approach close to zero. The amount of entanglement is shown as the black line and unlike for the case of initial two-qubit states from inside the basin, clearly there are peaks at $\frac{t_r}{4}$ and $\frac{3t_r}{4}$.

There are changes that can be observed on some of the dynamics at these two-qubit attractor times, even with a small error value $\Delta = 0.1$. At time $\frac{t_r}{4}$ the linear entropy can be seen to have a shallower dip, indicating that the approach of the entropy to zero weakens with increasing decoherence. On the other hand, the probability of the two qubits being in the two-qubit attractor state $\left|\psi_{2,att}^{+}\right\rangle$ decreases where the approach of the probability to unity weakens although a little less susceptible with increasing decoherence. Similar attributes can be observed at

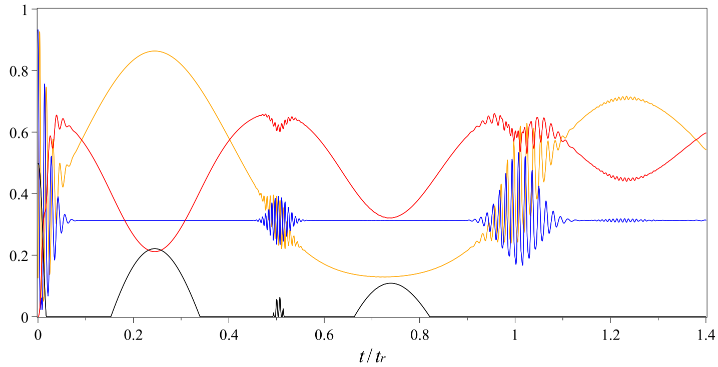

(a) $\Delta = 0.1$

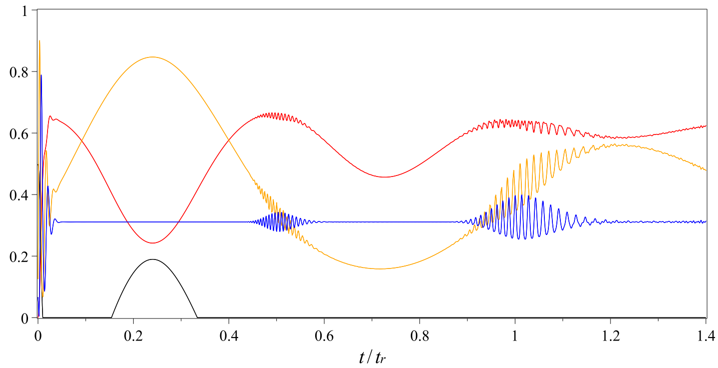

(b) $\Delta = 0.3$

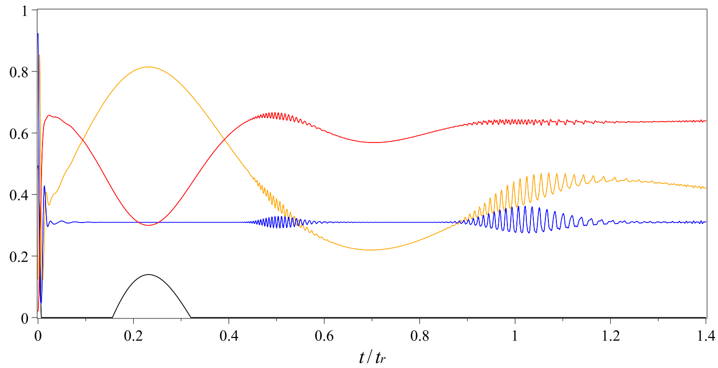

(c) $\Delta = 0.5$

Figure 6.2.2: Plots comparing qubits linear entropies (red), probability of the two-qubit state $|ee\rangle$ (blue), the probability of being in the two-qubit attractor state $\left|\psi^{+}_{2,att}\right\rangle$ (orange), and concurrence $\varsigma(t)$ (black) for two qubits-field mode models of initial qubit state $\frac{1}{\sqrt{20}}\,|ee\rangle + \sqrt{\frac{19}{20}}\,|ee\rangle$, $\bar{n} = 36$ and the initial phase of the radiation field $\theta = 0$, with decoherence effects in dipole interaction strength. Figure (a) shows the differences in the system with $\Delta = 0.1$, (b) shows the differences in the system with $\Delta = 0.3$ and (c) shows the differences in the system with $\Delta = 0.5$.

the second two-qubit attractor time $\frac{3t_r}{4}$ but with two-qubit attractor state $\left|\psi^-_{2,att}\right\rangle$. This indicates that the two-qubit state which was already a mixed state has become more mixed with the increment in the error distribution width. Significant changes can also be spotted on the entanglement between the two qubits at these two-qubit attractor times. The quantity can be seen to reduce rapidly with the error distribution increment. With an error at the scale of $\Delta = 0.3$, a lesser value of entanglement peak is observed at $\frac{t_r}{4}$, and the quantity even vanishes completely at time $\frac{t_r}{4}$. These changes show that the error in the dipole interaction strength has very significant effects on the purity of the two-qubit subsystem as well as the two-qubit entanglement at the respective attractor times for the case of an initial two-qubit state from outside the basin of attraction.

Besides at the two-qubit attractor times, we can also observe changes to the system as a function of increasing error distribution width at the two-qubit revival time $\frac{t_r}{2}$ as well as the one-qubit revival time t_r too. At these times, there is suppression of the revival oscillations in probability of the two qubits being in the two-qubit attractor state $\left|\psi^+_{2,att}\right\rangle$ and both qubits being in the excited state $|ee\rangle$. This can be seen by blue and orange curves where the quantities become flatter at both times with the increasing decoherence.

At the one-qubit revival time t_r, the two-qubit state can be factorised out of the wavefunction, so the entropy is predicted to be zero. However, Figure 6.2.2 shows otherwise where the entropy dips are less pronounced with increasing decoherence. Similarly, the two-qubit entanglement measurement also suffers with increasing decoherence due to the dipole interaction strength mismatches. If an ideal revival was to occur at the revival time of interaction, the entanglement should have the same concurrence value as at the start where $\varsigma(0) = \varsigma(t_r)$. However the quantity is now affected and the entanglement revivals decrease with increasing decoherence. The black line shows that the entanglement peaks at both times completely disappear with error distribution width $\Delta = 0.3$. This indicates that the expected revival of entanglement between the qubits is sensitive to the increasing qubit-field dipole interaction strength errors.

6.3 Collapse, Revival and Decoherence of Entanglement in Two-Qubit Big Spin Model

We have considered and seen the effects of errors in the dipole interaction strength modelled a distribution given by Equation (6.2.21) on the two-qubit Jaynes-

Cummings model. We averaged the density matrix of the system over this error distribution and used a discrete approximation given by Equation (6.2.22) to calculate the time evolutions of the decohering system.

In this section, we apply the similar analysis on the two-qubit big spin interacting model. We will consider a similar error distribution and density matrix approximation to observe the effect of errors in the dipole interaction strength to the system. To do this, we consider a condition where the frequency of the big spin ω_N is at resonance with the frequency of both qubits Ω_1 and Ω_2 and we find the eigenvalues of the Hamiltonian (4.3.2). After we rearrange the states with the same number of excitations, Equation (4.3.43) becomes

$$
\begin{aligned}
\hat{H}_{2,N}\left|\Psi_2\right\rangle_N = \sum_{n=0}^{N} \Bigg[& \Bigg(\hbar\omega_N(n+1)a_{ee,n} + \hbar\sqrt{(n+1)\Big(1-\frac{n}{N}\Big)} \\
& \times \left(\lambda_1 a_{ge,n+1} + \lambda_2 a_{eg,n+1}\right)\Bigg) \left|ee,n\right\rangle_N \\
& + \Bigg(\hbar\omega_N(n+1)a_{eg,n+1} + \hbar\lambda_1\sqrt{(n+2)\Big(1-\frac{n+1}{N}\Big)} \\
& \times a_{gg,n+2} + \hbar\lambda_2\sqrt{(n+1)\Big(1-\frac{n}{N}\Big)}a_{ee,n}\Bigg) \left|eg,n+1\right\rangle_N \\
& + \Bigg(\hbar\omega_N(n+1)a_{ge,n+1} + \hbar\lambda_1\sqrt{(n+1)\Big(1-\frac{n}{N}\Big)} \\
& \times a_{ee,n} + \hbar\lambda_2\sqrt{(n+2)\Big(1-\frac{n+1}{N}\Big)}a_{gg,n+2}\Bigg) \left|ge,n+1\right\rangle_N \\
& + \Bigg(\hbar\omega_N(n+1)a_{gg,n+2} + \hbar\sqrt{(n+2)\Big(1-\frac{n+1}{N}\Big)} \\
& \times \left(\lambda_1 a_{eg,n+1} + \lambda_2 a_{ge,n+1}\right)\Bigg) \left|gg,n+2\right\rangle_N \Bigg] \\
& + \hbar\omega_N a_{gg,0}\left|gg,0\right\rangle_N + \hbar\lambda_2 a_{gg,1}\left|ge,0\right\rangle_N + \hbar\lambda_1 a_{gg,1}\left|ge,0\right\rangle_N \\
& + \Big(\hbar\lambda_1 a_{eg,0} + \hbar\lambda_2 a_{ge,0}\Big)\left|gg,1\right\rangle_N + \hbar\omega_N(N+1)a_{ee,N}\left|ee,N\right\rangle_N \\
& + \hbar\omega_N N a_{eg,N}\left|eg,N\right\rangle_N + \hbar\omega_N N a_{ge,N}\left|ge,N\right\rangle_N \\
& + \Big(\hbar\omega N a_{ee,N-1} + \hbar\lambda_1 a_{ge,N} + \hbar\lambda_2 a_{eg,N}\Big)\left|ee,N-1\right\rangle_N .
\end{aligned} \tag{6.3.1}
$$

We then put this equation into a matrix form of

$$\hat{H}\,|\Psi_2\rangle_N = \sum_{n=0}^{N-2} \begin{pmatrix} \nu_{1,1} & \nu_{1,2} & \nu_{1,3} & \nu_{1,4} \\ \nu_{2,1} & \nu_{2,2} & \nu_{2,3} & \nu_{2,4} \\ \nu_{3,1} & \nu_{3,2} & \nu_{3,3} & \nu_{3,4} \\ \nu_{4,1} & \nu_{4,2} & \nu_{4,3} & \nu_{4,4} \end{pmatrix} |\Psi_2\rangle_N \tag{6.3.2}$$

where

$$\begin{aligned}
\nu_{1,1} &= \hbar\omega_N(n+1) & \nu_{1,2} &= \hbar\lambda_2\sqrt{(n+1)\left(1-\tfrac{n}{N}\right)} \\
\nu_{1,3} &= \hbar\lambda_1\sqrt{(n+1)\left(1-\tfrac{n}{N}\right)} & \nu_{1,4} &= 0 \\
\nu_{2,1} &= \hbar\lambda_2\sqrt{(n+1)\left(1-\tfrac{n}{N}\right)} & \nu_{2,2} &= \hbar\omega_N(n+1) \\
\nu_{2,3} &= 0 & \nu_{2,4} &= \hbar\lambda_1\sqrt{(n+2)\left(1-\tfrac{n+1}{N}\right)} \\
\nu_{3,1} &= \hbar\lambda_1\sqrt{(n+1)\left(1-\tfrac{n}{N}\right)} & \nu_{3,2} &= 0 \\
\nu_{3,3} &= \hbar\omega_N(n+1) & \nu_{3,4} &= \hbar\lambda_2\sqrt{(n+2)\left(1-\tfrac{n+1}{N}\right)} \\
\nu_{4,1} &= 0 & \nu_{4,2} &= \hbar\lambda_1\sqrt{(n+2)\left(1-\tfrac{n+1}{N}\right)} \\
\nu_{4,3} &= \hbar\lambda_2\sqrt{(n+2)\left(1-\tfrac{n+1}{N}\right)} & \nu_{4,4} &= \hbar\omega_N(n+1)
\end{aligned}$$

We can then find the eigenvalues of Matrix (6.3.2) where for $n=0$ we get

$$E_{0,n} = E_{d,n} = \hbar\omega(n+1), \tag{6.3.3}$$

and for $1 \leq n \leq N-2$ the eigenvalues are

$$\begin{aligned}
E_{\pm,n} &= \hbar\omega_N(n+1) \\
&\quad \pm \frac{\hbar}{2}\Bigg[(4n+6-\frac{4}{N}(n+1)^2)(\lambda_1^2+\lambda_2^2) \\
&\quad + 2\sqrt{(4n+6-\frac{4}{N}(n+1)^2)^2\lambda_1^2\lambda_2^2+(\lambda_1-\lambda_2)^2(\lambda_1+\lambda_2)^2}\Bigg]^{1/2}
\end{aligned} \tag{6.3.4}$$

and with $\xi = 4n+6-\frac{4}{N}(n+1)^2$, we have

$$E_{\pm,n} = \hbar\omega_N(n+1) \pm \frac{\hbar}{2}\left[\xi(\lambda_1^2+\lambda_2^2)+2\sqrt{\xi^2\lambda_1^2\lambda_2^2+(\lambda_1-\lambda_2)^2(\lambda_1+\lambda_2)^2}\right]^{1/2}. \tag{6.3.5}$$

For the lower energy levels, the eigenvalues are given by

$$E_{\pm,-1} = \pm\hbar\sqrt{\lambda_1^2+\lambda_2^2} \tag{6.3.6}$$

$$E_{d,-1} = 0 \tag{6.3.7}$$

$$E_{g,0} = -\hbar\omega_N \tag{6.3.8}$$

and the upper energy levels we have

$$E_{\pm,N-1} = \hbar\omega_N \pm \hbar\sqrt{\lambda_1^2+\lambda_2^2} \tag{6.3.9}$$

$$E_{d,N-1} = \hbar\omega_N N \tag{6.3.10}$$

$$E_{e,N} = \hbar\omega_N (N+1) \tag{6.3.11}$$

From these eigenvalues, we find the corresponding eigenvectors that are given as

$$|\pm, n\rangle_2 = P\,|ee, n\rangle \pm Q\,|eg, n+1\rangle + R\,|ge, n+1\rangle + S\,|gg, n+2\rangle \tag{6.3.12}$$

$$|0, n\rangle_2 = -\frac{P_0}{\sqrt{P_0^2+S_0^2}}\,|ee, n\rangle + \frac{S_0}{\sqrt{P_0^2+S_0^2}}\,|gg, n+2\rangle \tag{6.3.13}$$

$$|d, n\rangle_2 = \frac{Q_0}{\sqrt{Q_0^2+R_0^2}}\,|ge, n+1\rangle - \frac{R_0}{\sqrt{Q_0^2+R_0^2}}\,|eg, n+1\rangle \tag{6.3.14}$$

where

$$P = \frac{(\lambda_1+\lambda_2)\sqrt{(n+1)(1-\frac{n}{N})}}{\left(\xi(\lambda_1^2+\lambda_2^2+\lambda_1\lambda_2) + \sqrt{\xi^2\lambda_1^2\lambda_2^2 + (\lambda_1-\lambda_2)^2(\lambda_1+\lambda_2)^2}\right)^{1/2}} \tag{6.3.15}$$

$$Q = \frac{\left(\xi(\lambda_1^2+\lambda_2^2) + 2\sqrt{\xi^2\lambda_1^2\lambda_2^2 + (\lambda_1-\lambda_2)^2(\lambda_1+\lambda_2)^2}\right)^{1/2}}{2\left(\xi(\lambda_1^2+\lambda_2^2+\lambda_1\lambda_2) + \sqrt{\xi^2\lambda_1^2\lambda_2^2 + (\lambda_1-\lambda_2)^2(\lambda_1+\lambda_2)^2}\right)^{1/2}} \tag{6.3.16}$$

$$R = \frac{\left(\xi(\lambda_1^2+\lambda_2^2)+2\sqrt{\xi^2\lambda_1^2\lambda_2^2+(\lambda_1-\lambda_2)^2(\lambda_1+\lambda_2)^2}\right)^{1/2}}{2\left(\xi(\lambda_1^2+\lambda_2^2+\lambda_1\lambda_2)+\sqrt{\xi^2\lambda_1^2\lambda_2^2+(\lambda_1-\lambda_2)^2(\lambda_1+\lambda_2)^2}\right)^{1/2}} \tag{6.3.17}$$

$$S = \frac{(\lambda_1+\lambda_2)\sqrt{(n+2)(1-\frac{n+1}{N})}}{\left(\xi(\lambda_1^2+\lambda_2^2+\lambda_1\lambda_2)+\sqrt{\xi^2\lambda_1^2\lambda_2^2+(\lambda_1-\lambda_2)^2(\lambda_1+\lambda_2)^2}\right)^{1/2}} \tag{6.3.18}$$

$$P_0 = (\lambda_1+\lambda_2)\sqrt{(n+1)(1-\frac{n}{N})} \tag{6.3.19}$$

$$Q_0 = \frac{1}{2}\left(\xi(\lambda_1^2+\lambda_2^2)+2\sqrt{\xi^2\lambda_1^2\lambda_2^2+(\lambda_1-\lambda_2)^2(\lambda_1+\lambda_2)^2}\right)^{1/2} \tag{6.3.20}$$

$$R_0 = \frac{1}{2}\left(\xi(\lambda_1^2+\lambda_2^2)+2\sqrt{\xi^2\lambda_1^2\lambda_2^2+(\lambda_1-\lambda_2)^2(\lambda_1+\lambda_2)^2}\right)^{1/2} \tag{6.3.21}$$

$$S_0 = (\lambda_1+\lambda_2)\sqrt{(n+2)(1-\frac{n+1}{N})} \tag{6.3.22}$$

Note that by letting the two couplings tend to the same λ, we recover the eigenvalues and eigenvectors for the case of two-qubit big spin model with $\lambda_1 = \lambda_2 = \lambda$ as described in Chapter 4. We find the exact solution to this system's Hamiltonian and by using the state transformation given by Equations (4.3.44) to (4.3.48), we set the states into the interaction picture and get the following solution

$$
\begin{aligned}
|\Psi_2(t)\rangle_N = |C_S\rangle + \sum_{n=0}^{N-2} \Bigg(\Bigg[C_n C_{ee} \bigg(2P^2 \cos\Big(\frac{t}{2}\sqrt{Z}\Big) + \frac{S_0^2}{P_0^2+S_0^2} \bigg) + C_{gg} C_{n+2} \\
\times \bigg(2PS \cos\Big(\frac{t}{2}\sqrt{Z}\Big) - \frac{P_0 S_0}{P_0^2+S_0^2} \bigg) - iC_{n+1} P \sin\Big(\frac{t}{2}\sqrt{Z}\Big) (C_{eg}+C_{ge}) \Bigg] |ee,n\rangle \\
+ \Bigg[-i \sin\Big(\frac{t}{2}\sqrt{Z}\Big) \Big(C_n C_{ee} P + C_{n+2} C_{gg} S \Big) \\
+ C_{n+1} Q \cos\Big(\frac{t}{2}\sqrt{Z}\Big) (C_{eg}+C_{ge}) + C_{n+1} C (C_{eg}-C_{ge}) \Bigg] |eg,n+1\rangle \\
+ \Bigg[-i \sin\Big(\frac{t}{2}\sqrt{Z}\Big) \Big(C_n C_{ee} P + C_{n+2} C_{gg} S \Big) \\
+ C_{n+1} Q \cos\Big(\frac{t}{2}\sqrt{Z}\Big) (C_{eg}+C_{ge}) - C_{n+1} C (C_{eg}-C_{ge}) \Bigg] |ge,n+1\rangle \\
+ \Bigg[C_{ee} C_n \bigg(2PS \cos\Big(\frac{t}{2}\sqrt{Z}\Big) - \frac{P_0 S_0}{P_0^2+S_0^2} \bigg) + C_{gg} C_{n+2} \\
\times \bigg(2S^2 \cos\Big(\frac{t}{2}\sqrt{Z}\Big) + \frac{P_0^2}{P_0^2+S_0^2} \bigg) - iC_{n+1} S \sin\Big(\frac{t}{2}\sqrt{Z}\Big) (C_{eg}+C_{ge}) \Bigg] |gg,n+2\rangle \Bigg)
\end{aligned}
\tag{6.3.23}
$$

where $Z = \xi(\lambda_1^2+\lambda_2^2) + 2\sqrt{\xi^2\lambda_1^2\lambda_2^2 + (\lambda_1-\lambda_2)^2(\lambda_1+\lambda_2)^2}$ and $|C_S\rangle$ are all other states outside the sum given by

$$
\begin{aligned}
|C_S\rangle = \hbar\omega_N a_{gg,0} |gg,0\rangle_N + \hbar\lambda_2 a_{gg,1} |ge,0\rangle_N + \hbar\lambda_1 a_{gg,1} |ge,0\rangle_N \\
+ (\hbar\lambda_1 a_{eg,0} + \hbar\lambda_2 a_{ge,0}) |gg,1\rangle_N + \hbar\omega_N (N+1) a_{ee,N} |ee,N\rangle_N \\
+ \hbar\omega_N N a_{eg,N} |eg,N\rangle_N + \hbar\omega_N N a_{ge,N} |ge,N\rangle_N \\
+ (\hbar\omega N a_{ee,N-1} + \hbar\lambda_1 a_{ge,N} + \hbar\lambda_2 a_{eg,N}) |ee,N-1\rangle_N .
\end{aligned}
\tag{6.3.24}
$$

6.3.1 Initial two-qubit state from inside the basin of attraction

We use solution given by Equation (6.3) and error modelling properties by Equations (6.2.21) and (6.2.22) to plot relevant time evolutions of a two-qubit big spin model with mismatch in the qubits' dipole interaction coupling to the spin coherent state. We calculate the probability of the two qubits being in the excited states $P_{ee}(t)$, the linear entropy of the two-qubit subsystem $S_q^L(t)$, the probability of the two qubits being in the attractor state $P^+_{2,att}(t)$ and the measure of entanglement, concurrence $\varsigma(t)$ of the two-qubit subsystem. We show the time evolutions in Figure 6.3.1 for three error distribution widths. We consider the case of an initial two-qubit state from inside the basin of attraction and we compare the results with the case of uniform dipole interaction coupling depicted as Figure 4.3.1 and Figure 4.3.4.

We have seen in Section 4.2.3, for the case of $\lambda_1 = \lambda_2$ in a large photon number approximation, at the attractor time $\frac{t_r}{4}$ qubits and the big spin are disentangled. The two-qubit subsystem is a two-qubit attractor state which is a pure state. Therefore, in 4.3.1 we can see the linear entropy line (red) approaching close to zero while the probability line (orange) of the two qubits being in the two-qubit attractor state $\left|\psi^{+}_{2,att}\right\rangle$ approaching close to unity. At this time too, the system is expected to have no entanglement between the two qubits, therefore the concurrence should remain flat near zero. However, in Figure 6.3.1 we can observe changes on most of these quantities with an increasing error in the system. The plots show that the linear entropy and two-qubit attractor state probabilities deviating further from the pure state properties at $\frac{t_r}{4}$. A weaker approach to zero in the red entropy curves, as well as a weaker approach to unity in the orange probability curves are observed with respect to the increment in the error distribution width, indicating the purity of the two-qubit subsystem has been affected.

In large $\bar{n}$ and $N \to \infty$ approximations, another interesting observation can be made at time $\frac{t_r}{2}$, where the two-qubit subsystem and the big spin are expected to once again disentangled, which is indicated by the linear entropy curve goes very close to zero. Although the numerical plots do not accurately display this condition, we can still see dips in the red curve in Figure 4.3.1. Furthermore, with decoherence in the system, we can also see that there is an increase in the entropy value and shallower dips and later their disappearance in the red curves with respect to the increasing error distribution width Δ as depicted in Figure 6.3.1. This shows that there is an addition in the two-qubit mixture due to the decoherence in the system.

At this two-qubit revival time $\frac{t_r}{2}$ too, we can also see changes in the two-qubit probabilities, either for both qubits being in the excited state $|ee\rangle$, or for the qubits being a two-qubit attractor state $\left|\psi^{+}_{2,att}\right\rangle$. As the error distribution width increased, significant reductions in the revival amplitudes of both quantities can be seen from the blue and orange lines in Figure 6.3.1. With $\Delta = 0.5$ the curves become almost flat lines, and similar condition can also be observed at time t_r.

Besides the above quantities, the entanglement between the two qubits is also affected by the decoherence in the system. In a perfect system with large $\bar{n}$, at time $\frac{t_r}{2}$ the concurrence is expected to recover its initial value, so that

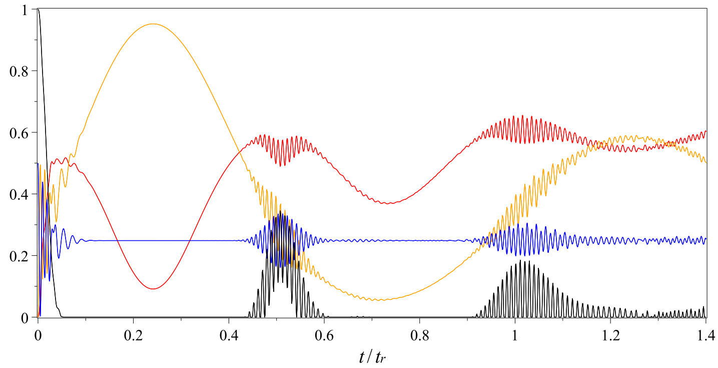

(a) $\Delta = 0.1$

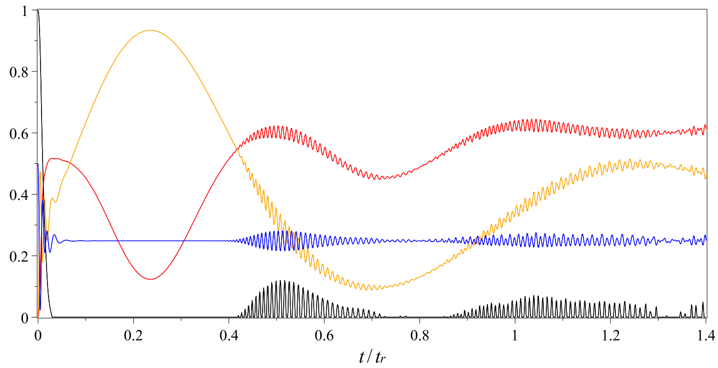

(b) $\Delta = 0.3$

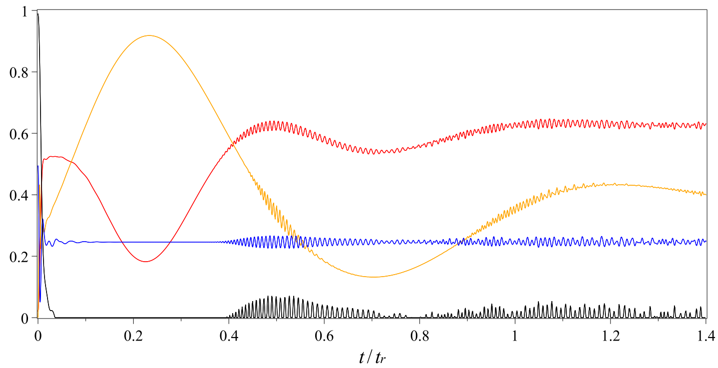

(c) $\Delta = 0.5$

Figure 6.3.1: Plots comparing qubits linear entropies (red), probability of the two-qubit state $|ee\rangle$ (blue), the probability of being a two-qubit attractor state $\left|\psi^{+}_{2,att}\right\rangle_N$ (orange), and concurrence $\varsigma(t)$ (black) for two-qubits big spin models of initial qubit state $\frac{1}{\sqrt{2}}(|ee\rangle + |gg\rangle)$, $|\zeta|^2 = 25$, $N = 150$ and the big spin's initial phase $\phi = 0$, with decoherence effects in the dipole-interaction strength. Figure (a) shows the differences in the system with $\Delta = 0.1$, (b) shows the differences in the system with $\Delta = 0.3$ and (c) shows the differences in the system with $\Delta = 0.5$.

$\varsigma(0) = \varsigma(\frac{t_r}{2})$. This is however not happening in a system with decoherence in the dipole interaction strength as shown by a black line in Figure 6.3.1. It can be seen that the revival peaks at this time decrease significantly with the increment of error distribution widths. However, it is very interesting to note that there is still some entanglement revival showing in the two-qubit subsystem even with $\Delta = 0.5$, indicating a good robustness of this interacting model against the decoherence in the dipole interaction strength, and thus providing some promise for experimental investigations.

6.4 Initial two-qubit state from outside basin of attraction

To understand the effects of decoherence in the dipole-interaction strength on the two-qubit big spin model with an initial two-qubit state from outside the basin of attraction, we plot Figure 6.4.1. The figure shows the linear entropy $S_q^L(t)$ (red), the probability of both qubits being in the excited state $P_{ee}(t)$ (blue), the probability of the two-qubit being an attractor state $P_{2,att}^{+}(t)$ (orange) and also the concurrence $\varsigma(t)$ (black) to show the dynamics of the entanglement between the two qubits.

We have seen in Section 4.2.6 that for the case of $\lambda_1 = \lambda_2$ and with initial two-qubit states from outside the basin of attraction, the two-qubits state cannot be factorised out of the wavefunction at the two-qubit attractor times of the system. This means that at time $\frac{t_r}{4}$ and $\frac{3t_r}{4}$, the two-qubit state is not a pure attractor. These facts are reflected in Figure 4.3.2 where the probability of the two qubits being in the two-qubit attractor state is far from unity at the first attractor time, and only has a shallow dip at the second. The linear entropy also does not approach close to zero at these times. With decoherence in the system, we can observe changes in the dynamics of these quantities. With an error distribution width $\Delta = 0.1$ a shallower dip in the entropy curve, indicating a weaker approach to zero at time $\frac{t_r}{4}$ is shown in Figure 6.4.1. The probability $P_{2,att}^{+}(t)$ has also deceased and shows a weaker approach to unity at this time. These changes suggest that the two-qubit subsystem has becomes more mixed with the increment of decoherence. Similar observations can be made at time $\frac{3t_r}{4}$ but with two-qubit attractor state $\left|\Psi_{2,att}^{-}\right\rangle$.

The effects of the errors can also be seen at the two-qubit revival time $\frac{t_r}{2}$ as well as at t_r. The revival magnitude of the two-qubit attractor state probability

$P_{2,att}^{+}(t)$ as well as the two-qubit oscillation $P_{ee}(t)$ reduce with the increment of the error distribution width. With $\Delta = 0.5$ the revivals in both quantities are very small and the curves are almost flat lines. Further more, at $\frac{t_r}{2}$, we can see that there is a decrement in the purity of the two-qubit subsystem where the entropy value has become larger than zero and the dip in the red line are no longer visible as the error distribution width increases to $\Delta = 0.3$.

Another interesting change can also be observed in the dynamics of the entanglement between the two qubits. Significant reductions in the peaks of the black curves are seen in Figure 6.4.1 with the increment of error distribution width at time $\frac{t_r}{4}$ and $\frac{3t_r}{4}$. Although the peak at the second attractor time vanishes completely with $\Delta = 0.1$, we can still see the sign of entanglement revival at the $\frac{t_r}{4}$ even with $\Delta = 0.5$. At the two-qubit revival time $\frac{t_r}{2}$ and t_r, this quantity suffers a very significant suppression. The entanglement between the two qubits vanishes completely with error distribution width $\Delta = 0.3$ at $\frac{t_r}{2}$ and the curve is completely flat at t_r with $\Delta = 0.1$. These reductions show that the entanglement of the two qubits are very sensitive to the decoherence in the system at these times for the case of initial two-qubit states from outside the basin of attraction.

6.5 Summary

We have considered both the two-qubit Jaynes-Cummings model as well as the two-qubit big spin model, with the effect of decoherence in the dipole interaction strengths. With two qubits in the system, in principle the dipole interaction strength has two independent parameters λ_1 and λ_2. Therefore, in order to simplify and make the investigations calculationally practical, we reduced this to a single parameter by detuning the dipole strength of one of the qubits, so that $\lambda_2 = \lambda_1 + \delta$.

We then analysed both systems with the field mode and the big spin by taking a desired case of zero difference in the dipole interaction strengths. For each example we considered an ensemble of systems with a distribution of errors, subject to a Gaussian distribution peaked at zero, with different chosen error widths. We have considered two cases of initial states *i.e* from inside and outside the basins of attraction, and demonstrated how the decoherence introduced by these errors affect both interacting systems.

From these studies, we have demonstrated that both the two-qubit Jaynes-Cummings model as well as the two-qubit big spin model react in a similar manner

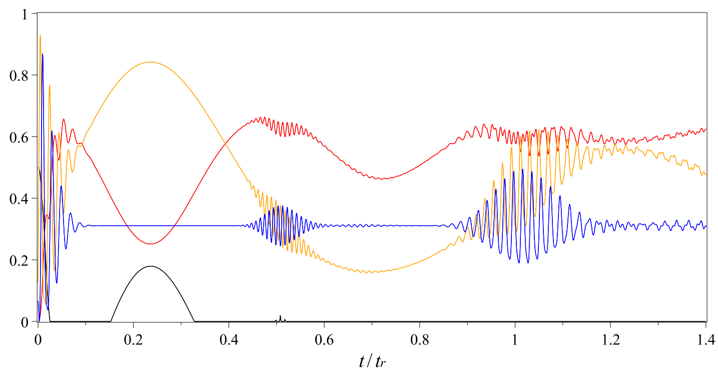

(a) $\Delta = 0.1$

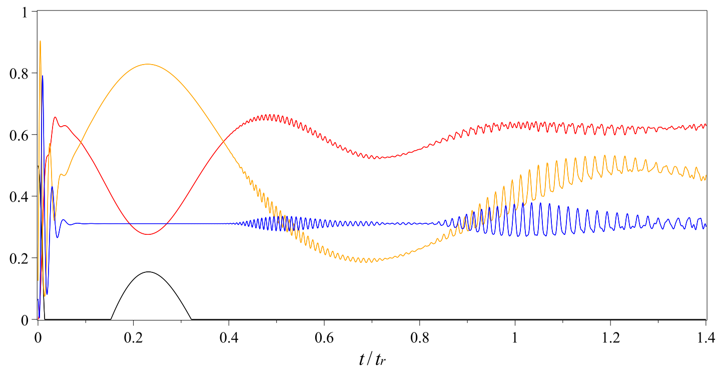

(b) $\Delta = 0.3$

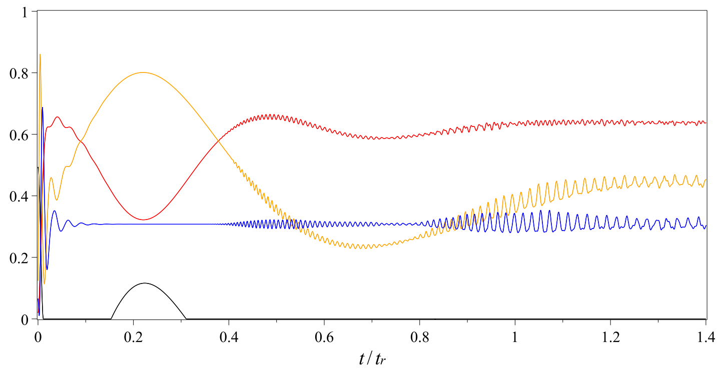

(c) $\Delta = 0.5$

Figure 6.4.1: Plots comparing qubits linear entropies (red), probability of the two qubits state $|ee\rangle$ (blue), probability of the two qubits being a two-qubit attractor state $\left|\psi^{+}_{2,att}\right\rangle_N$ (orange), and concurrence $\varsigma(t)$ (black) for two-qubit big spin model of initial qubit state $\frac{1}{\sqrt{15}}\,|ee\rangle + \sqrt{\frac{14}{15}}\,|gg\rangle$, $|\zeta|^2 = 25$, $N = 150$ and the big spin's initial phase $\phi = 0$, with decoherence effects in the dipole-interaction strength. The figures show the differences in the system with (a) $\Delta = 0.1$, (b) $\Delta = 0.3$ and (c) $\Delta = 0.5$.

to the errors introduced. Both systems show similar behaviors for each equivalent initial state regimes. All relevant quantities like the probability of the two qubits being in the attractor state, the probability of the two qubits being in the excited state, the linear entropy and the concurrence considered in both interacting systems show similar effects with increasing error distribution width.

Besides the presented results, we can also make an observation on the way that the time evolutions of both two-qubit models change with respect to decoherence. Similar to Chapter 5, we use two-qubit entanglement as an example to exhibit the decrement in this quantity with respect to the increasing error distribution width. We plot Figure 6.5.1 that compares the changes in concurrence for both two-qubit models by considering all initial two-qubit state regimes. We plot the amounts of concurrence ς for their specific value of Δ at time $\frac{t_r}{2}$ for the case of initial state from inside the basin of attraction, and at time $\frac{t_r}{4}$ for the case of initial state form outside the basin of attraction. We can see that there are significant gaps in the amount of two-qubit entanglement between the two models, but similar trends of decrement can be observed in this quantity for both two-qubit models as the results of increasing decoherence.

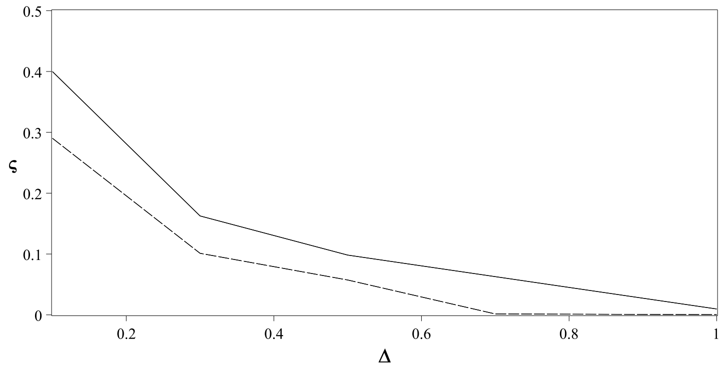

(a) Two-qubit state from inside the basin of attraction at time $\frac{t_r}{2}$

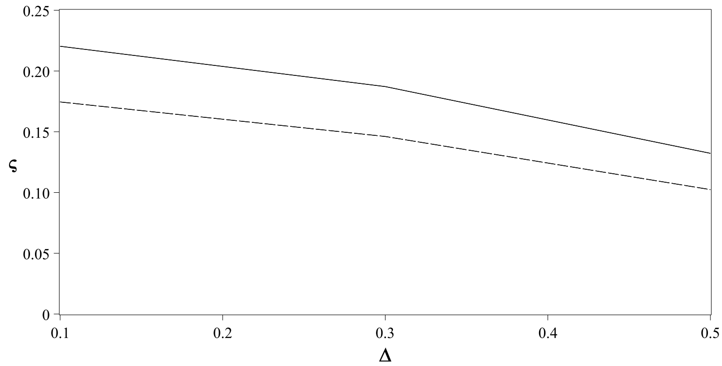

(b) Two-qubit state from outside the basin of attraction at time $\frac{t_r}{4}$

Figure 6.5.1: Measure of entanglement (concurrence) versus error distribution width (decoherence) for two-qubit Jaynes Cummings model (solid line) and two-qubit big spin (dashed line) model.

Chapter 7

Two-Qubit Big Spin Interacting System With Small N

7.1 Introduction

The calculations we have presented for the two-qubit big spin models in the previous Chapters 4, 5 and 6 have been performed with $N = 150$ and a spin coherent state parameter $|\zeta|^2 = 25$. These conditions are used such that N is large enough to make a good comparison with the field mode case and to enable comparison with the two-qubit Jaynes-Cummings model.

However, in order to consider the potential for experiments that could be realistic with current or near future systems, it is interesting to consider smaller values for N. Such consideration for the one-qubit big spin system have been studied by S. Dooley *etal*. [62, 63] where they demonstrated that even with a small value of N, we can still observe the fractional revival in systems of few spins.

In this chapter, we extend our study by exploring the regime of small qubit number in the big spin. We will investigate to ascertain the smallest N that maintains the relevant time evolutions in the two-qubit big spin system, especially the occurrence of qubit-qubit entanglement. We will study this model by considering interacting systems with errors as modelled in Section 3.2.2 for both cases of non-zero errors in detuning and non-zero errors in dipole interaction strength.

7.2 Rabi Oscillation, Linear Entropy, Attractor State and Two-Qubit Entanglement

Similar to the case of a two-qubit big spin system with a large value of N studied in Section 4.3.5 and Section 4.3.6, we will evaluate our two-qubit big spin system with a small value of N in two sets of initial two-qubit states. We have demonstrated that for a large value of N, the time evolutions of a two-qubit big spin system is bounded by a basin of attraction given by Equation (4.3.83). Starting the system with an initial two-qubit state from inside or outside this basin of attraction gives us different behaviours in the relevant quantities. Therefore, in this section we will replicate the similar numerical analysis to observe the differences in the system with a small value of N.

7.2.1 Initial two-qubit state from inside the basin of attraction

To exhibit the changes in the time evolutions of the two-qubit big spin system with an initial two-qubit state form inside the basin of attraction given by Equation (4.3.83), we plot Figure 7.2.1. The figure shows the differences in the system for three small values of N, where we can see the evolutions of the relevant quantities in the system with respect to the increment in the size of the big spin, N. The changes can clearly be seen in the the probability of the two qubits being in the excited states $P_{ee}(t)$, the probability of the two qubits being in an attractor state $P^{+}_{2,att}(t)$ and the linear entropy $S^{L}_{q}(t)$ of the two-qubit subsystem. From Figure 7.2.1, with the increment in the size of the big spin, we can see these quantities start to resemble the attributes displayed by the two-qubit big spin model with a large value of N. With $N = 20$ shown in Figure 7.2.1(a), these quantities appear to be rather noisy which is a similar manner to the dynamics produced by the one-qubit Jaynes-Cummings model with small size coherent states [64]. Such a noisy appearance is not due to actual noise, but rather the complicated quantum dynamics of a modest size system. However, the appearance of the important events become more obvious with the increment of the big spin's size N.

We can start to observe interesting dynamics of Rabi oscillations in a system with $N = 30$. The two-qubit state probability $P_{ee}(t)$ that is depicted by the blue line collapses until time $\frac{t_r}{4}$, before the quantity starts to revive and peaks at time $\frac{t_r}{2}$. This can be seen in Figure 7.2.1(b) even though it is not as smooth as seen in Figure 4.3.1 for a system with $N = 150$. We can also note the appearance of a dip in the red line and a peak in the orange line at $\frac{t_r}{4}$. The two-qubit linear entropy $S_q^L(t)$ approaches zero meanwhile the two-qubit attractor state probability $P_{2,att}^+(t)$ approaches unity at this time. This suggests that, at this point there is a sign of disentanglement between the two-qubit subsystem and as we know from Section 4.3.4, these are the properties of a two-qubit attractor state. So, it is clear that with a big spin with size as small as $N = 30$, we may start to see the signature of a two-qubit attractor state, and thus the spin coherent state.

Similar phenomena as at time $\frac{t_r}{4}$ are also expected at the second attractor time $\frac{3t_r}{4}$ if the size of the big spin is large, but with the orthogonal two-qubit attractor state $\left|\psi_{2,att}^-\right\rangle$. However, with such small N values, the effects are not clearly visible as shown in Figure 7.2.1. The value of linear entropy $S_q^L(t)$ is large for all times, which is the similar case for the two-qubit attractor state probability $P_{2,att}^+(t)$. These indicate no significant disentanglement between the two-qubit and the big spin and the mixture of the two-qubit subsystem is high. In fact, no interesting observations can be made on the system at time larger than $\frac{t_r}{2}$ since the time evolutions produced are rather noisy except a small sign of disentanglement between the two qubits and the big spin at approximately times $\frac{t_r}{2}$ and t_r.

To observe the changes in the entanglement between the two qubits, we plot Figure 7.2.2, that shows the concurrence $\varsigma(t)$ for a two-qubit big spin system with three values of N. It was shown in Section 4.3.6 that with an initial state from inside the basin of attraction and $N = 150$, we can observe the event of collapse and revival of the two-qubit entanglement. This is where the quantity smoothly goes to zero, revives and has a peak at time $\frac{t_r}{2}$. With $|\zeta|^2 = 9$, some signature for this phenomenon can be seen for $N \sim 20$ and this is more apparent in the case of $N = 30$ as presented in the figure. From this Figure 7.2.2, we can see that the collapse and revival of the two-qubit entanglement are rather noisy in comparison to the larger N results shown in Figure 4.3.4. However, there is still clear evidence for revival of the entanglement between the two qubits with small values of N.

We can also note that at the beginning of the interaction, there are fluctuations in the in the two-qubit entanglement especially in Figure 7.2.2(a) for the system with $N = 20$. This can be explained by the dynamics in the trade-off between entanglement and entropy [49]. We know from Section 4.3.6 that in the evolutions of two qubits interacting with N spins, there will be exchange in the value of the two-qubit entanglement for the value of the two-qubit big spin entanglement. This means that the two-qubit entanglement fluctuations require some disentanglement

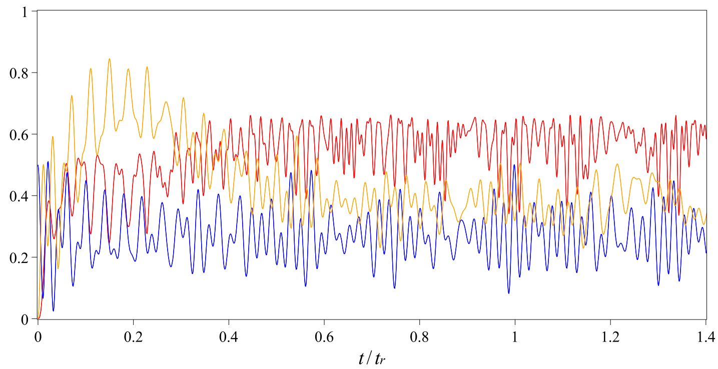

(a) $N = 20$

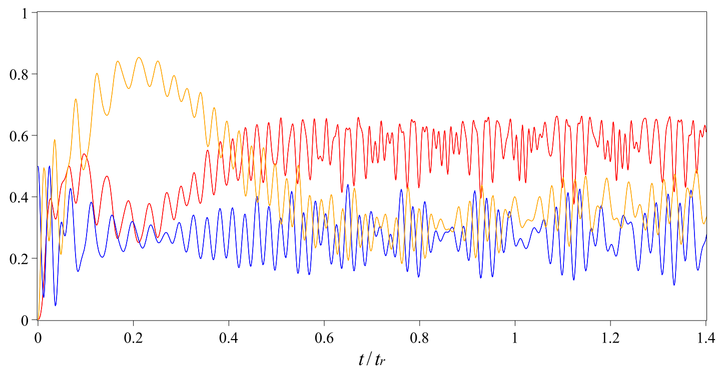

(b) $N = 30$

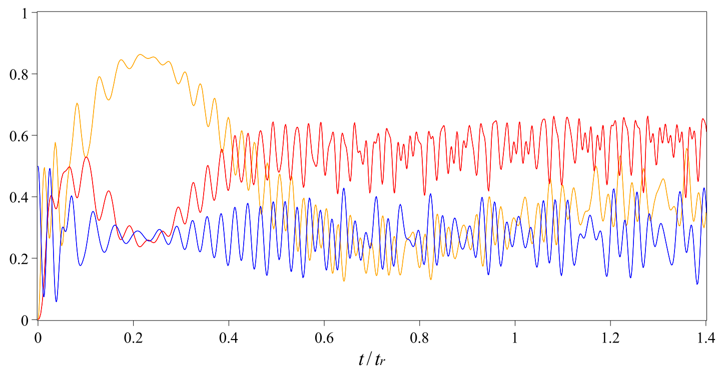

(c) $N = 40$

Figure 7.2.1: Plots comparing qubits linear entropies (red), probability of the two qubits state $|ee\rangle$ (blue) and the probability of being in the two-qubit attractor state $\left|\psi^{+}_{2,att}\right\rangle_N$ (orange) for two qubits-big spin models of initial qubit state $\frac{1}{\sqrt{2}}(|ee\rangle + |gg\rangle)$, $|\zeta|^2 = 9$ and the big spin's initial phase $\phi = 0$. Figure (a) shows the system with $N = 20$, (b) shows the system with $N = 30$ and (c) shows the system with $N = 40$.

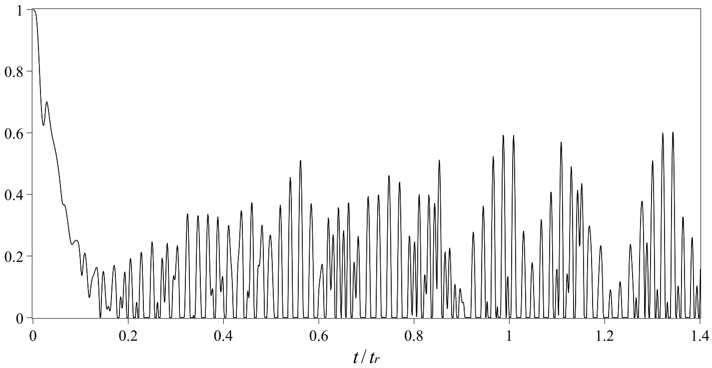

(a) $N = 20$

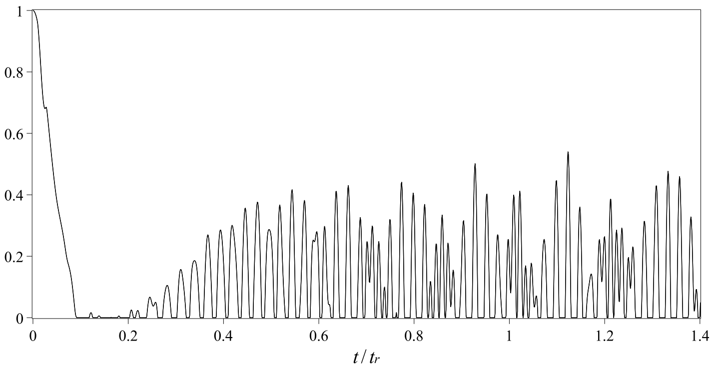

(b) $N = 30$

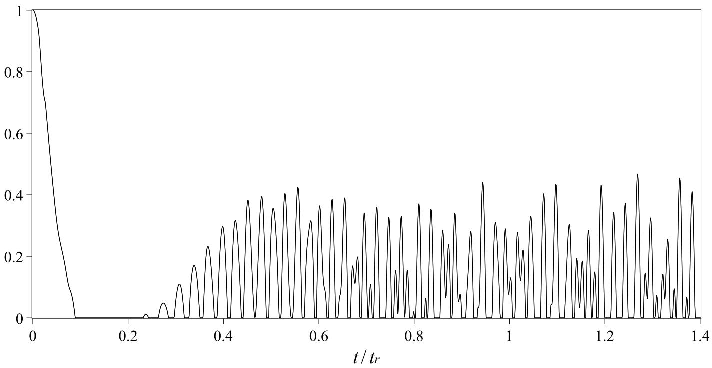

(c) $N = 40$

Figure 7.2.2: Plots comparing the concurrence $\varsigma(t)$ for two qubits-big spin models of initial qubit state $\frac{1}{\sqrt{2}}(|ee\rangle + |gg\rangle)$, $|\zeta|^2 = 9$ and the big spin's initial phase $\phi = 0$. Figure (a) shows the system with $N = 20$, (b) shows the system with $N = 30$ and (c) shows the system with $N = 40$.

fluctuations of the two qubits from the big spin qubits. These variations in the disentanglement between the two qubits and the big spin cause the fluctuations in the two-qubit entanglement with a small N value.

Not only it introduces fluctuations in the two-qubit entanglement, the two-qubit and big spin disentanglement variations also put a limit on the quantity. From Figure 7.2.2 we can note that at larger time, most of the peaks in the two-qubit entanglement fluctuations are higher with $N = 20$ as compared to the case of $N = 30$ and $N = 40$. There are linear entropy points that drop lower for the smallest N indicating disentanglement between the two qubits and the big spin, and it is become harder to achieve as N increases which then limit how big the two-qubit entanglement can get. This is the reason we see suppression in the concurrence fluctuations with bigger big spin's sizes.

7.2.2 Initial two-qubit state from outside the basin of attraction

We also plot Figure 7.2.3 and Figure 7.2.4 to show the time evolutions of the two-qubit big spin system with an initial two-qubit state that lies outside the basin of attraction. We plot the graphs for three different values of small N. The first figure shows the probability of the two-qubit state being in the excited state $P_{ee}(t)$, the probability of the two-qubit state being in an attractor state $P^{+}_{2,att}(t)$ and the linear entropy $S^{L}_{q}(t)$ of the two-qubit subsystem, while the latter shows the concurrence $\varsigma(t)$ that represents the entanglement of the two qubits.

From Figure 7.2.3, we can see that similar to the case of the system with an initial two-qubit state from inside the basin of attraction, the quantities change with the increment of N. Although seemingly noisy evolutions are shown, these start to resemble the system with a large value of N as plotted in Figure 4.3.5, as the number increases. With also $N = 30$, the visibility of significant events like the collapse and revival in the two-qubit probability $P_{ee}(t)$, the peak in the two-qubit attractor state probability $P^{+}_{2,att}(t)$ and the dip in the linear entropy $S^{L}_{q}(t)$ line start to become clearer at time $\frac{t_r}{4}$.

From Section 4.3.5 too, we know that at time $\frac{t_r}{4}$ the two-qubit state will not approach the two-qubit attractor state that is unentangled and pure. So, at this particular time the linear entropy remains high and the value of the two-qubit attractor state probability $P^{+}_{2,att}(t)$ will not approach close to unity. These properties are also visible in the system with small value of N as shown in Figure 7.2.3. However, even with $N = 40$, we still cannot see any interesting phenomenon in the system at later times. These quantities are noisy and no clear important events can be observed. No revival peaks at $\frac{t_r}{2}$ and t_r are developed in the two-qubit probability $P_{ee}(t)$, and no dips in the linear entropy $S_q^L(t)$ at $\frac{t_r}{2}$, $\frac{3t_r}{4}$ and t_r are visible, which are the cases for a system with a large value of N.

Figure 7.2.4 is plotted by using similar parameters as used in Figure 7.2.3. From Section 4.3.6, we know that the concurrence exhibits the 'sudden death and birth' property if the two qubits start with a state selected from outside the basin of attraction. In Figure 7.2.4 we can start to spot such an event at approximately time $\frac{t_r}{4}$ in a system with a big spin of size $N = 30$. We also know that this peak is the result of $\eta_0 \neq 0$ in Equation (4.3.82) and it becomes more apparent in a system with $N = 40$ where a revival peak appears and then disappears again with a finite gradient. Similar observation can be made at time $\frac{t_r}{2}$ where in a system with a large value of N, the entanglement between the two qubits will again reappear. However, with a small size big spin, the revival peak is very low and again, the appearance of 'sudden death and birth' becoming clearer with $N = 40$.

No further observations on the 'death and birth' of entanglement between the two qubits can be made on a system with small N at later times, as the dynamics appear to be very noisy. However, similar to the case of initial two-qubit state from inside the basin of attraction, the peaks in the concurrence fluctuations are higher at most of the points in a system with $N = 20$ as compared to $N = 30$ and $N = 40$. As discussed in the previous section, we know that this is due to the variations in the disentanglement between the two qubits and the big spin which also permits fluctuations in the two-qubit entanglement in a small N regime. The results can be seen especially at the beginning of Figure 7.2.3(a) where there are fluctuations in the concurrence line at which the quantity starts to collapse. However, these variations in the entanglement between the two qubits and the big spin are actually suppressed with the increment in N as can be seen in the linear entropy plots in Figure 7.2.4. This also means that the fluctuations in the two-qubit entanglement are also suppressed with bigger big spin's sizes.

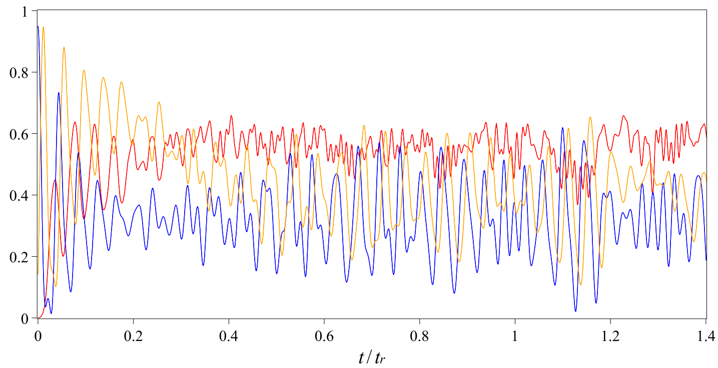

(a) $N = 20$

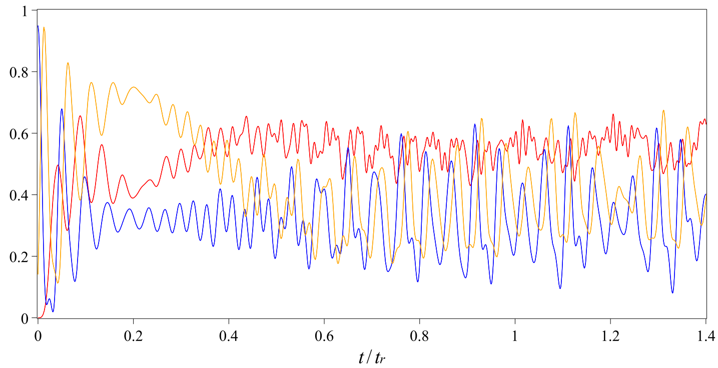

(b) $N = 30$

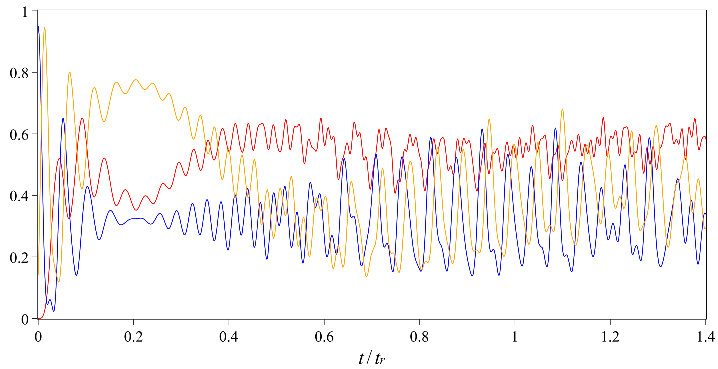

(c) $N = 40$

Figure 7.2.3: Plots comparing qubits linear entropies (red), probability of the two qubits state $|ee\rangle$ (blue) and the probability of being in the two-qubit attractor state $\left|\psi^{+}_{2,att}\right\rangle_N$ (orange) for two qubits-big spin models of initial qubit state $\frac{1}{\sqrt{20}}|ee\rangle + \frac{\sqrt{19}}{\sqrt{20}}|gg\rangle$, $|\zeta|^2 = 9$ and the big spin's initial phase $\phi = 0$. Figure (a) shows the system with $N = 20$, (b) shows the system with $N = 30$ and (c) shows the system with $N = 40$.

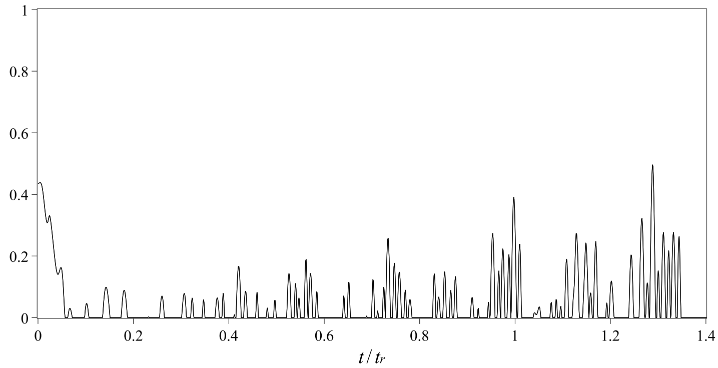

(a) $N = 20$

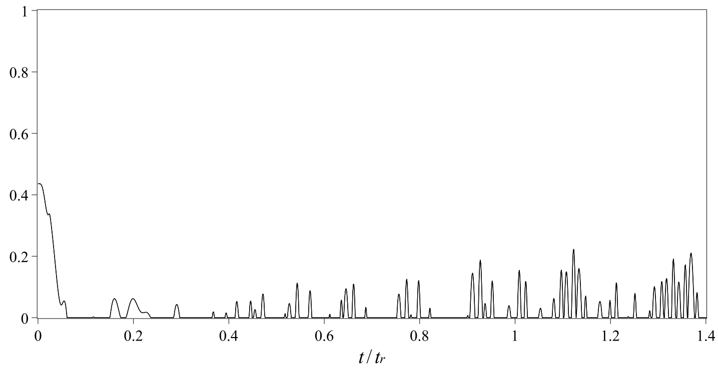

(b) $N = 30$

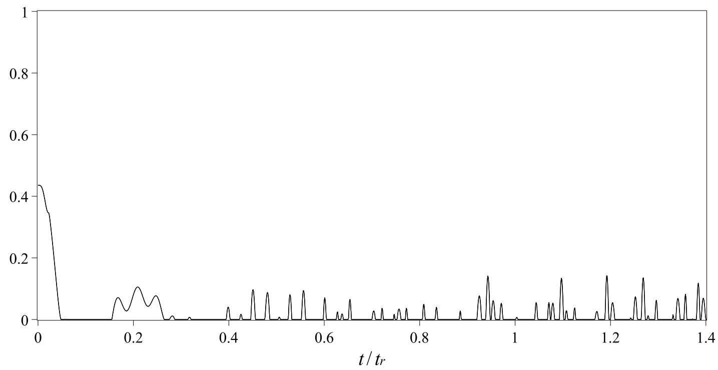

(c) $N = 40$

Figure 7.2.4: Plots comparing the concurrence $\varsigma(t)$ for two qubits-big spin models of initial qubit state $\frac{1}{\sqrt{20}}\left|ee\right\rangle + \frac{\sqrt{19}}{\sqrt{20}}\left|gg\right\rangle$, $|\zeta|^2 = 9$ and the big spin's initial phase $\phi = 0$. Figure (a) shows the system with $N = 20$, (b) shows the system with $N = 30$ and (c) shows the system with $N = 40$.

7.3 Collapse, Revival and Decoherence of Entanglement in Two-Qubit Jaynes-Cummings Model With Non-Zero Error in Frequency Detunings

In the previous section, we presented numerical results for a two-qubit big spin system with a small number of qubits N in the big spin. We also demonstrated that for a system with an initial two-qubit state from inside the basin of attraction, we start to observe the event of collapse and revival in the two-qubit entanglement with $N = 30$, and for the case of an initial two-qubit state from outside the basin of attraction, we start to clearly see the event of death / birth of two-qubit entanglement with $N = 40$. Therefore, in this and the following sections, we will respectively use these big spin sizes to consider an erroneous two-qubit big spin system for both initial two-qubit states.

To observe the effects of non-zero detunings in a two-qubit big spin system with small N, we apply similar analysis we applied to the system with a large number of N considered in Section 5.3.1. We again consider the case where the big spin‘s frequency ω_N is positioned in between the two qubits frequencies, Ω_1 and Ω_2 such that $\hbar\delta_1 = \hbar(\Omega_1 - \omega_N)$ and $\hbar\delta_2 = -\hbar(\Omega_2 - \omega_N)$ as shown in Figure 5.2.1. We use a similar error distribution modelled by Equation (5.2.21) and we average the density matrix of the system over this error distribution with a discrete approximation as given by Equation (5.2.22).

7.3.1 Initial two-qubit state from inside the basin of attraction

We reproduce the results in Section 5.3.1 by replacing the big spin's size with $N = 30$ and we plot Figure 7.3.1 and Figure7.3.2 to show the non-zero detuning effects on the two-qubit big spin system with small number of N. The first figure shows the dynamics in the linear entropy and the two-qubit probabilities, while the latter shows the collapse and revival of the two-qubit entanglement. We can compare the results of our analysis in this section with the results of a system with no detuning effects plotted in Figure 7.2.1(b) and Figure 7.2.2(b).

In Figure 7.3.1, at time $\frac{t_r}{4}$ we can see some reductions in the amplitudes of the two-qubit probabilities and the entropy as the error distribution width Δ increases. The dynamics in the oscillations of the two qubits being in excited state $P_{ee}(t)$, the probability of the two qubit being in an attractor state $P^{+}_{2,att}(t)$, as well as the entropy $S^{L}_{q}(t)$ of the two-qubit subsystem are getting weaker at this time with a higher value of error. However, there is neither increment nor decrement in the value of these quantities at this time as compared to the system with $N = 30$ and no detuning effects as shown in Figure 7.3.1(b). This indicates that there are no significant changes in the purity of the two-qubit subsystem and the amount of entanglement between the two qubits and the big spin at the attractor time. This also means that we may still observe the two-qubit attractor state as well as the spin cat state with such small N.

Further changes in the amplitudes of these quantities can also be seen at time $\frac{t_r}{2}$ and time t_r. Greater reductions are observed with respect to the increment of error distribution width, and with $\Delta = 2.0$, these quantities are almost flat lines at time t_r. In Section 4.3.4, we have shown that in a system with a large value of N, there are dips in the linear entropy at these times and in Figure 7.2.1(b) there are signs that this event occurs. However, from Figure 7.3.1, we see that these dips are being filled in as the decoherence is increased. This is not due to entanglement with the big spin (or less disentanglement), but rather due to increased mixture of the two-qubit system because of the decoherence.

From Figure 7.3.2, interesting observations can be made on the dynamics of the entanglement between the two qubits in a system with $N = 30$. The plotted black line in the figure suggests that at times $\frac{t_r}{2}$ and t_r, the concurrence $\varsigma(t)$ is also affected by the non-zero detunings in the system. At these times, the peaks in the quantity reduce with the increasing error distribution width as compared to the non-zero detuning case as depicted in Figure 7.2.2. This suggests that weaker entanglements between the two qubits are observed with larger decoherence. As discussed earlier, the decoherence has increased the mixture of the two-qubit subsystem as suggested by fewer and smaller dips at time $\frac{t_r}{2}$ and t_r in the entropy line in Figure 7.3.1. Not only it affects the purity of the two qubits subsystem, such increment also limits the maximum fluctuation heights of the entanglement between the two qubits. This is due to the relationship between the two-qubit linear entropy and the two-qubit entanglement [49], and can be seen by the black concurrence line in Figure 7.3.2 that gets lower with the increasing error distribution width. However, it is very surprising to learn that the robustness of the quantity in a system with a small N value against the error as high as $\Delta = 2.0$. A revival peak can still be seen at time $\frac{t_r}{2}$ although it disappears completely at time t_r and the event of collapse and revival of entanglement becomes more apparent.

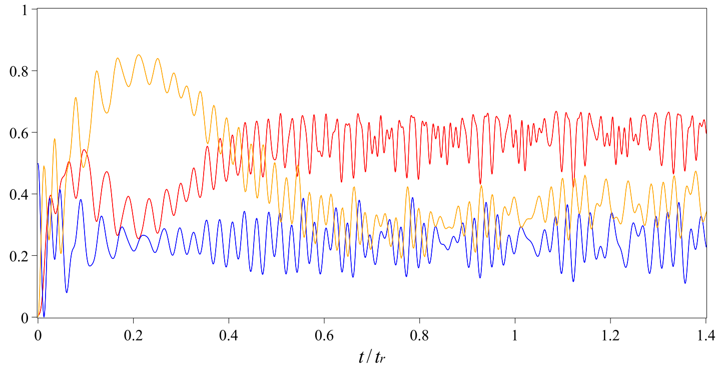

(a) $\Delta = 0.5$

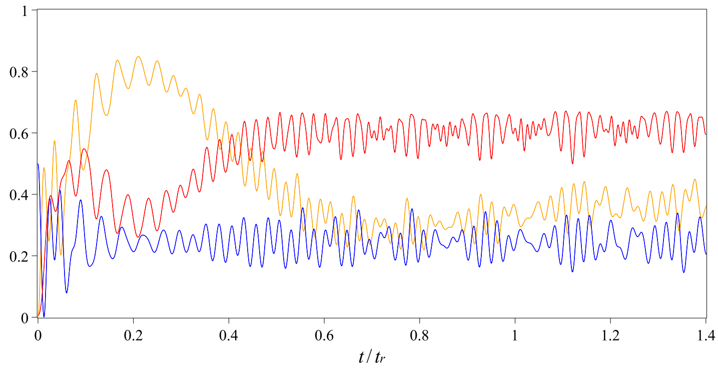

(b) $\Delta = 1.0$

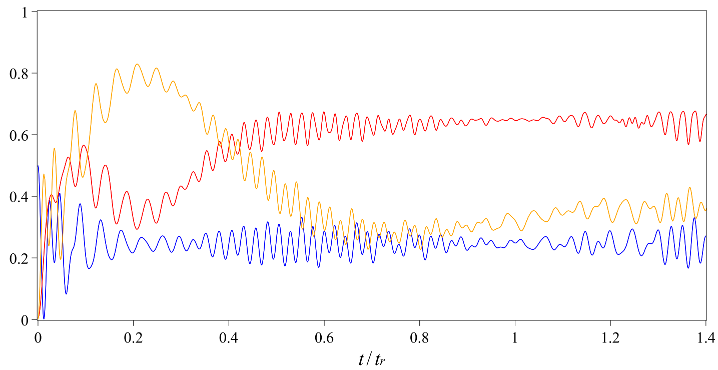

(c) $\Delta = 2.0$

Figure 7.3.1: Plots comparing qubits linear entropies (red), probability of the two qubits state $|ee\rangle$ (blue), probability of the two qubit being in an attractor state $\left|\psi^{+}_{2,att}\right\rangle_N$ (orange) for two qubits-big spin models of initial qubit state $\frac{1}{\sqrt{2}}(|ee\rangle + |gg\rangle)$, $|\zeta|^2 = 9$, $N = 30$ and the big spin's initial phase $\phi = 0$, with errors in detunings, Δ. Figure (a) shows the differences in the system with $\Delta = 0.5$, (b) shows the differences in the system with $\Delta = 1.0$ and (c) shows the differences in the system with $\Delta = 2.0$.

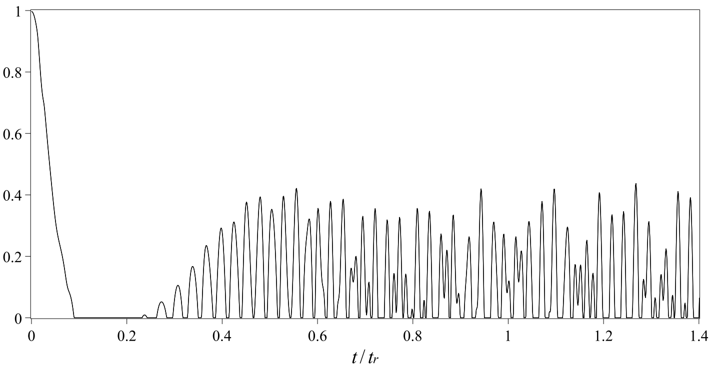

(a) $\Delta = 0.5$

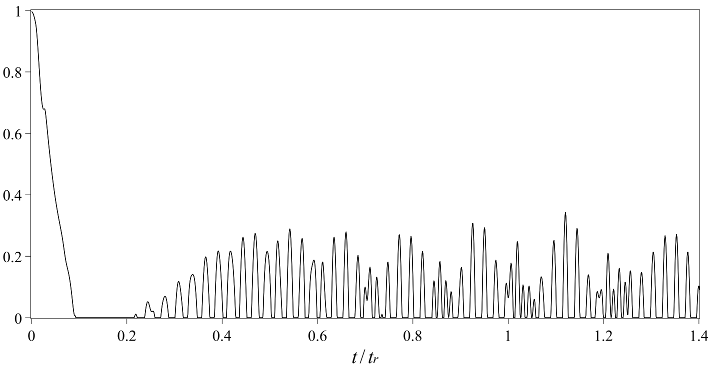

(b) $\Delta = 1.0$

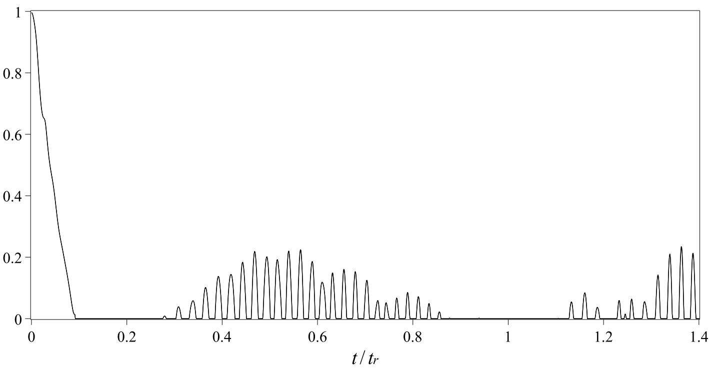

(c) $\Delta = 2.0$

Figure 7.3.2: Plots comparing the concurrence $\varsigma(t)$ for two qubits-big spin models of initial qubit state $\frac{1}{\sqrt{2}}(|ee\rangle + |gg\rangle)$, $|\zeta|^2 = 9$, $N = 30$ and the big spin's initial phase $\phi = 0$, with errors in detunings, Δ. Figure (a) shows the differences in the system with $\Delta = 0.5$, (b) shows the differences in the system with $\Delta = 1.0$ and (c) shows the differences in the system with $\Delta = 2.0$.

7.3.2 Initial two-qubit state from outside the basin of attraction

We also plot Figure 7.3.3 and Figure 7.3.4 to show the time evolutions of the two-qubit big spin system with an initial two-qubit state that lies outside the basin of attraction with non-zero detunings. We plot the graphs for three different values of error distribution widths Δ, where in the first figure we show the probability of the two-qubit state being in the excited state $P_{ee}(t)$, the probability of the two-qubit state being in an attractor state $P^{+}_{2,att}(t)$ and the linear entropy $S^{L}_{q}(t)$ of the two-qubit subsystem, and in the second graph we show the concurrence $\varsigma(t)$ that represent the entanglement of the two qubits.

With an initial two-qubit state from outside the basin of attraction, we compare the time evolutions of this non-zero detuning two-qubit big spin model plotted as Figure 7.3.3 with the resonant case two-qubit big spin system with $N = 40$ shown in 7.2.3(c). From our observations, we can see some changes in these quantities with respect to the increment in the error distribution width. Similar to the case of a system with an initial two-qubit state from inside the basin of attraction, there is some reduction in the amplitude of these quantities as a larger value of Δ is used.

We know that with an initial two-qubit state from outside the basin of attraction, the two-qubit states cannot be factorised out of the wavefunction at time $\frac{t_r}{4}$. Therefore at this time, the two-qubit is a mixed and entangled state. The linear entropy is high and the value two-qubit attractor state probability $P^{+}_{2,att}(t)$ does not approach close to unity as displayed in Figure 7.2.3(c). As comparisons, from Figure 7.3.3 we can see that similar to the case of initial two-qubit states from inside the basin of attraction, no significant changes can be observed on these quantities at this time. Even with an error distribution width as high as $\Delta = 2.0$, there is no change in the values of these quantities, indicating no significant decoherence effects in the two-qubit big spin system that starts with an initial two-qubit state from outside the basin of attraction, with $N = 40$ at time $\frac{t_r}{4}$. In addition to that, at later times, although there is no clear visibility of the significant events like the collapse and revival in the two-qubit probability $P_{ee}(t)$ and only small signs of dips in the linear entropy $S^{L}_{q}(t)$ at times $\frac{t_r}{2}$ and t_r, we can still see the suppression in the plots of these quantities. Furthermore, these small dips in entropy get filled in as the decoherence increases, and this puts some limits on the two-qubit occurrence of two-qubit entanglement.

In Figure 7.3.4 we plot the concurrence $\varsigma(t)$ of the system for three different values of error to exhibit the changes in the entanglement between the two qubits

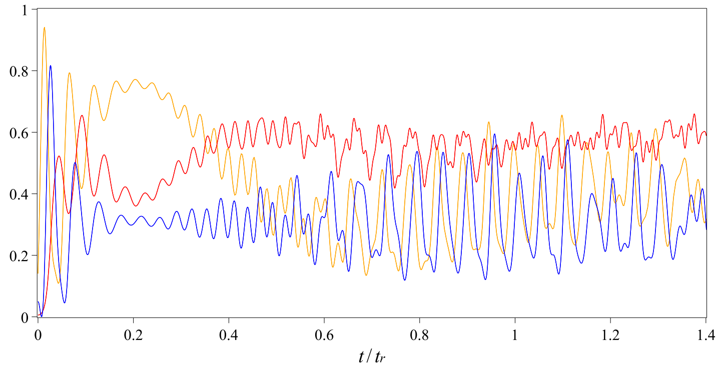

(a) $\Delta = 0.5$

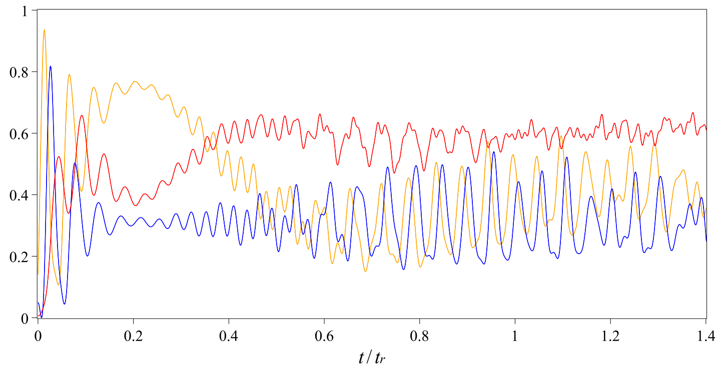

(b) $\Delta = 1.0$

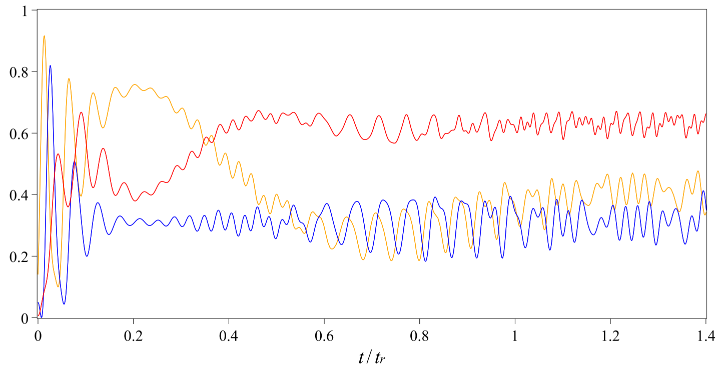

(c) $\Delta = 2.0$

Figure 7.3.3: Plots comparing qubits linear entropies (red), probability of the two qubits state $|ee\rangle$ (blue) and the probability of being in the two-qubit attractor state $\left|\psi^{+}_{2,att}\right\rangle_N$ (orange) for two qubits-big spin models of initial qubit state $\frac{1}{\sqrt{20}}|ee\rangle + \frac{\sqrt{19}}{\sqrt{20}}|gg\rangle$, $|\zeta|^2 = 9$, $N = 40$ and the big spin's initial phase $\phi = 0$ with errors in detunings, Δ. Figure (a) shows the system with $\Delta = 0.5$, (b) shows the system with $\Delta = 1.0$ and (c) shows the system with $\Delta = 2.0$.

with the increment in the decoherence. We compare the results with Figure 7.2.4(c) which shows the dynamics in the quantity for a system with no detunings and $N = 40$. In the figure there are revival peaks in the quantity approximately at times $\frac{t_r}{4}$ and $\frac{t_r}{2}$ and they exhibit the event of 'sudden death and birth' of entanglement. By comparing both figures, we can see that there is no significant change in the quantity at time $\frac{t_r}{4}$. There is still revival and the peak of the concurrence remains even with $\Delta = 2.0$. However, at time at time larger than $\frac{t_r}{2}$, the dynamics of the concurrence show fluctuations for $\Delta = 0.5$, but then these are suppressed to almost a completely flat line when we increase the error distribution width to $\Delta = 1.0$, and with $\Delta = 2.0$ the fluctuations have completely vanished.

7.4 Collapse, Revival and Decoherence of Entanglement with Non-Zero Error in Dipole Interaction Strength

Earlier in this chapter, we have studied a two-qubit big spin system with small values of N and then we extended our research to observe the effects of errors in the frequency detunings on the time evolutions. These analyses are actually replications of Chapter 4 and Chapter 5, but with $N = 30$ or $N = 40$ instead of $N = 150$, depending on whether the initial two-qubit state is respectively coming from the inside or outside the basin of attraction. We have also seen in Chapter 6 that not only can we study the effects of errors in the frequency detunings, we can also apply the similar analysis on the non-zero mismatch in the interaction strength between each qubit and the big spin. Therefore, in this section we will reproduce our analysis in Chapter 6 but with small values of N to see the changes in the time evolutions of the system as an effect of errors in the dipole interaction strength λ.

7.4.1 Initial two-qubit state from inside the basin of attraction

We plot Figure 7.4.1 and Figure 7.4.2 to show the effects of non-zero mismatch in the dipole interaction strength on the two-qubit big spin system with $N = 30$. The first figure shows the dynamics in the linear entropy $S_q^L(t)$, the probability of the two qubits being in an excited state $P_{ee}(t)$ and two-qubit attractor state probability $P_{2,att}^{+}(t)$. In the second graph, we plot the concurrence $\varsigma(t)$ to show the events of collapse and revival of the two-qubit entanglement. We can then

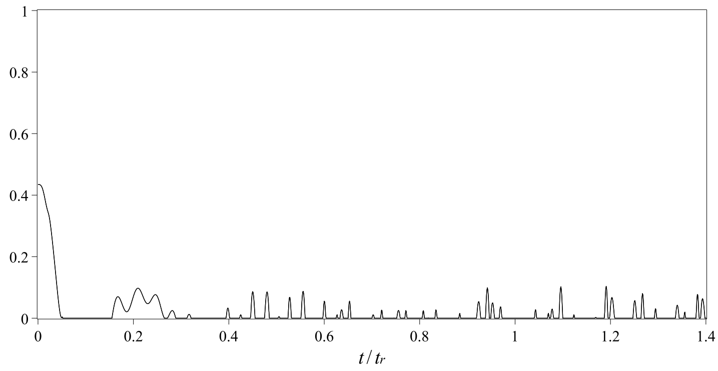

(a) $\Delta = 0.5$

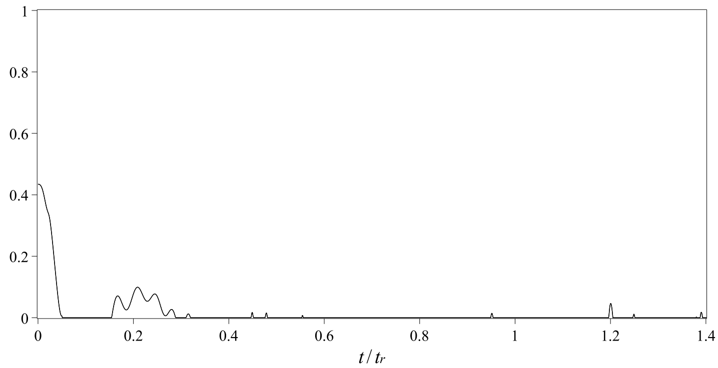

(b) $\Delta = 1.0$

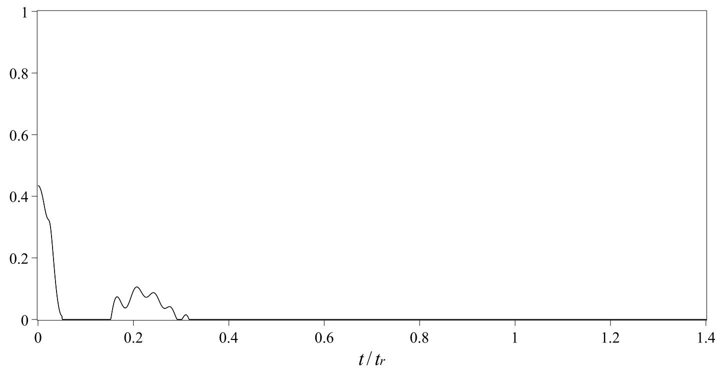

(c) $\Delta = 2.0$

Figure 7.3.4: Plots comparing the concurrence $\varsigma(t)$ for two qubits-big spin models of initial qubit state $\frac{1}{\sqrt{20}}\left|ee\right\rangle + \frac{\sqrt{19}}{\sqrt{20}}\left|gg\right\rangle$, $|\zeta|^2 = 9$, $N = 40$ and the big spin's initial phase $\phi = 0$ with errors in detunings, Δ. Figure (a) shows the system with $\Delta = 0.5$, (b) shows the system with $\Delta = 1.0$ and (c) shows the system with $\Delta = 2.0$.

compare the plots with the results of an ideal system depicted as Figure 7.2.1(b) and Figure 7.2.2(b).

Based on the comparisons between the plots in Figure 7.4.1 and Figure 7.2.1(b), at time $\frac{t_r}{4}$ we can see increment in value of the linear entropy $S_q^L(t)$ and decrement in the value of the two-qubit attractor state probability $P_{2,att}^{+}(t)$. These quantities deviate further from the attractor state properties as the error distribution width Δ increases. This indicates that there is an addition in the two-qubit mixture due to errors in the dipole interaction strength. We can also note that there is suppression in the amplitude of the variations in linear entropy, as well as the two-qubit probabilities especially at time $\frac{t_r}{2}$ and at the one-qubit revival time t_r. The revivals in these quantities are weaker with the increment in the error distribution width and almost flat with $\Delta = 0.5$. These changes in the system are similar to the case of a two-qubit big spin system with $N = 150$ under the same error parameters that we considered in Section 6.3.1.

It is also very interesting to note that as compared to the system with no error in the dipole interaction strength shown in Figure 7.2.1(c) the visibility of some important dynamics in the quantities are clearer with the decoherence effects. The events such as collapse in the $P_{ee}(t)$ curve and its revival at times $\frac{t_r}{2}$ and t_r can be seen although there are very small dips in the linear entropy line after time $\frac{t_r}{4}$ as they are being filled in with increasing decoherence.

Besides the above quantities, the effects of decoherence in the system can also be seen on the entanglement between the two qubits. The first obvious effect on this quantity against the error distribution width Δ is the collapse on the concurrence curve at the beginning of the interactions. The time for the quantity to drop until it reaches near zero is shorter with larger error values. This effect is similar to the case of $N = 150$ we considered in Section 6.3.1, but different to the case of errors in the detuning that we considered in the last section, where no changes in this quantity can be observed regardless of the increasing decoherence. We can also note that the fluctuations in the collapsing line these arise in the small N dynamics are suppressed with increasing error distribution width Δ. This is due the suppression of the variations in the linear entropy with increasing decoherence.

In a perfect system with a very large N, the concurrence is expected to recover its initial value at the two-qubit revival time, so that $\varsigma(0) = \varsigma(\frac{t_r}{2})$. This is however not happening in a system with $N = 30$ and errors in the dipole interaction strength as shown in Figure 7.4.2. With such small size of the big spin and

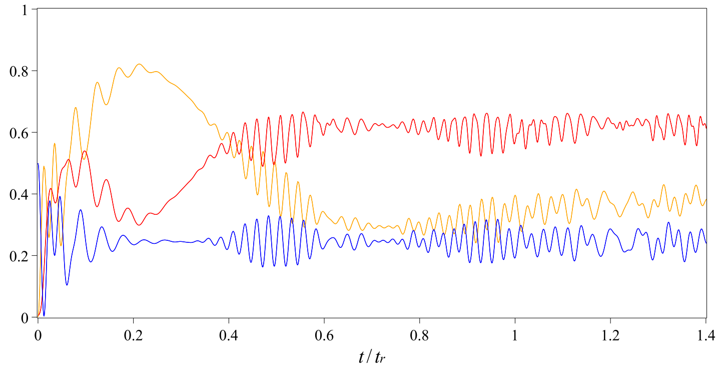

(a) $\Delta = 0.1$

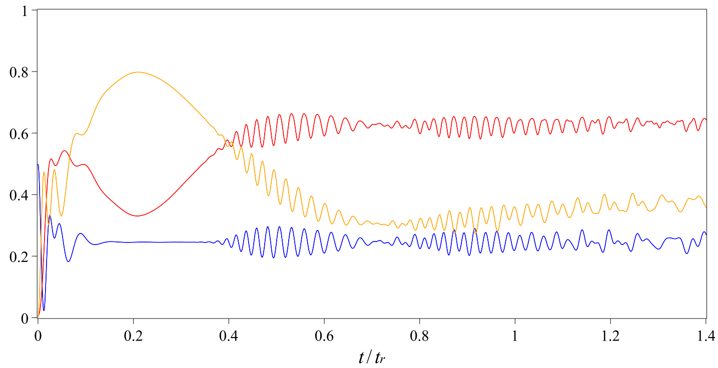

(b) $\Delta = 0.3$

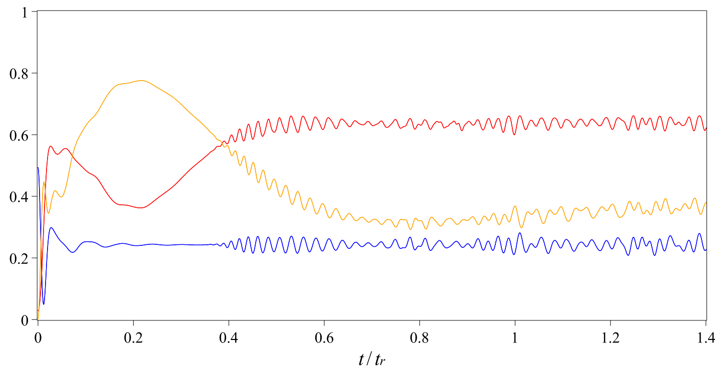

(c) $\Delta = 0.5$

Figure 7.4.1: Plots comparing qubits linear entropies (red), probability of the two qubits state $|ee\rangle$ (blue), probability of the two qubit being in an attractor state $\left|\psi^{+}_{2,att}\right\rangle_N$ (orange) for two qubits-big spin models of initial qubit state $\frac{1}{\sqrt{2}}(|ee\rangle + |gg\rangle)$, $|\zeta|^2 = 9$, $N = 30$ and the big spin's initial phase $\phi = 0$, with errors in dipole interaction strength, Δ. Figure (a) shows the differences in the system with $\Delta = 0.1$, (b) shows the differences in the system with $\Delta = 0.3$ and (c) shows the differences in the system with $\Delta = 0.5$.

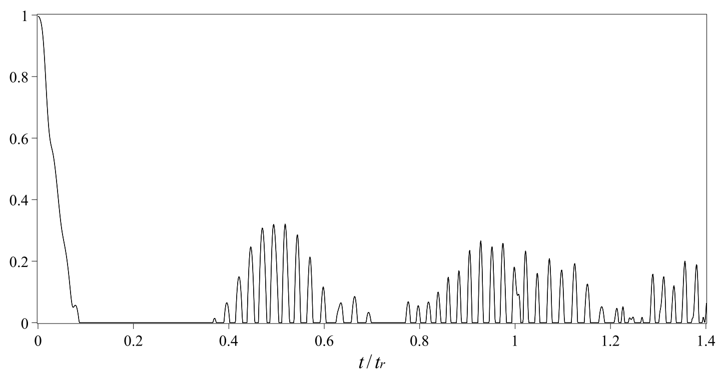

(a) $\Delta = 0.1$

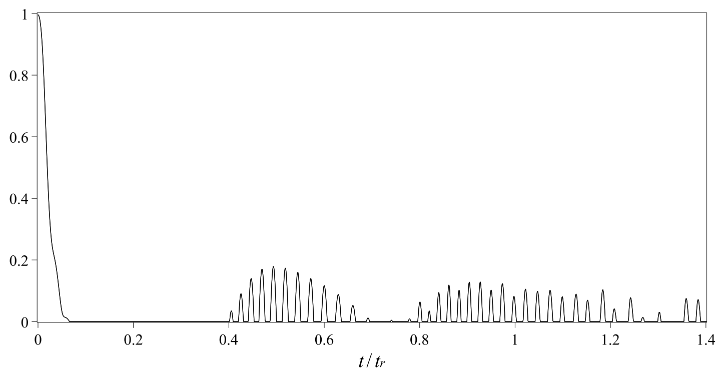

(b) $\Delta = 0.3$

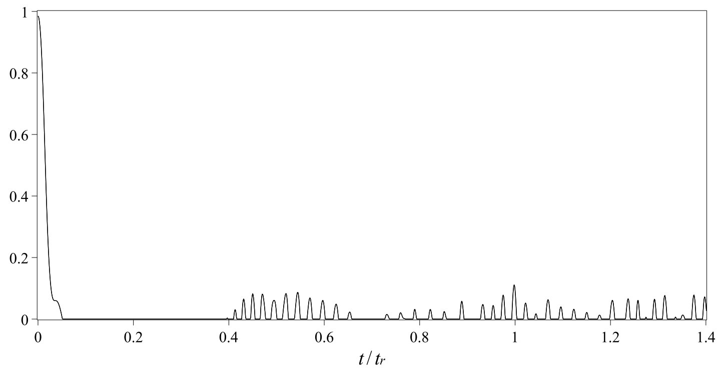

(c) $\Delta = 0.5$

Figure 7.4.2: Plots comparing the concurrence $\varsigma(t)$ for two qubits-big spin models of initial qubit state $\frac{1}{\sqrt{2}}(|ee\rangle + |gg\rangle)$, $|\zeta|^2 = 9$, $N = 30$ and the big spin's initial phase $\phi = 0$, with errors in dipole interaction strength, Δ. Figure (a) shows the differences in the system with $\Delta = 0.1$, (b) shows the differences in the system with $\Delta = 0.3$ and (c) shows the differences in the system with $\Delta = 0.5$.

decoherence, there cannot be a complete revival in the concurrence. It can be seen that the revival peaks at time $\frac{t_r}{2}$ decrease significantly with the increment of error distribution widths and this can be explained by the linear entropy curve in Figure 7.4.1 that have the dips filled in at this time. There is increment in the value of the linear entropy of the two-qubit subsystem at this time due to the decoherence, and this puts more limit on the entanglement between the two qubits which results in the suppression of the concurrence curve. Similar observations on the connection between the linear entropy and the concurrence can be made at time t_r. However, it is very interesting to note that the event of collapse and revival of entanglement is more apparent with the decoherence effects, and in additional to that, there is still some entanglement revival showing in the two-qubit system even with $\Delta = 0.5$, indicating a good robustness of the system against the decoherence in the dipole interaction strength, even with a small value on N.

7.4.2 Initial two-qubit state from outside the basin of attraction

Figure 7.4.3 shows the effects of decoherence on the linear entropy $S_q^L(t)$, the probability of the two qubits being in an excited state $P_{ee}(t)$ and the probability of two-qubit attractor state $P_{2,att}^{+}(t)$ in two-qubit big spin system with an initial two-qubit state from outside the basin of attraction and $N = 40$. Some obvious changes in the dynamics of these quantities especially on their revival amplitudes at times $\frac{t_r}{2}$ and t_r can be observed. There are reductions in the peaks of these quantities as an effect of errors in the dipole interaction strength. With the increment in the error distribution width Δ, the peaks become lower and the curves are almost flat with $\Delta = 0.5$. However, it is very interesting to note that as compared to the system with no error in the dipole interaction strength shown in Figure 7.2.3(c) the visibility of the events of collapse and revival in the $P_{ee}(t)$ curve has become clearer. The dips in the linear entropy line are also become apparent and the decoherence effects can be observed at times $\frac{t_r}{2}$ and t_r where these dips are filled in and with $\Delta = 0.5$, the variations in the red curve are significantly reduced.

Another interesting observation can be made at the two-qubit attractor time $\frac{t_r}{4}$. This is where we can see the dip in the red line becomes shallower as the error increases, and at the same time the peak of the two-qubit attractor state probability $P_{2,att}^{+}(t)$ shows a weaker approach to unity. These indicate that the two-qubit subsystem has become more mixed with the increment of decoherence in the system as the result of non-zero mismatch in the qubits-big spin dipole interaction strength.

Significant changes can also be observed in the dynamics of the entanglement between the two qubits with respect to the non-zero mismatch in the dipole interaction strength. Similar to the case of initial state from inside the basin of attraction, the collapse time of the concurrence curve at the beginning of the interactions is shorter with increasing Δ as shown in Figure 7.4.4. Reductions in the amplitudes of the peaks in the concurrence curves are also observed with the increment of error distribution width especially at time $\frac{t_r}{4}$, where with $\Delta = 0.5$, only a small peak is visible. This indicates that the sensitivity of the entanglement between the two qubits is high towards the decoherence. As compared to Figure 7.2.4(c), the peak at time $\frac{t_r}{2}$ as well as the signature of entanglement between the two qubits at later times vanishes completely. This is due to the changes in the purity of the whole system as a result of decoherence, which can be explained by the increment in the linear entropy curve in Figure 7.4.3. As the decoherenc increases, the mixture of the two-qubit state also increases, and this suppresses the maximum possible entanglement of the two qubits, which results in the lower peaks of the concurrence.

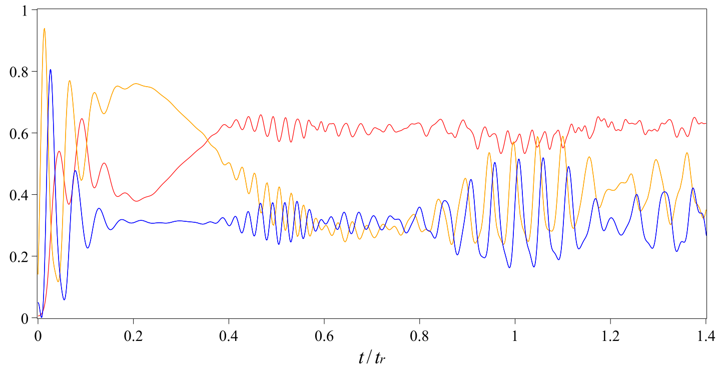

(a) $\Delta = 0.1$

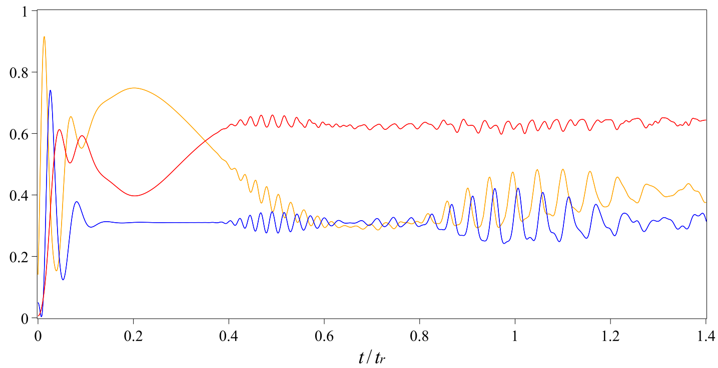

(b) $\Delta = 0.3$

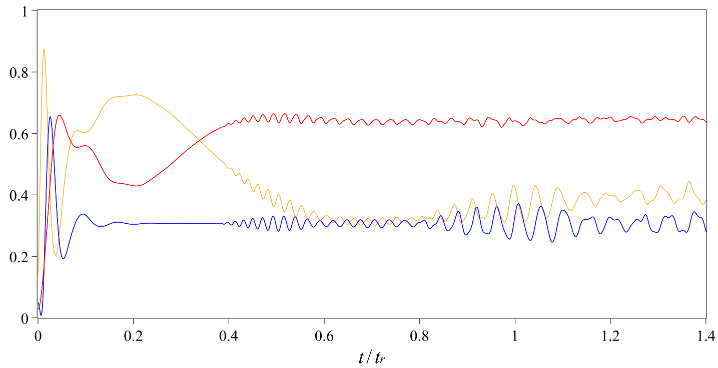

(c) $\Delta = 0.5$

Figure 7.4.3: Plots comparing qubits linear entropies (red), probability of the two qubits state $|ee\rangle$ (blue), probability of the two qubit being in an attractor state $\left|\psi^{+}_{2,att}\right\rangle_N$ (orange) for two qubits-big spin models of initial qubit state $\frac{1}{\sqrt{20}}|ee\rangle + \frac{\sqrt{19}}{\sqrt{20}}|gg\rangle$, $|\zeta|^2 = 9$, $N = 40$ and the big spin's initial phase $\phi = 0$, with errors in dipole interaction strength, Δ. Figure (a) shows the differences in the system with $\Delta = 0.1$, (b) shows the differences in the system with $\Delta = 0.3$ and (c) shows the differences in the system with $\Delta = 0.5$.

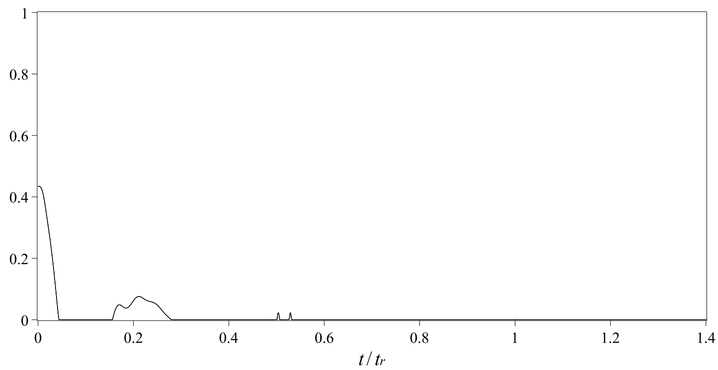

(a) $\Delta = 0.1$

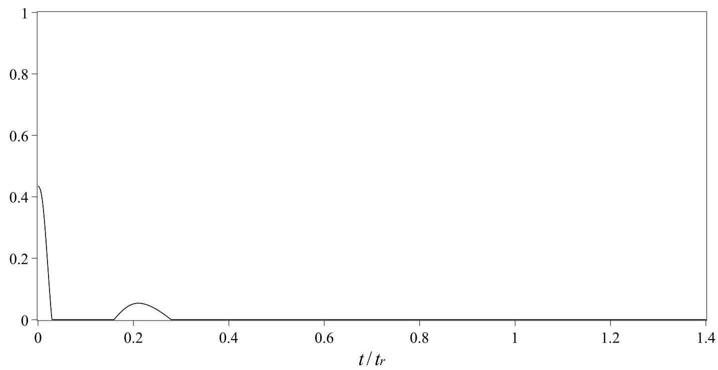

(b) $\Delta = 0.3$

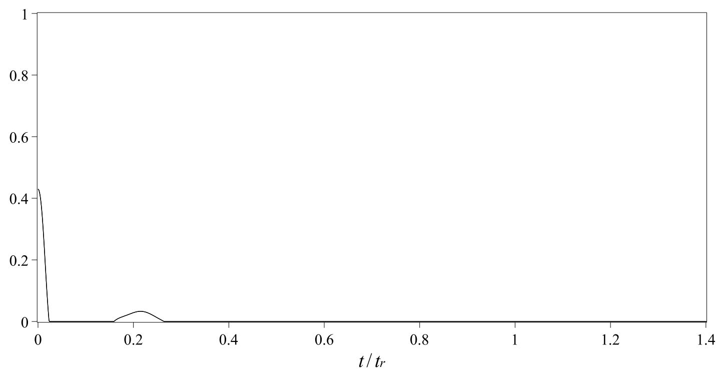

(c) $\Delta = 0.5$

Figure 7.4.4: Plots comparing the concurrence $\varsigma(t)$ for two qubits-big spin models of initial qubit state $\frac{1}{\sqrt{20}}\left|ee\right\rangle + \frac{\sqrt{19}}{\sqrt{20}}\left|gg\right\rangle$, $|\zeta|^2 = 9$, $N = 40$ and the big spin's initial phase $\phi = 0$, with errors in dipole interaction strength, Δ. Figure (a) shows the differences in the system with $\Delta = 0.1$, (b) shows the differences in the system with $\Delta = 0.3$ and (c) shows the differences in the system with $\Delta = 0.5$.

7.5 Summary

In this chapter, we have considered a two-qubit big spin model with small values of N. We have then further analysed the system with decoherence effects we have taken into account errors in the system as the results of non-zero detunings, as well as non-zero mismatch in the dipole interaction strength. These are analogous calculations to those of the second parts of Chapter 4, 5 and 6, but with small values of N.

The studies suggest that, if the system starts with a two-qubit state from inside the basin of attraction, with $N = 30$ we can start to observe the important events of the relevant time evolutions. On the other hand, with an initial two-qubit state from outside the basin of attraction, these properties are visible with $N = 40$.

Analogous to the case of a two-qubit big spin system with $N = 150$, the effects of decoherence on the system are clearly apparent. Both errors in the detunings as well as the dipole interaction strength will change the dynamics of the time evolutions. It is very interesting to note the results of our analysis show that the effects of the latter are larger than the former. This means errors in the dipole interaction strength have more impact on the linear entropy, two-qubit probabilities and the concurrence, as compared to the errors in detunings. However, it is also very interesting to see that the entanglement between the two qubits has a very good robustness against these errors, which provide some positive promise for experimental investigations with realistic values of N.

Chapter 8

Conclusion

In this thesis, we have anaylsed, discovered and discussed many interesting phenomena resulting from the interactions of a qubit subsystem with another non-classical subsystem of either a coherent state of a field or a spin coherent state (called the big spin). We started by reproducing the calculations involved in solving a one-qubit Jaynes-Cummings model in order to understand the mathematical process used in a system of which a single qubit interacting with a coherent field. We reproduced the works by C. Jarvis by following a similar method used in her works [27, 64], where we first formulated the Hamiltonian of the system, found the eigenvalues and the eigenvectors of such Hamiltonian and then, by solving the time-dependent Schrödinger equation, we found the exact solutions for the model. This process was very helpful in the subsequent studies especially when we applied a similar calculation method to investigate the dynamics and time evolutions of a single qubit interacting with the big spin. Although this work was originally introduced by S. Dooley [29, 63], he used a different mathematical method to solve the one-qubit big spin system.

By identifying the correspondence between the parameters of both systems, we have shown the similarities in the attributes of the one-qubit big spin model with the one-qubit Jaynes-Cummings model. Both models exhibit the collapse and revival of qubit probability where at the beginning of the interaction, there is a decay or collapse in the value of the quantity. This is then followed by a period of time in which the oscillations (or variations) in the dynamics totally disappear before these reappear and peak at the revival time t_r. As explained in Chapter 2, these are the results of the destructive and constructive interference between different frequency amplitudes of each subsystem. We also have shown that within a similar parameter regime, we can generate a quantum state known as the Schrödinger cat state of the big spin. It is a state where the big spin is in a superposition of two coherent states with opposite phase and contains all the information about the initial state of the single qubit that interacted with the big spin. These make the spin Schrödinger cat state a very useful state and has found its applications in quantum metrology [79, 80]. Among the advantages of this particular state over other forms of entangled states usually used to achieve high precision beyond the Standard Quantum Limit in quantum metrology are its robustness against particle losses, and the ease of experimental preparation [80].

We then continued our research by considering the case of non-resonant frequencies in both single qubit interacting models, where we divided this particular study into two parts. Firstly, we let the systems evolve with a fixed value of non-zero detuning. Again, for the case of one-qubit Jaynes-Cummings model, this work was already done by C. Jarvis [27, 64]. We however, reproduced her results as comparisons to our one-qubit big spin case. From the study, we found that with a finite non-zero detuning there are changes in the qubit state probability, the revival time, the purity of the qubit subsystem, as well as in the probability of the qubit being in attractor state. There are shifts in the dynamics of these quantities, where these move in the same magnitude of the changes in the non-zero detuning value, and these happen to both one-qubit Jaynes-Cummings, as well as one-qubit big spin models.

In the second part of the study on one-qubit models with non-zero detuning, we considered the case for which we expected the interacting systems to evolve with the behaviours seen in a practical system with resonance frequencies. Therefore, we developed a model for the case of a desired system with zero detuning, but with potential errors subject to a probabilistic distribution, leading to additional mixture in the qubit's reduced density matrix. In this thesis, we used a Gaussian distribution (of variable width Δ) as an example to represent the errors in an actual system, which is very useful for experimental works. However, the error model is not limited to only this specific example, but can be applied with any other form of probabilistic distributions, depending on the systems being observed. Due to calculation complexity, we have also proposed a discrete approximation to evaluate the density matrix of the qubit by averaging it over the errors as given by Equation (3.2.7). The study suggests that unlike for the case of a fixed non-zero detuning value that shifts the revival of qubit probabilities, by considering errors as a distribution of detunings, the revivals in such quantities are suppressed at a particular revival time t_r. This is because of the revivals that occur at different time as a result of different detunings in the ensemble distribution have been averaged. More significant suppression effects are observed with a larger value of error Δ, which also affected the purity of the qubit subsystem at the revival time t_r. It is also very interesting to note that, from our numerical analysis, we found that the one-qubit big spin model has a better robustness against errors as compared to the one-qubit Jaynes-Cummings model.

In Chapter 4 of this thesis, we expanded the dimension of our study on the interacting models by introducing an additional qubit into the systems with the assumptions that $\lambda_1 = \lambda_2$ and $\omega = \Omega_1 = \Omega_2$. This means that we considered the case for which there is no error or mismatch in the dipole interaction strengths of the two qubits, and their frequencies are at resonance with the applied field. Similar to the single qubit cases, we reproduced the works by C. Jarvis [27, 64] on the two-qubit Jaynes-Cummings model. Under the same assumptions on the dipole strengths and frequencies, we then applied similar extension, analysis and calculation methods to find the exact and approximate solutions, and therefore observed the dynamics of the two-qubit big spin model. We showed that the phenomena of 'attractor states' can also be found in a two-qubit model, and it is simply a direct product of two one-qubit attractor states. We also demonstrated that the occurrence of such states depend on the initial conditions of the two qubits, which enabled us to quantify a set of initial conditions that leads to a phenomenon called the 'basin of attraction'.

Different to the single qubit case, in a two-qubit interacting model, we managed to study the entanglement properties between the two qubits. The two-qubit subsystem exhibits interesting entanglement properties, where the dynamics are also influenced by the initial conditions. For a system that starts with a state from inside the 'basin of attraction', we observed phenomena called the 'collapse and revival of entanglement'. This is the event in which the entanglement disappears with a Gaussian envelope, smoothly approaches zero, and then returns to its initial value at a later time. A different entanglement dynamics were observed for a system with an initial two-qubit state from outside the 'basin of attraction'. In this regime of initial conditions, the systems exhibit the event of 'sudden death and birth of entanglement' where the entanglement vanishes with a finite gradient.

Not only do they influence the occurrence of a two-qubit attractor state and the dynamics of the entanglement between the two qubits, the initial conditions also shows significant effects on the occurrence of the spin Schrödinger cat states. In the large number of spins N approximations, we have shown that if the system starts with a two-qubit initial state from inside the basin of attraction, at times $\frac{t_r}{4}$ and t_r the wavefunction can be factorised into the two-qubit and big spin subsystems, and therefore, there is no entanglement present between the two parts. At these times too, the big spin is in a superposition of two essentially orthogonal coherent states, called the 'spin cat state' that contains the information about the initial state of the two qubits. However, this is not the case if the two-qubit initial state is from outside the basin of attraction. The disentanglement between the two-qubit and the big spin subsystems is not complete, and therefore prohibits the occurrence of the spin Schrödinger cat states.

As mentioned earlier, the interacting models with an additional qubit that we considered in Chapter 4 were analysed with assumptions that the dipole interaction strengths of each qubit are uniform, and the qubits are interacting with the coherent fields or the big spin at approximately the same frequencies. With two qubits in the systems, we had the opportunity to extend the scope of our study by considering the case where these assumptions are eliminated. In any physical realisation of interaction between two qubits and a field mode (or a big spin), there will always be the potential for errors and thus decoherence. Therefore, in Chapter 5, we considered the case of frequency mismatch in our interacting systems. We explored the effects of detunings on these two-qubit models where we let the field mode's frequency ω positioned in between the two qubits frequencies Ω_1 and Ω_2. This means that there are mismatches in the frequencies of each component for both the two-qubit Jaynes-Cummings model, as well as the two-qubit big spin model.

This was followed by Chapter 6 that studied the effects of having non-uniform dipole interaction strengths of the two qubits for both models. Such mismatch in the couplings of the two qubits might arise due to spatial positioning errors for physically identical fundamental qubits, or be caused by fabrication and positioning errors in the case of manufactured qubits. We let the difference in the parameter take the form of $\lambda_1 = \lambda_2 + \delta$. We then analysed the system with respect to the mismatches (or errors) in the detunings as well as the couplings, as modelled for the single qubit case in Chapter 3. Again, similar to the case of two-qubit models with resonant frequencies, we observed the time evolutions of the systems with initial qubit states from inside and outside the basin of attraction.

Studies on both forms of error have revealed many interesting new findings. Observations on the main features of the two-qubit Jaynes-Cummings model and two-qubit big spin model showed that both systems responded in a similar way towards the errors introduced. Changes in the two-qubit state probability, the occurrence of a two-qubit attractor state, the linear entropy of the two-qubit subsystem and the entanglement between the two qubits are seen in most of these erroneous systems especially at the two-qubit revival time $\frac{t_r}{2}$ and one-qubit revival time t_r. At these times, be it a two-qubit Jaynes-Cummings or two-qubit big spin model, either with error in the detuning or with error in the dipole interaction strengths, all of the stated features show some significant changes in their time evolutions. With the increasing (dimensionless) error distribution width Δ, the two-qubit state probabilities show reductions in the amplitude of their revival, the linear entropy increases, and the concurrence revives with lower amplitudes. These changes are due to the disturbance in the purity of the qubit system as a result of decoherence, which can be explained by the increment in the linear entropy. As the decoherence increases, the mixture of the two-qubit state also increases, and this suppresses the maximum possible entanglement of the two qubits, which results in the lower peaks of the concurrence. It is also very interesting to note that the visibility of these effects are more apparent in the two-qubit interacting systems with errors in the dipole interaction strength as compared to the systems with detuning errors. For example, in a two-qubit big spin model that starts with an initial two-qubit state from inside the basin of attraction, it takes only $\Delta = 0.3$ for a system with error in the dipole interaction strength to reduce the concurrence value to $\varsigma(t_r) \approx 0.2$, in contrast to $\Delta = 2.0$ for a system with error in the detuning.

Similar effects on those quantities were also observed at times $\frac{t_r}{4}$ and $\frac{3t_r}{4}$ in both two-qubit models with error in the dipole interaction strength. Given that either the initial two-qubit states are from inside or outside the basin of attraction, the two-qubit state probabilities, the linear entropy and the concurrence change in a similar behaviour as they were observed at times $\frac{t_r}{2}$ and t_r with respect to the increment of error. However, a unique observation was noticed on both two-qubit systems with errors in the detunings at times $\frac{t_r}{4}$ and $\frac{3t_r}{4}$. There are no significant changes in any of the quantities at these times regardless of the initial state of the two qubits. In another words, at these times there are no decoherence effects on the purity of the two-qubit subsystem, the level of entanglement between the two qubits, the occurrence of the two-qubit attractor state and therefore the generation of Schrödinger cat state of the field and the big spin, even with error distribution width as high as $\Delta = 2.0$. This indicates a very good robustness of these interacting systems against errors in the frequencies at these particular times.

We ended our research with Chapter 7 that discusses the robustness of the two-qubit big spin models against errors as described in Chapter 5 and 6, with a small number N of spins in the big spin. We first investigated and ascertained the smallest N that maintains the relevant time evolutions of this system. We started to observe the signature of important events of the relevant time evolutions with $N = 30$ if the system starts with a two-qubit state from inside, and with $N = 40$ if the system starts with a two-qubit state from outside the basin of attraction. Similar considerations were also made as in the previous two chapters, where we considered a two-qubit big spin interacting system with errors as modelled in Section 3.2.2 for both cases of non-zero errors in detuning as well as non-zero errors in dipole interaction strength, and subject to the basin of attraction. Analogous to the system with $N = 150$, we also found that the errors in the dipole interaction strength have more impact on the linear entropy, two-qubit state probabilities and the two-qubit entanglement, as compared to the errors in detunings. We also noted a very good robustness in some of these quantities against these errors, which provide some positive promise for experimental investigations with realistic values of N.

In the future, an immediate extension to this work would be to consider a larger number of qubits N_q to interact with the big spin of size N. It would be very interesting to investigate the dynamics of the interacting systems with large number of qubits especially when we have the two components with an equal size, such that the system evolves with Hamiltonian

$$\hat{H}_{N,N} = \hbar\omega_N \left(\hat{J}^z + \frac{N}{2}\right) + \frac{\hbar}{2}\sum_{i=1}^{N_q}\Omega_i\hat{\sigma}_i^z + \frac{\hbar}{\sqrt{N}}\sum_{i=1}^{N_q}\lambda_i(\hat{J}^+\hat{\sigma}_i^- + \hat{J}^-\hat{\sigma}_i^+). \tag{8.0.1}$$

In this thesis, we have considered the parameters in the regime of $\frac{1}{\sqrt{N}} < \zeta < \sqrt{N}$, where $1 \ll N$. Therefore, it would be very interesting to explore the possibilities to study the qubit-big spin system with different parameters from outside of this regime. For example, S. Dooley and T.P. Spiller have made an analysis on the evolution of single qubit interacting with an initial spin coherent state that has $\theta = \frac{\pi}{2}$ in Equation (1.2.28), or equivalently the value of Equation (1.2.29) becomes $\zeta = 1$ [62]. By doing this, they found a way of generating a 'multiple-Schrödinger' cat state which is a superposition of many spin-coherent states. We may then extend our two-qubit big spin model into these similar parameters and observe the interesting features resulting from such system.

There are many possible experimental set ups that can be implemented and taking into account the decoherence effects we discussed in Chapter 3, 5, 6 and 7. One of such systems is superconducting qubit like a two-qubit gate operations of superconducting circuits, in which two qubits are interacting with a fundamental superconducting oscillator mode with a detuning factor in the frequencies [81, 82, 83]. For an example, we consider a similar set up of superconducting qubits as considered in [84]. With a characteristic energy of 1 GHZ and the dipole-interaction strength as given by Equation (8) in the paper, we can calculate the dimensionless qubit-field coupling for the superconducting system, which is $\lambda = 0.095$. Integrating these values into the cases of our studies in Chapter 5, we obtain our two-qubit revival time at $\frac{t_r}{2} = 5.25\mu s$. As explained previously in the relevant chapters, this is the time for the first entanglement revival in our two-qubit subsystem. It is very interesting to note that the calculated characteristic two-qubit revival time is much shorter the system's typical decoherence time of $100\mu s$. This comparison shows us that there is potential experimental possibility at the current time to observe the interesting dynamics in the interacting systems we considered in this study. Furthermore, an interaction between two qubits and 7 spin chain as a quantum bus in a superconducting system has been proposed in [84] with very encouraging results.

There are also numerous other platforms for physical realisation where the applications of an interacting model in which a collection of N spins are considered instead of the field mode. For example, a system of multiple superconducting qubits with uniform coupling to one or more microwave field modes operated in their qubit limit (zero or one excitation) could be used in the physical implementation of Circuit QED [85, 86, 87, 88, 89, 90, 91]. Similarly, ion trap or atomic systems [92, 93, 94, 95] that utilises ions or atoms coupled to various cavity modes operated with two-level excitation could also be considered. Another possible application is in the molecular fabrication [96, 79] where one or more specific spins couple to a system of N other spins to envisage designer molecules besides the applications in quantum dots [97, 98] through an interaction of an electron spin with nuclear spin for quantum computation using semiconductor. These examples are among many other systems that could be studied in the near future.

Bibliography

[1] W. J. Munro, K. Nemoto, G. J. Milburn, and S. L. Braunstein, "Weak-force detection with superposed coherent states," *Physical Review A*, vol. 66, no. 2, p. 023819, 2002.

[2] A. Gilchrist, K. Nemoto, W. J. Munro, T. Ralph, S. Glancy, S. L. Braunstein, and G. Milburn, "Schrödinger cats and their power for quantum information processing," *Journal of Optics B: Quantum and Semiclassical Optics*, vol. 6, no. 8, p. S828, 2004.

[3] J. Joo, W. J. Munro, and T. P. Spiller, "Quantum metrology with entangled coherent states," *Physical review letters*, vol. 107, no. 8, p. 083601, 2011.

[4] J. A. Dunningham, "Using quantum theory to improve measurement precision," *Contemporary Physics*, vol. 47, no. 5, pp. 257–267, 2006.

[5] P. Knott, T. Proctor, A. Hayes, J. Cooling, and J. Dunningham, "Practical quantum metrology with large precision gains in the low-photon-number regime," *Physical Review A*, vol. 93, no. 3, p. 033859, 2016.

[6] V. Giovannetti, S. Lloyd, and L. Maccone, "Quantum metrology," *Physical review letters*, vol. 96, no. 1, p. 010401, 2006.

[7] L. Pezzé and A. Smerzi, "Entanglement, nonlinear dynamics, and the heisenberg limit," *Physical review letters*, vol. 102, no. 10, p. 100401, 2009.

[8] S. Boixo, A. Datta, M. J. Davis, S. T. Flammia, A. Shaji, and C. M. Caves, "Quantum metrology: dynamics versus entanglement," *Physical review letters*, vol. 101, no. 4, p. 040403, 2008.

[9] S. Haroche and J.-M. Raimond, "Cavity quantum electrodynamics," *Scientific American*, vol. 268, pp. 54–60, 1993.

[10] A. Wallraff, D. I. Schuster, A. Blais, L. Frunzio, R.-S. Huang, J. Majer, S. Kumar, S. M. Girvin, and R. J. Schoelkopf, "Strong coupling of a single photon to a superconducting qubit using circuit quantum electrodynamics," *Nature*, vol. 431, no. 7005, pp. 162–167, 2004.

[11] P. R. Berman, "Cavity quantum electrodynamics," 1994.

[12] J. I. Cirac and P. Zoller, "Quantum computations with cold trapped ions," *Physical review letters*, vol. 74, no. 20, p. 4091, 1995.

[13] D. Schuster, A. Houck, J. Schreier, A. Wallraff, J. Gambetta, A. Blais, L. Frunzio, J. Majer, B. Johnson, M. Devoret, *et al.*, "Resolving photon number states in a superconducting circuit," *Nature*, vol. 445, no. 7127, pp. 515–518, 2007.

[14] E. T. Jaynes and F. W. Cummings, "Comparison of quantum and semiclassical radiation theories with application to the beam maser," *Proceedings of the IEEE*, vol. 51, no. 1, pp. 89–109, 1963.

[15] I. I. Rabi, "Space quantization in a gyrating magnetic field," *Physical Review*, vol. 51, no. 8, p. 652, 1937.

[16] J. You and F. Nori, "Quantum information processing with superconducting qubits in a microwave field," *Physical Review B*, vol. 68, no. 6, p. 064509, 2003.

[17] A. Blais, J. Gambetta, A. Wallraff, D. Schuster, S. Girvin, M. Devoret, and R. Schoelkopf, "Quantum-information processing with circuit quantum electrodynamics," *Physical Review A*, vol. 75, no. 3, p. 032329, 2007.

[18] J.-H. An, M. Feng, and C. Oh, "Quantum-information processing with a single photon by an input-output process with respect to low-q cavities," *Physical Review A*, vol. 79, no. 3, p. 032303, 2009.

[19] H. Azuma, "Quantum computation with the jaynes-cummings model," *Progress of Theoretical Physics*, vol. 126, no. 3, pp. 369–385, 2011.

[20] B. Mischuck and K. Mølmer, "Qudit quantum computation in the jaynes-cummings model," *Physical Review A*, vol. 87, no. 2, p. 022341, 2013.

[21] A. Blais, R.-S. Huang, A. Wallraff, S. Girvin, and R. J. Schoelkopf, "Cavity quantum electrodynamics for superconducting electrical circuits: An architecture for quantum computation," *Physical Review A*, vol. 69, no. 6, p. 062320, 2004.

[22] J. Gea-Banacloche, "Collapse and revival of the state vector in the jaynes-cummings model: An example of state preparation by a quantum apparatus," *Phys. Rev. Lett.*, vol. 65, pp. 3385–3388, Dec 1990.

[23] C. Gerry and P. Knight, *Introductory quantum optics*. Cambridge university press, 2005.

[24] T. Yu and J. Eberly, "Finite-time disentanglement via spontaneous emission," *Physical Review Letters*, vol. 93, no. 14, p. 140404, 2004.

[25] Y. Qing, Y. Ming, and C. Zhuo-Liang, "Sudden death of entanglement between two atoms with initial tripartite entangled state in the Tavis-Cummings model," *Chinese Physics Letters*, vol. 25, no. 3, p. 825, 2008.

[26] T. Yu and J. Eberly, "Sudden death of entanglement," *Science*, vol. 323, no. 5914, pp. 598–601, 2009.

[27] C. Jarvis, D. Rodrigues, B. Györffy, T. Spiller, A. Short, and J. Annett, "Dynamics of entanglement and 'attractor' states in the Tavis-Cummings model," *New Journal of Physics*, vol. 11, no. 10, p. 103047, 2009.

[28] C. Jarvis, D. Rodrigues, B. Györffy, T. Spiller, A. Short, and J. Annett, "Collapse and revival of "Schrödinger cat" states," *JOSA B*, vol. 27, no. 6, pp. A164–A169, 2010.

[29] S. Dooley, F. McCrossan, D. Harland, M. J. Everitt, and T. P. Spiller, "Collapse and revival and cat states with an N-spin system," *Physical Review A*, vol. 87, no. 5, p. 052323, 2013.

[30] P. A. M. Dirac, *The principles of quantum mechanics*. No. 27, Oxford university press, 1981.

[31] P. O. Löwdin, *Linear algebra for quantum theory*. Wiley, 1998.

[32] R. J. Glauber, "Coherent and incoherent states of the radiation field," *Physical Review*, vol. 131, no. 6, p. 2766, 1963.

[33] M. A. Nielsen and I. Chuang, “Quantum computation and quantum information,” 2002.

[34] F. Arecchi, E. Courtens, R. Gilmore, and H. Thomas, “Atomic coherent states in quantum optics,” *Physical Review A*, vol. 6, no. 6, p. 2211, 1972.

[35] J. Radcliffe, “Some properties of coherent spin states,” *Journal of Physics A: General Physics*, vol. 4, no. 3, p. 313, 1971.

[36] E. Schrödinger, “Die gegenwärtige situation in der quantenmechanik,” *Naturwissenschaften*, vol. 23, no. 48, pp. 807–812, 1935.

[37] N. Bohr and A. Einstein, “Quantum theory and measurement, edited by JA Wheeler and WH Zurek,” 1984.

[38] L. Amico, R. Fazio, A. Osterloh, and V. Vedral, “Entanglement in many-body systems,” *Reviews of modern physics*, vol. 80, no. 2, p. 517, 2008.

[39] V. Vedral, “The role of relative entropy in quantum information theory,” *Reviews of Modern Physics*, vol. 74, no. 1, p. 197, 2002.

[40] J. S. Bell, “On the einstein podolsky rosen paradox. physics, 1 (3), 195-200,” 1964.

[41] N. Linden and S. Popescu, “On multi-particle entanglement,” *arXiv preprint quant-ph/9711016*, 1997.

[42] A. Peres, “Separability criterion for density matrices,” *Physical Review Letters*, vol. 77, no. 8, p. 1413, 1996.

[43] M. B. Plenio and S. Virmani, “An introduction to entanglement measures,” *arXiv preprint quant-ph/0504163*, 2005.

[44] J. Von Neumann, *Mathematical foundations of quantum mechanics.* No. 2, Princeton university press, 1955.

[45] A. Wehrl, “General properties of entropy,” *Reviews of Modern Physics*, vol. 50, no. 2, p. 221, 1978.

[46] S. Bose and V. Vedral, “Mixedness and teleportation,” *Physical Review A*, vol. 61, no. 4, p. 040101, 2000.

[47] H. Araki and E. H. Lieb, “Entropy inequalities,” *Communications in Mathematical Physics*, vol. 18, no. 2, pp. 160–170, 1970.

[48] V. Vedral, M. Plenio, K. Jacobs, and P. Knight, "Statistical inference, distinguishability of quantum states, and quantum entanglement," *Physical Review A*, vol. 56, no. 6, p. 4452, 1997.

[49] W. J. Munro, D. F. James, A. G. White, and P. G. Kwiat, "Maximizing the entanglement of two mixed qubits," *Physical Review A*, vol. 64, no. 3, p. 030302, 2001.

[50] C. H. Bennett, D. P. DiVincenzo, J. A. Smolin, and W. K. Wootters, "Mixed-state entanglement and quantum error correction," *Physical Review A*, vol. 54, no. 5, p. 3824, 1996.

[51] W. K. Wootters, "Entanglement of formation of an arbitrary state of two qubits," *Physical Review Letters*, vol. 80, no. 10, p. 2245, 1998.

[52] S. Hill and W. K. Wootters, "Entanglement of a pair of quantum bits," *Physical review letters*, vol. 78, no. 26, p. 5022, 1997.

[53] W. K. Wootters, "Entanglement of formation and concurrence.," *Quantum Information & Computation*, vol. 1, no. 1, pp. 27–44, 2001.

[54] D. Cavalcanti, F. G. Brandão, and M. T. Cunha, "Are all maximally entangled states pure?," *Physical Review A*, vol. 72, no. 4, p. 040303, 2005.

[55] T.-C. Wei, K. Nemoto, P. M. Goldbart, P. G. Kwiat, W. J. Munro, and F. Verstraete, "Maximal entanglement versus entropy for mixed quantum states," *Physical Review A*, vol. 67, no. 2, p. 022110, 2003.

[56] R. F. Werner, "Quantum states with einstein-podolsky-rosen correlations admitting a hidden-variable model," *Physical Review A*, vol. 40, no. 8, p. 4277, 1989.

[57] C. H. Bennett, G. Brassard, S. Popescu, B. Schumacher, J. A. Smolin, and W. K. Wootters, "Purification of noisy entanglement and faithful teleportation via noisy channels," *Physical review letters*, vol. 76, no. 5, p. 722, 1996.

[58] F. Verstraete, K. Audenaert, and B. De Moor, "Maximally entangled mixed states of two qubits," *Physical Review A*, vol. 64, no. 1, p. 012316, 2001.

[59] M. J. Everitt, W. Munro, and T. Spiller, "Quantum-classical crossover of a field mode," *Physical Review A*, vol. 79, no. 3, p. 032328, 2009.

[60] E. T. Jaynes and F. W. Cummings, "Comparison of quantum and semiclassical radiation theories with application to the beam maser," *Proceedings of the IEEE*, vol. 51, no. 1, pp. 89–109, 1963.

[61] M. Tavis and F. W. Cummings, "Exact solution for an n-molecule-radiation-field Hamiltonian," *Physical Review*, vol. 170, no. 2, p. 379, 1968.

[62] S. Dooley and T. P. Spiller, "Fractional revivals, multiple-Schrödinger-cat states, and quantum carpets in the interaction of a qubit with N qubits," *Physical Review A*, vol. 90, no. 1, p. 012320, 2014.

[63] S. Dooley, *Quantum revivals and generation of non-classical states in an N spin system.* PhD thesis, University of Leeds, 2014.

[64] C. E. A. Jarvis, *Dynamics of Entanglement for Qubits in a Cavity.* PhD thesis, University of Bristol, 2009.

[65] K. Fujii, "Introduction to the rotating wave approximation (rwa): Two coherent oscillations," *Journal of Modern Physics*, vol. 8, no. 12, p. 2042, 2017.

[66] J. H. Eberly, N. Narozhny, and J. Sanchez-Mondragon, "Periodic spontaneous collapse and revival in a simple quantum model," *Physical Review Letters*, vol. 44, no. 20, p. 1323, 1980.

[67] F. Cummings, "Stimulated emission of radiation in a single mode," *Physical Review*, vol. 140, no. 4A, p. A1051, 1965.

[68] J. Gea-Banacloche, "Atom-and field-state evolution in the Jaynes-Cummings model for large initial fields," *Physical Review A*, vol. 44, no. 9, p. 5913, 1991.

[69] V. Bužek, H. Moya-Cessa, P. Knight, and S. Phoenix, "Schrödinger-cat states in the resonant jaynes-cummings model: Collapse and revival of oscillations of the photon-number distribution," *Physical review A*, vol. 45, no. 11, p. 8190, 1992.

[70] P. Knight and B. Shore, "Schrödinger-cat states of the electromagnetic field and multilevel atoms," *Physical Review A*, vol. 48, no. 1, p. 642, 1993.

[71] S. Chumakov, A. Klimov, and J. Sanchez-Mondragon, "Collective atomic dynamics in a strong quantum field," *Optics communications*, vol. 118, no. 5, pp. 529–536, 1995.

[72] T. Meunier, A. Le Diffon, C. Ruef, P. Degiovanni, and J.-M. Raimond, "Entanglement and decoherence of n atoms and a mesoscopic field in a cavity," *Physical Review A*, vol. 74, no. 3, p. 033802, 2006.

[73] S. Chumakov, A. B. Klimov, and J. Sanchez-Mondragon, "General properties of quantum optical systems in a strong-field limit," *Physical Review A*, vol. 49, no. 6, p. 4972, 1994.

[74] D. Rodrigues, C. Jarvis, B. Györffy, T. Spiller, and J. Annett, "Entanglement of superconducting charge qubits by homodyne measurement," *Journal of Physics: Condensed Matter*, vol. 20, no. 7, p. 075211, 2008.

[75] B. W. Shore and P. L. Knight, "The jaynes-cummings model," *Journal of Modern Optics*, vol. 40, no. 7, pp. 1195–1238, 1993.

[76] G. Ramon, C. Brif, and A. Mann, "Collective effects in the collapse-revival phenomenon and squeezing in the Dicke model," *Physical Review A*, vol. 58, no. 3, p. 2506, 1998.

[77] J. Eberly and T. Yu, "The end of an entanglement," *Science*, pp. 555–557, 2007.

[78] M. Yönaç, T. Yu, and J. Eberly, "Sudden death of entanglement of two jaynes–cummings atoms," *Journal of Physics B: Atomic, Molecular and Optical Physics*, vol. 39, no. 15, p. S621, 2006.

[79] S. Simmons, J. A. Jones, S. D. Karlen, A. Ardavan, and J. J. Morton, "Magnetic field sensors using 13-spin cat states," *Physical Review A*, vol. 82, no. 2, p. 022330, 2010.

[80] J. Huang, X. Qin, H. Zhong, Y. Ke, and C. Lee, "Quantum metrology with spin cat states under dissipation," *Scientific reports*, vol. 5, 2015.

[81] X.-Y. Lü, S. Ashhab, W. Cui, R. Wu, and F. Nori, "Two-qubit gate operations in superconducting circuits with strong coupling and weak anharmonicity," *New Journal of Physics*, vol. 14, no. 7, p. 073041, 2012.

[82] L. DiCarlo, J. Chow, J. Gambetta, L. S. Bishop, B. Johnson, D. Schuster, J. Majer, A. Blais, L. Frunzio, S. Girvin, *et al.*, "Demonstration of two-qubit algorithms with a superconducting quantum processor," *Nature*, vol. 460, no. 7252, pp. 240–244, 2009.

[83] J. Majer, J. Chow, J. Gambetta, J. Koch, B. Johnson, J. Schreier, L. Frunzio, D. Schuster, A. Houck, A. Wallraff, *et al.*, "Coupling superconducting qubits via a cavity bus," *Nature*, vol. 449, no. 7161, pp. 443–447, 2007.

[84] K. N. Wilkinson, M. P. Estarellas, T. P. Spiller, and I. D'Amico, "Rapid and robust generation and distribution of epr pairs with spin chains," *arXiv preprint arXiv:1708.05650*, 2017.

[85] R. McDermott, R. Simmonds, M. Steffen, K. Cooper, K. Cicak, K. Osborn, S. Oh, D. Pappas, and J. M. Martinis, "Simultaneous state measurement of coupled josephson phase qubits," *Science*, vol. 307, no. 5713, pp. 1299–1302, 2005.

[86] A. Niskanen, K. Harrabi, F. Yoshihara, Y. Nakamura, S. Lloyd, and J. Tsai, "Quantum coherent tunable coupling of superconducting qubits," *Science*, vol. 316, no. 5825, pp. 723–726, 2007.

[87] M. Neeley, R. C. Bialczak, M. Lenander, E. Lucero, M. Mariantoni, A. O'Connell, D. Sank, H. Wang, M. Weides, J. Wenner, *et al.*, "Generation of three-qubit entangled states using superconducting phase qubits," *Nature*, vol. 467, no. 7315, pp. 570–573, 2010.

[88] M. Neeley, M. Ansmann, R. C. Bialczak, M. Hofheinz, E. Lucero, A. D. O'Connell, D. Sank, H. Wang, J. Wenner, A. N. Cleland, *et al.*, "Emulation of a quantum spin with a superconducting phase qudit," *Science*, vol. 325, no. 5941, pp. 722–725, 2009.

[89] L. DiCarlo, M. Reed, L. Sun, B. Johnson, J. Chow, J. Gambetta, L. Frunzio, S. Girvin, M. Devoret, and R. Schoelkopf, "Preparation and measurement of three-qubit entanglement in a superconducting circuit," *Nature*, vol. 467, no. 7315, pp. 574–578, 2010.

[90] M. Reed, L. DiCarlo, S. Nigg, L. Sun, L. Frunzio, S. Girvin, and R. Schoelkopf, "Realization of three-qubit quantum error correction with superconducting circuits," *Nature*, vol. 482, no. 7385, pp. 382–385, 2012.

[91] G. Kirchmair, B. Vlastakis, Z. Leghtas, S. E. Nigg, H. Paik, E. Ginossar, M. Mirrahimi, L. Frunzio, S. M. Girvin, and R. J. Schoelkopf, "Observation of quantum state collapse and revival due to the single-photon kerr effect," *Nature*, vol. 495, no. 7440, pp. 205–209, 2013.

[92] J. G. Bohnet, B. C. Sawyer, J. W. Britton, M. L. Wall, A. M. Rey, M. Foss-Feig, and J. J. Bollinger, "Quantum spin dynamics and entanglement generation with hundreds of trapped ions," *Science*, vol. 352, no. 6291, pp. 1297–1301, 2016.

[93] F. Reiter, A. Sørensen, P. Zoller, and C. Muschik, "Autonomous quantum error correction and application to quantum sensing with trapped ions," *arXiv preprint arXiv:1702.08673*, 2017.

[94] P. Schindler, D. Nigg, T. Monz, J. T. Barreiro, E. Martinez, S. X. Wang, S. Quint, M. F. Brandl, V. Nebendahl, C. F. Roos, *et al.*, "A quantum information processor with trapped ions," *New Journal of Physics*, vol. 15, no. 12, p. 123012, 2013.

[95] D. Gorman, E. Megidish, B. Hemmerling, and H. Haeffner, "Quantum simulation of spin-bath dynamics with trapped ions," *Bulletin of the American Physical Society*, 2017.

[96] J. A. Jones, S. D. Karlen, J. Fitzsimons, A. Ardavan, S. C. Benjamin, G. A. D. Briggs, and J. J. Morton, "Magnetic field sensing beyond the standard quantum limit using 10-spin noon states," *Science*, vol. 324, no. 5931, pp. 1166–1168, 2009.

[97] D. J. Reilly, J. M. Taylor, J. R. Petta, C. M. Marcus, M. P. Hanson, and A. C. Gossard, "Exchange control of nuclear spin diffusion in a double quantum dot," *Physical review letters*, vol. 104, no. 23, p. 236802, 2010.

[98] E. Chekhovich, M. Makhonin, A. Tartakovskii, A. Yacoby, H. Bluhm, K. Nowack, and L. Vandersypen, "Nuclear spin effects in semiconductor quantum dots," *Nature materials*, vol. 12, no. 6, pp. 494–504, 2013.